Volume 66A
Number 1
Jan.–Feb. 1962

Physics and Chemistry

U.S. DEPARTMENT OF COMMERCE

SECTION A

JOURNAL OF RESEARCH

NATIONAL BUREAU OF STANDARDS

Journal of Research

of the

National Bureau of Standards

A. Physics and Chemistry

JAN.–FEB. • 1962

VOLUME • 66A

NUMBER • 1

Editor: C. W. Beckett

Associate Editors: D. D. Wagman
J. M. Richardson

Publication dates:
Feb. 1, Apr. 1, June 1, Aug. 1, Oct. 1, Dec. 1, 1962.

JOURNAL OF RESEARCH

The National Bureau of Standards Journal of Research reports research and development in the fields of activity shown at right. Also included from time to time are survey articles on topics closely related to the Bureau's scientific and technical program.

The Journal is published in four separate sections as follows:

A. Physics and Chemistry

Contains papers of interest primarily to scientists working in these fields. Issued six times a year. Annual subscription: domestic, $4.00; foreign, $4.75.

B. Mathematics and Mathematical Physics

Presents studies and compilations designed mainly for the mathematician and the theoretical physicist. Issued quarterly. Annual subscription: domestic, $2.25; foreign, $2.75.

C. Engineering and Instrumentation

Reports research and development results of interest chiefly to the engineer and the applied scientist. Issued quarterly. Annual subscription: domestic, $2.25; foreign, $2.75.

D. Radio Propagation

Reports work in radio propagation, upper atmospheric physics and communications. Issued six times a year. Annual subscription: domestic, $4.00; foreign, $4.75.

U.S. DEPARTMENT OF COMMERCE
Luther H. Hodges, Secretary

NATIONAL BUREAU OF STANDARDS
A. V. Astin, Director

Functions and Activities

The functions of the National Bureau of Standards are set forth in the Act of Congress, March 3, 1901, as amended. These include the development and maintenance of the national standards of measurement and the provision of means and methods for making measurements consistent with these standards; the determination of physical constants and properties of materials; the development of methods and instruments for testing materials, devices, and structures; advisory services to government agencies on scientific and technical problems; invention and development of devices to serve special needs of the Government; and the development of standard practices, codes, and specifications. The work includes basic and applied research, development, engineering, instrumentation, testing, evaluation, calibration services, and various consultation and information services. The Bureau also serves as the Federal technical research center in a number of specialized fields. The scope of activities of the National Bureau of Standards is suggested in the following listing of the divisions and sections engaged in technical work.

Washington, D.C.

Electricity. Resistance and Reactance. Electrochemistry. Electrical Instruments. Magnetic Measurements. Dielectrics. High Voltage.

Metrology. Photometry and Colorimetry. Refractometry. Photographic Research. Length. Engineering Metrology. Mass and Scale. Volumetry and Densimetry

Heat. Temperature Physics. Heat Measurement. Cryogenic Physics. Equation of State. Statistical Physics.

Radiation Physics. X-ray. Radioactivity. Radiation Theory. High Energy Radiation. Radiological Equipment. Nucleonic Instrumentation. Neutron Physics.

Analytical and Inorganic Chemistry. Pure Substances. Spectrochemistry. Solution Chemistry. Standard Reference Material. Applied Analytical Research.

Mechanics. Sound. Pressure and Vacuum. Fluid Mechanics. Engineering Mechanics. Rheology. Combustion Controls.

Organic and Fibrous Materials. Rubber. Textiles. Paper. Leather. Testing and Specifications. Polymer Structure. Plastics. Dental Research.

Metallurgy. Thermal Metallurgy. Chemical Metallurgy. Mechanical Metallurgy. Corrosion. Metal Physics. Electrolysis and Metal Deposition.

Mineral Products. Engineering Ceramics. Glass. Refractories. Enameled Metals. Crystal Growth. Physical Properties. Constitution and Microstructure.

Building Research. Structural Engineering. Fire Research. Mechanical Systems. Organic Building Materials. Codes and Safety Standards. Heat Transfer. Inorganic Building Materials.

Applied Mathematics. Numerical Analysis Computation. Statistical Engineering. Mathematical Physics. Operations Research.

Data Processing Systems. SEAC Engineering Group. Components and Techniques. Digital Circuitry. Digital Systems. Analog Systems. Applications Engineering.

Atomic Physics. Spectroscopy. Infrared Spectroscopy. Solid State Physics. Electron Physics. Atomic Physics.

Instrumentation. Engineering Electronics. Electron Devices. Electronic Instrumentation. Mechanical Instruments. Basic Instrumentation.

Physical Chemistry. Thermochemistry. Surface Chemistry. Organic Chemistry. Molecular Spectroscopy. Molecular Kinetics. Mass Spectrometry.

Office of Weights and Measures.

Boulder, Colo.

Cryogenic Engineering. Cryogenic Equipment. Cryogenic Processes. Properties of Materials. Gas Liquefaction.

Ionosphere Research and Propagation. Low Frequency and Very Low Frequency Research. Ionosphere Research. Prediction Services. Sun-Earth Relationships. Field Engineering. Radio Warning Services.

Radio Propagation Engineering. Data Reduction Instrumentation. Radio Noise. Tropospheric Measurements. Tropospheric Analysis. Propagation-Terrain Effects. Radio-Meteorology. Lower Atmosphere Physics.

Radio Standards. High Frequency Electrical Standards. Radio Broadcast Service. Radio and Microwave Materials. Atomic Frequency and Time Interval Standards. Electronic Calibration Center. Millimeter-Wave Research. Microwave Circuit Standards.

Radio Systems. Applied Electromagnetic Theory. High Frequency and Very High Frequency Research. Modulation Research. Antenna Research. Navigation Systems. Space Telecommunications.

Upper Atmosphere and Space Physics. Upper Atmosphere and Plasma Physics. Ionosphere and Exosphere Scatter. Airglow and Aurora. Ionospheric Radio Astronomy.

Order all publications from the Superintendent of Documents
U.S. Government Printing Office, Washington 25, D.C.

Use of funds for printing this publication approved by the Director of the Bureau of the Budget (June 19, 1961).

JOURNAL OF RESEARCH of the National Bureau of Standards—A. Physics and Chemistry
Vol. 66A, No. 1, January–February 1962

Absolute Isotopic Abundance of Terrestrial Silver*

William R. Shields, Ernest L. Garner, and Vernon H. Dibeler

(September 28, 1961)

Isotopic abundance ratios are reported for a commercial silver nitrate, 13 samples of native silver, and 11 silver minerals of various compositions and from widely distributed deposits. Collateral measurements of known mixtures of nearly pure silver isotopes permit the determination of absolute abundance ratios. Native silver from Cobalt, Ontario, previously reported as exhibiting statistically significant variation, is re-examined. Additional measurements are reported for samples from the same nugget and from the same region. Except for the original observation, no significant variation from normal abundance is observed for any of the samples. The Ag^{107}/Ag^{109} ratio obtained from pooling the data is 1.07597 with a 95 percent confidence limit of ± 0.00055 for the effect of random errors and a total uncertainty of ± 0.00135 when an allowance for the possible effects of known sources of systematic error is included.

1. Introduction

In a recent determination of the absolute isotopic abundance ratio of silver, Shields, Craig, and Dibeler [1][1] carefully measured the Ag^{107}/Ag^{109} ratio for several samples of native silver. They reported a statistically significant variation in the ratio for one sample from Cobalt, Ontario compared with six samples from other localities. Previous investigations of a possible variation in the isotope ratio of natural silver have been limited to processed bulk silver [2] or to a very few mineral samples. Hess, Marshall, and Urey [3] have reported no variation among four samples of terrestrial silver and one sample of Toluca Troilite. However, their limit for detection of variation was about 2 percent of the isotope ratio. Murthy [4] has recently made a more precise comparison of Toluca Troilite with commercial silver nitrate and finds about a 2 percent enrichment of Ag^{107} in the troilite. As the apparent variation reported for Cobalt silver is only a fraction of this amount, a careful re-examination has been made of native silver samples, including some from the Cobalt area. In addition, measurements have been made on a number of silver minerals from widely scattered deposits to provide a broader basis for establishing a limit to the natural variation in the isotope abundance of terrestrial silver.

2. Experimental Procedure

The mass spectrometer used in this research is a 12-in. radius-of-curvature, 68° deflection with 60° magnet, single focusing, surface emission instrument. The triple filament source uses all rhenium ribbons 1×30 mils. The usual techniques were employed for preparing sample filaments for surface emission using of the order of 100 μg of sample. No extraneous material was required or used to produce satisfactory emission characteristics for Ag^+ ions.

Ion currents were measured with a vibrating reed electrometer. Isotope ratios were measured both by comparison of the Ag^{107} and Ag^{109} ion currents collected alternately on the Faraday collector and by a ratio-record method using an expanded scale recorder.[2]

All ratio measurements of the calibration mixtures and the commercial and natural samples were obtained under standardized conditions of essentially constant sample size and nominal ion currents of 1×10^{-11} amp. The latter was controlled by adjustment of the filament temperatures. Observations were made on a strict time schedule as illustrated in figure 1. The plot represents a typical set of uncorrected data for eight analyses of a commercial silver nitrate. Each analysis consists of three ratios observed at 10-min intervals starting 20 min after filaments are turned on. Curve A represents the set of

[2] This circuit and other details of construction of the instrument used in this work will be published elsewhere.

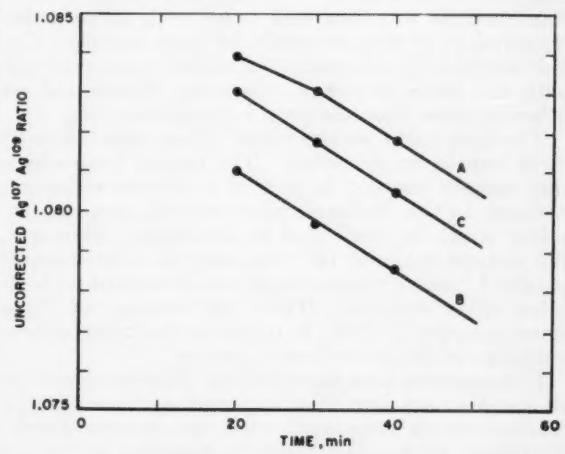

FIGURE 1. *Typical uncorrected ratio measurements for commercial silver nitrate as a function of time.*

Of eight analyses, curves A and B represent the highest and lowest observed ratios, respectively. Curve C represents the average of all eight analyses.

*This work was supported in part by the U.S. Atomic Energy Commission.
[1] Figures in brackets indicate the literature references at the end of this paper.

data with the highest observed Ag^{107}/Ag^{109} ratios, curve B represents the lowest ratios, and curve C represents the average ratios of all eight analyses. A variation in abundance ratio with time is observed. Mass spectra were obtained by varying the magnetic field by means of a reversible motor-driven control Helipot.

Except as otherwise indicated, the natural silver samples were obtained from collections of the U.S. National Museum, Smithsonian Institution through the courtesy of Paul E. Desautels and selected by Thomas W. Stern of the U.S. Geological Survey. Details of the preparation and measurement of the native silver samples and of the calibration mixtures of nearly pure isotopes are given by Shields, et al., [1]. The mineral samples were prepared for analysis by Rolf A. Paulson using well-known procedures and taking care to prevent contamination or separation of isotopes during the solution process. No effort was made to purify mineral samples to better than 80 percent silver. Native silver samples were not purified.

3. Results and Discussion

Tables 1, 2, and 3 summarize the data for the various silver samples examined in this study. Column 1 gives the U.S. National Museum catalog number, when applicable. Columns 2 and 3 identify the ore and locality, respectively. Column 4 lists the absolute Ag^{107}/Ag^{109} ratios and column 5 gives the 95 percent confidence limit for the effect of random errors in the analytical procedure. The data for silver nitrate reference obtained with each group of samples is given in each table.

The native silver samples of table 1 were analyzed by mass scanning. Each sample was analyzed four times with eighteen ratio pairs taken within each analysis. The mineral silver samples in table 3 were analyzed with a ratio recording measuring circuit. Each sample was analyzed twice with three ratios observed at 10 min intervals for each sample. Cobalt samples (1), (2), and (3) of table 2 were analyzed with the ratio recording measuring circuit and all other samples were analyzed by mass scanning.

The high value for the cobalt (1) sample (table 2) must remain unreconciled. The nugget from which this sample was cut is part of a private collection donated to the National Museum and some uncertainty must be attributed to its origin. However, the isotope ratio of the two samples subsequently obtained from the same nugget are in accord with all other silver samples. Thus, the average of these three samples (1.0764) is taken as the value representative of the silver from this area.

It is apparent that the observed differences among all samples are less than expected on the basis of random errors associated with the measurements. Therefore, all samples must be regarded as having the same isotope abundance ratio within these limits (0.2 percent of the ratio). Nevertheless, it is interesting to note that in general the isotope abundance ratios for natural silver samples are lower than that of the commercial silver nitrate. This is presently attributed to the lower silver purity in the natural samples compared with the chemically pure silver nitrate from the commercial and calibration samples.

TABLE 1. *Native Silver Samples*

U.S.N.M. Catalog No.	Composition	Locality	Ag^{107}/Ag^{109}	Analytical error [a]
----------	Silver Nitrate	Commercial material lot 90138	1.0755	0.0013
65154	Native Silver	Silver King Mine, Pinal Co., Arizona	1.0734	
5791	Native Silver	Ontonagon, Lake Superior District, Mich.	1.0766	
81784	Native Silver	Gagnon Mine, Butte Mont.	1.0744	.0025
112858	Native Silver	El Mochito Mine, Honduras	1.0746	
C-162	Native Silver	Chihuahua, Mexico	1.0755	
62845	Native Silver	Kongsberg, Norway	1.0744	

[a] This uncertainty is the 95 percent confidence limit for the effect of random errors in the analytical procedure.

TABLE 2. *Cobalt Silver Samples*

U.S.N.M. Catalog No.	Composition	Locality	Ag^{107}/Ag^{109}	Analytical error [c]
----------	Silver Nitrate	Commercial material lot 90138	1.0763	0.0009
C-140 (1) [a]	Native Silver	Cobalt, Ontario, Canada	1.0783 (1)	
C-140 (2) [a]	Native Silver	Cobalt, Ontario, Canada	1.0758 (2)	.0015
C-140 (3) [a]	Native Silver	Cobalt, Ontario, Canada	1.0753 (3)	
----------	Native Silver [b]	Silver Miller Mine, Cobalt Camp	1.0746	
----------	Native Silver [b]	Nova Scotia Mine, Cobalt Camp	1.0743	
----------	Native Silver [b]	Silver Banner Mine, Cobalt Camp	1.0736	.0025
----------	Native Silver [b]	Great Bear Lake,	1.0745	

[a] Three chips cut from different sides of the same nugget.
[b] Kindly supplied by the Canadian Geological survey through Dr. Frank E. Senftle, U.S.G.S.
[c] See footnote to table 1.

TABLE 3. *Mineral Silver Samples*

U.S.N.M. Catalog No.	Composition	Locality	Ag^{107}/Ag^{109}	Analytical error [a]
----------	Silver Nitrate	Commercial material, lot 90138	1.0758	0.0008
80263	Bromyrite	Australia	1.0752	
R-1215	Cerargyrite	Arizona	1.0750	
R-1226	Embolite	Australia	1.0756	
C-816	Freibergite	Bolivia	1.0754	
96041	Naumannite	Idaho	1.0751	
C-330	Hessite	Transylvania	1.0754	.0015
62877	Argentite	Germany	1.0752	
R-1144	Polybasite	Mexico	1.0743	
C-5638	Stephanite	Germany	1.0757	
9525	Pyrargyrite	Germany	1.0750	
92933	Proustite	Chile	1.0746	

Silver nitrate summary	Ag^{107}/Ag^{109}	Analytical error [a]	Total uncertainty [b]
Shields, Craig, and Dibeler (1960)	1.07547	±0.00126	±0.00206
Pooled data—present work	1.07597	±0.00055	±0.00135

[a] See footnote to table 1.
[b] Analytical error plus an allowance for possible effect due to known sources of systematic error.

It has been observed consistently that the Ag^{107}/Ag^{109} ratio for a given sample regardless of origin was low if any difficulty was experienced in obtaining the standardized intensity level for the Ag^+ ion current or otherwise required higher-than-normal filament temperatures.

The proper means of obtaining the "best estimate" of the Ag^{107}/Ag^{109} ratio is not obvious. However, the total number of measurements of the commercial silver nitrate, lot 90138, greatly exceeds all other samples. Furthermore, this material is isotopically indistinguishable from the other samples. If all the information observed to date for the commercial silver nitrate is pooled, the unbiased estimate of $Ag^{107}/Ag^{109}=1.07597$. The 95 percent confidence limit for the effect of random errors on this combined value is ± 0.00055. This limit of error plus a limit for possible systematic error gives the overall limit for the $Ag/^{107}/Ag^{109}$ ratio of ± 0.00135. The value for the ratio does not differ significantly from that previously reported by Shields et al., but can be stated with a smaller uncertainty.

4. References

[1] W. R. Shields, D. N. Craig, and V. H. Dibeler, J. Amer. Chem. Soc. **82,** 5033–5036 (1960).

[2] E. A. C. Crouch, E. R. Preece, I. G. Swainbank, and A. H. Turnbull, Nature **184,** No. 4683 (Suppl.), 358 (1959).

[3] D. C. Hess, R. R. Marshall, and H. C. Urey, Science, **126,** 1291–1293 (1958).

[4] U. R. Murthy, Phys, Rev. Letters **5,** No. 12, 539–541 (1960).

(Paper 66A1–135)

JOURNAL OF RESEARCH of the National Bureau of Standards—A. Physics and Chemistry
Vol. 66A, No. 1, January–February 1962

Temperature of a Copper Arc

Charles H. Corliss

The temperature of a copper arc in air has been measured by comparing 31 sets of transition probabilities for spectra of 20 elements with spectral-line intensities from those elements separately added to the copper. The intensities are taken from the recently published NBS Tables of Spectral-line Intensities and the transition probabilities from the literature. The individual determinations are discussed. The set of determinations is shown to follow a Gaussian distribution about a mean of 5100 °K. The average deviation of the determinations is 470 °K and the standard deviation of the mean is 110 °K. This temperature may be used in the evaluation of thousands of atomic transition probabilities from the intensities in the new tables. The effect of the uncertainty in the temperature on derived transition probabilities is evaluated as a function of excitation potential.

1. Introduction

Physicists have a natural interest in measuring quantities of extraordinary magnitude. This is especially true when the quantity measured permits new or more accurate evaluations of physical constants.

Such a quantity is the temperature of the electric arc in air between metallic electrodes. Well above the melting points of all materials and the boiling points of nearly all, the arc provides one of the hottest locations generally available in the physical laboratory. In such an arc it is possible to study the properties of atoms whose behavior is described by Boltzmann's law.

One particular arc, the temperature of which is especially interesting is the arc between copper electrodes, in which the spectra reported in the NBS Tables of Spectral-line Intensities were excited [1].[1] It happens that the temperature of this arc is susceptible of measurement by means of these very spectral-line intensity data. In itself, this would tempt us to carry out the determination; the fact that an accurate value of the temperature may enable us to evaluate transition probabilities for the 25,000 classified lines in the NBS Tables makes the temptation irresistible.

The arc has been described in the NBS Tables [1]. It was struck between two copper pellets ¼ inch in diameter, ¼ inch long, and weighing 1.5 grams each. The pellets were formed in a hydraulic press at 5000 psi from fine copper powder. Two pellets were mounted in water cooled clamps, cathode above the anode, with an arc gap of 3 mm. A direct current of 10 amperes, controlled by resistive ballast, was drawn from a 220-volt line. Exposures with which the spectra were taken varied in duration from 1 sec to 5 min depending on spectrographic efficiency and photographic plate sensitivity in different spectral regions. Separate sets of spectrograms were made for each element, using for each exposure fresh pellets to which an element had been added in the proportion of 1 atom of the element for every 1000 atoms of copper. The element was thoroughly mixed with the copper powder before pressing.

[1] Figures in brackets indicate the literature references at the end of this paper.

A lens at the slit of the spectrograph formed an image of the arc which fell entirely within the aperture of the grating, consequently the spectra represented radiation from all parts of the arc.

The method of temperature measurement adopted here is based on comparisons of published experimental transition probabilities of atomic lines with the intensities of the same lines measured in the copper arc. This method yields a temperature which is precisely that appropriate to the calculation of transition probabilities from our intensities.

If N_n atoms in the arc column are in an excited state n, the number of transitions per second to a lower state m will be N_nA_{nm} where A_{nm} is Einstein's probability coefficient of spontaneous emission [2]. The power from the transition is

$$I=h\nu N_nA_{nm} \tag{1}$$

where I is the intensity of the emitted line, h is Planck's constant, ν is the frequency of the line and $h\nu$ is the energy of a single photon. The temperature enters the comparison through its role of populating the upper level in accordance with Boltzmann's law

$$N_n=N_0\frac{g_n}{g_0}e^{-\frac{E}{kT}} \tag{2}$$

where N_0 is the population of the ground state and g_0 is its statistical weight $(2J+1)$, g_n is the statistical weight of the upper level, E is the energy of the upper level, k is Boltzmann's constant and T is the absolute temperature.

Substituting (2) into (1) we have

$$I=\frac{N_0}{g_0}h\nu g_nA_{nm}e^{-\frac{E}{kT}}. \tag{3}$$

Substituting $\nu=c/\lambda$, where c is the velocity of light and λ the wavelength of the line, and changing into logarithmic form (base 10), (3) becomes

$$\log\frac{I\lambda}{g_nA_{nm}}=\log\frac{N_0hc}{g_0}-\frac{0.434E}{kT}. \tag{4}$$

The first term on the right of (4) is a constant for

any particular element in this arc. We set it equal to C and solve for T. Introducing a value for k,

$$T=-\frac{625E}{\log\frac{I\lambda}{gA}-C} \tag{5}$$

where T is in °K, $gA=g_nA_{nm}$ and E is in units of 10^3 cm^{-1} which we will call kilokaysers (1 kK= 1000 cm^{-1}) in accordance with a suggestion of Meggers [3]. The value of T is most conveniently obtained from a plot of log $I\lambda/gA$ versus E for each spectrum in which relative values of gA are known. The constant C does not affect the slope of the line from which T is determined.

The ordinate is equivalent to log N_n/g_n so the plot is in effect a display of the population of excited levels in the atom as a function of the level value. Plots for eight sets of transition probabilities taken from the literature and compared with our intensities are given in figures 1 to 8. The straightness of the plots clearly shows that the observations are in accord with the Boltzmann distribution. The population of levels of equal statistical weight declines exponentially with increasing energy values.

If the f-value is known instead of A, we may use Ladenburg's [4] equation

$$g_nA_{nm}=\frac{8\pi^2e^2}{mc}\frac{g_mf_{mn}}{\lambda^2} \tag{6}$$

for converting eq (5) to the form

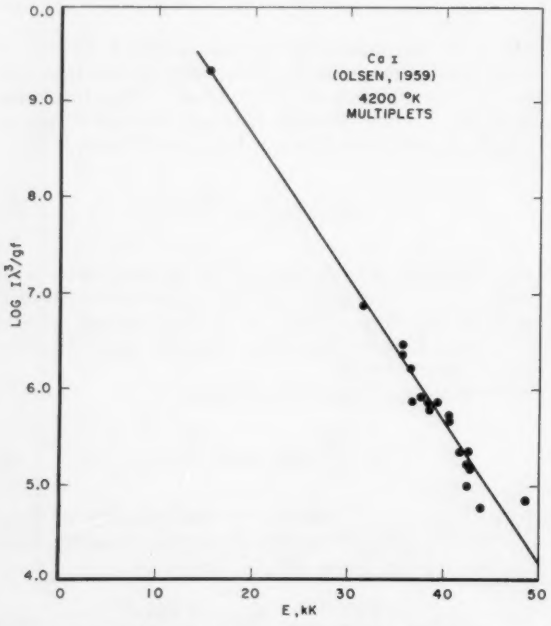

FIGURE 1. *Log ratio of intensity $\times\lambda^3$ to gf-value for multiplets of* Ca I *in the copper arc plotted versus upper level.*

An arc temperature of 4200 °K is derived from the slope of the line of best fit.

$$T=\frac{-625E}{\log\frac{I\lambda^3}{gf}-C'} \tag{7}$$

where $gf=g_mf_{mn}(=g_nf_{nm})$, and C' is a constant.

We assume that the temperature of the arc was constant during the exposure of each of the hundreds of spectrograms in which our intensity observations were made. Great care was taken in the preparation of the electrodes and in the operation of the arc to insure uniformity in the experimental conditions from exposure to exposure. The NBS intensity data used in the 31 temperature determinations reported in section 4 of this paper are taken from about 50 separate exposures. It will be shown in the discussion that the variation in the determinations arises, at least in part, from systematic errors amongst the sets of transition probabilities.

2. Excitation in the Arc in Air at Atmospheric Pressure

The question arises whether we should be able to assign a valid temperature which can be used to describe the intensity of spectral lines emitted in accordance with eq (3). If there are several processes of excitation at work, each operating at a different effective temperature, then eq (3) is not valid. In a classical investigation, Ornstein and Brinkman [5] have shown that excitation in the column of the ordinary arc in air is controlled by collisions between atoms and molecules in a strictly thermal fashion. The same process is responsible for ionization and dissociation. They found that the excitation was well described by Boltzmann's law and that ionization followed Saha's equation, which also demands a thermal aggregation of particles. Experiments by Elenbaas described by Cobine [6] show that in arcs at pressures above 20 mm Hg, the electron and gas

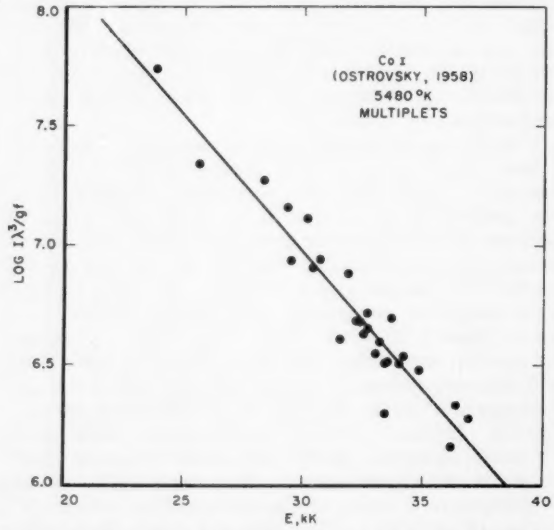

FIGURE 2. *Log ratio of intensity $\times\lambda^3$ to gf-value for multiplets of* Co I *in the copper arc plotted versus upper level.*

An arc temperature of 5480 °K is derived from the slope of the line of best fit

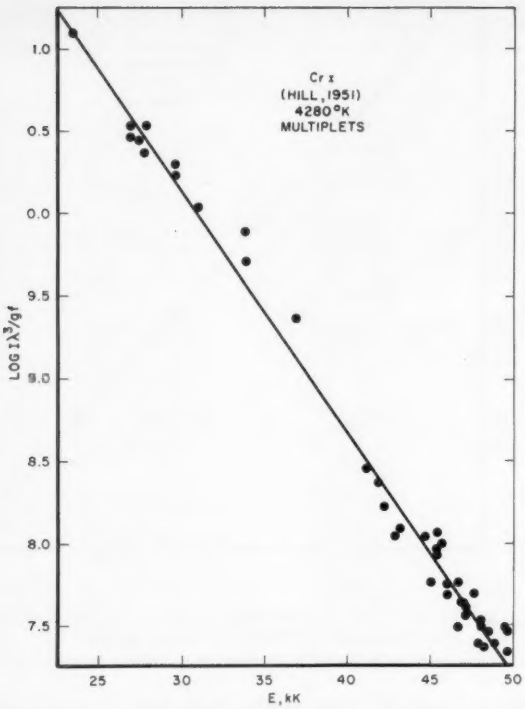

FIGURE 3. *Log ratio of intensity $\times\lambda^3$ to gf-value for multiplets of* Cr I *in the copper arc plotted versus upper level.*

An arc temperature of 4280 °K is derived from the slope of the line of best fit.

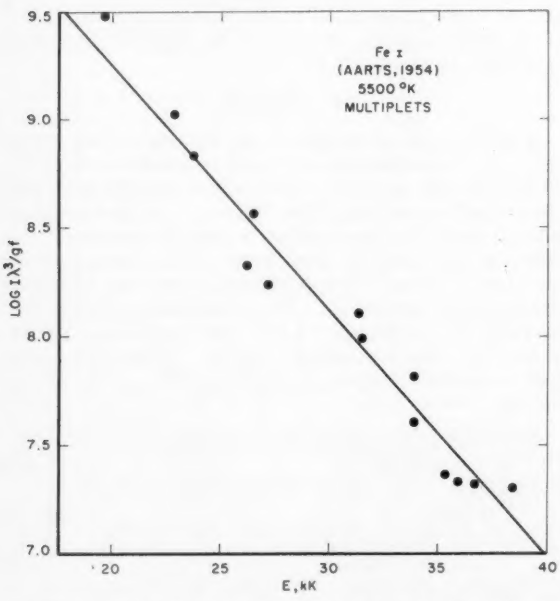

FIGURE 4. *Log ratio of intensity $\times\lambda^3$ to gf-value for multiplets of* Fe I *in the copper arc plotted versus upper level.*

An arc temperature of 5500 °K is derived from the slope of the line of best fit.

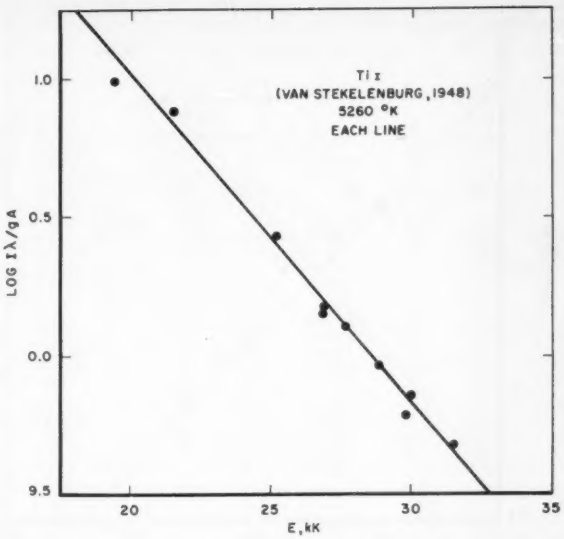

FIGURE 5. *Log ratio of intensity $\times\lambda$ to gA for lines of* Ti I *in the copper arc plotted versus upper level.*

An arc temperature of 5260 °K is derived from the slope of the line of best fit.

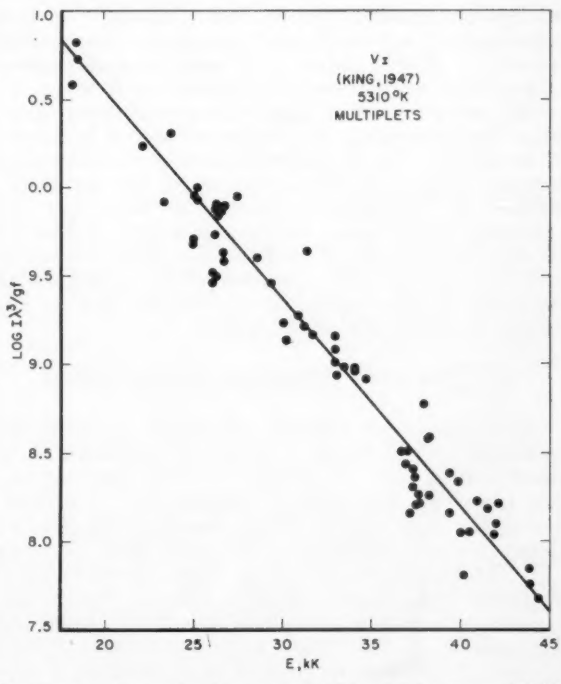

FIGURE 6. *Log ratio of intensity $\times\lambda^3$ to gf-value for multiplets of* V I *in the copper arc plotted versus upper level.*

An arc temperature of 5310 °K is derived from the slope of the line of best fit.

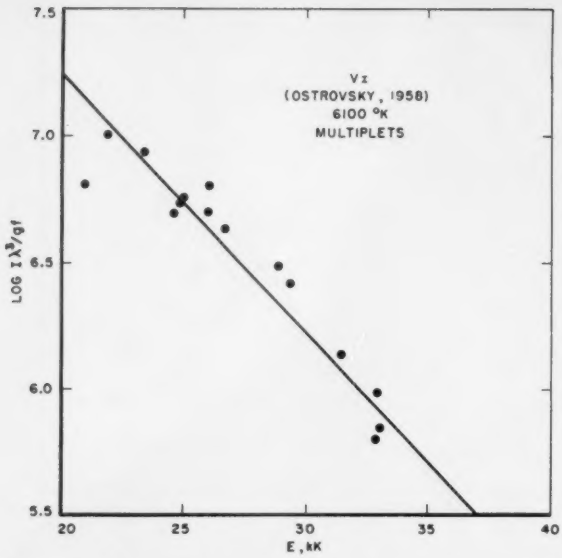

FIGURE 7. *Log ratio of intensity $\times\lambda^3$ to gf-value for multiplets of* V I *in the copper arc plotted versus upper level.*

An arc temperature of 6100 °K is derived from the slope of the line of best fit.

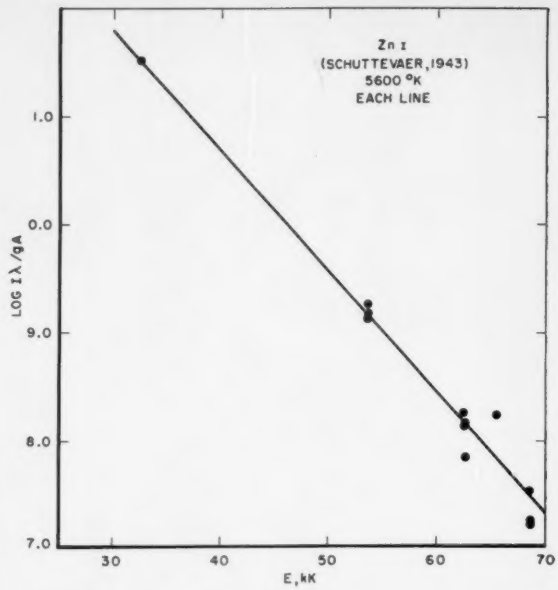

FIGURE 8. *Log ratio of intensity $\times\lambda$ to gA for lines of* Zn I *in the copper arc plotted versus upper level.*

An arc temperature of 5600 °K is derived from the slope of the line of best fit.

temperatures are equal. Suits [7] has measured the gas temperature and positive ion temperature in arcs at atmospheric pressure and found them equal within an experimental error of 300 °K.

The investigations quoted above are of interest in considering excitation in arcs. However, in this investigation we need not depend on them. The remainder of this paper is devoted to a discussion of graphical evaluations of temperature from eq (5) or (6), using 31 sets of transition probabilities taken from the literature. Examples are shown in figures 1 through 8. The linearity of these plots establishes beyond doubt that the excitation in our arc is described by Boltzmann's law. The fact that the excitation does follow Boltzmann's law enables us to calculate transition probabilities from intensities and conversely. The question of the existence of complete thermodynamical equilibrium per se becomes irrelevant for our purpose.

3. Choice of Transition Probabilities

The values of relative transition probabilities available for comparison with our intensities may be divided into four categories: (1) Experimental values based on independent temperature determinations; (2) experimental values based on temperature determinations obtained with data from category (1); (3) values calculated by quantum-mechanical methods (e.g., Hartree-Fock); and (4) values calculated with the approximate theory of Bates and Damgaard. Several trials with data from categories (3) and (4) resulted in plots of eq (7) exhibiting such a large scatter of points that no reasonably reliable temperature could be derived. Allen [8], in a similar investigation, states that use of Bates and Damgaard values leads to impossibly high arc temperatures, particularly in complex spectra. Category (2) is obviously inadmissible for our purposes, since such a set of data would merely duplicate the information from category (1) with which it was calibrated.

We are left with the experimental data of category (1) for our temperature determination. These data are reviewed up to 1954 by R. B. King [9] who noted about 2000 known values. The number has since increased to about 2200.

4. Results

A rather complete search of the published literature on experimental transition probabilities disclosed 31 sets of data suitable for comparison with the intensities in the NBS Tables. All independent sets of data with more than 4 lines in common with those of our tables (and from which temperatures could be derived) were included, with one exception discussed in section 5. The results are summarized in table 1. Column 1 gives the spectrum investigated by the authors in col. 2. The data came from 5 laboratories, indicated in col. 3, and listed below.

Physical Institute of the State University at Leningrad	11 sets
Physical Laboratory of the University of Utrecht	10 sets
Norman Bridge Laboratory of the California Institute of Technology	7 sets
Physical Institute, Academy of Sciences USSR, Moscow	2 sets
Zeeman Laboratory at the University of Amsterdam	1 set

TABLE 1. *Individual determinations of copper arc temperature*

Spectrum	Author	Laboratory	Date	Ref.	Method	No. of lines	Range of E	ΔE	T	Dev.
							kK	*kK*	°*K*	°*K*
Ag I	Terpstra et al.	Utrecht	1958	[10]	Arc	8	43–54	11	4600	500
Ba I	Kruithof	Utrecht	1943	[11]	Arc	10	26–35	9	4250	850
Ba I	Ostrovsky et al.	Leningrad	1960	[12]	Hook	54	13–36	23	5000	100
Ca I	Schuttevaer et al.	Utrecht	1943	[13]	Arc	12	32–43	11	4880	220
Ca I	Olsen et al.	California	1959	[14]	Furn. abs.	63	15–49	34	4200	900
Cd I	Hengstum et al.	Utrecht	1956	[15]	Arc	15	51–65	14	5080	20
Cd I	Penkin et al.	Leningrad	1960	[16]	Hook and em.	13	51–65	14	4750	350
Co I	King et al.	California	1955	[17]	Furn. abs.	181	24–46	22	5380	280
Co I	Ostrovsky et al.	Leningrad	1958	[18]	Hook	79	24–37	13	5480	380
Cr I	Hill et al.	California	1951	[19]	Furn. abs.	137	24–50	26	4280	820
Fe I	King et al.	California	1938	[20]	Furn. abs.	180	19–52	33	4820	280
	Carter	California	1949	[21]	Furn. em.					
Fe I	Sobolev (table 3)	Moscow	1943	[22]	Arc	15	33–46	13	4850	250
Fe I	Sobolev (table 5)	Moscow	1943	[22]	Arc	32	27–40	13	5320	220
Fe I	Aarts et al.	Amsterdam	1954	[23]	Furn. em.	59	20–38	18	5500	400
Ga I	Ostrovsky et al.	Leningrad	1958	[24]	Hook	5	25–35	10	5750	650
Hg I	Schouten et al.	Utrecht	1943	[25]	Arc	8	62–71	9	6250	1150
In I	Ostrovsky et al.	Leningrad	1958	[24]	Hook	5	24–33	9	4510	590
K I	van der Held et al.	Utrecht	1936	[26]	Flame	6	13–27	14	5100	0
Mg I	Kersten et al.	Utrecht	1941	[27]	Arc	18	41–58	17	5780	680
Mn I	Ostrovsky et al.	Leningrad	1957	[28]	Hook	9	18–36	18	3900	1200
Ni I	King	California	1948	[29]	Furn. abs.	89	28–37	9	4660	440
Sc I	Ostrovsky et al.	Leningrad	1957	[30]	Hook	33	16–33	17	5100	0
Sr I	Schuttevaer et al.	Utrecht	1943	[13]	Arc	8	15–40	25	4410	690
Ti I	King et al.	California	1938	[20]	Furn. abs.	204	19–40	21	5080	20
Ti I	van Stekelenburg et al.	Utrecht	1948	[31]	Arc	28	19–32	13	5260	160
Ti I	Ostrovsky et al.	Leningrad	1956	[32]	Hook	56	19–34	15	5400	300
Tl I	Filippov et al.	Leningrad	1933	[33]	Hook	5	26–43	17	6400	1300
V I	King	California	1947	[34]	Furn. abs.	224	18–42	24	5310	210
V I	Ostrovsky	Leningrad	1958	[18]	Hook	78	21–33	12	6100	1000
Zn I	Schuttevaer et al.	Utrecht	1943	[35]	Arc	12	31–69	38	5600	500
Zn I	Penkin et al.	Leningrad	1960	[16]	Hook and em.	12	54–68	14	5160	60

The date of publication is given in col. 4 and the reference number, as listed at the end of this paper, in col. 5. The method used in the paper is indicated in col. 6. In general, the several laboratories use different methods. At Leningrad the anomalous dispersion of the vapor in the neighborhood of the absorption lines from a furnace is employed according to the "hook" method of Rogestwensky [36], sometimes with variations. The temperature of the tube furnace is measured with an optical pyrometer. At Utrecht measurements are made usually with the arc method originated by Ornstein and his co-workers [5] and carried on by Professor Smit [37]. In that procedure, the temperature is usually measured from the intensity distribution in the CN bands in the spectrum. The California experiments generally follow the method of total absorption as developed by King and King [38]. The furnace temperature is measured with an optical pyrometer.

The number of spectral lines utilized in each determination is given in col. 7. The largest numbers are from California. The minimum and maximum values of upper excitation potential and the differences between them are given in cols. 8 and 9. These determine the range of the abscissae of the plots and thus affect to some extent the precision of the slope determination. The temperature determined from the slope of the plot appears in col. 10 and its deviation from the mean value in col. 11. The average value of the 31 individual determinations is 5100 °K and the average deviation is 470 °K (9%). The standard deviation of an individual determination, which is a measure of the scatter of the determinations, is given by

$$\sigma=\sqrt{\frac{\Sigma \text{ dev.}^2}{n-1}}$$

and is equal to 600 °K (12%). The standard deviation of the mean, which measures the precision of the result, is given by

$$\sigma_m=\sqrt{\frac{\Sigma \text{ dev.}^2}{n(n-1)}}$$

and is equal to 110 °K (2%). The median value is also 5100 °K.

It is of interest to compare the results from the three major contributors of transition probability data. This is done in table 2. The three mean values agree amongst themselves within their uncertainties. Another test of the data was made by selecting 12 sets of data which, on the basis of small scatter and uniform distribution of the points, and adequate range of E, seemed to give promise of better determinations. The average of these 12 is 5000 °K with an average deviation of 500 °K. These values are not significantly different from the general averages. The above mentioned tests provide some confidence in the adoption of an unweighted mean as the best value for the temperature.

Eight of the plots from which the temperatures were derived are reproduced in the figures. In each figure is given the spectrum, the reference from which the transition probabilities were taken, the temperature derived from the plot and a note whether each point on the plot represents a single spectral line or the average value for a multiplet.

617296—62——2

TABLE 2. *Comparison of laboratories*

Spectrum	Temp.	Dev.
California		
Ca I	4200	620
Cr I	4280	540
Ni I	4660	240
Fe I	4820	0
Ti I	5080	260
V I	5310	490
Co I	5380	560
Avg	4820	390
$\sigma = 470$		
Leningrad		
Mn I	3900	1330
In I	4510	720
Cd I	4750	480
Ba I	5000	230
Sc I	5100	130
Zn I	5160	70
Ti I	5400	170
Co I	5480	250
Ga I	5780	520
V I	6100	870
Tl I	6400	1170
Avg	5230	540
$\sigma = 720$		
Utrecht		
Ba I	4250	870
Sr I	4410	710
Ag I	4600	520
Ca I	4880	240
Cd I	5080	40
K I	5100	0
Ti I	5260	140
Zn I	5600	480
Mg I	5780	660
Hg I	6250	1130
Avg	5120	480
$\sigma = 630$		

5. Discussion of Results

It might not be amiss to discuss briefly the individual determinations. Ag gave a good plot, but with only a small range of E and a small number of lines. The Leningrad Ba data are excellent, except for low values of gf for 4132 and 3889 A which were probably caused by the proximity of strong lines at 4130 and 3891 A. The Utrecht Ba plot is good. Both plots of Cd are good and they agree well. Both Ca plots are excellent; the California one covers an unusually long range of E (see fig. 1). The plot of the Co data from California is long and straight but shows some scatter: the Leningrad one is shorter but with less scatter (see fig. 2). The low temperature which is obtained with the California Cr data has been noticed by several other people and is discussed by Goldberg, Muller, and Aller [39]. Otherwise a good plot is obtained (fig. 3). A set of Cr data from Leningrad shows such a large scatter and small range of E that no temperature could be derived [28].

In the California Fe plot, all the lines below 3200 A stand above the line. These were ignored in deriving the slope. The Moscow Fe data show a rather large scatter but yield satisfactory temperatures. The same paper [22] gives a set of data for Bi, which, although apparently in good order, yields a temperature of 8700 °K, which differs from the general mean by six times the standard deviation and it has been rejected, as noted above. The Amsterdam Fe data form an excellent plot with a good range of E and a small scatter (see fig. 4).

The Ga and In data are deficient in number and involve only resonance lines which are generally subject to various experimental difficulties, but they give a satisfactory plot. The plot for Hg covers too short a range of E because the NBS intensity of the resonance line was affected by self-absorption and could not be used. K represents the only data obtained from flames, and, although necessarily deficient in number of lines, yields a satisfactory plot. It involves the resonance lines, which showed no self-absorption in the NBS spectra. The Mg data show a good distribution and a very small scatter. The Mg resonance line was omitted because of self-absorption in the NBS line. The Mn resonance lines fall high on the Mn plot, indicating too low a value of gf from the hook method, and they were not used in finding the slope. Ni gives a good plot but with a small range of E. As in the case of Mn, the resonance lines of Sc are high on the plot and were ignored in determining the slope. The hook method apparently tends to give low values for the strongest lines. The Utrecht Sr data make a nice plot over a good range of E. Another set of Sr data obtained by Eberhagen at Göttingen [40] by using the Kiel water-arc forms a set of points with too large a scatter to permit a determination of temperature.

Data for Ti are available from three laboratories. The California set has a large number of points well distributed over a long range of E and a very small scatter. A preliminary plot of these data is shown in ref. [1]. The Utrecht data are fewer and have a smaller range, but shown almost no scatter. The maximum vertical deviation of a point from the best line is 0.09 log units which represents a maximum deviation of 23 percent (see fig. 5). The Leningrad data have more points but a considerable scatter. It may be mentioned at this point that Miss Rountree [41] has calculated a temperature for our arc from our Ti data and King's. Her value is slightly high because she omitted the λ^3 factor of eq (7). The Tl data from Leningrad have been frequently cited in the Russian literature. There are only 5 lines in common with ours. The fact that the temperature derived from these data shows the maximum deviation in the group of 31 values may arise from the location of 4 of the 5 lines in the short wavelength regions below 2800 A where the accuracy of the intensities declines. The V data from California have the largest number of lines in the group and the plot shows a moderate scatter of points well distributed over a long range of E, permitting an accurate determination of T. It shows no suggestion of curvature, indicating strict adherence to Boltz-

mann's law (see fig. 6). The Leningrad data cover a shorter range of E (see fig. 7). The Utrecht data for Zn cover the longest range of E of the whole group and give a very straight plot (see fig. 8). The Leningrad data omit the intersystem line at 3075 A and so have a more restricted range of E.

Taken as a whole, the results exhibit a nearly normal (Gaussian) distribution of values (see table 3). Consideration of the results in table 1 suggests that the effective temperature of the copper arc is substantially constant and that the variations arise from systematic errors in the various sets of transition probabilities. For example, the two sets of gf-values for V I exhibited in figures 6 and 7 are compared with the same intensity numbers in each case. The temperature difference of 780 °K between the values from each plot can arise only from systematic errors inherent in the two sets of gf-values. Similarly, the transition probabilities of van Hengstum and Smit [15] for Cd I are systematically smaller relative to those of Penkin and Redko [16] at the larger values of E, so although the identical NBS intensity numbers are used, the two plots yield temperatures which differ by 330 °K. The diversity of methods represented and the independent nature of the laboratories leads us to suppose that these systematic errors have offset one another to some extent in contributing to the general average value.

Various correlation plots have been made to determine other systematic influences on the derived temperatures. There appears to be no correlation with the number of lines used, with atomic number, with range of E (abscissae of the plots), with magnitude of E, nor with ionization potential.

TABLE 3. *Distribution of individual temperature determinations about the mean, in intervals of σ.*

Interval	3300–3900	3900–4500	4500–5100	5100–5700	5700–6300	6300–6900
Individual determinations	3900	4200 4250 4280 4410	4510 4600 4660 4750 4820 4850 4880 5000 5080 5080 5100	5100 5160 5260 5310 5320 5380 5400 5480 5500 5600	5750 5780 6100 6250	6400
Observed fraction	0.03	0.13	0.36	0.32	0.13	0.03
Expected (Gaussian)	.02	.14	.34	.34	.14	.02

6. Effect of Uncertainty in Temperature on Uncertainty in Derived Transition Probability

The purpose of determining the best value of the temperature of the copper arc is to enable us to calculate values of gA or gf from the intensities of the classified lines in the NBS Tables of Spectral-line Intensities. We must find out how the uncertainty of the value of T will influence the uncertainty of the gA or gf.

If we differentiate eq (3) with respect to T and divide the result by eq (3) we have

$$\frac{d(gA)}{gA}=-\frac{E}{kT}\frac{dT}{T}.$$

Introducing numerical values we find

$$\frac{d(gA)}{gA}=-\frac{E}{3.54}\frac{dT}{T}.$$

Now if $\frac{dT}{T}$ is 2 percent, then

$$\frac{d(gA)}{gA}=-0.00565\ E.$$

Similarly

$$\frac{d(gf)}{gf}=-0.00565\ E.$$

The magnitude of the error for values of the upper level from 10 to 100 kilokaysers is given in table 4, assuming a temperature of 5100 °K and an uncertainty in the temperature of 2 percent. Most of the lines in the NBS tables have upper levels less than 50 kK, so most of the errors introduced by the temperature error will be less than 30 percent. This is about the same as the errors in the intensity numbers themselves.

TABLE 4. *Error in gf of gA corresponding to a 2 percent error in T at 5100 °K*

E in kK	% error in gf or gA
10	6
20	11
30	17
40	23
50	28
60	34
70	40
80	45
90	51
100	56

7. Conclusion

A temperature for the copper arc in which the intensities published in the NBS Tables of Spectral-line Intensities [1] were measured has been determined. Comparison of NBS intensities with 1650 published transition probabilities for 20 different spectra yields the value

5100±110 °K.

With this parameter, relative transition probabilities for the 25,000 classified lines in the NBS Tables can be computed.

Further studies are in progress to determine the state of ionization of each element in the arc. This will allow the relative values for each spectrum to be adjusted to the same scale. It may then be possible to calibrate the scale on an absolute basis as Allen

has done [42]. All the pertinent data for the 25,000 lines are on punched cards and the computation can be performed very quickly, once the proper parameters and factors have been determined.

The author acknowledges the kind encouragement of W. F. Meggers and the helpful assistance of K. G. Kessler. The idea for this work came during a staff meeting lecture given by H. P. Broida many years ago. The work was greatly facilitated by the new NBS Data Center on Atomic Physics and its curator, Miss Barbara Glennon.

8. References

[1] W. F. Meggers, C. H. Corliss, and B. F. Scribner, Tables of Spectral-line Intensities, NBS Monograph 32 (1961), (U.S. Government Printing Office, Washington, D.C.)
[2] A. Einstein, Phys. Z. **18,** 121 (1917).
[3] Transactions of the Joint Commission for Spectroscopy, J. Opt. Soc. Am. **43,** 410 (1953).
[4] R. Ladenburg, Z. Physik **4,** 451 (1921).
[5] L. S. Ornstein and H. Brinkman, Physica **1,** 797 (1934).
[6] J. D. Cobine, Gaseous Conductors, p. 290, Dover Publications, New York (1958).
[7] C. G. Suits, Physics **6,** 190 and 315 (1935).
[8] C. W. Allen and A. S. Asaad, Mon. Not. Roy. Astronom. Soc. **115,** 571 (1955).
[9] R. B. King, Proc. of Conf. on Stellar Atmospheres, Indiana Univ. (1954).
[10] J. Terpstra and J. A. Smit, Physica **24,** 937 (1958).
[11] A. M. Kruithof, Physica **10,** 493 (1943).
[12] Y. I. Ostrovsky and N. P. Penkin, Optics and Spectroscopy **9,** 371 (1960).
[13] J. W. Schuttevaer, M. J. de Bont, and T. H. van den Broek, Physica **10,** 544 (1943).
[14] K. H. Olsen, P. M. Routly, and R. B. King, Astrophys. J. **130,** 688 (1959).
[15] J. P. A. van Hengstum and J. A. Smit, Physica **22,** 86 (1956).
[16] N. P. Penkin and T. P. Red'ko, Optics and Spectroscopy **9,** 360 (1960).
[17] R. B. King, B. Parnes, M. Davies, and K. H. Olsen, J. Opt. Soc. Am. **45,** 350 (1955).
[18] Y. I. Ostrovsky and N. P. Penkin, Optika i Spektroskopiya **5,** 345 (1958).
[19] A. J. Hill and R. B. King, J. Opt. Soc. Am. **41,** 315 (1951).
[20] R. B. King and A. S. King, Astrophys. J. **87,** 24 (1938).
[21] W. W. Carter, Phys. Rev. **76,** 962 (1949).
[22] N. N. Sobolev, J. Exp. Theoret. Phys. **13,** 131 (1943).
[23] J. Aarts, D. Harting, and C. J. Bakker, Physica **20,** 1250 (1954).
[24] Y. I. Ostrovsky and N. P. Penkin, Optika i Spektroskopiya **4,** 719 (1958).
[25] J. W. Schouten and J. A. Smit, Physica **10,** 661 (1943).
[26] E. F. M. van der Held and J. H. Heierman, Physica **3,** 31 (1936).
[27] J. A. H. Kersten and L. S. Ornstein, Physica **8,** 1124 (1941).
[28] Y. I. Ostrovsky and N. P. Penkin, Optika i Spektroskopiya **3,** 193 (1957).
[29] R. B. King, Astrophys. J. **108,** 87 (1948).
[30] Y. I. Ostrovsky and N. P. Penkin, Optika i Spektroskopiya **3,** 391 (1957).
[31] L. H. M. van Stekelenburg and J. A. Smit, Physica **14,** 185 (1948).
[32] Y. I. Ostrovsky, G. F. Parchevsky, and N. P. Penkin, Optika i Spektroskopiya **1,** 821 (1956).
[33] A. Filippov and W. Prokofiev, Z. Physik **85,** 647 (1933).
[34] R. B. King, Astrophys. J. **105,** 376 (1947).
[35] J. W. Schuttevaer and J. A. Smit, Physica **10,** 502 (1943).
[36] D. S. Rogestwensky and N. P. Penkin, J. Phys. U.S.S.R. **5,** 319 (1941).
[37] J. A. Smit, Physica **12,** 683 (1946).
[38] R. B. King and A. S. King, Astrophys. J. **82,** 377 (1935).
[39] L. Goldberg, E. A. Muller, and L. H. Aller, Astrophys. J. Supplement No. 45 **5,** 1 (1960).
[40] A. Eberhagen, Z. Physik **143,** 392 (1955).
[41] J. C. Rountree, Annales d'Astrophysique **23,** 633 (1960).
[42] C. W. Allen and A. S. Asaad, Mon. Not. Roy. Astron. Soc. **117,** 36 (1957); C. W. Allen, ibid. **117,** 622 (1957); C. W. Allen, ibid, **121,** 299 (1960).

(Paper 66A1–136)

JOURNAL OF RESEARCH of the National Bureau of Standards—A. Physics and Chemistry
Vol. 66A, No. 1, January–February 1962

Melting Process and the Equilibrium Melting Temperature of Polychlorotrifluoroethylene

John D. Hoffman and James J. Weeks

(October 2, 1961)

A new method of estimating the equilibrium melting temperature, T_m, of a polymer is described, and applied to polychlorotrifluoroethylene (PCTFE). Experimentally determined values of the so-called observed melting point, T_m'(obs), are plotted as a function of the isothermal crystallization temperature, T_x. When freed of secondary effects, such as recrystallization, the data fit a straight line of positive slope on a T_m'(obs) versus T_x plot, T_x being the abscissa. This line is then extrapolated to its intersection with the line T_m'(obs) $= T_x$. The temperature at this intersection is T_m. This intersection is at 224 °C for PCTFE, and T_m is quoted as 224±1 °C. (The highest melting point actually attained for a specimen was 218.2 °C.) The value of T_m estimated using the extrapolation procedure is compared with that estimated using the customary method of slow stepwise warming.

A theoretical justification is given for making the type of plot mentioned above. The most important assumption used in the theory is that one of the dimensions of the growing crystal retains a value rather close to that of the appropriate growth nucleus during an isothermal crystallization, the other two dimensions being large in comparison. Combination of this with the fact that the relevant dimension of the growth nucleus will vary as the reciprocal of the degree of supercooling leads to the prediction of melting points that increase linearly with crystallization temperature. The assumption that one of the dimensions of the crystal retains a value fairly close to that of a growth nucleus can readily be justified on the basis of polymer crystal growth with chain folds. Its justification in the case of the customary bundlelike mode of crystallization is less clear. It is demonstrated experimentally that even the largest detectible crystals in PCTFE are only about 70 percent thicker than a primary nucleus, when secondary effects are minimized.

The application of the theory to systems other than PCTFE is discussed briefly, and some preliminary measurements on polyethylene mentioned. Some points relating to the shape of the melting curves of highly crystalline polymers are also brought out.

1. Introduction

The present investigation was begun largely because of our interest in learning more about the factors that influence the melting behavior of polychlorotrifluoroethylene (PCTFE) specimens that were crystallized in bulk. Such factors as the rate of heating used in the melting run, the initial degree of crystallinity, and the temperature of the original crystallization were studied. One basic fact emerged early in the work: the temperature of the original crystallization had an important influence on the experimentally observed melting point. Under appropriate experimental conditions, the observed melting point, T_m'(obs) increased markedly and nearly linearly as the crystallization temperature, T_x, was increased. It naturally occurred to us that such data might be extrapolated in such a way as to permit the equilibrium melting temperature, T_m, to be determined. The concept that T_m'(obs), T_m, and T_x might be simply related to one another was apparently first mentioned by Lauritzen and Hoffman [1][1]. For a simplified model, they showed that $T_m'(\text{obs}) = (T_m + T_x)/2$. A somewhat more general derivation is given in the present paper. The melting point data on PCTFE are extrapolated to obtain an estimate of T_m. A number of secondary effects, such as the recrystallization that may occur on slow warming, are discussed.

It is of interest to know the equilibrium melting temperature of a polymer for a number of reasons. Among these is the fact that this quantity is required in the analysis of crystal growth rate data in order to establish the degree of supercooling $\Delta T = T_m - T_x$. The results of our studies on the isothermal growth of spherulitic crystallization in PCTFE at various temperatures will be reported shortly [2].

The equilibrium melting temperature of a polymer may be defined as the melting point of an assembly of crystals, each of which is so large that size (i.e., surface) effects are negligible, with the provision that each such large crystal is in equilibrium with the normal polymer liquid. (Small crystals will tend to melt well below T_m). A further provision is that the crystals at the melting point have the equilibrium degree of crystal perfection consistent with the minimum of free energy at T_m. The melting phenomena may take place at too high a temperature if the liquid polymer is oriented to an appreciable extent.

The above definition of T_m for a polymer is in principle similar to that for the true melting point of a pure compound of the nonpolymeric type, whether it be a molecular, ionic, or metallic crystal. However, the formation within a reasonable period of time of polymer crystals that are sufficiently large to meet the requirement that surface effects be negligible presents a most difficult practical problem. Polymers as they are ordinarily crystallized tend to melt out well below T_m because the crystals are

[1] Figures in brackets indicate the literature references at the end of this paper.

small, and perhaps somewhat too imperfect. The result is that an attempt to make a direct measurement of T_m for a polymer is not necessarily rewarded by a result that is sufficiently free of crystal size effects.

Before going on to give the theory and the analysis of the data, it is useful to indicate in a preliminary way the point of view that will be taken concerning the combination of circumstances that (a) causes the observed melting point of a linear polymer of high molecular weight to increase with increasing crystallization temperature and (b) renders it improbable that the equilibrium melting temperature can actually be attained in a real polymer specimen in an experiment of reasonable duration.

From nucleation theory we know that a dimension x of either a primary or secondary (growth) nucleus will vary as $1/(\Delta T)$. If the nucleus grows on all its faces, a large crystal that will melt extremely close to the true melting point will form. This is evidently what occurs with ordinary crystals. On the other hand, if some restriction on growth exists for one dimension, so that the resultant crystallite continues to maintain this dimension at a small value close to x while growing to large size in the other two, the crystal will melt out well below T_m. Thus, if one dimension of a polymer crystal persisted at or near the value appropriate to a nucleus during the growth process, it is seen that the observed melting point would be distinctly higher the greater the temperature of crystallization. As noted earlier, PCTFE exhibits such behavior. (Preliminary work reveals that similar behavior occurs for polyethylene.) The first systematic study showing an increase of melting point with an increase of crystallization temperature was that of Wood and Bekkedahl on natural rubber [3,4].

Even if one dimension of a polymer crystal remained at a value x near the primary or secondary nucleus size while growing to large size in the other two dimensions, it is readily seen that a large and high melting crystal would in theory be formed by carrying out the crystallization very near to T_m where ΔT is small. However, crystallization of a polymer specimen within a few degrees of T_m, so that it would be certain to melt within say 1 or 2 °C of T_m, will generally be prevented by kinetic factors. The growth rate of polymer crystals is nucleation rather than diffusion controlled anywhere near to T_m, with the result that the rate of crystallization becomes exponentially slower as the crystallization temperature is raised. Depending on the polymer, the rate of isothermal crystallization generally becomes excessively slow somewhere between 5 and 20 °C below even the nominal melting point. On this basis, one must expect to be frequently confronted with the problem of the depression of the observed melting point well below the true equilibrium melting temperature because of small crystal size. In a slow warming run, certain secondary mechanisms, to be discussed in some detail later, may operate in such a manner as to permit a further increase of crystal size. However, these effects (melting out followed by recrystallization; chain mobility in the crystal) will tend to be increasingly ineffective the higher the temperature. Hence, it is to be expected that even the slowest of the warming rates useful in practice may not lead to a specimen which actually melts at T_m, even though the dependence of T_m' (obs) on T_x will be more subdued than with more rapid warming.

A slow stepwise warming technique has been advocated by Mandelkern [5,6] as a method of attaining or closely approaching T_m in a real polymer specimen. From an operational standpoint, this method places emphasis on secondary processes such as the recrystallization that occurs with very slow warming as a method of obtaining large crystals and a high melting point in a specimen, rather than on initially crystallizing at the highest practicable temperature to achieve the same end. The question naturally arises as to how close the results obtained with the slow stepwise warming technique, as it is applied in practice, are to both the T_m value obtained by the extrapolation method, and the actual melting points of specimens obtained with initial crystallization at a high temperature. In order to obtain information on these points, a slow stepwise warming run was carried out on PCTFE. Data on polyethylene are also discussed in connection with this problem. Evidence is cited that suggests that the slow stepwise warming technique, as it has been employed in practice, gives melting points that are at least a few degrees below T_m.

The data on PCTFE analysed in this paper lead to the definite conclusion that one dimension of the crystal is small and close to that of a nucleus. (The preliminary data on polytheylene lead to a similar conclusion.) A discussion is given concerning the origin of this phenomenon. One of the models discussed is that of polymer crystal growth with chain folds, and the other is the familiar bundlelike model of polymer crystal growth. It is indicated that the retention of one dimension of the grown crystal near that of a growth or primary nucleus can be defended on theoretical grounds for a folded crystal, but that difficulties arise in the case of the bundlelike system. On this and other grounds, it is concluded that it is highly probable that the melting behavior of PCTFE is to be explained in terms of the model with chain folds.

2. Theory

2.1. Crystals With Chain Folds

The principal objective of this section is to derive an expression relating the observed melting point T_m'(obs) of a polymer with chain folded crystals to the crystallization temperature T_x and the equilibrium melting temperature T_m. The general type of experiment to which the theory applies is the following. A specimen is crystallized isothermally at T_x after being cooled from the melt. The melting point T_m'(obs) relevant to T_x is determined by warming the specimen at a specified rate by a method which locates the temperature at which the last detectible trace of crystallinity disappears. The experiment is then repeated for different T_x values.

The development given mentions the theoretical justification for assuming that one dimension of a folded crystal retains a value close to that of a primary or growth nucleus. Consideration is also given to the secondary mechanisms, such as recrystallization, that may occur in experimental studies and allow some increase in this restricted dimension. The shape of the melting curves is also discussed.

Consider the free energy of formation of a crystal with chain folds of the type shown in figure 1a. Define the dimension **l** as the step height of the crystal, and denote the other two dimensions **a** and **b**. Let σ and σ_e be the lateral and end surface free energy, respectively. Then the free energy of formation of a crystal may be written as

$$\Delta\phi_c = 2ab\sigma_e + 2al\sigma + 2bl\sigma - abl(\Delta f), \qquad (1)$$

where (Δf) is the free energy difference between the supercooled liquid phase and the bulk crystal phase. The latter quantity may be written

$$\Delta f = \frac{(\Delta h_f)(\Delta T)}{T_m} = \frac{(\Delta h_f)(T_m - T_x)}{T_m} \qquad (2)$$

to a sufficient approximation.[2] The quantity (Δh_f) is the heat of fusion in erg cm^{-3}. The quantities **a**, **b**, and **l** are in cm, and the surface free energies are in erg cm^{-2}. Thus $\Delta\phi_c$ is given in ergs for the whole crystal.

By setting $\Delta\phi_c = 0$, one finds

$$T_m'(l) = T_m\left\{1 - \frac{2\sigma_e}{(\Delta h_f)\mathbf{l}}\right\} \qquad (3)$$

for the melting point of a folded crystal where **l** is small compared to **a** and **b** [1,7]. The equilibrium melting temperature is seen to correspond to a crystal that has very large **a**, **b**, and **l** dimensions.

Even in the case where **a** and **b** are only several times larger than **l**, eq (3) is a fair approximation because σ_e will in general be substantially larger than σ. The ratio σ/σ_e will usually be within a factor of 2 or so of 0.1 [7]. The quantity σ_e will usually lie between 25 to 40 erg cm^{-2} to perhaps 150 to 175 erg cm^{-2}, depending on the work required to make a fold, and the cross-sectional area of the polymer molecule [7]. Thus, the terms $-4\sigma/(\Delta h_f)\mathbf{a}$ and $-4\sigma/(\Delta h_f)\mathbf{b}$ which appear in the exact form of eq (3) will be less important than the term $-2\sigma_e/(\Delta h_f)\mathbf{l}$ even if **a** and **b** are only a few times larger than **l**. In the case $\mathbf{a} >> \mathbf{l}$ and $\mathbf{b} >> \mathbf{l}$, eq (3) may be regarded as exact.

For completeness, the terms $4\mathbf{a}\epsilon + 4\mathbf{b}\epsilon$ where ϵ is the edge free energy in erg cm^{-1} could have been included in eq (1), but this would not have affected the result for $\mathbf{T}_m'(\mathbf{l})$. The edge free energy reflects the extra work that may be required to cause a fold to lie on a flat surface in from the fold plane, rather than in the plane of the chain folds or even outside it [1,7].

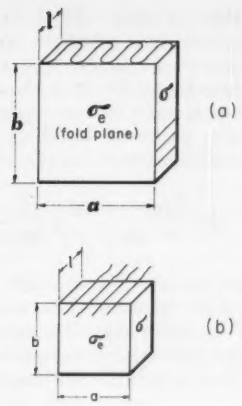

FIGURE 1. *Models of polymer crystals.*

(a) Lamellar crystal with chain folds.
(b) Bundlelike crystal.

The assumption $\Delta\phi_c = 0$ is equivalent to the statement that the melting of crystals of finite size occurs when the free energy of the crystal, surface energy included, is the same as that of the supercooled liquid.

We must now pause and ask if it is reasonable to assume that **l** remains at a small value while the folded crystal grows to large dimensions in the **a** and **b** directions.

There is a strong theoretical justification for this restriction of **l** in the case of polymer crystals grown in the chain folded pattern. This has been discussed in detail in a series of three papers by Lauritzen and Hoffman [1,7], and Lauritzen [8]. Reference [1] deals mainly with the formation of chain folded platelets in dilute solution. Reference [7] deals with the formation of chain folded crystals in bulk, and how aggregates of such crystals can form typical lamellar spherulites. Reference [8] treats the problem of the fluctuation of step height within a given folded crystal as it grows in the **a** and **b** direction. The following is a summary of a number of points relevant to the present discussion concerning crystallization with chain folds. The original papers should be consulted for details.

It can be shown that at a given degree of supercooling the step height of the growth nucleus will not fall below $2\sigma_e/(\Delta f)$, because no increase of stability even with extended growth in the **a** and **b** directions is achieved thereby. (It is easily seen from eq (1) that $\Delta\phi_c$ always has a positive value when $\mathbf{l} = 2\sigma_e/(\Delta f)$ no matter what values are assigned to **a** and **b**. Thus a stable crystal with this step height, i.e., one with $\Delta\phi_c$ negative, cannot be formed). If the edge free energy ϵ is included in the calculation, this lower limit becomes $\mathbf{l} = (2\sigma_e + \epsilon/\mathbf{b}_0)/(\Delta f)$, where $\mathbf{b}_0$ is the thickness of the monomolecular growth layer.

[2] The expression $\Delta f = [(\Delta h_f)(\Delta T)/T_m][T_x/T_m]$, which takes account of the fact that the entropy difference between the supercooled liquid and crystalline phase falls below $(\Delta h_f)/T_m$ when $T_x < T_m$ is somewhat more accurate than eq (2). (See Ref. [9]). However, we need not complicate the analysis at this point by using the more accurate expression for (Δf) if it is understood that the results may require modification if T_x/T_m falls much below about 0.9.

The explanation of why the **l** dimension of the growth nucleus will not increase markedly as the folded crystal grows to large size in the **a** and **b** dimensions is based on the fact that the maximum steady-state growth rate in the **a** and **b** dimensions refers to a certain value of **l**. The value of **l** that leads to the maximum growth rate is [1,7]

$$\mathbf{l}_g^* = \frac{(2\sigma_e + \epsilon/\mathbf{b}_o)}{(\Delta f)} + \frac{kT}{\mathbf{b}_o\sigma}. \qquad (4a)$$

The quantity $kT/\mathbf{b}_o\sigma$ will generally run from 10 to 30A. If **l** for a given crystal becomes temporarily larger than $\mathbf{l}_g^*$, the activation barrier becomes high, thus reducing the rate of crystal growth in the **a** and **b** directions. For a relatively large value of ϵ, eq (4) will be

$$\mathbf{l}_g^* = \frac{4\sigma_e}{(\Delta f)} = \mathbf{l}_p^*, \qquad (4b)$$

where $\mathbf{l}_p^*$ is the step height of a primary (homogeneous) nucleus. Crystals with values of **l** in excess of those given by eqs (4a) and (4b) will occasionally occur, but these will not grow as rapidly in the **a** and **b** directions as those with a step height $\mathbf{l}_g^*$. Once a chain folded crystal is formed, it will not tend to grow rapidly in the **l** direction because of the folds.[3] Through fluctuations, a step height that is too large will gradually tend toward $\mathbf{l}_g^*$ as growth in the **a** and **b** directions takes place [8]. The tendency of the step height of a folded crystal to maintain itself close to that of the growth nucleus is also predicted by the theoretical studies of Frank and Tosi [10] and Price [11].

At a supercooling of 20° C, eqs (4) predict values of $\mathbf{l}_g^*$ in the neighborhood of roughly 50 to 500 A [7]. There is no restriction to such a small value implicit in the model for growth in the **a** and **b** directions. Thus, there is a theoretical justification for the assumptions $\mathbf{a} >> \mathbf{l}$ and $\mathbf{b} >> \mathbf{l}$ used in the derivation of eq (3) for a polymer crystal formed on the chain folded pattern.

The considerations outlined above provide a reasonable theoretical justification for the assumption that the mean value of the step height **l** of a folded crystal will maintain itself at a value close to that of a primary or growth nucleus, while the other two dimensions become much larger. The various factors that can lead to a preponderance of crystals with chain folds over bundle-like crystals during crystallization from the supercooled bulk phase are discussed in some detail in reference [7].

From an experimental standpoint, there is ample reason to consider polymer crystals with chain folds for material crystallized from dilute solution. Keller [12] has clearly demonstrated that the platelets formed under these conditions are chain folded when removed from the solution and dried, and that the step height increases with decreasing supercooling as required by eqs (4a) and (4b). The question of whether chain folded crystals exist in polymer crystallized from the supercooled bulk phase has proved to be more difficult to answer. Recently however, Geil has demonstrated that chain folds must exist in polypropylene crystallized from the melt [13]. This work provides strong experimental confirmation of the view that the lamellae in spherulites consist of chain folded crystals (cf. ref. [7]). Any chain folded structures formed in bulk will doubtless possess some chains protruding from the plane of the chain folds, and chains of a similar character forming interlamellar links.

We return now to the question of the application of eq (3) to melting point data. The melting point T_m' (obs) is defined operationally as the temperature where the last detectible trace of crystallization disappears. For crystals at the melting point defined in this way, the value of **l** that is relevant in eq (3) is not the average value of **l**, but rather a somewhat larger value that represents the thicker and therefore the higher melting crystals in the system. In this situation, it is convenient to assume that

$$\mathbf{l} = \beta\mathbf{l}_p^* = \beta\left\{\frac{4\sigma_e T_m}{(\Delta h_f)(T_m - T_x)}\right\}, \qquad (5)$$

where $\mathbf{l}_p^*$ is given by (4b) and β is a constant. This states simply that the mean step height of the crystals that melt out last, i.e., those corresponding to T_m'(obs), is β times as large as the mean step height of a primary nucleus, or the mean step height of a growing crystal with fairly large ϵ.

Some discussion of the expected values of β and the implications of this approximation is necessary.

The theory of chain folded nucleation and growth suggests a rather narrow number distribution of step heights **n**(**l**) of the general type shown in figure 2 by the dashed line. The particular distribution illustrated was calculated on the assumption that the grown lamellae have the same step height distribution as that of the primary (homogeneous) nuclei

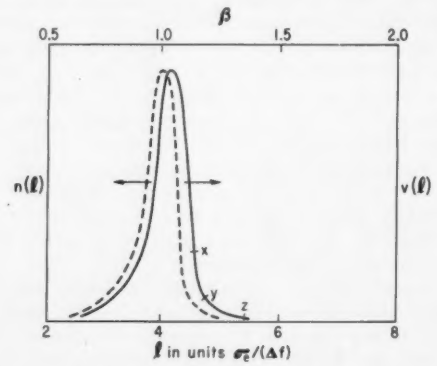

FIGURE 2. *Distribution of lamellar thickness for crystals with chain folds (schematic).*

– – – – denotes number distribution **n**(**l**).
——— denotes volume distribution **v**(**l**).
x, y, and z indicate increasing β with increasing detector sensitivity.

[3] In some cases, diffusion mechanisms involving chain mobility in the crystal may allow a gradual increase of **l** in a grown crystal with the passage of time. This effect is discussed later in the paper.

[1, 7]. This corresponds to the case where the growth nucleus has a large ϵ. The assumption that the step height distribution of the grown lamellae is the same as that of the primary nuclei is crude. However, a detailed calculation [8] of the distribution of step heights formed in the growth process within a given lamella, and the deviation of the average height of each lamella compared with the rest, gives a distribution which for the present purpose has similar properties. Hence our general conclusions concerning β will not rest on the assumption of homogeneous initiation.

It is seen in figure 2 that there is a rather sharp maximum in $\mathbf{n}(\mathbf{l})$ at $\mathbf{l}_g^*=4\sigma_e/(\Delta f)$. However, some crystals are thinner than $\mathbf{l}_g^*$, and a significant number are thicker. It is the melting of these thicker crystals that will be observed near the melting point as it has been defined. However, for the purpose of analysing melting points obtained from specific volume-temperature ($\overline{V}-T$) curves, we must really ask what the volume of such crystals is, rather than the number. We may in general expect the thicker crystals to have a larger volume, thus shifting the righthand side of the volume distribution function $\mathbf{v}(\mathbf{l})$ slightly to the right in the plot shown in figure 2 (see solid curve). Thus, for the case where the mean step height of the growing crystal is $\mathbf{l}_g^*=4\sigma_e/(\Delta f)$, we must expect β to be somewhat in excess of unity. Further, the sensitivity of the detector will have an influence on the observed value of β. This is shown in figure 2 at points x, y, and z, which correspond to slightly different β values. Thus, in the case of large ϵ, we may expect β to be near or slightly greater than unity. In the case where ϵ is negligible, β may be expected to be somewhat below unity.

Insertion of (5) into (3) gives

$$T_m'(\text{obs})=T_m(1-1/2\beta)+\frac{T_x}{2\beta}. \qquad (6)$$

This equation describes a family of straight lines on a plot of T_m'(obs) *versus* T_x. *The equilibrium melting temperature is the intersection of one of these lines with the line* $T_m'(\text{obs})=T_x$. A schematic plot of T_m'(obs) against T_x for some β values is shown in figure 3.

The expression $T_m'(\text{obs})=(T_m+T_x)/2$ given earlier [1] corresponds to the case $\beta=1$.

The depression of the observed melting point below the equilibrium melting temperature predicted by eq (6) for even the higher range of β is quite large. Equation (6) was derived on the basis that no secondary processes enter and cause $\mathbf{l}$ to increase as the polymer is stored, or while it is being warmed during the melting run. Such processes can be imagined, and their effect is discussed below.

Melting out of Thin Crystals followed by Recrystallization

According to eq (3) a given chain folded lamella, or portion of a lamella, will melt out as the polymer is heated. The thinner lamellae, or sections thereof, will melt out first. The (possibly somewhat oriented) supercooled liquid produced by a melting crystal at $\mathbf{T}_m'(\mathbf{l})$ during the warming process will tend to recrystallize at $\mathbf{T}_m'(\mathbf{l})$, forming a crystal with the larger value of $\mathbf{l}$ characteristic of this higher crystallization temperature. This new and thicker lamella will have a higher $\mathbf{T}_m'(\mathbf{l})$ value than the one originally melted out. The recrystallization will tend to be slower the higher the temperature because it involves a nucleation mechanism.[4] As a consequence, for a specified warming rate, the T_m'(obs) values obtained for high T_x values are apt to be more nearly correct than those obtained for low T_x values. Thus a β value obtained under conditions where recrystallization occurs during the warming process will tend to be too large. Also, the value of T_m obtained by extrapolation of melting data involving recrystallization is apt to be somewhat low. These two features are illustrated schematically in figure 3 in conjunction with the case $\beta=1$ (see dotted line).

The effect of recrystallization after melting out can be lessened by increasing the rate of warming during the melting run.

Possibility of Isothermal Increase of $\mathbf{l}$ *Resulting from Chain Mobility in a Folded Crystal*

In the derivation of eq (6), it was assumed that the step height $\mathbf{l}$ remained at a certain value, originally determined by the crystallization temperature, until it was melted out. This assumption implies that the polymer chains comprising the folded crystal have insufficient mobility to permit the rather complex rearrangements that would be required to permit the step height of a folded crystal to increase while still in the crystalline state. This assumption is probably correct in at least some

[4] Detailed investigations of the recrystallization process carried out by Kovacs and coworkers verify this statement (private communication from Dr. A. J. Kovacs, Strasbourg).

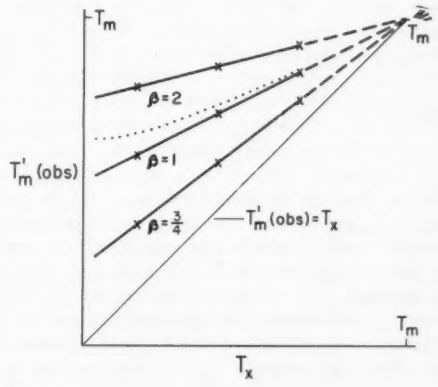

FIGURE 3. *Theoretical* $T_m'(obs)$ *versus* T_x *plot.*

x—x—x denotes T_m'(obs) *versus* T_x for various β values in experimentally accessible range (no secondary effects assumed). ..... illustrates type of effect caused by recrystallization or chain mobility effects for $\beta=1$ line.

cases, but in others the mobility of the chains might permit an isothermal increase of the step height on prolonged storage. The driving force for the increase of the step height will always exist below $\mathbf{T}_m'(\mathbf{l})$ for a lamellar crystal as it is formed in the kinetic crystal growth process. (It should be recalled that a folded crystal possesses a small and temperature-dependent mean step height $\mathbf{l}_g^*$ because a crystal of this step height has the maximum rate of growth in the **a** and **b** directions, and *not* because a crystal with this step height is the most stable at the crystallization temperature from a thermodynamic viewpoint [1,7]). In view of the fact that a thin chain folded lamellar crystal could increase its stability (and hence, its melting point) by becoming thicker, through complex chain rearrangements fostered by chain mobility in a crystal, it seems useful to indicate how this would affect the present analysis. Reneker has suggested some interesting mechanisms involving defects such as point dislocations that could lead to a slow increase of **l** for folded crystals [14].

If gradual thickening due to mobility of segments in a folded crystal occurred, the melting points corresponding to various T_x values would all be raised somewhat, the effect on $\mathbf{T}_m'(\mathbf{l})$ being least at the higher crystallization temperatures because of the greater thickness of the lamellae. In this sense, the effect of mobility would resemble the effect of recrystallization (increased β, low extrapolated T_m value). There is, however, one important difference between the two effects: thickening of a lamella due to chain mobility in the crystal (if it occurs at all) could take place anywhere in the interval T_x to $\mathbf{T}_m'(\mathbf{l})$, whereas thickening of a lamella due to melting out followed by recrystallization could occur only after a lamella had been heated to $\mathbf{T}_m'(\mathbf{l})$. Thus, if the observed melting point (at a given warming rate) depends markedly on the residence time at T_x, isothermal thickening of the lamellae due to chain mobility should be suspected. If the observed melting points are insensitive to the residence time at T_x, but are dependent on the melting rate, then the existence of simple melting out followed by recrystallization is indicated. (This does not preclude some increase of step height due to chain mobility effects at low T_x values at residence times shorter than those that are experimentally practicable.)

From this standpoint, the most reliable melting point data for the determination of T_m and β for a polymer where either or both effects occur to a measurable extent would be obtained on specimens where the initial crystallinity was low (short residence time at T_x), where fairly rapid melting rates were used, and where the greatest reliance is placed on T_m'(obs) data obtained for high T_x values.

The effect of orientation of the polymer liquid will be to increase the T_m'(obs) values. Such an effect may occur in samples where orientation is initially present due to severe stress applied to the melt phase, but this can generally be circumvented. Also, the crystallization process itself may locally orient the supercooled liquid phase of the polymer somewhat. Where a fast melting run is found to be necessary to minimize recrystallization and lamellar thickening resulting from chain mobility, some residual effect of orientation may appear, but this should be minimized by making measurements on specimens of low initial crystallinity.

In its simplest interpretation, the process we have termed "melting out" refers to the conversion of a crystal of a specified step height at a certain temperature given by equation (3) to a thermodynamic state of identical free energy and a molecular state similar to that of the normal supercooled liquid at the same temperature. While the chain molecules in the normal supercooled liquid may well be somewhat alined locally, this interpretation certainly implies a considerable disorientation of the chains during the "melting out" process. (This does not necessarily imply, however, that any ensuing recrystallization process will lead to a crystal with a different crystallographic orientation than the one originally melted out. For example, the presence of undestroyed nuclei in the form of unmelted lamellae, or portions of a lamella, could easily lead to the same orientation for the newly-formed crystal.) A more complex process than this might actually occur when at a certain temperature the free energy of a lamella, or portion thereof, becomes equal to that of the normal supercooled liquid. For example, a very thin (and nearly unstable) crystal might, when heated slightly find the route to a larger step height more rapid through the chain mobility mechanism than through the melting out with disorientation→recrystallization mechanism. In this case, the distinction we have drawn between the melting out→recrystallization, and the increase of step height through chain mobility, mechanisms would become rather artificial. Nevertheless, for a crystallization conducted fairly close to T_m, where the step height is large, one must expect the disappearance of the crystals on warming to correspond to the formation of liquid-like polymer in a state of disorientation at least fairly similar in nature to the normal supercooled liquid.

Despite the possibilities for an increase of step height after the formation of a folded crystal, it is commonly to be expected that a system of chain folded crystals will exhibit a marked dependence of melting point on the original crystallization temperature. In the limiting case where secondary effects resulting from recrystallization and chain mobility are minimized by appropriate experimental techniques, values of β ranging from somewhat below to somewhat above unity should be found, and a reliable value of T_m determined by the extrapolation method. When these secondary effects enter, β will be larger than normal, and the extrapolated T_m value will be somewhat low.

Shape of the Melting Curves

The theory indicates that the sharpness of the melting process near T_m will increase as the crystallization temperature is increased. This is a natural

consequence of the fact that T_m'(obs) approaches T_m less rapidly than does T_x. This is illustrated schematically in figure 4 for the case $\beta=1$ on the assumption that no recrystallization or chain mobility effects occur during the melting run. The actual shape of the melting curve was drawn in such a manner as to conform to the type of distribution function for $\mathbf{v}(\mathbf{l})$ shown schematically in figure 2. The small wing on the right-hand side of the $v(\mathbf{l})$ distribution may in some cases manifest itself as a small "tail" on the melting curve near the liquidus line as shown in the inset in figure 4.

It can be shown to a first approximation that the breadth of the melting process, say as measured by the function $dT/d\overline{V}$ somewhat below T_m'(obs), will vary approximately as ΔT. Recrystallization and chain mobility effects will in general tend to sharpen the melting curves.

The foregoing discussion indicates from a theoretical standpoint that one way to achieve a very sharp melting point for a polymer of very high molecular weight, i.e., one that reproduces the typical sharp first-order phase transition characteristic of the melting of pure non-chain molecular crystals,[5] would be to crystallize the polymer at very low supercooling. However, the rapidly decreasing rate of crystallization as T_m is approached (which culminates in a rate that is zero at T_m), together with the tendency of the step height to maintain itself, must be expected to defeat the actual attainment of either the equilibrium melting temperature or the very sharp equilibrium melting curve. The melting of each individual crystal of step height $\mathbf{l}$ at $\mathbf{T}_m'(\mathbf{l})$ is properly regarded as a sharp first-order phase transition. The melting curve of a real polymer with a distribution of $\mathbf{l}$ is represented here as the sum of a vast number of such events, and may be designated as a "diffuse" or "unsharp" first-order transition (cf. remarks of Mandelkern on the melting of linear homopolymers [15]).

2.2. Bundlelike Crystals

The model is illustrated schematically in figure 1b. The length is denoted l, and the other two dimensions a and b. The end surface free energy is called σ_e, and the lateral surface free energy is called σ. (Note that bold face symbols are used for chain folded crystals, and ordinary face type for bundlelike crystals).

The free energy of formation of a bundlelike crystal may be set down in a manner analogous to eq (1). Using steps similar to those noted in section 2.1, one obtains

$$T_m'(l)=T_m\left\{1-\frac{2\sigma_e}{(\Delta h_f)l}\right\} \tag{7}$$

as the melting point of a bundlelike crystal that has large a and b dimensions and a small l dimension. The same result is obtained if the crystal is assumed to be a cylinder of revolution about the l direction.

[5] An observable depression of the observed melting point below T_{fusion} is of course to be expected for ordinary molecular crystals if they are small enough. Because the growth of most such crystals is inherently three-dimensional, they become large, and the depression due to surface effects of the type that is so apparent in polymers is to be measured in tenths to thousandths of a degree, rather than in degrees.

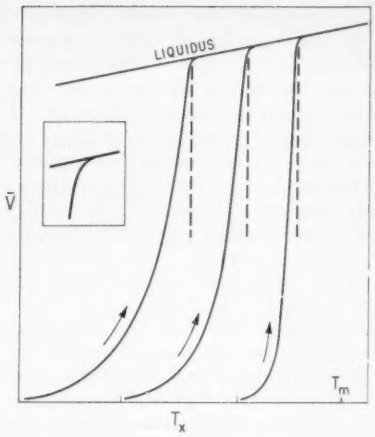

FIGURE 4. *Theoretical melting curves (schematic).*

The curves are based on the type of distribution shown in figure 2. Increasing T_x sharpens melting process. Inset shows "tail" that may appear near liquidus line.

The length of a homogeneous nucleus for such a crystal is

$$l_p^*=\frac{4\sigma_e}{(\Delta f)}. \tag{8}$$

The length of a coherent lateral growth nucleus is $l_g^*=2\sigma_e/(\Delta f)$. These results are in general similar to those obtained for the corresponding folded crystal. Both l_p^* and l_g^* vary with temperature as $1/\Delta T$.

One could proceed from eqs (7) and (8) to derive an expression for a bundlelike crystal formally equivalent to eq (6) *only* in the case where it is reasonable to define β by the relation $l=\beta l_p^*$. Recalling that we are interested in explaining cases where T_m'(obs) is clearly well below T_m when T_x is in the practicable crystallization range, it follows that l must retain a value reasonably close to that of either the primary or growth nucleus length, i.e., β must be reasonably close to unity. (Values of β between 1 and 2 are found in the present study.) To the best of our knowledge, the assumption that the l dimension of a bundlelike crystal will retain a value fairly close to l_p^* or l_g^* as the crystal grows to large size in the a and b directions has never been justified on theoretical grounds. If the assumption $l=\beta l_p^*$ cannot be justified for the bundlelike mode of growth, then it would follow that the melting behavior of a polymer that conformed to an expression of the form of eq (6), with β in the stipulated range, would most appropriately be interpreted in terms of the chain fold model, where such a β value can readily be justified.

We have considered several conceptions of how the growth of a bundlelike crystal might be much slower in the l direction than in the a and b directions. The result is that it appears to be difficult to defend the assumption $l=\beta l_p^*$ with β anywhere near unity for a bundlelike crystal. The following describes the approaches used:

(1) A calculation of the growth rate in the l direction, and in the a and b directions, was made using classical nucleation theory. The effect of entanglements was ignored, and it was assumed that no cumulative strain existed at the bundle ends. This model implies a more rapid growth rate in the l direction [7], since the end surface free energy of a polymer crystal is generally agreed to be much larger than the lateral surface free energy. This model evidently does not correspond to the crystal habit exhibited by most real polymers, which generally grow most rapidly in the two directions tranverse to the chain axes, rather than in the chain axis direction.

(2) The assumption that the cumulative strain that may occur in the diffuse end surface of a bundlelike crystal might abort growth in the l direction was examined [7]. In the bundlelike system, polymer chain molecules actually pass through the end surfaces, and connect the crystalline and supercooled liquid phases together. Since there is a density difference between the two phases, cumulative strain may exist in the end of the bundle. This model raises a serious question concerning whether a *large* bundlelike crystal can be formed at all, and definitely rules out of existence a strictly bundlelike crystal with a flat end surface where the chains are perpendicular to this surface. The concept of cumulative strain does not imply that the restriction on growth in the l direction would be such as to allow l to be even approximately proportional to l_x^* or l_y^*. Crystals aborted by cumulative strain would in general tend to melt quite close to the crystallization temperature. Rather than giving a clue as to the melting behavior of bundlelike crystals, this model suggests one important reason why crystals with chain folds form instead. Crystals with chain folds effectively evade strain resulting from the density difference of the supercooled liquid and crystal phases, since relatively few chains pass through the end (folded) surfaces.

(3) The concept that chain entanglements cause a bundlelike crystal to cease growth in the l direction once it has reached the nucleus length was examined. This special assumption does not appear to be readily justifiable. The same type of entanglements that one must assume are continually resolved as the critical-sized nucleus is being built up would have to suddenly become exceedingly effective just as the length l_x^* was attained. Recalling that l_x^* is strongly dependent on temperature, such a mechanism for the persistence of the one dimension of a bundlelike crystal near l_x^* seems improbable.

On the basis of the above, it is regarded as unlikely that the interpretation of the melting behavior of a polymer conforming with eq (6) with β values in the general vicinity of unity is to be based on a bundlelike model. To derive the analogue of eq (6) for the bundlelike model, the arbitrary assumption $l=\beta l_y^*$ with $\beta \sim 1$ has to be introduced, and this apparently has no clear justification.

As noted previously, the typical lamellar structures so often seen in polymers crystallized from the unoriented melt are most readily explained in terms of growth of a substantially chain folded character [7, 13]. Thus, in cases where it is known that the melting process refers to the disappearance of typical lamellar spherulitic structures on warming, the chain fold model discussed in 2.1 is clearly more appropriate than the analogous treatment with the bundlelike model.

3. Experimental

3.1. Materials

The specimens of PCTFE, $-(CF_2CFCl)_n-$, that were used in this work were laboratory samples of Kel-F grade 300 polymer that were kindly supplied to us by the Minnesota Mining and Manufacturing Company. The number average molecular weight was stated to be about 415,000. The polymer was supplied in the form of molded sheets about 2 mm thick. When crystallized as described below the polymer is highly spherulitic.

3.2. Melting Runs With High χ_{Initial} and Moderately Slow Melting

The objective of this part of the study was to determine, with moderately slow warming, the melting point of PCTFE specimens that had been isothermally crystallized to a high degree of crystallinity, χ.

A sample weighing from 1 to 3 g was first heated in an air bath far above any possible value of T_m to a temperature denoted T_1 in order to establish a reproducible thermal history. (T_1 was usually 305 °C.) Then it was quickly suspended in a silicone oil bath which was operating at the crystallization temperature, T_x, and an isothermal crystallization carried out to the desired degree of crystallinity. The temperature of the sample in the bath was known to better than 0.1 °C.

Melting data were obtained on such specimens by warming them in the silicone oil bath, and plotting the specific volume—temperature ($\overline{v}$-T) curves. The specific volume data were precise to within 0.0002 cm^3g^{-1}. This was sufficient to detect a melting point T_m''(obs) corresponding to the disappearance of all but the last four tenths of a percent of crystallinity. Details concerning the apparatus used have been given elsewhere [16]. The T_m''(obs) values cited are accurate to within about 0.2 °C.

In carrying out the melting run, the sample was first warmed rapidly from T_x to about 205 °C in an attempt to minimize recrystallization. The melting point T_m''(obs) was then determined with moderately slow warming above 205 °C. Counting from the time 205 °C was reached, most of the melting runs were carried out within 4 to 6 hours, but a few were carried out over a period of many days in order to check the effect of the rate of heating. In all these runs, most of the time above 205 °C was spent in carefully approaching the melting point. The degree of crystallinity at the beginning of each warming run, χ_{Initial}, was calculated from the specific volume using the crystallinity scale established by Hoffman and Weeks [16].

T_x values from about 170 to 200 °C were practicable with the above procedure. It is difficult to carry out an isothermal crystallization much below 170 °C on a sample of convenient size because of self-heating attending the rapid crystallization. Above about 200 °C, the rate of crystallization becomes intolerably slow.

In a few cases, the melting points were determined by mounting the crystallized specimens on a hot stage on a polarizing microscope, and observing the temperature at which birefringence disappeared.

For most of the runs, the samples were cooled to room temperature after crystallizing at T_x, and then rewarmed and the melting curve obtained. It was demonstrated that this did not alter T'_m(obs), as it relates to T_x, by carrying out similar runs without first cooling to room temperature. The hierarchy of small crystals introduced below T_x on cooling to room temperature simply melt out first when the sample is rewarmed.

The initiation of the crystals in the samples is principally by heterogeneous nucleation. The bulk crystallization isotherms follow the Avrami relation, $\chi=1-\exp[-Zt^n]$, where t is time, with $n=2$ to $n=3$, for the first 30 to 50 percent of the crystallization. The crystallization becomes much less rapid as the temperature is increased. Thus the rate constant Z has the strongly negative temperature coefficient characteristic of a nucleation controlled growth mechanism. The $n=3$ exponent results from three-dimensional growth, mainly spherulites in the body of the specimen born at or near $t=0$. In thin samples with a large amount of surface, an $n=1$ component due to surface nucleation causes the overall bulk isotherm to tend toward $n=2$. Above $\chi=0.4$ to 0.5, the crystallization rather abruptly slows down with the consequence that long periods of time are required to attain high χ values.

3.3. Melting Runs With High χ_{Initial} and Fast Melting

After conducting the investigation described above and analysing the data, it became apparent that recrystallization and other secondary effects had almost certainly increased some of the melting points somewhat.

In order to reduce recrystallization and other secondary effects during the melting process as much as possible, and thereby obtain T'_m(obs) values that reflected the T_x values more precisely, a rapid melting procedure was adopted.

Specimens were heated to T_1 and then crystallized at T_x as described in section 3.2. Then they were placed (without first cooling to room temperature) in a silicone oil bath operating quite close to the anticipated melting point, i.e., 1 or 2 °C below the T'_m(obs) value obtained with a moderate warming rate. It was then determined, usually by the volume-temperature ($\overline{V}$–T) technique, whether or not the sample had melted out when it came to the temperature of the bath. By successive experiments with baths at closely spaced temperatures, T'_m(obs) could be rather closely bracketted. This procedure is equivalent to a melting run of about 20 minutes duration, most of this interval being spent very close to T'_m(obs).

3.4. Melting Runs With Low χ_{Initial} and Fast Melting

These runs were carried out primarily with the aim of determining the effect of storage time on the melting points for a given rate of melting.

The runs were carried out in the same manner as those described in section 3.3, except that the specimens were not allowed to crystallize as long prior to being melted out.

As noted in section 3.2, the runs with high χ_{Initial} values ($\chi=0.40$ to 0.65) and moderate melting rates were carried out on specimens about 2 mm thick and weighing about 3 g. In these experiments, and in the high χ_{Initial} runs with rapid melting, the $\overline{V}-T$ method detects the disappearance of all but the last 0.4 percent of crystals. However, in this low χ_{Initial} runs ($\chi=0.05$ to 0.11) the sensitivity was less, partly because somewhat smaller samples were used, but mostly because of the lower crystallinity. The sensitivity in these runs was such that the observed melting point corresponded to 3 percent crystallinity in the specimen. After some investigation of the slopes of the $\overline{V}-T$ curves in the melting range, it was found that adding 0.6 °C to each observed melting point gave a T'_m(obs) value that corresponded to the disappearance of all but the last 0.4 percent of the crystals. This correction is actually somewhat smaller the higher T_x, but adding the constant value 0.6 °C gives results accurate to about ±0.2 °C in the experimental range, which is sufficient for the intended purpose.

3.5. Melting Point by the Slow Stepwise Warming Method

A specimen of PCTFE was initially crystallized at 180 °C. (The melting run was carried out with the specimen suspended in silicone oil so that the specific volume could be measured.) It was then warmed to a higher temperature and allowed to stand until the specific volume appeared to settle down to a "rest" value. Then the temperature was raised again, and the process repeated. The total duration of the melting part of the run was 35 days. The average rate of warming was 5 °C per day up to 205 °C, 1 °C per day up to 210 °C, and 0.5 °C per day up to the melting point.

3.6. The Melting Point of Specimens Crystallized at High Temperatures Using Seeds

The objective of this part of the work was to obtain the highest actual melting temperature for a specimen of PCTFE using the general concept that a high isothermal crystallization temperature will lead to a high melting point.

As indicated in section 3.2 the rate of crystallization becomes so slow around T_x=200 °C in the normal runs that it is not convenient to carry out isothermal crystallizations at higher temperatures. Therefore seeds from a previous crystallization were used to accelerate the crystallization process.

The seed crystal run was carried out in the following manner. First, the specimen was heated to 305 °C and then crystallized isothermally at 180 °C to a degree of crystallinity of over 0.5. Then it was warmed to a T_1 value of 215.6 °C. This melted out the vast majority of the crystals present, and gave a specific volume that was indistinguishable from the liquidus. However, numerous seed crystals were present. (The presence of seed crystals was indicated by the fact that the subsequent crystallization at a specified value of T_x was considerably more rapid than the crystallization would have been at the same T_x in a normal run.) The sample was then transferred from the T_1 bath to another bath operating at T_x, and the crystallization carried to a fairly high χ value. Then the melting point was determined from a $\overline{V}-T$ curve with a moderate warming rate as described in section 3.2.

4. Results

Three typical melting curves for PCTFE of the type that were used to obtain the T'_m(obs) versus T_x data are shown in figure 5. The particular ones shown refer to the high $\chi_{initial}$ runs with moderate melting rate. The melting point relevant to each T_x value is seen to be clearly defined within narrow limits, and the definite character of the increase of T'_m(obs) with increasing T_x is also clearly evident. The other types of runs yield melting curves (not shown) that also lead to clearly discernible melting points.

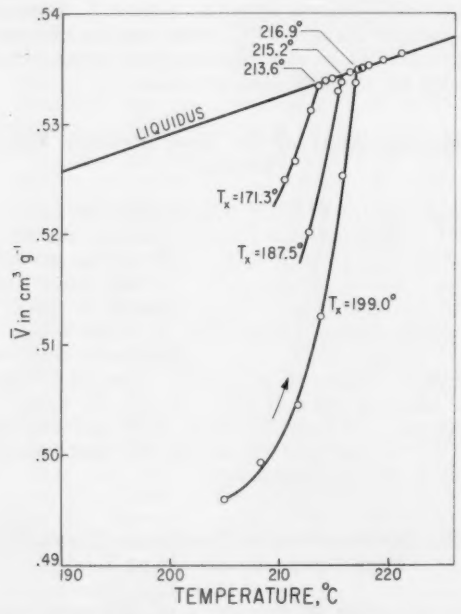

FIGURE 5. *Melting curves of PCTFE obtained for runs with high $\chi_{initial}$ and moderate melting rate.*

Note increase of T'_m(obs) and increase of sharpness of melting process with rising T_x.

The T'_m(obs) versus T_x data for each of the three types of runs mentioned in sections 3.2, 3.3, and 3.4 are given in table 1, together with certain other information. The data are plotted in figure 6.

TABLE 1. *T'_m(obs) versus T_x data for PCTFE* [a]

Initial melt temperature, T_1	Isothermal crystallization temperature, T_x	χ at T_x after crystallization, $\chi_{initial}$	Approximate time required to attain $\chi_{initial}$	Observed melting point, T'_m(obs)	Remarks
		A. Runs with high $\chi_{initial}$ and moderate melting rate [b]			
°C	°C			°C	
305	169.6–170.2	~0.40	~5 min	213.8	T_x measured with thermocouple in sample.
305	171.3	.49	20 min	213.6	T_x certain to about 0.5 °C.
305	172.5–173.0	~.40	5½ min	213.9	T_x measured with thermocouple in sample.
305	179.8	.49	20 min	213.8	
305	180.2	.52	1 hr	214.1	
305	187.5	.49	85 min (est)	215.2	
305	190.1	.63	10 d	215.2	
305	190.2	.49	93 min	215.4	
305	195.8	.55	16 hr	216.4	
305	196.0	.65	2 d	216.0	
325	199.0	.65	34 d	216.9 217.2	Melting point from $\overline{V}-T$ data. Melting point determined optically.
305	199.6	.53	4 d	216.9	
		B. Runs with high $\chi_{initial}$ and fast melting [b]			
305	172.5–173.0	~0.40	5½ min	211.2	Melting point obtained visually.
305	180.1	.48	20 min	212.8	
305	185.0	.50	45 min	213.4	
305	190.1	.48	96 min	214.6	
305	196.7	.54	15 hr	216.5	
305	199.5	.50	3 d	217.3	
		C. Runs with low $\chi_{initial}$ and fast melting [c]			
305	185.9	0.07 (est.)	8 min	212.9	
305	189.8	.05 (est.)	17 min	213.6	
305	192.9	.09	51 min	215.0	
305	193.5	.09	101 min	215.0	
305	196.1	.11	5.2 hr	215.8	
305	199.3	.09	15.6 hr	216.8	
305	201.5	.09	66 h	217.3	

[a] Unless noted otherwise, the T'_m(obs) data were obtained from $\overline{V}-T$ curves.

[b] In these tables the directly observed T'_m(obs) data are given, and refer to the disappearance of all but the last 0.4 percent of crystals.

[c] The T'_m(obs) data given in this table have all been increased by 0.6 °C above the value actually observed in order to correspond to the disappearance of all but the last 0.4 percent of crystals. The values actually observed referred to the disappearance of all but the final 3 percent of crystallinity.

Table 2 gives the results of the runs mentioned in sections 3.5 and 3.6 where, with previous seeding, crystallization at the highest practicable temperature was used to attain high melting points for PCTFE. Also shown in the same table is the result for the slow stepwise warming run on PCTFE.

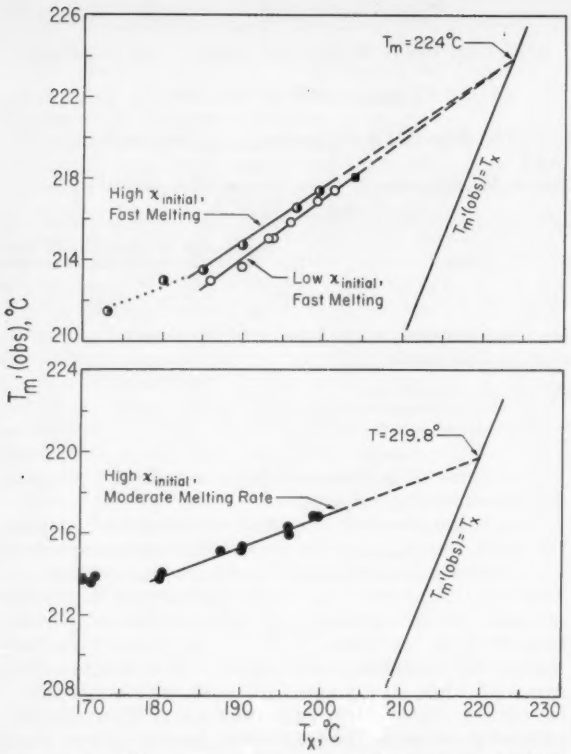

FIGURE 6. *$T_m'(obs)$ versus T_x plots obtained for PCTFE.* ——— shows best straight line that fits data in experimentally accessible region, — — — — shows extrapolation to line $T_m'(obs) = T_x$.

The upper diagram shows data where recrystallization effects are minimized except where noted by dotted line. The lower diagram shows data that are strongly affected by recrystallization, except at the highest T_x values.

Point ■ is seed crystal run from table 2.

TABLE 2. *Additional melting point data on PCTFE*

A. Melting point obtained using seed crystals to attain fast crystallization at high T_x

Seeding temperature [a]	Isothermal crystallization temperature, T_x	χ at T_x after crystallization, $\chi_{initial}$	Time at T_x required to attain $\chi_{initial}$	Observed melting point, T_m'(obs)	Remarks
°C	°C			°C	
215.6	203.9	0.36	7 d	218.0	Melting point from $\overline{V}$—T data, moderate melting rate.
				218.2	Optical melting point, moderate melting rate.

B. Melting point by slow stepwise warming method

Original crystallization temperature	Melting point ($\overline{V}$—T method)	Time required for run	Remarks
°C	°C		
180	216.4	35 d	Slight discoloration observed toward end of run; specimen sorbed small amount of silicone oil.

[a] Thermal history prior to seeding: Sample heated to 305 °C, crystallized to high χ at 180 °C, and then warmed to seeding temperature. The sample was then lowered to T_x and crystallized for the time indicated.

5. Analysis and Interpretation of Melting Data of PCTFE

5.1. Preliminary Observations on T_m'(obs) Versus T_x Data

The optically determined melting point, and that obtained on a portion of the same specimen from $\overline{V}$–T curves, are very nearly the same. This is evident from certain entries cited in table 1. This result was also confirmed in a number of other studies not specifically reported. This provides a useful check of the data. However, the optical melting points have not been used in the analysis of β, or in estimating T_m by the extrapolation method.

It is evident from table 1 that heating to the T_1 values in the range indicated for a given type of run erased the previous thermal history of the specimen so far as the dependence of T_m'(obs) on T_x is concerned.

Although the main point of this paper is not that of differentiating between the effects on the melting point of melting out followed by recrystallization on warming on the one hand, and any isothermal increase of crystal size on storage at T_x due to chain mobility effects on the other, it will prove useful to comment briefly on this prior to undertaking the main analysis. Orientation effects are also discussed.

It is readily seen from table 1 and figure 6 that in the rapid melting runs there is a small effect of residence time at T_x: the high $\chi_{initial}$ run is from 0.5 to 0.8 °C above the data for low $\chi_{initial}$. This implies that a small increase of the smallest crystal dimension due to chain mobility may have occurred isothermally at T_x in the high $\chi_{initial}$ run, where the residence time was substantially longer. Some of the increase of T_m'(obs) in the rapid melting run with high $\chi_{initial}$ may be a result of residual liquid phase orientation arising from the crystallization process itself, but this is not considered likely (see below).

The T_m'(obs) data for runs with high $\chi_{initial}$ and moderate warming rates are well above any of the rapid melting run data for T_x values in the range 170 to ~185 °C. (Compare upper and lower diagrams in fig. 6.) Some of this excess in the melting point values for the moderate melting rate runs could be due to an increase of crystal size of the same general character that takes place on isothermal storage, but the greater part of it is probably a result of melting out followed by recrystallization during the warming part of the runs. Mandelkern and coworkers have clearly demonstrated in certain polymers (see for example [5]) that an incremental increase in temperature from T_i to T_j leads first to a distinct increase of volume at T_j followed by a slow decrease. This was interpreted as melting out of small crystals followed by recrystallization to form larger crystals. The initial increase of volume at T_j noted by these workers is in our opinion much too large to be ascribed solely to chain mobility effects: an increase of step height due to chain mobility leads, in the first approximation, only to a change of the shape of a crystal, and not its total

volume. Similar volume changes were noted in PCTFE in specimens warmed rapidly from room temperature to a fixed temperature fairly near the melting point, showing that melting out of small crystals followed by recrystallization can in fact occur in this polymer.

Near and above T_x=198 °C, all three types of run give very similar melting points, showing a general lack of sensitivity to heating rate and residence time. Even the seed crystal run in table 2 is consistent in this respect. Our general conclusion from the above is that, for T_x values above 198 °C, the T_m'(obs) data as obtained are essentially free of significant recrystallization and chain mobility effects.

Between a T_x of 185 and 198 °C, each rapid melting run is evidently a simple linear continuation of the T_m'(obs) versus T_x points above 198 °C, where the data are evidently mostly free of secondary effects as noted above. Accordingly, we conclude that the melting points obtained with fast melting from T_x=185 °C up to the highest T_x values employed are most representative of the original crystallization mechanism.

When considered as a whole, the present evidence for PCTFE indicates that melting out followed by recrystallization is a substantially more important cause of an increase of step height (and hence T_m'(obs)) after the lamella is originally formed than the chain mobility effect. In accord with the expectations cited in section 2.1, all the secondary effects are minimized at high temperatures for a wide range of storage times and warming rates. The fact that recrystallization is minimized at lower temperatures by rapid melting is also in accord with expectation.

Finally, we must concern ourselves with the possibility that abnormal liquid orientation effects have artificially raised the T_m'(obs) values. First we indicate that the specimens exhibited no marked birefringence after melting out at T_m'(obs). It was concluded from this that there was never any serious degree of orientation in the specimens on a macroscopic scale. Any liquid orientation would have to be on a local scale, presumably induced by the crystallization process. From the standpoint of T_m'(obs) versus T_x data, one would expect orientation of this type to manifest itself in the following way: under equivalent conditions of initial crystallinity and crystallization temperature, a fast melting run should give a higher T_m'(obs) than a slow run because of the greater opportunity for randomization of orientation in the slow run. Just the reverse occurs in PCTFE.

5.2. Determination of β

The T_m'(obs) versus T_x plots used to determine β are shown in figure 6.

A least-squares fit of the data in the straight line region yields the following equations where the temperature is in °C:

$$T_m'(\text{obs})=187.17°+0.1486\ T_x \qquad (9)$$

(180.2 to 199.6 °C for high χ_{initial}, moderate melting rate)

$$T_m'(\text{obs})=163.22°+0.2709 T_x \qquad (10)$$

(185.0 to 199.5 °C for high χ_{initial}, fast melting)

$$T_m'(\text{obs})=157.89°+0.2952 T_x \qquad (11)$$

(185.9 to 201.5 °C low χ_{initial}, fast melting).

TABLE 3. *Estimates of T_m by extrapolation method and values of β for PCTFE*

Run	β	Temperature at intersection of extrapolated T_m'(obs) *versus* T_x line and line $T_m'(\text{obs})=T_x$
		°C
Low χ_{initial}, fast melting	1.69	224.0
High χ_{initial}, fast melting	1.85	223.9
High χ_{initial}, moderate melting rate	(3.36)	(219.8)

The value of β obtained from eqs (9–11) using eq (6) are shown in table 3.

The value β=1.69 obtained with the fast melting run with low χ_{initial} is in reasonable agreement with the theoretical expectations mentioned in section 2.1. This result means that even the largest detectible crystals in the system are only about 70 percent thicker than the mean value of a primary nucleus (or a growth nucleus with large ϵ). The rapid melting run with high χ_{initial} gives β=1.85, which is still not far from theoretical expectation. The slightly greater β value in this case may be a result of chain mobility effects due to the longer residence time at T_x. (The run with high χ_{initial} and moderate melting rate is known to be strongly affected by recrystallization at low T_x, and is included principally to show how abnormally large β values will be found when such data are analysed.)

We regard the remarkable tendency of the step height of even the largest observable crystals in the system to maintain values close to the nucleus dimension during the crystallization process in PCTFE as being most readily understood in terms of the crystals with chain folds. As discussed in section 2.1, a β value running from somewhat below to somewhat above unity can be given a reasonable direct theoretical justification for a system of chain folded crystals, but no such justification seems to have been given for the bundle-like model.

Further evidence that the chain fold model is appropriate to the case of melting phenomena in PCTFE is as follows. PCTFE crystallized in bulk is known to be spherulitic [2, 17], and definite evidence is available showing that the spherultic texture in this polymer is distinctly lamellar [18, 19]. Our microscopic observations have shown that melting points obtained from $\overline{V}$–T curves may be closely identified with the disappearance of the last vestige of the lamellar spherulitic crystallinity. Since the basic features of lamellar spherulites are most reasonably interpreted in terms of structures possessing chain folds [7, 13], it follows that the melting behavior described for PCTFE is most appropriately interpreted in terms of chain folded crystals.

5.3. Estimate of T_m by Extrapolation Method

The general situation with regard to the extrapolation of the T_m'(obs) versus T_x data to the line $T_m'(\text{obs}) = T_x$ is shown in figure 6.

Table 1 brings out the enormous increase of crystallization time that is incurred by raising T_x. This places an upper limit on the T_m'(obs) value that can be achieved in a run of reasonable duration. An examination of figure 6 shows that to obtain an observed melting point of 220 °C, the crystallization would have to be carried out close to 210 °C. Our studies of the kinetics of crystallization of PCTFE [2] indicate that without seeding it would take at least one year to achieve a crystallinity of 10 percent at this temperature. (The rate constant Z mentioned in section 3.2 varies approximately as $\exp[-\Delta H^*/RT] \exp[-K_1/T^2(\Delta T)]$, and the latter term, which has a strongly negative temperature coefficient, is dominant anywhere near T_m. Hence there is a very rapid increase in the time required to achieve a given degree of crystallinity as the crystallization temperature is raised.) Seeding might be used to shorten the time, but long crystallization times would still be needed.

The data obtained with a long residence time at T_x (high χ_{initial}) and moderate melting rates lead to an intersection at $T=219.8$ °C (table 3). This may be safely regarded as a lower limit for T_m, since recrystallization is known to have raised T_m' (obs) at the lower T_x values, and thus artificially lowered the point of intersection.

As noted previously, the most reliable value of T_m should be found with data obtained by rapid melting of specimens with low χ_{initial}, since recrystallization and chain mobility effects are then minimized. Also, in fast melting runs, the effects of residual orientation should be minimized by employing low initial crystallinites. The run with low χ_{initial} and rapid melting gives $T_m=224.0$ °C. The rapid melting run with high χ_{initial} gives the practically identical result $T_m=223.9$ °C. One gathers from this that any orientation, chain mobility, and recyrstallization effects that occurred in the high χ_{initial} run as compared with the low χ_{initial} rapid melting run were either compensatory or small.

Accordingly, the "best" value of the equilibrium melting temperature of PCTFE as obtained by the extrapolation method is quoted as

$$T_m = 224 \pm 1 \text{ °C.} \qquad (12)$$

The standard deviation of each of the fast melting runs is only 0.5 °C at T_m. The larger error of ±1 °C is used to allow for other factors, for example undetected curvature in the T_m'(obs) versus T_x lines used in the extrapolation.

Note that the estimated value of T_m is about 6 °C above the highest melting point actually obtained on any PCTFE specimen (see $T=218.2$ °C run in table 2). It will be seen subsequently that this state of affairs is not unique to PCTFE.

The present study provides a simple explanation for the low melting points in the range 212 to 215 °C that have been reported in the past for PCTFE. When PCTFE samples of ordinary size, say 2 to 5 mm thick, are heated well above the melting point, and then allowed to cool in air, most of the crystallization tends to take place between 165 and 175 °C. This happens because the crystallization is rapid in this region, and because the heat evolved is sufficient to maintain a specimen of the size mentioned in this range for a time. (The heating and cooling procedure described corresponds to the molding → cooling procedure often used in practice). A glance at table 1 shows that a sample crystallized in this range will melt between about 212 and 215 °C, depending on the melting rate.

5.4. Shape of Melting Curves

Some evidence was obtained suggesting that the breadth of the melting process diminishes as the crystallization temperature increases, i.e., as ΔT decreases, as shown schematically in figure 4. An example of this behavior is seen in figure 5: The quantity $dT/d\overline{V}$ near the liquidus is clearly larger for the $T_x=171.3°$ curve than it is for the $T_x=199.0$ °C curve. To a rough approximation, $dT/d\overline{V}$ for these runs appears to vary as ΔT. However, there was considerable scatter in the $dT/d\overline{V}$ data for these high χ_{initial} runs with moderate melting rates. It seems probable that much of this scatter was due to the secondary effects that occurred during the melting process. No $dT/d\overline{V}$ data of the required accuracy were obtained with fast warming rates.

A number of the melting curves for high χ_{initial} with moderate melting revealed a small "tail" of the type depicted in the inset in figure 4. This tail corresponds to the melting out of something less than the last one or two percent of the crystals and usually occurred over a range of less than one degree.

6. Discussion

6.1. Comparison of Extrapolated T_m Value With That Estimated by the Slow Stepwise Warming Method

It has been recommended that the equilibrium melting temperature of a polymer be measured by slow stepwise warming [5, 6]. The polymer may be initially crystallized under any of a number of conditions. The stepwise warming is to be carried out so that the specific volume settles down to its "rest" value after each incremental increase of temperature. The method evidently relies in large part on melting out followed by recrystallization and other secondary effects to achieve large and high melting crystals. This method of estimating T_m is discussed below in the light of the present work.

In the case of PCTFE, it appears that the "T_m" value of 216.4 °C obtained by the slow stepwise warming method is somewhat below the true equilibrium melting temperature. This statement holds even if one questions the T_m value of 224 °C obtained by the extrapolation method, since specimens melting at 218.0 to 218.2 °C can be made rather

easily by crystallizing the polymer at high temperatures (table 2). Thus, the melting point obtained by the slow stepwise warming method is at least 1.6 °C low. If the extrapolation method is valid, as the present study suggests, then the melting point obtained by the stepwise warming method is about 7.5 °C below T_m.

The slow stepwise warming run carried out on PCTFE may not be a completely fair test of the method. Some silicone oil was taken up by the specimen, and some discoloration possibly indicative of slight degradation was observed. On this basis, the melting point of 216.4 °C might be thought to be lower than that which would be found in a more ideal stepwise warming run of the same duration. Note, however, that the isothermal run of 34 days duration mentioned in table 1(A) does not lead to a melting point that is out of line with those found in much shorter runs. (The specimens in the shorter runs did not become discolored or take up any significant amount of silicone oil.)

In order to check further on the relative value of the stepwise warming method and the extrapolation method, we initiated a study on linear polyethylene (Marlex 50). Here the T_m value found from a T_m'(obs) versus T_x plot was compared with (a) the value $T_m = 137.5 \pm 0.5$ °C found by Quinn and Mandelkern for Marlex 50 by the stepwise warming method [6], and (b) the convergence temperature of the orthorhombic form of the *n*-paraffins as determined by the careful analysis of Broadhurst [20], which includes new data on n-$C_{94}H_{190}$. A detailed report of both the T_m'(obs) versus T_x studies (still in progress) and the convergence temperature work will be given elsewhere, but the following brief summary is relevant here.

The observed melting point for polyethylene increases markedly with increasing T_x, corresponding to $\beta \cong 1$ in eq (6). At this writing, the extrapolated value of T_m is 143 ± 2 °C. (A somewhat more precise value may be expected when the work is completed.) This compares favorably with the convergence temperature of 141.1 ± 2.4 °C found by Broadhurst. The latter may be taken as an independent estimate of T_m, since the crystal structure of polyethylene is orthorhombic. As in PCTFE, secondary effects attributable to recrystallization and chain mobility in the crystal were found. A specimen crystallized at $T_x = 130.0$ °C for two weeks (high χ_{Initial}, moderate warming rate) gives T_m''(obs) = 137.7 °C, which is practically identical to the result obtained by Quinn and Mandelkern using the slow stepwise warming technique.

The T_m'(obs) versus T_x plot containing the point T_m'(obs) = 137.7 ° C has a definite positive slope similar to that found in PCTFE, and gives a strong impression that crystallization at a higher temperature would give a significantly higher melting point. This would, of course, take a long time to verify because of the rapidly diminishing crystallization rate, but the implication remains clear.

From the above, it seems improbable that T_m is below 140 °C for linear polyethylene, suggesting that the slow stepwise warming method, as applied in this case, gave a melting point that was at least 2.5 °C below T_m. Our present best estimate is that T_m for polyethylene is about 3.5 to 5.5° C above the melting point given by the slow stepwise warming method, i.e., T_m is between 141 and 143 °C.

It is considered that the value $\beta \cong 1$ found for polyethylene implies that crystallization with chain folds occurs in this polymer.

Some further discussion of the slow stepwise warming method is of interest.

The stepwise warming technique has a tendency to yield the same melting point for polymer crystallized in a variety of ways and at different temperatures prior to the start of the slow stepwise warming run. This result is readily understandable in terms of the concepts outlined in this paper.

Assume for the sake of discussion that two specimens are at hand, and that the one consists mostly of small crystals formed at high supercooling, and the other of medium-sized crystals formed at moderate supercooling. By the time that both specimens have been warmed to a temperature sufficient to melt out the medium-sized crystals, the small ones will also have melted out. Then the recrystallization and other secondary effects occurring in both specimens on sufficiently slow warming will tend to occur under conditions of equivalent supercooling. Thus, the larger crystals formed at these higher temperatures must be expected to eventually develop a quite similar size distribution in each case. Then at some temperature near (but still below) T_m, the negative temperature coefficient of the recrystallization and other secondary mechanisms will in the allotted time effectively prevent the formation of still larger crystals, and the melting point consistent with the patience of the investigator will have been reached. Because of the similarity in crystal size, both specimens will melt close to the same temperature, but this temperature will be somewhat below T_m. Interestingly, the sameness of the observed melting point with slow stepwise warming for a polymer initially crystallized in various ways has been cited as evidence that the melting temperature so found was in fact the equilibrium melting temperature. Such evidence could actually mean merely that the largest crystals in the preparation were of roughly the same size, and is not adequate as a proof of the attainment of T_m.

In view of the foregoing, it is considered improbable that the slow stepwise warming technique, as it has been applied in practice, actually gives the equilibrium melting temperature. The slow stepwise warming technique has the advantage of simplicity, and obviously minimizes orientation effects, but the presently available evidence is that melting points obtained in this way are apt to be several degrees below T_m.

The present work presents an alternative to the slow stepwise warming technique if the objective is to obtain the highest melting point for a real specimen in a given period of time. The bulk of the allotted time is spent in an isothermal crystallization at the highest temperature where a reasonable

amount of crystallization will develop. Then the specimen is warmed and the melting point determined. The latter step would most wisely be carried out on several specimens for a series of moderate and fairly slow warming rates. Seeding may be used to achieve an increased rate of crystallization at high T_x values if feasible. This general procedure forms large crystals in the specimen in the beginning, and does not rely largely on secondary mechanisms to achieve the same end. The present evidence suggests that this method is at least as efficient in producing a high melting point in a specimen in a given period of time as the slow stepwise warming technique. It should be understood that T_m cannot actually be attained by either method in a real specimen because of the extreme slowness of both crystallization and recrystallization near T_m, and the tendency of the step height of a chain folded crystal to maintain itself (see section 6.3).

The extrapolation method of estimating T_m proposed in this paper is not without its pitfalls. In order to avoid recrystallization and other secondary effects, it is desirable to use fairly rapid melting rates. However, the use of such melting rates may fail to allow residual orientation effects in the liquid to disipate, and thus increase the observed melting points somewhat. In the case of PCTFE this effect is evidently small enough so that it is not unambiguously identifiable. It is believed that residual orientation would in any case be subdued by dealing with samples of low crystallinity. The evidence is that the extrapolation method, as applied using low χ_{Initial} and fairly rapid melting, is accurate in the case of polyethylene, and it is likewise believed correct within the stated limits of error for PCTFE. Nevertheless, investigations with other polymers should not for the time being be confined merely to runs with low χ_{Initial} and rapid melting, since unusually large secondary or orientation effects may appear in some instances. The proposed extrapolation method has the distinct advantage of being associated with a simple theory whose main points (such as a linear increase of T_m'(obs) with increasing T_x) can be verified in the region where the kinetics of crystallization allow data to be obtained. The method also provides additional information of interest, for instance that concerning β.

6.2. Crystal Size Versus Volume Imperfections as Principal Cause of T_m'(obs) Falling Below T_m

The treatment in this paper deals with the lowering of the melting point of a polymer that is caused by a restriction of one crystal dimension, **l**, to a small size. This restriction is incurred in the original isothermal crystallization. Thus, crystal size rather than volume imperfections have been taken as the main source of the fact that T_m'(obs) falls well below T_m. We must now raise the question concerning whether this point of view is reasonable in PCTFE.

Geil has found from electron micrographs that the lamellae in an air-cooled specimen of PCTFE are approximately 250 A thick [19]. As noted earlier, a specimen that is air-cooled tends to crystallize at around 175 °C, corresponding to $\Delta T \cong 50$ °C. This work may be taken as proving the existence of very thin crystals in PCTFE of the general type that must be expected to have a melting point many degrees below T_m.

A simple calculation using eq (3) may be used to lend credence to this statement. For PCTFE, we have $T_m = 497.2$ °K, $\Delta h_f = 9.1 \times 10^8$ erg cm^{-3} [21]; further, $\mathbf{l} \cong 250$ A $= 2.5 \times 10^{-6}$ cm for polymer that is air cooled. The quantity σ_e in eq (3) must be estimated. Recent theoretical studies suggest that the lower range of σ_e for chain folded crystals will be 25–50 erg cm^{-2} [7]. (A value in this range is also consistent with the surface free energy parameters obtained from studies of the radial growth rate of PCTFE spherulites [2].) Using $\sigma_e = 40$ erg cm^{-2} in eq (3), it is found that the melting point of the crystal of average thickness will be about 17.5 °C below T_m. Considering the fact that the observed melting point refers to the largest crystals in the system, we would estimate with $\beta = 1.7$ that the depression should be about 10 °C, corresponding to T_m'(obs) = 214 °C. This is close to what is observed for air-cooled specimens (section 5.3).

The foregoing calculation is tendered as a partial justification for analysing the present experiments in terms of crystal size effects, rather than ascribing the observed depressions incurred by low crystallization temperatures mainly to volume imperfections. The latter may exist in excess concentration, and play some role in lowering the observed melting point, but it is very doubtful that this role is the major one. No crystal is "perfect" at its melting point, and a polymer crystal at this temperature must be expected to have an equilibrium concentration of volume defects, e.g., a certain number of small chain ends incorporated in the lattice. However, such equilibrium defects are not to be considered as lowering the melting point. From our point of view, the important "imperfections" that influence the melting behavior of high molecular weight linear polymers with no stereochemical irregularities are the high energy chain folded surfaces and the thinness of the crystals.

6.3. The Concept of the Equilibrium Melting Temperature

The present work does not in any way deny the existence of an equilibrium melting temperature for a highly crystallizable linear polymer. It does however bring out the reasons why this temperature will be impossible (or at least exceedingly difficult) to attain in a real polymer specimen. These reasons are:

(1) One dimension of a polymer crystal, **l**, is small and varies with the crystallization temperature as $1/(\Delta T)$ because of the nature of the nucleation-controlled growth mechanism in chain folded systems.

(2) The smallness of this one dimension is sufficient to significantly reduce the melting point.

(3) Attempts to produce crystals with a large **l** dimension by crystallizing at high temperatures,

i.e., small (ΔT), are rendered difficult and eventually impracticable by the rapidly increasing crystallization times involved as ΔT is diminished. This effect is again due to the nucleation controlled character of the growth process.

(4) Efforts to increase the **l** dimensions of the chain folded crystals by recrystallization and other secondary mechanisms (using either prolonged storage or slow warming) are increasingly inefficient as the melting point is approached. Near the melting point, nucleation effects strongly inhibit recrystallization, and the large lamellar thickness together with the existence of the folds prevent internal diffusion (chain mobility) from further increasing the step height.

In short, our studies strongly suggest that T_m could be closely approached (say within 1 or 2 °C) in a real specimen only in an experiment of extraordinary duration. In this situation, we have turned to estimating T_m using a method that essentially extrapolates to the temperature appropriate to infinite **l**. Despite its lack of attainability in a real specimen in an experiment of reasonable duration, T_m is clearly to be regarded as a real property of thermodynamic significance.

The present work suggests that the true equilibrium melting curve for a linear polymer of very high molecular weight with no stereochemical irregularities would strongly resemble the very sharp first-order transition commonly associated with ordinary pure molecular crystals. The equilibrium melting curve refers to the melting of an assembly of crystals, each having very large **a**, **b**, and **l** dimensions. The melting of each such crystal would refer to the equilibrium G (infinite crystal)$=G$ (liquid) at T_m, where G is the Gibbs free energy. As noted earlier, it is unlikely that such a state will be readily attained in a real polymer system. However, the increasing sharpness of the melting process in PCTFE and polyethylene that is observed as higher and higher initial crystallization temperatures are employed points to the validity of the above concept. The melting point of a small polymer crystal refers to the metastable equilibrium G (small crystal)$=G$ (slightly supercooled liquid) at $T_m'(\mathbf{l})$, or T_m'(obs) if the larger crystals in an assembly are considered. As long as the time scale is specified, so that no change of crystal size takes place during the melting experiment, and provided that the slightly supercooled liquid is in its normal state, T_m'(obs) is also a quantity of thermodynamic significance. There is no fundamental objection to applying thermodynamics to metastable equilibria.

7. References

[1] J. I. Lauritzen, Jr., and J. D. Hoffman, J. Research NBS **64A** 73 (1960).
[2] J. D. Hoffman and J. J. Weeks, manuscript in preparation.
[3] L. A. Wood and N. Bekkedahl, J. Appl. Phys. **17** 362 (1946).
[4] L. A. Wood and N. Bekkedahl, J. Research NBS **36** 489 (1946).
[5] D. E. Roberts and L. Mandelkern, J. Am. Chem. Soc. **77** 781 (1955).
[6] F. A. Quinn, Jr. and L. Mandelkern, J. Am. Chem. Soc. **80** 3178 (1958).
[7] J. D. Hoffman and J. I. Lauritzen, Jr., J. Research NBS **65A** 297 (1961).
[8] J. I. Lauritzen, Jr., manuscript in preparation.
[9] J. D. Hoffman, J. Chem. Phys. **29** 1192 (1958)
[10] F. C. Frank and M. P. Tosi, Proc. Roy. Soc. (London), **A263,** 323 (1961).
[11] F. P. Price, J. Chem. Phys. **35,** 1884 (1961).
[12] A. Keller, Phil. Mag. **2** 1171 (1957); A. Keller and A. O'Connor, Discussions, Faraday Soc. **25** 114 (1958).
[13] P. H. Geil, J. Appl. Phys. (in press).
[14] D. H. Reneker, J. Polymer Sci. (in press).
[15] L. Mandelkern, Chem. Revs. **56** 903 (1956).
[16] J. D. Hoffman and J. J. Weeks, J. Research NBS **60** 465 (1958).
[17] F. P. Price, J. Am. Chem. Soc. **74** 311 (1952).
[18] E. W. Fischer, Z. Naturforschung, **12A** 753 (1957).
[19] Private communication, P. H. Geil, Wilmington.
[20] M. Broadhurst, National Bureau of Standards, manuscript in preparation.
[21] A. M. Bueche, J. Am. Chem. Soc. **74** 65 (1952).

(Paper 66A1–137)

JOURNAL OF RESEARCH of the National Bureau of Standards—A. Physics and Chemistry
Vol. 66A, No. 1, January–February 1962

Tritium-Labeled Compounds VIII. Confirmation of the Position of the Tritium in D-Glucose-*6-t* and D-Glucitol-*5-t*[1]

Lorna T. Sniegoski and Horace S. Isbell

(August 29, 1961)

The radiochemical purity of D-glucose-*6-t* and D-glucitol-*5-t* was established by oxidation of the labeled compounds and determination of the radioactivity of the products. The results show that, in each instance, the tritium is present solely in the position cited.

1. Introduction and Discussion

Carbohydrates position-labeled with tritium have proved useful for studying reaction mechanisms and for investigating complex biological problems. In order to interpret the results of studies conducted with tritium-labeled carbohydrates, it is essential that the position of the tritium label be accurately known, and that the carbohydrate be labeled exclusively in the position cited.

As has previously been demonstrated, D-glucose-*1-t*, prepared by reduction of D-glucono-1,5-lactone either with sodium amalgam in tritiated water or with lithium borohydride-*t* in pyridine solution, is labeled exclusively at C–1 [1].[2] In the present study, it has been shown that the D-glucose-*6-t* and D-glucitol-*5-t* distributed under the NBS labeled-sugar project [2] are labeled exclusively at C–6 and C–5, respectively.

The compounds in question were synthesized by reduction of suitable substances with lithium borohydride-*t* [3]. D-Glucose-*6-t* was obtained by hydrolysis of 1,2-*O*-isopropylidene-D-glucose-*6-t* prepared by reduction of 1,2-*O*-isopropylidene-D-glucurono-6,3-lactone [4]. D-Glucitol-*5-t* was prepared by reduction of L-sorbose, and was separated by crystallization as the D-glucitol–pyridine complex [5].

It seemed possible that, in the reduction of the carbonyl group with lithium borohydride-*t*, enolization might occur between the carbonyl group and the adjacent group, leading to unsaturation and subsequent introduction of tritium at a position other than the desired one. This study was undertaken to determine whether each of the materials was labeled only in the position cited.

In order to prove the position of tritium, the labeled sugar was so oxidized as to remove all of the hydrogen or tritium at one position or more in the carbon chain, and the molar activity of the derivative was compared with that of the original compound.

Thus, in the analysis of D-glucose-*6-t*, a sample of the sugar was oxidized with dilute nitric acid to potassium hydrogen D-glucarate [6, 7]. This compound contains no hydrogen or tritium attached to C–1 or C–6. Radioassay of the purified potassium hydrogen D-glucarate showed that it contained no tritium. Consequently, all of the tritium in D-glucose-*6-t* is at C–1 or C–6.

Next, a sample of the D-glucose-*6-t* was oxidized with iodine by the Kline-Acree method [8] to potassium D-gluconate-*6-t*, which contains no hydrogen or tritium attached to C–1. The potassium D-gluconate-*6-t* was purified by recrystallization to constant activity, and was found to have the same molar activity as the D-glucose-*6-t*. Since all of the tritium in D-glucose-*6-t* must be at C–1 or C–6, and there is no tritium at C–1, all of the tritium in D-glucose-*6-t* must be at C–6.

In the determination of the position of the label in D-glucitol-*5-t*, a bacterial oxidation with *Acetobacter suboxydans* was conducted. *A. suboxydans* attacks only those compounds containing the

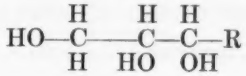

group in the D-configuration, oxidizing the penultimate group to a carbonyl group [9]. In the oxidation of D-glucitol, the hydrogen (or tritium) atom at C–5, the site of oxidation, is removed, to yield L-sorbose [10, 11]. When D-glucitol-*5-t* was oxidized, the resulting L-sorbose contained no radioactivity; hence there could have been no tritium at positions other than C–5 in the D-glucitol-*5-t*.

Radioactivity assays were made with a 2π, windowless, gas-flow, proportional counter. Materials of very low activity were counted in films of sodium *O*-(carboxymethyl)cellulose (CMC) on 2-in. planchets [12, 13]. Materials of higher activity were counted in solutions of formamide [14]. Table 1 gives a summary of the results.

TABLE 1. *Analysis of* D-*glucose*-6-t *and* D-*glucitol*-5-t

Compound analyzed	Positions of non-labile hydrogen or tritium [a]	Radioactivity	Percent of original radioactivity
		mc/mmole	
D-Glucose-*6-t*	1,2,3,4,5,6*	1.10	100
↓ Potassium hydrogen D-glucarate.	2,3,4,5	0.0	0
Potassium D-gluconate-*6-t*	2,3,4,5,6*	1.10	100
D-Glucitol-*5-t*	1,2,3,4,5*,6	0.075	100
↓ L-Sorbose	1,3,4,5,6	.0	0

[a] The asterisk indicates the tritium-bearing carbon atom.

[1] Part of a project on the production of radioactive carbohydrates sponsored by the Division of Research of the Atomic Energy Commission.

[2] Figures in brackets indicate the literature references at the end of this paper.

2. Experimental Procedures

2.1. Preparation of Derivatives of D-Glucose-*6-t*

a. Potassium Hydrogen D-Glucarate

A 5.669-mg sample of D-glucose-*6-t* (0.031 mmole, 1.10 mc/mmole) was combined with 101.9 mg (0.56 mmole) of nonradioactive D-glucose in a 50-ml porcelain casserole. Thirty milliliters of 1-*M* nitric acid was added, and the solution was concentrated to dryness on a steam bath. The residue was dissolved in distilled water, and the solution was transferred to a 100-ml standard-tapered flask, neutralized with 5-percent potassium carbonate solution to the phenolphthalein end-point, reacidified with glacial acetic acid, and concentrated under reduced pressure to a sirup. After the sirup had been transferred to a test tube with glacial acetic acid, potassium hydrogen D-glucarate crystallized. After about two hours, the mother liquor was removed from the potassium salt with a capillary pipet, and the solid was washed once with water. It was then recrystallized by dissolving it in the minimal amount of hot water, adding decolorizing carbon, and filtering through infusorial earth and decolorizing carbon. The yield after one recrystallization was 43 mg (29 percent). After three recrystallizations, the potassium hydrogen D-glucarate was radioassayed by counting in films of CMC. Both the sample and the background planchets (5 each) were counted to a total of 20,000 counts: they gave the same average number of counts per second.

b. Potassium D-Gluconate-*6-t*

A 36.7-mg sample of D-glucose-*6-t* (0.204 mmole, 1.10 mc/mmole) was placed in a 50-ml flask and dissolved in 1 ml of water. An excess of iodine, 4.79 ml of 0.0511-*M* solution (0.245 mmole), was added, followed by 6.16 ml of 0.0993-*M* sodium hydroxide (0.612 mmole), added dropwise while the contents of the flask were mixed. The solution was allowed to stand for about 10 min and was then passed through a column containing 5 ml of cation-exchange resin (Amberlite IR-120). To the effluent was added 0.5 mmole of freshly prepared silver carbonate, and the mixture was stirred until all iodide had been converted to silver iodide. The solid was removed by filtration, and the filtrate, which gave a negative test for iodide ion, was passed through 7 ml of cation-exchange resin. The effluent was concentrated under reduced pressure and then neutralized to the phenolphthalein end-point with dilute potassium hydroxide. The solution of potassium D-gluconate-*6-t* was filtered into a standard-tapered test tube, concentrated, and brought to crystallization by dropwise addition of methanol. After 1 day, 37 mg (77 percent) of potassium D-gluconate-*6-t* had separated. Radioassays of the compound in formamide solution after two and three recrystallizations gave activities of 1.10 and 1.09 mc/mmole, respectively.

2.2. Preparation of Derivative of D-Glucitol-*5-t*

a. L-Sorbose

A 181-mg sample of D-glucitol-*5-t* (1.0 mmole, 0.075 mc/mmole) was oxidized to L-sorbose with *A. suboxydans*, according to the procedure previously described for the oxidation of D-mannitol to D-fructose [15]. The broth and inoculum were prepared as before, but with D-glucitol (instead of D-mannitol) as the substrate. The agar slants used for maintenance of the culture were prepared from 10-ml aliquots of an aqueous suspension containing, by weight, 1.5 percent of agar, 1 percent of yeast extract, 0.3 percent of D-glucose, and 1 percent of calcium carbonate.

The L-sorbose, produced in a yield of 89 percent, was purified by several recrystallizations from methanol–2-propanol, and was assayed in films of CMC; it contained no radioactivity.

3. References

[1] H. S. Isbell, H. L. Frush, N. B. Holt, and J. D. Moyer, J. Research NBS **64A** (Phys. and Chem.) No. 2, 177 (Mar.–Apr. 1960).
[2] NBS Tech. News Bull. **43,** 130 (1959).
[3] H. S. Isbell and J. D. Moyer, J. Research NBS **63A** (Phys. and Chem.) No. 2, 177 (Sept.–Oct. 1959).
[4] H. S. Isbell, H. L. Frush, and J. D. Moyer, J. Research NBS **64A** (Phys. and Chem.) No. 4, 359 (July–Aug. 1960).
[5] H. L. Frush, H. S. Isbell, and A. J. Fatiadi, J. Research NBS **64A** (Phys. and Chem.) No. 5, 433 (Sept.–Oct. 1960).
[6] C. A. Browne and F. W. Zerban, Physical and chemical methods of sugar analysis, p. 726–7 (John Wiley & Sons, Inc., New York, N.Y., 1941).
[7] F. Schneider, Qualitative organic microanalysis, p. 143 (John Wiley & Sons, Inc., New York, N.Y., 1946).
[8] F. J. Bates and associates, Polarimetry, saccharimetry, and the sugars, NBS Circ. **440,** p. 210 (1942).
[9] R. M. Hann, E. B. Tilden, and C. S. Hudson, J. Am. Chem. Soc. **60.** 1201 (1938).
[10] P. A. Wells, J. J. Stubbs, L. B. Lockwood, and E. T. Roe, Ind. Eng. Chem. **29,** 1385 (1937).
[11] H. L. Frush and H. S. Isbell, J. Research NBS **59,** 289 (1957) (RP2800).
[12] H. S. Isbell, H. L. Frush, and R. A. Peterson, J. Research NBS **63A** (Phys. and Chem.) No. 2, 171 (Sept.–Oct. 1959).
[13] H. S. Isbell, H. L. Frush, and N. B. Holt, J. Research NBS **64A** (Phys. and Chem.) No. 4, 363 (July–Aug. 1960).
[14] A. Schwebel, H. S. Isbell, and J. D. Moyer, J. Research NBS **53,** 221 (1954) RP2537.
[15] L. T. Sniegoski, H. L. Frush, and H. S. Isbell, J. Research NBS **65A** (Phys. and Chem.) No. 5, 441 (Sept.–Oct. 1961).

(Paper 66A1–138)

JOURNAL OF RESEARCH of the National Bureau of Standards—A. Physics and Chemistry
Vol. 66A, No. 1, January–February 1962

Infrared Absorption Spectra in the Study of Mutarotational Equilibria of Monosaccharides

R. Stuart Tipson and Horace S. Isbell

(October 2, 1961)

The infrared absorption spectra (in the range of 5000 to 250 cm^{-1}) of 6 anomeric pairs of sugars and of 12 single anomers are presented, together with the spectra (in the range of 5000 to 667 cm^{-1}) of the dry lyophilizates of the respective equilibrium solutions of these 18 sugars in water.

Analysis of the spectra indicated the presence, in a number (possibly, in all) of the equilibrium mixtures, of some of the carbonyl form (aldehydo or keto) of the respective sugar. Conclusions as to the other components of each equilibrium mixture agreed with those derived from mutarotational studies, except for D-lyxose and D-ribose. Despite the reported absence of mutarotation for D-*gluco*-heptulose and D-*manno*-heptulose, the equilibrium mixture of each was found to contain one or more forms different from that originally dissolved.

1. Purpose and Scope of the Project

This project was primarily undertaken with the objective of gaining, for a number of monosaccharides, information regarding the composition of the sugar mixture obtained by dissolving one anomer of a sugar in water and allowing the solution to reach mutarotational equilibrium. Each such solution was freed from water by lyophilization; and the infrared absorption spectrum of the product was recorded and then compared with the spectrum of the crystalline anomer originally dissolved (and with that of the other anomer, if available).

The second objective was to record these spectra for use in (a) the identification of monosaccharides and (b) eventual assignment of conformation to each crystalline anomer. For 6 sugars, the infrared spectrum, in the range of 5000 to 667 cm^{-1}, was recorded for *both* crystalline anomers and for the equilibrium mixture. For 12 other sugars, only *one* crystalline anomer was available; its infrared spectrum and that of the corresponding equilibrium mixture were recorded in the above range. The infrared spectra in the range of 667 to 250 cm^{-1} were also recorded for the crystalline anomers.

2. Sugars Investigated

Table 1 gives a list of the sugars, their code numbers [1],[1] and an index to the spectrograms; the serial number of a sugar is the same as the number of its spectrogram, and the letter E is appended to designate an equilibrium mixture. The 24 anomers were classified into 4 groups; the members of each group have like configurational features.

[1] Figures in brackets indicate the literature references at the end of this paper. The references for tables 1 and 2 are given at the ends of the tables.

2.1. Sugars of the *xylo* Configuration

The members of this group have the general formula I, if they are pyranoid.

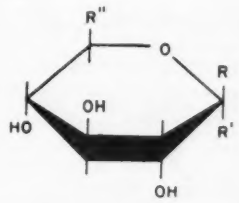

I

1. α-D-Xylose, R=H; R′=OH; and R″=H.
2. (?)-L-*xylo*-Hexulose (L-sorbose), R=OH and R′=CH_2OH, or vice versa; R″=H; and the molecule is the mirror image of that depicted.
5. α-D-Glucose, R=H; R′=OH; and R″=CH_2OH.
6. β-D-Glucose, R=OH; R′=H; and R″=CH_2OH.
7. α(?)-D-*gluco*-Heptulose, R=CH_2OH; R′=OH; and R″=CH_2OH.

2.2. Sugars of the *lyxo* Configuration

These sugars, if pyranoid, have the general formula II.

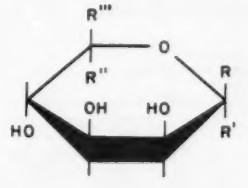

II

8. α-D-Lyxose, R=H; R′=OH; and R″ and R‴ =H.
9. β-D-Lyxose, R=OH; and R′, R″, and R‴=H.
10. (?)-D-*lyxo*-Hexulose (D-tagatose), R=CH_2OH and R′=OH, or vice versa; and R″ and R‴ =H.
11. 6-Deoxy-α-L-mannose (α-L-rhamnose) monohydrate, R=H; R′=OH; R″=H; R‴=CH_3; and the molecule is the mirror image of that depicted.
12. 6-Deoxy-β-L-mannose (β-L-rhamnose), R=OH; R′=H; R″=H; R‴=CH_3; and the molecule is the mirror image of that depicted.
13. α-D-Mannose, R=H; R′=OH; R″=H; and R‴ =CH_2OH.
14. β-D-Mannose, R=OH; R′=H; R″=H; and R‴ =CH_2OH.

TABLE 1. *Compounds measured and index to spectrograms*

Code	Sugar	References	Spectrogram
10.11?0	α-D-Xylose	1, 2	1
10.1100	D-Xylose (equilibrium)		1-E
10.71?0	(?)-L-*xylo*-Hexulose [a]	3, 4	2
10.7100	L-*xylo*-Hexulose (equilibrium)		2-E
10.21?09899	α-D-Glucose·0.5 NaCl·0.5 H_2O	5	3
10.21?099	α-D-Glucose, monohydrate	6, 7	4
10.2110 [b]	α-D-Glucose	2, 6 to 9	5
10.2100[99]	D-Glucose (equilibrium)		5, 6-E
10.21?0	β-D-Glucose	2, 7, 10	6
10.81?0	α(?)-D-*gluco*-Heptulose	11	7
10.8100	D-*gluco*-Heptulose (equilibrium)		7-E
10.12?0	α-D-Lyxose	2, 12 to 14	8
10.1200	D-Lyxose (equilibrium)		8, 9-E
10.12?0	β-D-Lyxose	2, 14	9
10.72?0	(?)-D-*lyxo*-Hexulose [c]	15	10
10.7200	D-*lyxo*-Hexulose (equilibrium)		10-E
10.22?0(6)8099	6-Deoxy-α-L-mannose, monohydrate [d]	2, 16	11
10.2200(6)8099	6-Deoxy-L-mannose (equilibrium)		11, 12-E
10.22?0(6)80	6-Deoxy-β-L-mannose	17 to 19	12
10.22?0	α-D-Mannose	2, 20	13
10.2200	D-Mannose (equilibrium)		13,14-E
10.22?0	β-D-Mannose	2, 21	14
10.82?0	(?)-D-*manno*-Heptulose	22	15
10.8200	D-*manno*-Heptulose (equilibrium)		15-E
10.26?09899	(?)-D-Gulose·0.5 $CaCl_2$·0.5 H_2O	2	16
10.26009899	D-Gulose·0.5 $CaCl_2$ (equilibrium)		16-E
10.13?0	β-D-Arabinose	23	17
10.1300	D-Arabinose (equilibrium)		17-E
10.73?09899	(?)-D-*arabino*-Hexulose [c]·0.5 $CaCl_2$·1.5 H_2O.	24	18
10.73009899	D-*arabino*-Hexulose·0.5 $CaCl_2$ (equilibrium).		18-E
10.73?0(3)11	3-*O*-Methyl-(?)-D-*arabino*-hexulose	25	19
10.7300(3)11	3-*O*-Methyl-D-*arabino*-hexulose (equilibrium).		19-E
10.82?0(3)7699	β-D-*manno*-3-Heptulose, monohydrate. [f]	26	20
10.8200(3)7699	D-*manno*-3-Heptulose (equilibrium) [f]		20-E
10.23?0(6)80	6-Deoxy-α-L-galactose [g]	27 to 30	21
10.2300(6)80	6-Deoxy-L-galactose (equilibrium)		21-E
10.23?0	α-D-Galactose	2, 31 to 34	22
10.2300	D-Galactose (equilibrium)		22,23-E
10.23?0	β-D-Galactose	2, 31 to 34	23
10.87?6899	2,7-Anhydro-β-D-*altro*-heptulose, [h] monohydrate.	35	24
10.8700+ 10.87?6899, etc. [i]	Mixture from acid treatment of compound 24 (equilibrium) [i]		24-E
10.14?0	β(?)-D-Ribose	36, 37	25
10.1400	D-Ribose (equilibrium)		25-E
10.24?0	α-D-Talose	2, 38, 39	26
10.2400	D-Talose (equilibrium)		26,27-E
10.24?0	β-D-Talose	39	27

[a] Trivial name: L-sorbose. [b] α-D-Glucopyranose has the CA conformation [T. R. R. McDonald and C. A. Beevers, Acta Cryst. **5**, 654 (1952)]. [c] Trivial name: D-tagatose. [d] Trivial name: α-L-rhamnose monohydrate. [e] Trivial name: D-fructose. [f] Kindly presented by R. Schaffer. [g] Trivial name: α-L-fucose. [h] Trivial name: sedoheptulosan. [i] See text, sec. 6.2.

15. (?)-D-*manno*-Heptulose, R=CH_2OH and R′ =OH, or vice versa; R″=H; and R‴ =CH_2OH.
16. (?)-D-Gulose·0.5 $CaCl_2$·0.5 H_2O, R=H and R′ =OH, or vice versa; R″=CH_2OH; R‴=H; and the molecule is the mirror image of that depicted.

2.3. Sugars of the *arabino* Configuration

These sugars, if pyranoid, have the general formula III.

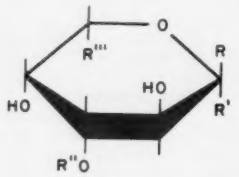

III

17. β-D-Arabinose, R=OH; R′=H; and R″ and R‴ =H.
18. (?)-D-*arabino*-Hexulose (D-fructose)·0.5 $CaCl_2$·1.5 H_2O, R=OH and R′=CH_2OH, or vice versa; and R″ and R‴=H.
19. 3-*O*-Methyl-(?)-D-*arabino*-hexulose, R=OH and R′=CH_2OH, or vice versa; R″=CH_3; and R‴=H.
20. β-D-*manno*-3-Heptulose monohydrate, R=OH; R′=$HOH_2C-\underset{OH}{\overset{H}{C}}$; and R″ and R‴=H.

References for Table 1

1. C. N. Riiber and O. Bjerkli, Kgl. Norske Videnskab. Selskabs, Skrifter No. 5 (1936).
2. H. S. Isbell and W. W. Pigman, J. Research NBS **18,** 141 (1937) RP969.
3. R. H. Smith and B. Tollens, Ber. deut. chem. Ges. **33,** 1285 (1900); H. H. Schlubach and J. Vorwerk, Ber. deut. chem. Ges. **66,** 1251 (1933).
4. W. W. Pigman and H. S. Isbell, J. Research NBS **19,** 443 (1937) RP1035.
5. O. L. Erdmann and K. G. Lehmann, J. prakt. Chem. [1] **13,** 111 (1838); Liebigs Ann. Chem. **28,** 334 (1835).
6. O. Hesse, Liebigs Ann. Chem. **277,** 302 (1893).
7. C. N. Riiber, Ber. deut. chem. Ges. **56,** 2185 (1923).
8. J. Nelson and F. Beegle, J. Am. Chem. Soc. **41,** 559 (1919).
9. R. F. Jackson, Bull. BS **13,** 633 (1916) S293.
10. C. S. Hudson and J. K. Dale, J. Am. Chem. Soc. **39,** 320 (1917).
11. W. C. Austin, J. Am. Chem. Soc. **52,** 2106 (1930).
12. E. Fischer and O. Bromberg, Ber. deut. chem. Ges. **29,** 581 (1896).
13. R. Weerman, Rec. trav. chim. **37,** 31 (1918).
14. W. N. Haworth and E. L. Hirst, J. Chem. Soc. **1928,** 1221.
15. T. Reichstein and W. Bosshard, Helv. Chim. Acta **17,** 753 (1934).
16. L. Berend, Ber. deut. chem. Ges. **11,** 1353 (1878).
17. E. Fischer, Ber. deut. chem. Ges. **29,** 324 (1896).
18. J. Minsaas, Kgl. Norske Videnskabs, Forh. **8,** 177 (1933).
19. E. L. Jackson and C. S. Hudson, J. Am. Chem. Soc. **59,** 1076 (1937).
20. P. A. Levene, J. Biol. Chem. **57,** 329 (1923); **59,** 129 (1924).
21. W. Alberda van Ekenstein, Rec. trav. chim. **15,** 221 (1896).
22. F. B. LaForge, J. Biol. Chem. **28,** 511 (1917).
23. C. S. Hudson and E. Yanovsky, J. Am. Chem. Soc. **39,** 1013 (1917).
24. H. S. Isbell and W. W. Pigman, J. Research NBS **20,** 773 (1938) RP1104.
25. C. G. Anderson, W. Charlton, W. N. Haworth, and V. S. Nicholson, J. Chem. Soc. **1929,** 1337.
26. R. Schaffer, Abstracts Papers Am. Chem. Soc. **139,** 4D (1961).
27. E. Votoček, Ber. deut. chem. Ges. **37,** 3859 (1904).
28. B. Tollens and F. Rorive, Ber. deut. chem. Ges. **42,** 2009 (1909).
29. J. Minsaas, Rec. trav. chim. **50,** 424 (1931).
30. H. S. Isbell, Circ. NBS **C440,** p. 716.
31. C. N. Riiber and J. Minsaas, Ber. deut. chem. Ges. **59,** 2266 (1926).
32. C. N. Riiber, J. Minsaas, and R. T. Lyche, J. Chem. Soc. **1929,** 2173.
33. T. M. Lowry and G. F. Smith, J. Phys. Chem. **33,** 9 (1929).
34. N. A. Sørensen, Kgl. Norske Videnskab. Selskabs, Skrifter No. 2 (1937).
35. F. B. LaForge and C. S. Hudson, J. Biol. Chem. **30,** 64 (1917).
36. H. S. Isbell, J. Research NBS **20,** 97 (1938) RP1069.
37. W. Alberda van Ekenstein and J. Blanksma, Chem. Weekblad **10,** 604 (1913).
38. P. A. Levene and R. S. Tipson, J. Biol. Chem. **93,** 631 (1931).
39. W. W. Pigman and H. S. Isbell, J. Research NBS **19,** 189 (1937) RP1021.

21. 6-Deoxy-α-L-galactose (α-L-fucose), R=OH; R′=H; R″=H; and R‴=CH_3.

22. α-D-Galactose, R=OH; R′=H; R″=H; R‴=CH_2OH; and the molecule is the mirror image of that depicted.

23. β-D-Galactose, R=H, R′=OH; R″=H; R‴=CH_2OH; and the molecule is the mirror image of that depicted.

Compound 24 (sedoheptulosan) has the following formula (IV).

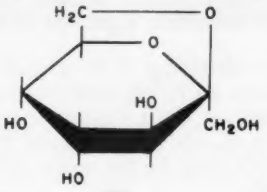

IV

24. 2,7-Anhydro-β-D-*altro*-heptulopyranose

2.4. Sugars of the *ribo* Configuration

The pyranoid forms of these sugars have the general formula V.

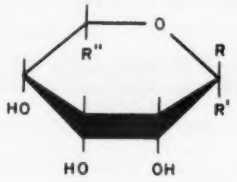

V

25. β-D-Ribose, R=OH; R′=H; and R″=H.

26. α-D-Talose, R=OH, R′=H; R″=CH_2OH; and the molecule is the mirror image of that depicted.

27. β-D-Talose, R=H, R′=OH; R″=CH_2OH; and the molecule is the mirror image of that depicted.

3. Previous Infrared Studies of These Sugars

3.1. Spectra Recorded for the Solid Phase

In 1950, Kuhn [2] recorded the spectra of 10 of the crystalline sugars, each in Nujol suspension, but, except for α-D-glucose (compound 5), he did not mention which anomer was employed. Sugars for which *only one* anomer is normally available were, presumably, sugars 1, 2, 21, 25, and the epimer of 17. The other five might have been 4 or 5, 5 or 6, 11 or 12, 13 or 14, and 22 or 23; by comparison of our spectrograms with his, we can now identify the anomers he employed as 4, 5, 11, 14, and 22. For sugars 5 and 14, the spectra were recorded for the range of 5000 to 667 cm^{-1}; for the 8 other sugars, from 1250 to 667 cm^{-1}. For sugar 14, Kuhn also recorded the spectrum of a film of the sugar, obtained by evaporation of an aqueous solution, which was probably either partially or completely equilibrated.

Four years later, the spectrum of sugar 5 ("α-glucose"; enantiomer not stated) as a mull in hexachlorobutadiene was recorded [3] for the range of approximately 3500 to 3200 cm^{-1}. In addition, Barker and coworkers [4] discussed bands in the range of 973 to 670 cm^{-1} shown by the spectra of the following 9 sugars in Nujol suspension: 1, 5, 6, 11, 14, 17, 21(?), 22, and 23. However, the spectra were published in insufficient detail to permit comparison with ours over a wide spectral range. Similarly, in 1957, Konkin and coworkers [5] published the spectra in the range of 3600 to 2700 cm^{-1} for a mull of each of the following sugars (anomer and suspension medium not specified): 1, 5 or 6, 13 or 14, enantiomer of 17, D-fructose, and 22 or 23. In the same year, Farmer [6] published the spectrum of sugar 5 ("α-glucose"; enantiomer not specified) in a potassium bromide pellet for the range of 5000 to 625 cm^{-1}. Finally, in 1959, Urbański and coworkers [7] recorded spectra and tabulated bands for 6 of these sugars in Nujol mulls for the range of 4000 to 750 cm^{-1}, but did not mention which anomer (of each) they employed. By comparison of our spectrograms with theirs, we have identified these sugar anomers as 1, 2, 5, 14, enantiomer of 17, and 25. [However, the equilibrium rotation that they recorded for D-ribose (sugar 25) is actually that for L-ribose, and their melting point for the D-glucose anomer they examined is closer to that for the β anomer (sugar 6) than for the α anomer (5).]

3.2. Spectra Recorded for the Liquid Phase

Long ago, Coblentz [8] recorded the infrared spectra of D-fructose and D-glucose monohydrate (sugar 4), presumably as supercooled melts, in the range of 10,000 to 1333 cm^{-1}. Rogers and Williams [9] listed absorption bands (3030 to 960 cm^{-1}) for equilibrated, saturated, aqueous solutions of L-xylose (enantiomer of 1–E), D-glucose (5,6–E), D-lyxose (8,9–E), D-mannose (13,14–E), D-arabinose (17–E), D-galactose (22,23–E), and D-fructose. Next, Barr and Chrisman [10] recorded the infrared spectrum (5556 to 3846 cm^{-1}) of a saturated, aqueous solution of D-arabinose (17–E). For other sugars, they smeared a concentrated aqueous solution of the sugar on a cover glass and heated gently for several hours, obtaining a thick sirup which, they claimed, contained practically no water; after this treatment, each sugar was probably present as its equilibrium mixture. The spectra of these evaporated films (for the range 5556 to 2174 cm^{-1}) were recorded for D-xylose (1–E), D-glucose (5,6–E), L-rhamnose (11,12–E), D-mannose (13,14–E), L-arabinose (enantiomer of 17–E), D-galactose (22,23–E), and D-fructose.

Finally, Parker [11] recorded the spectra (for the range of 1667 to 909 cm^{-1}) of 20-percent aqueous solutions (w/v) of L-arabinose (enantiomer of 17–E), D-ribose (25–E), and D-fructose, and of a 10-percent aqueous solution of D-galactose (22,23–E). In addition, he recorded the spectra (for the same range) of 20-percent aqueous solutions of α-D-glucose, β-D-glucose, and β-D-mannose (a) 2.5 minutes

after dissolution, and (b) at the end of mutarotation. By following the change in percent transmittance (at 1143 cm^{-1} for α- or β-D-glucose, and at 1163 cm^{-1} for β-D-mannose) with time, he was able to determine the mutarotation constants; these agreed well with those determined from measurements of change in optical rotation (see sec.4).

4. Mutarotational Studies of These Sugars by Optical Rotation

When a crystalline sugar is dissolved in water and the solution is allowed to stand, the optical rotation initially observed may change. An aldohexose or a 2-heptulose, in solution, may adopt one or more of eight modifications. Thus, for an aldohexose in which C–4 and C–5 are both D, the following structures may theoretically be present in the equilibrium solution. Of these, only the aldehydo form will show carbonyl absorption in the infrared spectrum.

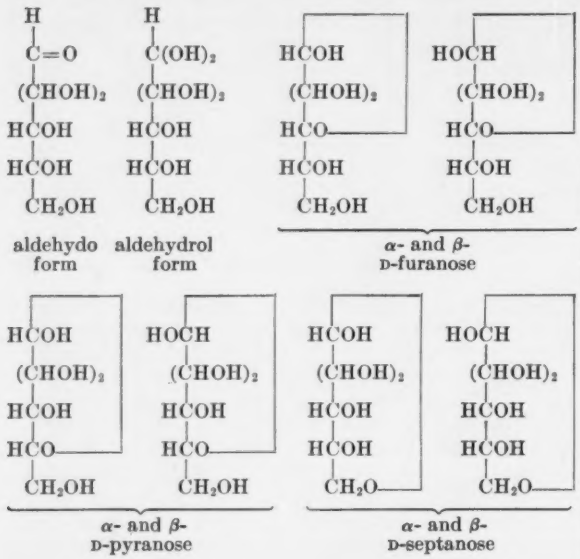

For an aldopentose or a 2-hexulose, the septanose forms are impossible, so that, for them, the maximum number of theoretically possible sugar components is six.

It is, of course, possible that the appearance of new species in the solution may be unaccompanied by any change in optical rotation. This would occur if (a) all the species present at any moment have the same optical rotation; (b) the initial and final rotations are the same, but, although intermediate rotations are different, mutarotation is so rapid that it is complete before observation of optical rotation has been started; or (c) an increase in rotation, caused by appearance (or disappearance) of one or more forms, is exactly balanced by a decrease resulting from disappearance (or appearance) of one or more other forms. In addition, there is the possibility that, at all times during establishment of equilibrium, the changes in rotation are so slight as to be virtually unobservable. On the other hand, in some instances, an apparent or spurious mutarotation, caused by a positive or negative heat of solution, might be observed, even though no new species actually appeared in the solution.

When dynamic equilibrium between the forms is reached, the proportion of each that is present in the solution depends on the structural, configurational, and conformational stability of each form.[2] Some indications as to the proportions of the various forms present in the equilibrium solution of some of the sugars in the present study have been obtained by observing the change in optical rotation, with time, when a crystalline anomer of the sugar is dissolved in pure water. The results [2] are given in table 2, from which it may be seen that, as regards mutarotational behavior, 4 groups of sugars may be distinguished.

In *group 1*, exhibiting little or no mutarotation, are the 2-ketoses 2, 7, 10, and 15; the equilibrium mixture for each of these sugars appears to consist almost entirely of one form (possibly the α- or β-pyranose), which may be the same as the crystalline sugar dissolved.

Group 2 sugars (the 2-ketoses 18 and 19, and, perhaps, the 3-ketose 20) exhibit mutarotation, and the equilibrium mixture apparently consists mainly of a single pyranose form together with the α- and β-furanose forms.

[2] A discussion, prepared by H. S. Isbell, of the sugars in solution is given in F. J. Bates and Associates, NBS Circular **440**, Chapter XXIX (1942).

TABLE 2. *Character of the mutarotation and composition of the equilibrium mixture, as determined by studies of changes of optical rotation*

Sugar		Mutarotation reaction	Equilibrium mixture	Reference
Name	No.			
(?)-L-*xylo*-Hexulose	2	slight; complex	almost entirely one form (pyranose) that is the same as for the crystals	1
α(?)-D-*gluco*-Heptulose	7	none	?	2
(?)-D-*lyxo*-Hexulose	10	none	almost entirely one form (pyranose)	3
(?)-D-*manno*-Heptulose	15	none	?	4
(?)-D-*arabino*-Hexulose ·0.5 $CaCl_2$·1.5H_2O	18	mutarotates	a single pyranose +α- and β-furanoses	5
3-*O*-Methyl-(?)-D-*arabino*-hexulose	19	mutarotates	?	6
β-D-*manno*-3-Heptulose	20	mutarotates	?	7
α-D-Xylose	1	first order	mainly α-pyranose+ β-pyranose	8
D-Glucose, α-;β-	5; 6	first order		8
D-Lyxose, α-;β-	8; 9	first order		8
6-Deoxy-L-mannose, α-;β-	11; 12	first order		8
D-Mannose, α-;β-	13; 14	first order		8
(?)-D-Gulose ·0.5 $CaCl_2$· 0.5 H_2O	16	first order		8
β-D-Arabinose	17	complex	α-pyranose+ β-pyranose+ α-furanose+ β-furanose	8
6-Deoxy-α-L-galactose	21	mutarotates		9
D-Galactose, α-;β-	22; 23	complex		8
β(?)-D-Ribose	25	complex		8
D-Talose, α-;β-	26; 27	complex		8, 10

References for Table 2

1. W. W. Pigman and H. S. Isbell, J. Research NBS **19**, 443 (1937) RP1035.
2. W. C. Austin, J. Am. Chem. Soc. **52**, 2106 (1930).
3. T. Reichstein and W. Bosshard, Helv. Chim. Acta **17**, 753 (1934).
4. F. B. LaForge, J. Biol. Chem. **28**, 511, 517 (1917).
5. H. S. Isbell and W. W. Pigman, J. Research NBS **20**, 773 (1938) RP1104.
6. C. G. Anderson, W. Charlton, W. N. Haworth, and V. S. Nicholson, J. Chem. Soc. **1929**, 1337.
7. R. Schaffer, Abstracts Papers Am. Chem. Soc. **139**, 4D (1961).
8. H. S. Isbell and W. W. Pigman, J. Research NBS **18**, 141 (1937) RP969.
9. A Günther and B. Tollens, Liebigs Ann. Chem. **271**, 86 (1892).
10. W. W. Pigman and H. S. Isbell, J. Research NBS **19**, 189 (1937) RP1021.

For *group 3* (aldoses 1, 5 and 6, 8 and 9, 11 and 12, 13 and 14, and 16), the mutarotation is a first-order reaction, and the equilibrium mixture consists mainly of the α- and β-pyranose forms.

The members of *group 4* (aldoses 17, 21, 22 and 23, 25, and 26 and 27) exhibit a complex mutarotation, and the equilibrium mixture appears to contain, at least, the α- and β-pyranose forms and the α- and β-furanose forms.

5. Discussion of the Spectra

5.1. Spectra of Sugars for Which Both Anomers Were Available

For D-glucose, D-lyxose, L-rhamnose, D-mannose, D-galactose, and D-talose, the infrared spectra were recorded for both of the cystalline anomers. Table 3 lists the bands shown by the α anomer but not by the β anomer of each of these sugars, and table 4 lists the bands shown by the β anomer but not by the α anomer of each. These bands will be discussed in a subsequent article dealing with the infrared spectra of pyranoid sugars.

5.2. Spectra of the Equilibrium Mixtures

In this discussion, the spectrum of the material obtained by lyophilizing the equilibrium solution of a sugar will be referred to as the "equilibrium spectrum" for that sugar. It was assumed that, during freezing and lyophilization, no change in composition of an equilibrium solution occurs; for some sugars, this assumption may be unwarranted, and crystallization of a new form, or of the original form, may take place.

The equilibrium spectra all showed a band near 1718 cm^{-1}, suggesting the presence, in every equilibrium mixture, of some of the carbonyl form (aldehydo or keto) of the respective sugar. The intensity of this band differed from sugar to sugar; for example, for D-mannose (13,14–E) and D-galactose (21,22–E), it was quite clearly present, whereas it was weaker for D-fructose (18–E) and D-glucose (5,6–E), and barely perceptible for some of the other sugars. This observation agrees with the results of Lippich [12], who found that the proportion of the carbonyl form present in the equilibrium solution is in the order D-mannose>D-galactose>D-fructose>D-glucose. Similarly, D-*manno*-2-heptulose (15–E), whose aqueous solution shows [13] an ultraviolet absorption maximum at 2650A, indicating the presence of the carbonyl form, exhibits an infrared absorption band at 1712 cm^{-1}. D-*manno*-3-Heptulose, which is a member of the D-*arabino* series, shows a much stronger carbonyl band (at 1727 cm^{-1}).

The equilibrium spectra of those sugars for which the spectra for *both* crystalline anomers were available were now studied. These equilibrium spectra were found to fall into 2 groups. In the *first group*

TABLE 3. *Bands (cm^{-1}) shown by the α anomer but not by the β anomer of six sugars.*

D-Glucose (5)	D-Lyxose (8)	L-Rhamnose·H_2O (11)	D-Mannose (13)	D-Galactose (22)	D-Talose (26)
[a]3413	----	----	----	----	3378
----	----	3247	3165	3195	----
3021	----	2950	2976	----	----
2899	----	2899	2924	2890	2865
----	----	2584	----	2532	2674
----	----	----	----	----	----
----	----	1669	----	----	----
1445	1437	----	1453	1447	----
1429	----	1429	----	----	1425
[a]1340	----	----	1385	----	1362
1297	----	----	1297	1328, 1314	----
1284	1285	----	----	1284	----
----	1244, 1220	----	1224	1250	----
----	1147	----	1199	1152	1144
1105	----	----	1104	1104	----
1050	----	1075	----	1070, 1046	1054
[a]996	----	----	972	997, 976	----
----	965	----	960	[b]958	952
----	----	----	915	----	908
----	867	[b]878	885	----	----
[a][b]838	852	[b]830	831	----	----
----	----	----	812, 804	----	802
[a][b]776	771	----	----	[b]766	----
----	----	----	707	----	715
----	----	658	679	660	676
621	627	----	----	----	----
----	583	570	565	----	----
557	549, 530	----	----	533	----
----	490	503	509	500	----
435	476	----	467	----	477
391	----	----	391	----	----
377	367	----	375	----	366
347	----	----	----	345	----
----	----	----	311	334, 329	----
----	294	301	----	300(?), 292	296
----	----	----	----	280	----

[a] These bands were mentioned by Urbański and co-workers [7].
[b] These bands were mentioned by Barker and co-workers [4].

TABLE 4. *Bands (cm^{-1}) shown by the β anomer but not by the α anomer of six sugars.*

D-Glucose (6)	D-Lyxose (9)	L-Rhamnose (12)	D-Mannose (14)	D-Galactose (23)	D-Talose (27)
----	----	----	----	----	3497
----	----	----	----	----	3436
3247	3257	----	----	3333	3247
----	----	----	----	----	3030
----	----	2915	----	----	2924
----	----	2874	2874	2857	2890
----	----	2747	----	----	2703
----	1473	----	1484	----	1511
----	1420	----	1433	1435	1439
1361	1374	----	1410	----	1393
----	----	----	----	----	1340
1311	1318	----	[b]1311	----	1290
1271, 1253	----	1259	----	1269	1248
----	----	----	----	1212	----
----	1163	1166	[b]1170	1166	1176
----	----	1131	----	1120	----
----	1092	1100	1089	1089	1074
1063	----	1052	----	----	----
----	----	----	----	1033	1032
----	----	1025	----	1019	----
----	----	----	[a][b]936	[a]945	935
[a]901	----	897	[a][b]899	[a]900	886
----	804	865	[a][b]862	----	879
----	----	777	[a][b]772	----	----
----	755	----	729	----	746
709	----	672	----	654	653
----	615	----	619	----	----
----	----	530	540	553(?)	548
519	513	----	----	----	495
460	464	----	----	----	----
----	446	----	448	----	----
----	416	421	426	----	----
----	----	325	285	----	----

[a] See footnote b to table 3.
[b] See footnote a to table 3.

TABLE 5. *Bands (cm^{-1}) in the infrared spectra of the equilibrium mixtures of four sugars, compared with corresponding bands for each anomer of these sugars.*

D-Glucose			L-Rhamnose			D-Mannose			D-Galactose		
5,6-E	5	6	11,12-E	11	12	13,14-E	13	14	22,23-E	22	23
3356	[a] 3322	3356	3378	3333	—	3378	3344	3367	3367	3390	3413
....	....	....	2985	2985	2976	2941	2976	—	....	....	....
2924	2941, 2899	2941	2933	2950, 2899	2915	2907	2924	—	2941	2941	2950
2717	2688	2747	2717	2703	2695	2747	2703	2688	....	....	....
1712	—	—	1724(?)	—	—	[b] 1724	—	—	[b] 1730	—	—
1647	—	—	1650	1669	—	....	....	....	....	....	....
....	....	....	1456	1449	1449	....	....	....	....	....	....
1420	1429	1412	1418	1429, 1403	1406	1418	1422	1422	1416	1425	1416
[b] 1364	—	1361	1385	1383	1379	1385	1385	1372	[b] 1379	—	1383
1321	—	1311	1330	1330	1342, 1323	[b] 1332	1332	1337	1330	1328	—
1282	1284	1271	....	....	....	....	....	....	....	....	....
1263	—	1253	1258	—	1259	1259	1255	[a] 1263	1256	1250	1269, 1241
1200	[a] 1202	1202	1229	1224	1225	1211	1208	[a] 1214	1220	—	1212
....	....	....	1176	—	1166	[c] 1166	—	[a c] 1170	....	....	....
[c] 1147	[a c] 1148	[c] 1155	1140	1143	1149	....	....	....	1144	1140	1133
[b] 1104	[a] 1111, 1105	1111	1125	1122	1121	1111	1111	[a] 1111	....	....	....
1080	[a] 1080	1082	1087	1086	1089	1082	1073	1089	1078	1081	1080
....	....	....	1066	1070	1052	1068	1067	[a] 1073	....	....	....
....	....	....	....	....	....	1059	—	1062	1046	1046	1054
1035	[a] 1026	1035	1018	—	1025	[b] 1029	1034	1035	....	....	....
[b] 995	[a] 996	—	978	979, [d] 976	979	973	972	—	986	997, 976	—
....	....	....	....	....	....	958	960	—	949	—	[d] 945
921	[a d] 916	[d] 914	....	....	....	934	—	[a d] 936	921	—	—
901	—	[d] 901	904	[d] 911	909	906	—	[a d] 899	894	[d] 890	[d] 900
....	....	....	864	[d] 878	865	870	—	[a d] 862	879	—	[d] 884
840	[a d] 838	—	834	[d] 834	834	829	831	—	....	....	....
....	....	....	808	[d] 805	806	808	812	—	802	[d] 792	—
771	[a d] 776	—	776	—	777	783	—	[a d] 772	786	[d] 792	[d] 781
708	—	709	718	714	718	719	707	729	701	707	700
....	....	....	678	—	672	....	....	....	....	....	....

[a] See footnote a to table 3.
[b] These bands were mentioned by Rogers and Williams [9].
[c] These bands were mentioned by Parker [11].
[d] See footnote b to table 3.

(see table 5), all bands observed in the equilibrium spectrum (excepting that for carbonyl, at about 1718 cm^{-1}) could be accounted for, either as being (a) distinctive of one anomer present (the bands matching those of one or both of the crystalline anomers) or (b) the resultant of overlapping of neighboring bands displayed by each of the two crystalline anomers, respectively. In this category (for which the equilibrium mixtures consist, presumably, of 3 sugar components, viz, the α- and β-pyranose forms and the open-chain form) were the equilibrium spectra of D-glucose (5,6–E), L-rhamnose (11,12–E), D-mannose (13,14–E), and (except for one band, at 921 cm^{-1}) D-galactose (22,23–E). For the *second group* (see table 6), consisting of D-lyxose (8,9–E) and D-talose (26,27–E), the equilibrium spectrum shows bands (besides the carbonyl band) that are *absent* from the spectrum of *either* of the crystalline anomers. These extra bands may be attributable to the presence of (a) the open-chain form, (b) one or both anomers of one or more ring-forms different from that in the crystalline anomers examined, or (c) the presence of different conformations of the sugar. It is possible that D-galactose should be included in the second group.

For the other crystalline sugars in table 1, only *one* anomer of each was available. On comparing

TABLE 6. *Bands (cm^{-1}) in the infrared spectra of the equilibrium mixtures of two sugars, compared with corresponding bands for each anomer of these sugars.*

D-Lyxose			D-Talose		
8,9-E	8	9	26,27-E	26	27
3448	3509	—	....	....	....
3356	3300	3322	3356	3300	3300
3257	—	3257	....	....	....
2933	2941	2933	2933	2950	2950, 2924
2717	2681	2674	....	....	....
1712(?)	—	—	1724	—	—
1464	1464	1460	....	....	....
1418	1397	1420	1416	1425	—
[a] 1344	1346	1344	1328	1323	1325
1258	1253	1256	1244	1238	1241
....	....	....	1167	—	1176
1136	1133	1130	1115	1115	1122
[a] 1106	1099	1107	1092	1085	1089
1075	1072	1075	....	....	....
1044	1047	1045	1048	1054	—
1005	1006	1006	995	—	—
982	—	—	963	—	—
945	—	—	937	—	935
899	—	—	....	....	....
882	887	883	877	874	879
846	852	840	864	—	871
808	809	809	810	816	812
766	771	—	758	765	765, 746
714	—	713	....	....	....
673	669	673	....	....	....

[a] See footnote b to table 5.

the equilibrium spectrum of each sugar with the spectrum of the corresponding crystalline sugar, two groups of spectra were noted. In the *first* group (see table 7) were the equilibrium spectra[3] of L-*xylo*-hexulose (2–E), D-*lyxo*-hexulose (10–E), D-gulose·0·5 $CaCl_2$ (16–E), D-*arabino*-hexulose·0.5 $CaCl_2$ (18–E), 3-*O*-methyl-D-*arabino*-hexulose (19–E), and D-ribose (25–E); in each of these spectra, all bands which could be clearly distinguished were also present in the spectrum of the crystalline anomer originally dissolved (although the equilibrium spectrum lacked the band-definition of some of the bands displayed by the crystalline anomer). Indeed, for L-*xylo*-hexulose, D-*lyxo*-hexulose, and D-ribose, *the equilibrium spectrum is scarcely distinguishable from that of the crystalline sugar.* (In addition, a considerable resemblance between the equilibrium spectra of D-ribose and D-talose is evident, and, in the range of 5000 to 962 cm^{-1}, the spectra are almost superimposable.)

The *second group* of equilibrium spectra (see table 8) consisted of those of D-xylose (1–E), D-*gluco*-heptulose (7–E), D-*manno*-heptulose (15–E), D-arabinose (17–E), D-*manno*-3-heptulose (20–E), and 6-deoxy-L-galactose (21–E). Each of these equilibrium spectra clearly showed some bands not displayed by the anomer originally dissolved. New species of each sugar were obviously present in the respective equilibrium mixture; for sugars 7 and 15 (see table 2), a change in optical rotation during equilibration either (a) does not occur or (b) is so slight that it has not been detected. Since, for these 6 sugars, the spectrum of the other anomer of each was unavailable, no decision as to the source of the new bands could be made.

Thus, as regards the composition of the equilibrium mixture, the conclusions earlier arrived at (from studies of mutarotation) agree (or do not *dis*agree) with those derived from the infrared spectra, *except for* D-lyxose and D-ribose.

A clearcut decision as to agreement between results derived by the two techniques could not be reached for D-*gluco*-heptulose and D-*manno*-heptulose (as a careful search for mutarotation has not been made for these sugars) or for D-gulose, D-*arabino*-hexulose, and 3-*O*-methyl-D-*arabino*-hexulose (as their equilibrium spectra were not sufficiently informative).

[3] The "equilibrium spectrum" of 2,7-anhydro-D-*altro*-heptulose also belonged to this group, but, as this anhydride had received a special treatment (see sec. 6.2), the compound is not included here.

TABLE 7. *Bands (cm^{-1}) in the infrared spectra of the equilibrium mixtures of six sugars, compared with corresponding bands for one anomer of each of these sugars.*

L-*xylo*-Hexulose		D-*lyxo*-Hexulose		D-Gulose·0.5 $CaCl_2$		D-*arabino*-Hexulose·0.5 $CaCl_2$		3-*O*-Methyl-D-*arabino*-hexulose		D-Ribose	
2–E	2	10–E	10	16–E	16	18–E	18	19–E	19	25–E	25
3390	[a] 3413	3401	3534	....	....	3378	3425	3401	3401	....	....
....	....	3333	3322	3331	3333	3333	3268	....	....	3356	[a] 3378
2941	2950	2941	2950	2941	2915	2950	2985, 2933	2950	2941	2933	2933
2907	2907	....	....	....	....	....	....	2865	2857	2890	2899
2688	2778	2703	2674	2732	2681	2717	2681	....	....	2703	2703
1712	—	1718	—	1724(?)	—	1712	—	1712	—	1718	—
....	....	....	....	1650	1667	1647	1656	....	....	....	....
1464	1466	1473	1471	1456	1462	....	....	1458	1451	1458	1456
....	....	1443	1443	....	....	....	....	....	....	....	....
1399	1397	1410	1408	1416	1410	1425	1425	1410	1435, 1397	1416	1414
1366	1366	1383	1379	....	....	....	....	....	....	....	....
1351	1350	1340	1340	....	....	[b] 1355	1368, 1339	1346	1355	1344	1362
1311	[a] 1312	1302	1304	1305	1300	....	....	....	....	....	....
....	....	1277	1272	....	....	....	....	....	....	....	....
1258	[a] 1258	1263	1264	1259	1241	1259	1250	....	....	1250	[a] 1245
....	....	1241	1239	....	....	1242	1238	1244	1241	....	....
1212	1215	....	....	....	....	....	....	....	....	1227	[a] 1220
1193	[a] 1193	1185	1171	....	....	1185	1183	1190	1190	....	....
1151	[a] 1151	1155	1153	1147	1138	1147	1143	....	....	1139	[a] 1130
1125	1126	....	....	....	....	....	....	1119	1126, 1111	1119	[a] 1117
1106	[a] 1109	1100	1101	1099	1103, 1095	[b] 1099	1112, 1091	....	....	....	....
1080	[a] 1081	1071	1073	....	....	1080	1083	1080	1087	1085	1085
1059	1062	1058	1056	1052	1057	1058	1068, 1049	....	....	....	....
1050	[a] 1049	1042	1038	....	....	....	....	....	....	1044	[a] 1041
1032	[a] 1031	....	....	....	....	....	....	....	....	....	....
1016	1014	1024	1021	....	....	....	....	....	....	....	....
994	[a] 992	....	....	....	....	....	....	1000	994	1004	1017
....	....	964	966	980	963	977	984	973	970	966	[a] 959
....	....	947	947	....	....	....	....	931	928	....	....
....	....	912	912	917	919	929	920	....	....	914	[a] 912
900	[a] 901	....	....	895	897	....	....	....	....	887	[a] 889
885	[a] 882	870	868	883	876	863	860	870	865	870	[a] 869
821	[a] 820	822	822	....	....	822	823	825	831	826	825
....	....	785	784	807	806	783	785	770	768	797	[a] 799
....	....	....	....	....	....	....	....	....	....	747	747
721	719	730	731	....	....	....	....	....	....	724	724
685	683	690	688	....	....	....	....	....	....	....	....

[a] See footnote a to table 3. [b] See footnote b to table 5.

TABLE 8. *Bands (cm^{-1}) in the infrared spectra of the equilibrium mixtures of six sugars, compared with corresponding bands for one anomer of each of these sugars.*

D-Xylose		D-*gluco*-Heptulose		D-*manno*-2-Heptulose		D-Arabinose		D-*manno*-3-Heptulose · H_2O		6-Deoxy-L-galactose	
1-E	1	7-E	7	15-E	15	17-E	17	20-E	20	21-E	21
3356	[b] 3333	3356	3413	3356	3401	3356	[b] 3356	3390	3401	3356	3344
....	....	....	....	....	....	....	....	2976	2950	2985	3021
....	....	2933	2959	2941	2933	2924	2959	....	....	....	....
2915	2899	2907	2907	....	....	....	....	....	....	2915	2899
2703	2732	2688	2703	2674	2695	2688	2674	....	....	2717	2732
1712(?)	—	1712(?)	—	1712	—	[a] 1718	—	1727	—	1718	—
1466	1464	....	....	....	....	....	....	1653	1653	1464	—
....	....	....	....	....	....	....	....	1420	1429	1441	1447
1418	1395	1420	—	1412	1404	1406	1404	....	....	1385	1391
[a] 1355	1357	1364	1361	....	....	1346	1357	1359	—	1370	1370
....	....	....	....	....	....	....	....	....	....	1312	1300
1269	—	1255	1263	1250	1264	1258	[b] 1259	1271	—	1247	1256
1244	[b] 1236	....	....	....	....	[a] 1218	[b] 1233	1247	—	1214	1221
1202	1202	1206	1198	1202	1199	....	....	....	....	....	....
....	....	1181	1186	....	....	1161	—	1181	1185	1168	1170
1145	[b] 1149	1111	1117	....	....	1139	[b] 1135	....	....	1126	1130
[a] 1088	[b] 1082	1083	1087, 1078	1096	1093	1096	[b] 1093	1100	1099	1095	1089
....	....	....	....	....	....	[a] 1085	—	1086	—	....	....
1057	1055	1059	1054	1057	1056	1062	1067	....	....	1068	1072
1048	[b] 1042	1040	—	....	....	1033	[b] 1055	1052	1050	1037	1041
1016	1018	1019	1013	1025	1021	....	....	....	....	....	....
979	989	989	986	....	....	1001	[b] 1001	996	—	998	999
....	....	960	—	950	952	....	....	952	—	965	[c] 963
936	[b] 935	....	....	....	....	947	[b] 945	915	918	949	—
898	[b] 904	907	—	903	906	917	—	902	895	900	—
....	....	879	871	....	....	888	[b] 894	....	....	....	....
....	....	....	....	....	....	869	—	....	....	858	—
....	....	832	827	840	—	844	[b] 844	824	818	....	....
812	—	....	....	822	816	....	....	....	....	814	[c] 819
....	....	....	....	....	....	786	[b] 786	789	783	770	[c] 772
759	[b] 762	....	....	744	—	....	....	....	....	758	—
....	....	716	714	704	702	....	....	....	....	....	....
655	—	....	....	....	....	....	....	....	....	667	666

[a] See footnote b to table 5. These authors studied the enantiomer for 1-E.
[b] See footnote a to table 3.
[c] See footnote b to table 3. Their observations were for the β anomer.

6. Experimental Procedures

6.1. Preparation and Purification of the Compounds

The individual compounds listed in table 1 were prepared by the methods given in the references cited. Each compound was recrystallized from an appropriate solvent until further recrystallization caused no change in its melting point or optical rotation.

For the preparation of 6-deoxy-β-L-mannose (compound 12), 11.1 g of compound 11 was dissolved in 200 ml of boiling absolute ethanol under reflux and the solution was evaporated under diminished pressure to a sirup; the material was freed from water by (4 times) dissolving it in 100 ml of absolute ethanol, adding 100 ml of benzene, and evaporating to dryness. The resulting colorless crystals (10 g) were dissolved in 220 ml of boiling acetone under reflux, and the solution was cooled, to give 5.9 g of a crystalline mixture of the α and β anomers of the anhydrous sugar, mp 114–116°. (Jackson and Hudson had supposed this material to be a compound.) The dry, finely powdered mixture was shaken with absolute ethanol (4 vols.) for 5 min at room temperature, the suspension was filtered with suction (rubber dam), the crystals were immediately re-extracted in the same way with the same volume of absolute ethanol, and the crystals were rapidly removed by suction filtration (rubber dam) and dried in a vacuum desiccator (Desiguard) over phosphorus pentaoxide at 0.1 mm; the crystals had mp 127–129°.

6.2. Preparation of the Equilibrium Mixtures

The crystalline compound (0.5 g) was weighed into a 25-ml volumetric flask, water was added, the solution was made to 25 ml with water, and the specific rotation was observed periodically until mutarotation was complete. For sugars displaying no mutarotation, the solution was kept overnight at room temperature. A portion (0.1 ml) was now transferred, by pipet, to a 5-ml flask containing 500 mg of potassium chloride. The pipet and the neck of the 5-ml flask were washed with water, and the washings were added to the flask contents, which were then brought to about 3 ml with water. The solution was frozen and lyophilized, giving a dry mass containing 0.4 mg (or its equivalent) of the sugar or sugar compound per 100 mg of potassium chloride.

For 2,7-anhydro-β-D-*altro*-heptulose (sedoheptulosan) monohydrate (compound 24), 0.25 g was dis-

solved in 20 ml of 1 percent aqueous hydrochloric acid, and the solution was heated, under reflux, in a boiling-water bath for 1 hr. The solution was de-ionized by passage through columns of (a) Duolite A–4(OH^-)(20 ml) and (b) a mixture of 2 ml of this resin with 2 ml of Amberlite IR–120 (H^+), with elution with water until the total volume of final effluent was 125 ml. One milliliter of this neutral effluent was added to 500 mg of potassium chloride in a 5-ml flask, 2 ml of water was added, and the solution was frozen and lyophilized, giving a dry mass containing the equivalent of 0.4 mg of compound 24 per 100 mg of potassium chloride. It should be noted that heating of a 0.07 *M* solution of sedoheptulosan monohydrate in 0.2 *N* hydrochloric acid for 1 hr at 100° affords [14] a mixture of 80.4 percent of sedoheptulosan monohydrate with 3.4 percent of 2,7-anhydro-*β*-D-*altro*-heptulofuranose, 14.8 percent of D-*altro*-heptulose, and 1.4 percent of 5-(1,2-dihydroxyethyl)-2-furaldehyde.

6.3. Preparation of the Pellets

For spectrophotometric study, samples of the individual compounds were prepared as pellets consisting of the crystalline compound suspended in an alkali-metal halide, exactly as previously described [15]. For the range of 5000 to 667 cm^{-1}, a concentration of 0.4 mg of the compound per 100 mg of potassium chloride was used. The spectrum of compound 20 in this range was also recorded at the same concentration in potassium iodide. For the range of 667 to 250 cm^{-1}, the following weights of compound per 100 mg of potassium iodide were used—compound 25 : 1 mg; compounds 5 and 17 : 1.34 mg; compounds 2 to 4 and 7 : 3 mg; and for the rest of the compounds: 2 mg. In this range, the spectrograms for compounds 16 and 18 in Nujol were recorded at several concentrations.

For the lyophilized, equilibrium mixtures, the dry lyophilizate (already containing the desired proportion of potassium chloride) was pressed directly into a pellet.

6.4. Measurement of Infrared Absorption

The spectrograms are shown in figures 1 and 2. Those in figure 1 for compound 20 and its equilibrium mixture (20–E) were recorded with a Beckman Model IR4 (double-beam) spectrophotometer equipped with prisms of sodium chloride. The others were recorded with a Perkin-Elmer Model 21 (double-beam) spectrophotometer equipped with a prism of sodium chloride (for the range of 5000 to 667 cm^{-1}) and of cesium bromide (for the range of 667 to 250 cm^{-1}), as previously described [15].

Some absorption attributable to water (in the compound, the alkali halide, or both) was observed at 1639 cm^{-1} and, attributable to atmospheric water vapor, in the far-infrared curves. These regions are drawn on the spectrograms with dashed lines which are not to be interpreted quantitatively.

6.5. Spectra Measured Under Different Conditions

Because of the possibility of interaction of the various sugars with the pelleting halide under high pressure (previously observed [16] for 8 out of 24 aldopyranosides), the spectra of the sugars were also recorded in a Nujol mull in the range of 667 to 250 cm^{-1}. For 16 of the 27 sugars, the spectra obtained with either medium matched well; for 5, the spectra in potassium iodide were not well defined, but matched those in Nujol (compounds 8, 9, 15, 16, and 26). However, the following compounds gave spectrograms that were *different* in Nujol and in potassium iodide: compounds 3, 14, 20, 24, 25, and 27.

In view of these observations, the spectra obtained with a Nujol mull were used exclusively for measuring the positions of absorption bands in the range of 667 to 250 cm^{-1}, not only for the sugars that gave unsatisfactory spectra in potassium iodide, but also (in order to keep the measurements strictly comparable) for the other sugars.

Farmer [6] had noted that, in the range of 5000 to 667 cm^{-1}, "*α*-glucopyranose" gave a spectrum in potassium iodide that differed from that in potassium bromide. We therefore recorded the spectra of compound 20 (a sugar that gave a poor spectrum in potassium iodide in the range of 667 to 250 cm^{-1}) in potassium iodide and in potassium chloride, at identical concentration in pellets of the same weight, for the range of 5000 to 667 cm^{-1}; the spectrum in potassium iodide was less detailed than that in potassium chloride.

The authors express their gratitude to J. D. Moyer for preparing and lyophilizing the equilibrated solutions. They also thank J. E. Stewart, J. J. Comeford, and F. P. Czech for recording the infrared absorption spectra.

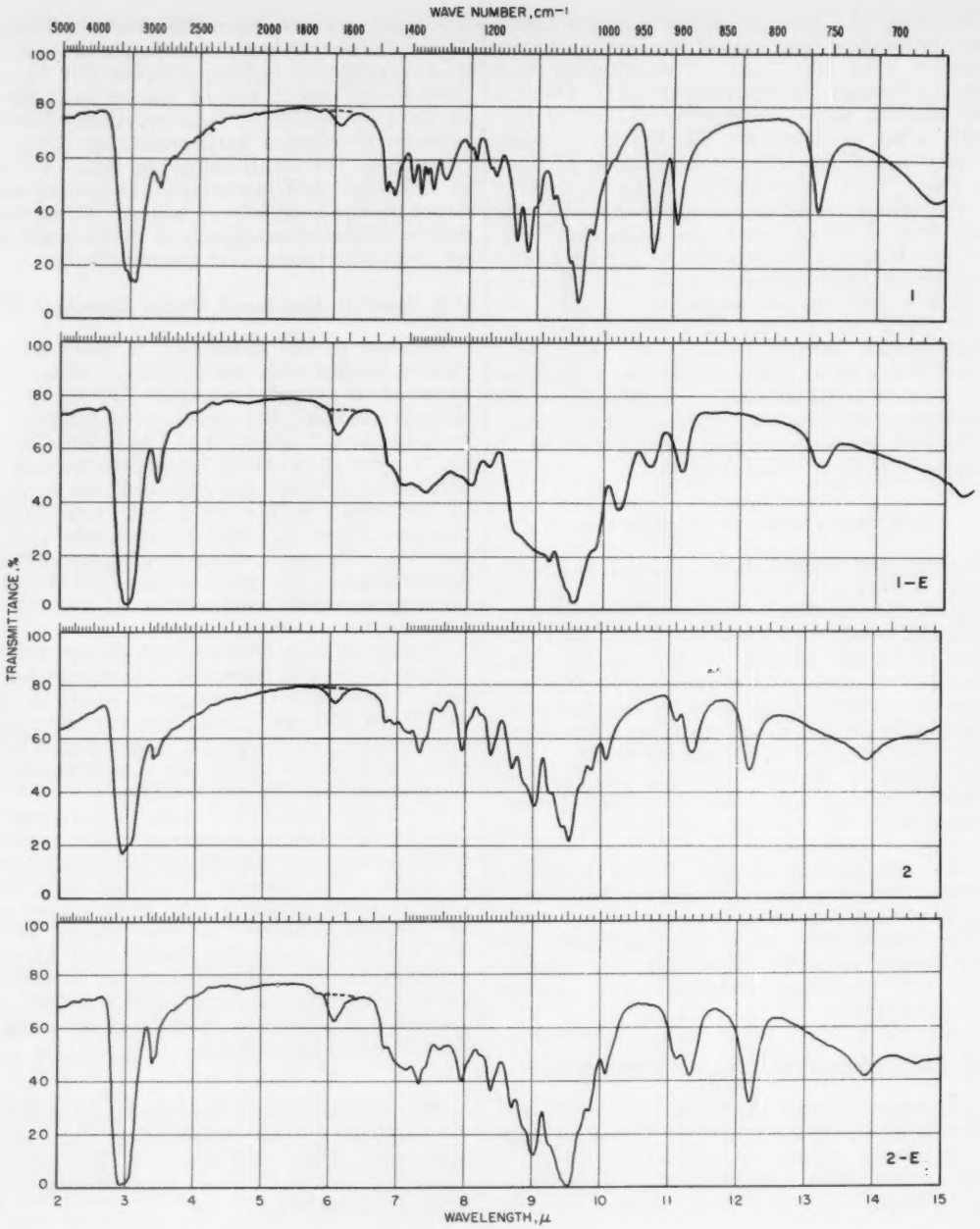

FIGURE 1. *Spectrograms of materials in potassium chloride pellets.*

1, α-D-Xylose; **1-E**, D-xylose (equilibrium); **2**, (?)-L-*xylo*-hexulose; **2-E**, L-*xylo*-hexulose (equil.).

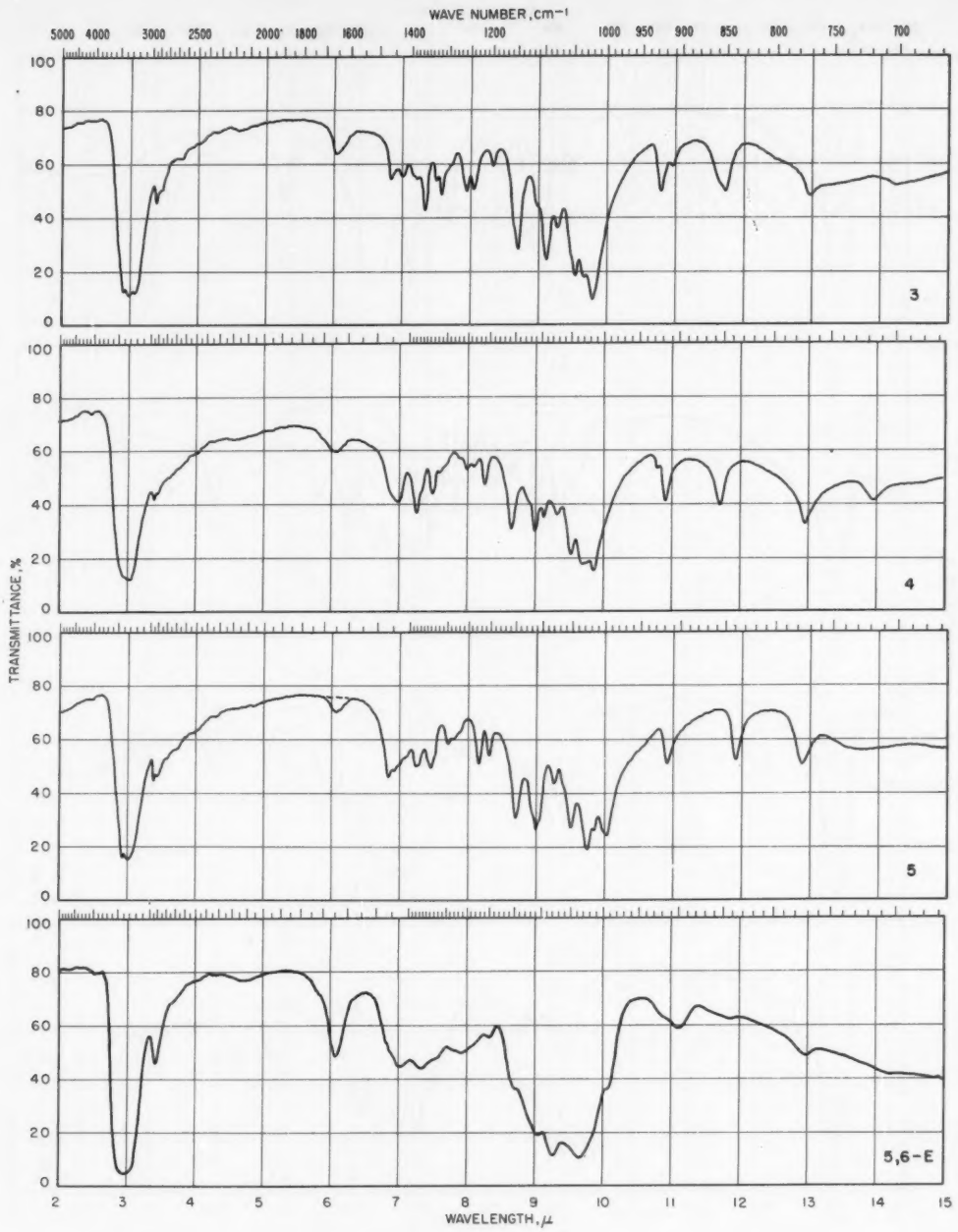

FIGURE 1. *Spectrograms of materials in potassium chloride pellets.*—Continued

3, α-D-glucose·0.5 NaCl·0.5 H_2O; **4,** α-D-glucose monohydrate; **5,** α-D-glucose; **5, 6-E,** D-glucose (equil.).

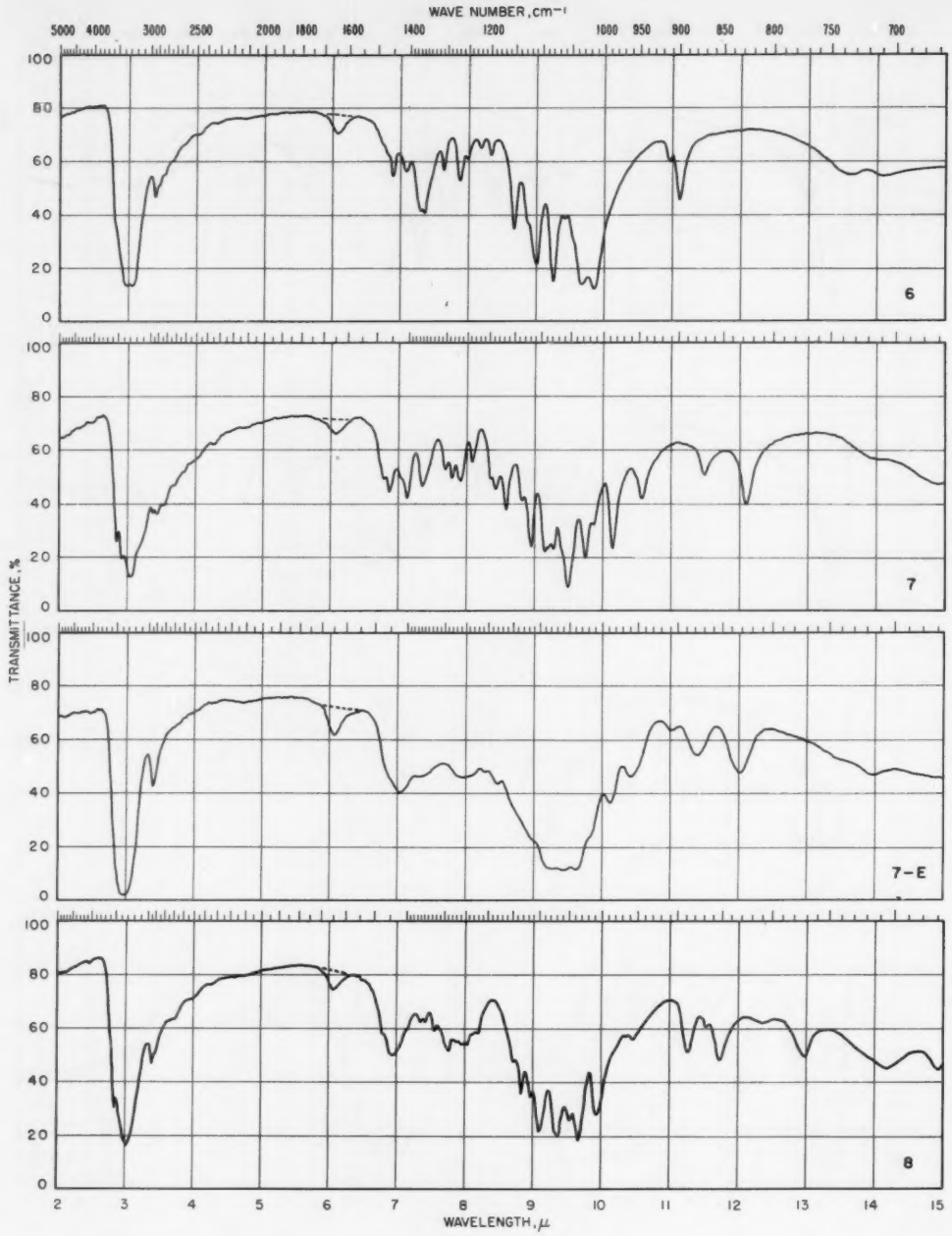

FIGURE 1. *Spectrograms of materials in potassium chloride pellets.*—Continued

6, β-D-glucose; 7, α(?)-D-*gluco*-heptulose; 7-E, D-*gluco*-heptulose (equil.); 8, α-D-lyxose.

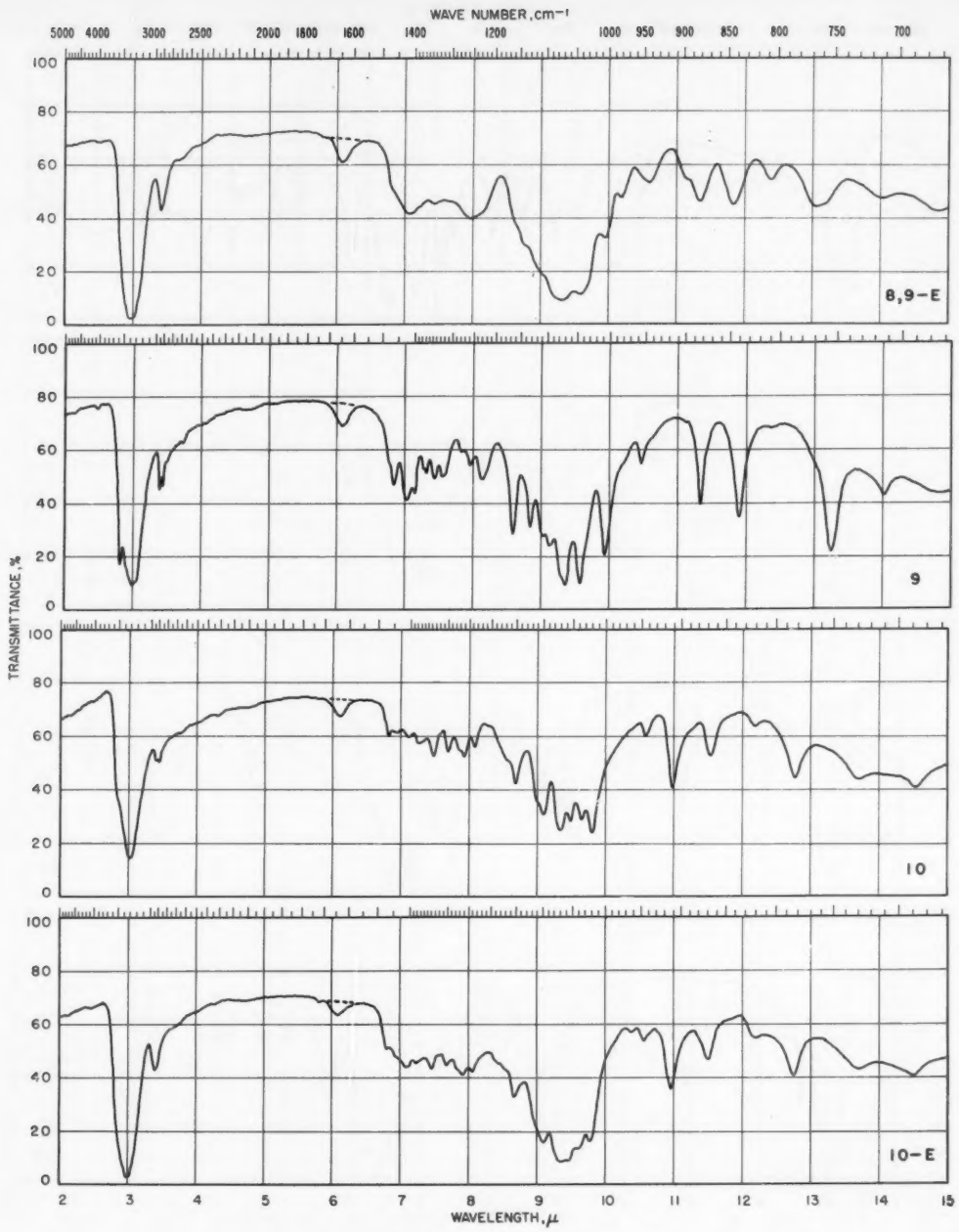

FIGURE 1. *Spectrograms of materials in potassium chloride pellets.*—Continued

8,9-E, D-lyxose (equil.); **9,** β-D-lyxose; **10,** (?)-D-*lyxo*-hexulose; **10-E,** D-*lyxo*-hexulose (equil.).

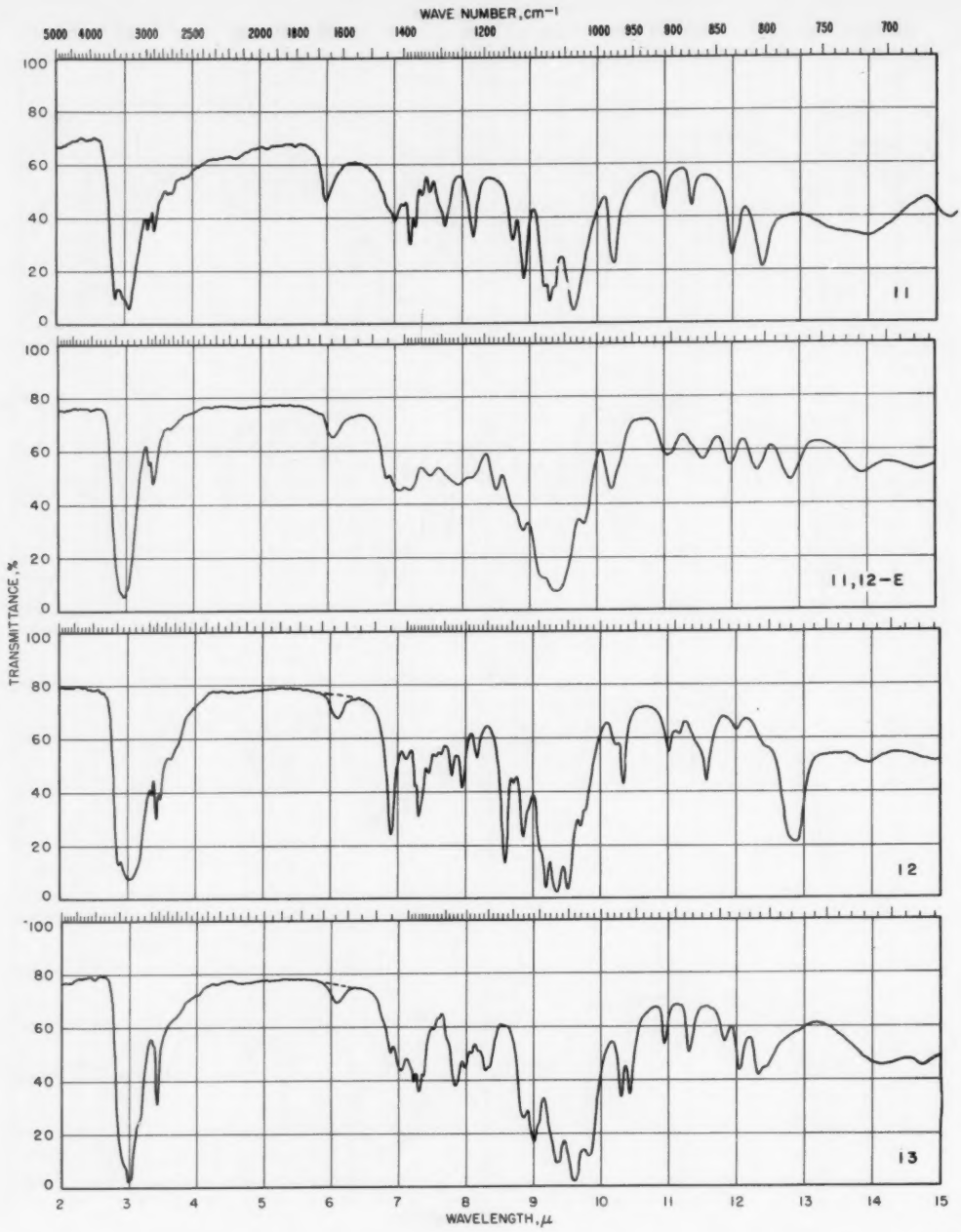

FIGURE 1. *Spectrograms of materials in potassium chloride pellets.*—Continued

11, 6-deoxy-α-L-mannose monohydrate; **11, 12-E,** 6-deoxy-L-mannose (equil.); **12,** 6-deoxy-β-L-mannose; **13,** α-D-mannose

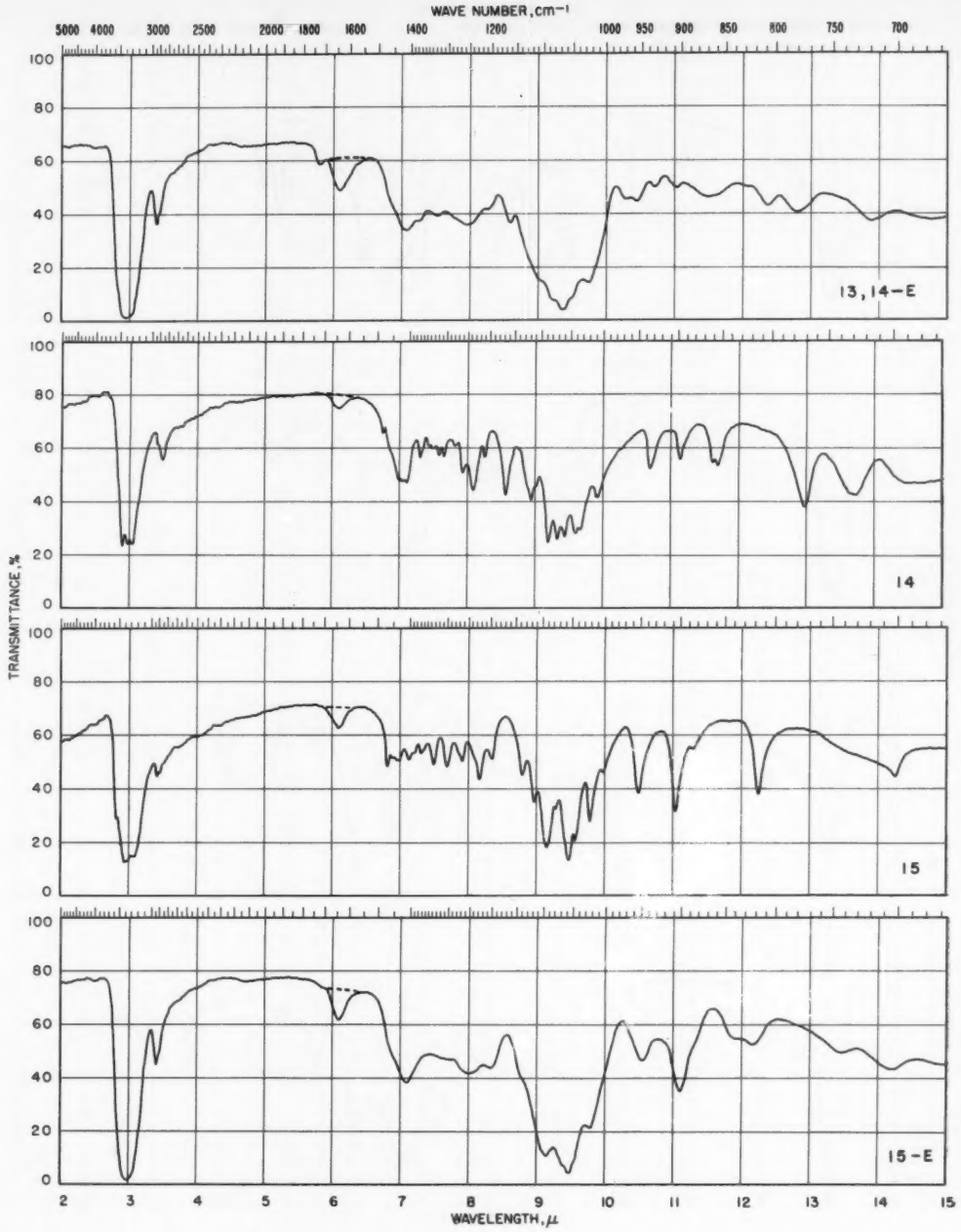

FIGURE 1. *Spectrograms of materials in potassium chloride pellets.*—Continued

13, 14-E, D-mannose (equil.); **14,** **β**-D-mannose; **15,** (?)-D-*manno*-heptulose; **15-E,** D-*manno*-heptulose (equil.).

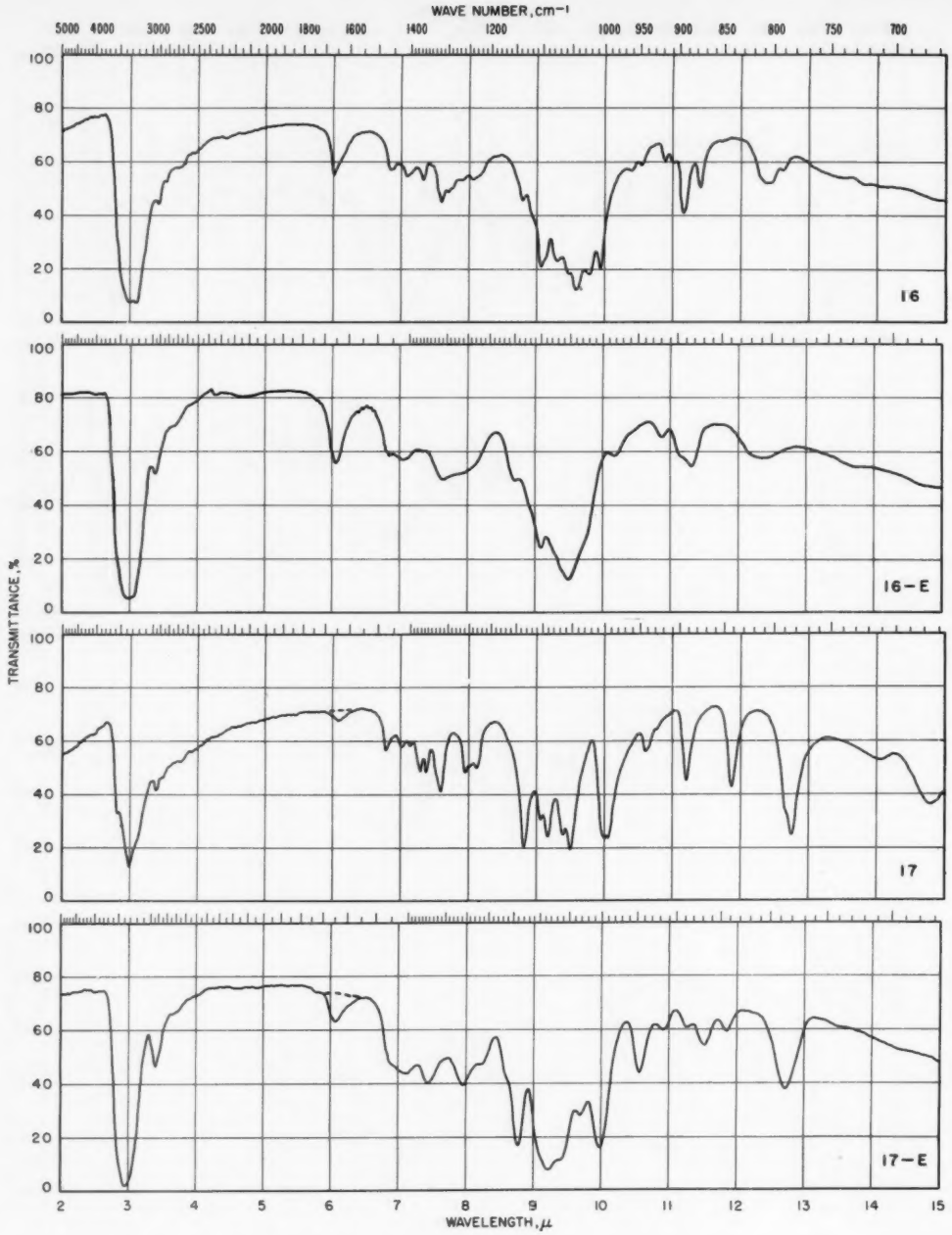

FIGURE 1. *Spectrograms of materials in potassium chloride pellets.*—Continued

16, (?)-D-gulose·0.5 $CaCl_2$·0.5 H_2O; **16-E**, D-gulose·0.5 $CaCl_2$ (equil.); **17**, *β*-D-arabinose; **17-E**, D-arabinose (equil.).

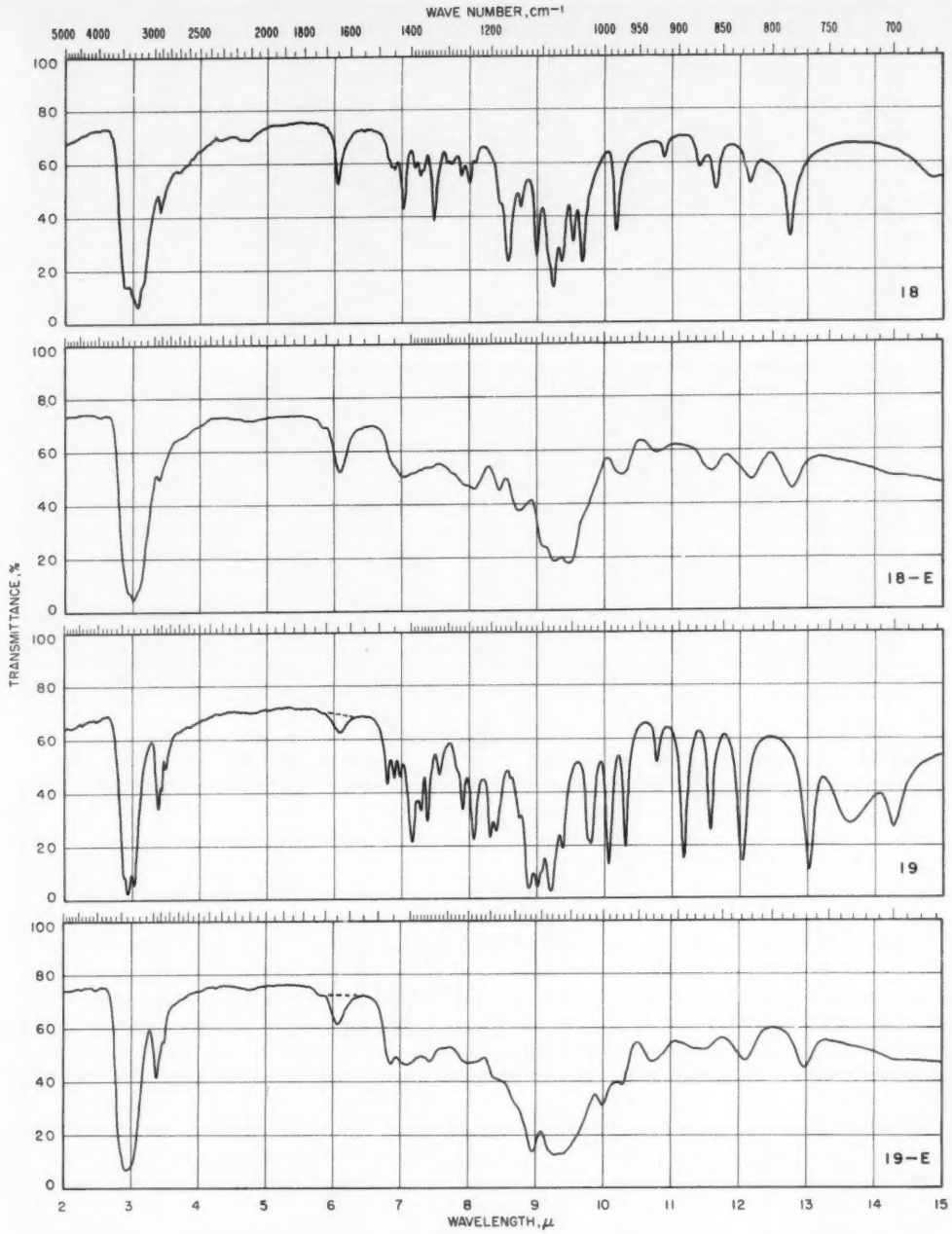

FIGURE 1. *Spectrograms of materials in potassium chloride pellets.*—Continued

18, (?)-D-*arabino*-hexulose·0.5 $CaCl_2$·1.5 H_2O; **18-E,** D-*arabino*-hexulose·0.5 $CaCl_2$ (equil.); **19** 3-*O*-methyl-(?)-D-*arabino*-hexulose; **19-E,** 3-*O*-methyl-D-*arabino*-hexulose (equil.).

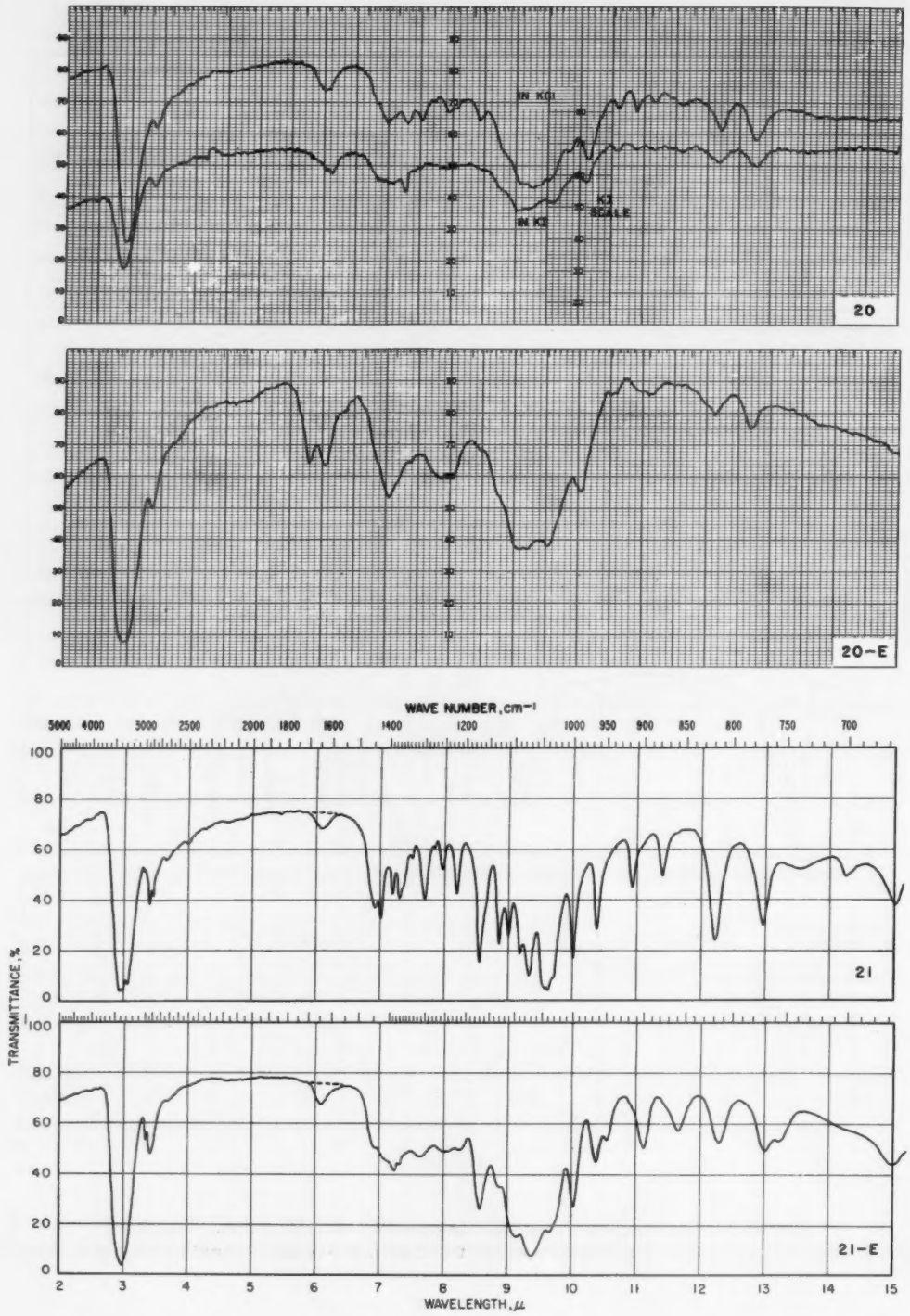

FIGURE 1. *Spectrograms of materials in potassium chloride pellets.*—Continued

20, β-D-*manno*-3-heptulose monohydrate; **20-E,** D-*manno*-3-heptulose (equil.); **21,** 6-deoxy-α-L-galactose; **21-E,** 6-deoxy-L-galactose (equil.).

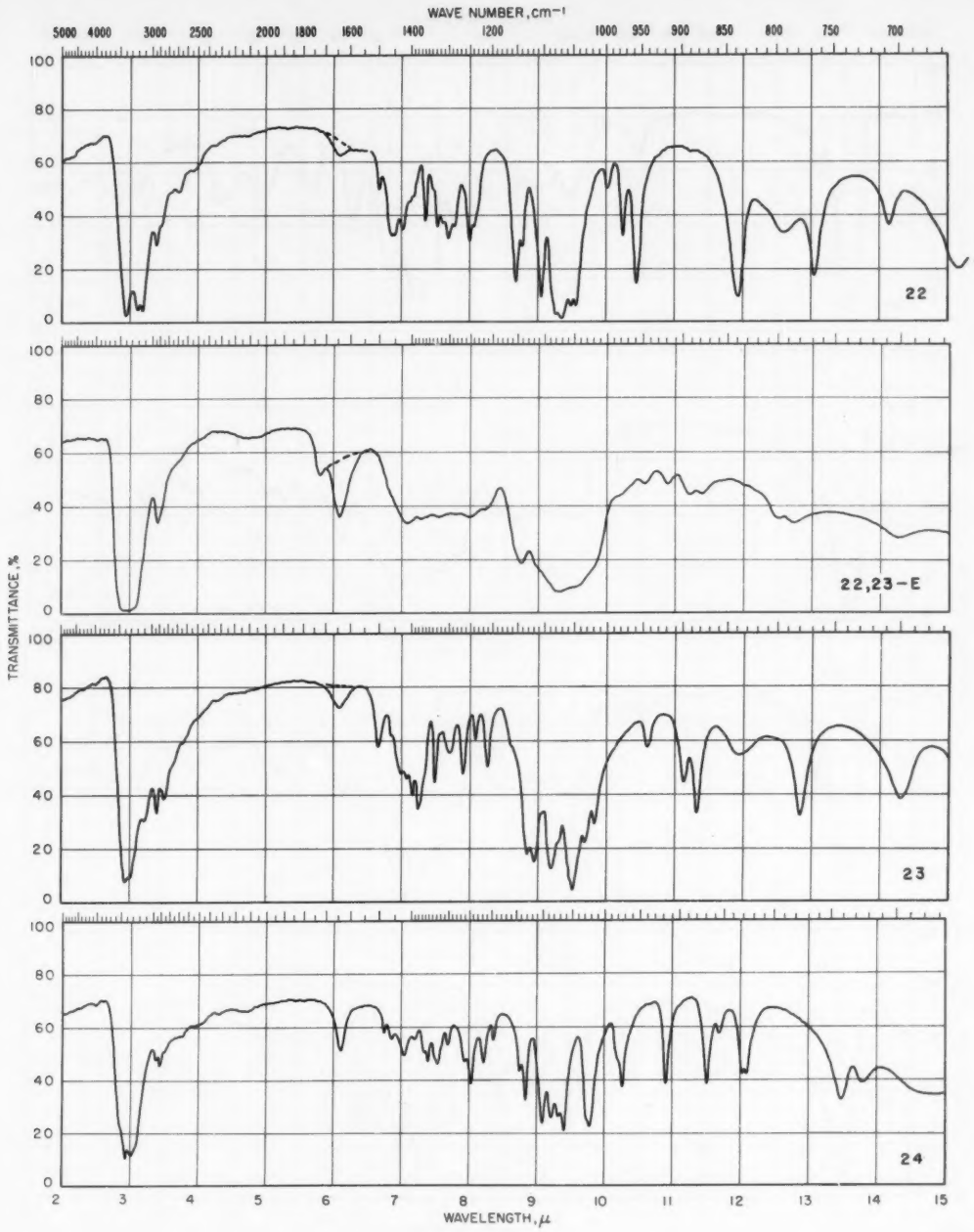

FIGURE 1. *Spectrograms of materials in potassium chloride pellets.*—Continued

22, α-D-galactose; **22,23-E,** D-galactose (equil.); **23,** β-D-galactose; **24,** 2,7- anhydro-β-D-*altro*-heptulose monohydrate.

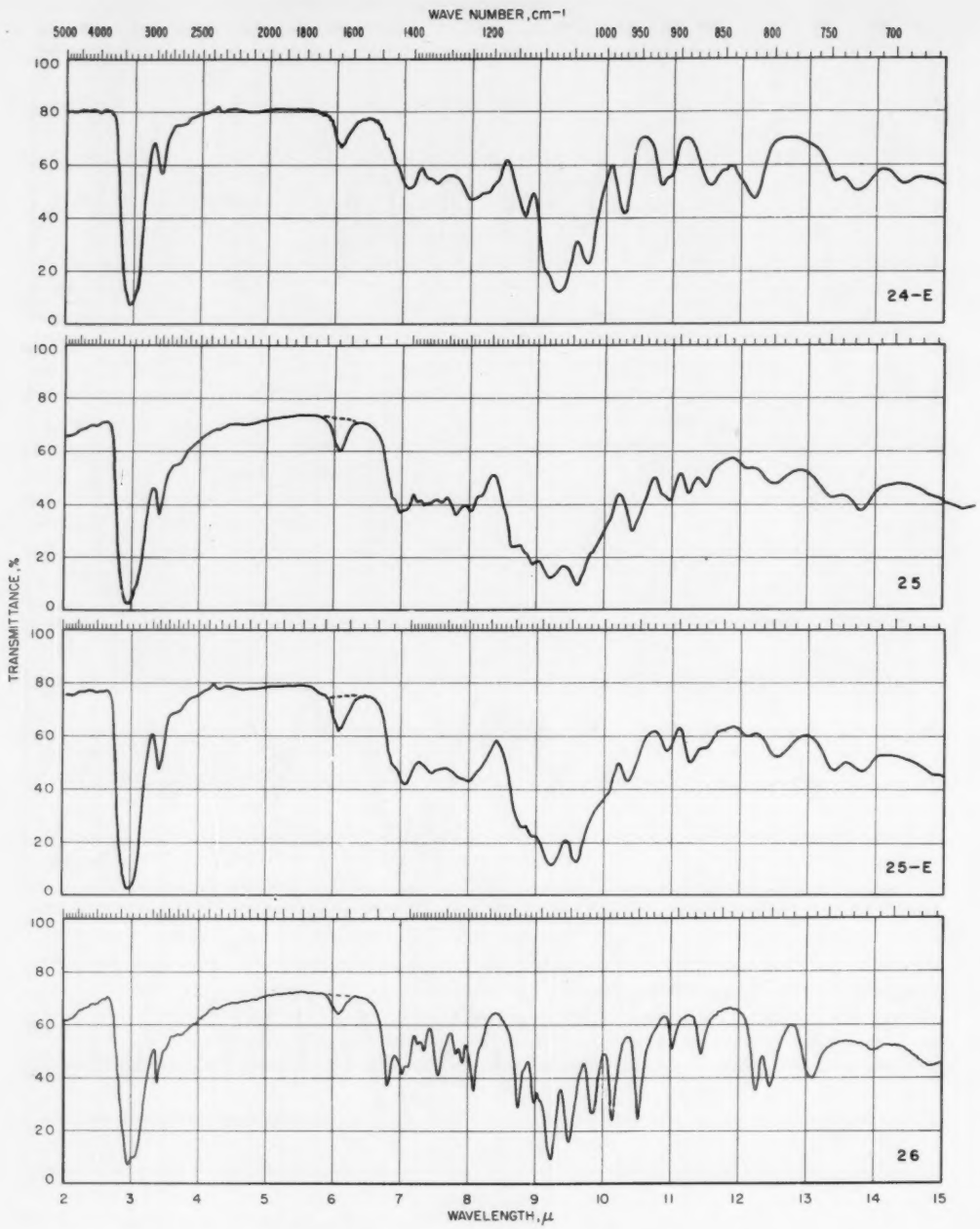

FIGURE 1. *Spectrograms of materials in potassium chloride pellets.*—Continued

24-E, mixture from treatment of compound 24 with 1 percent hydrochloric acid; **25,** β(?)-D-ribose; **25-E,** D-ribose (equil.); **26,** α-D-talose.

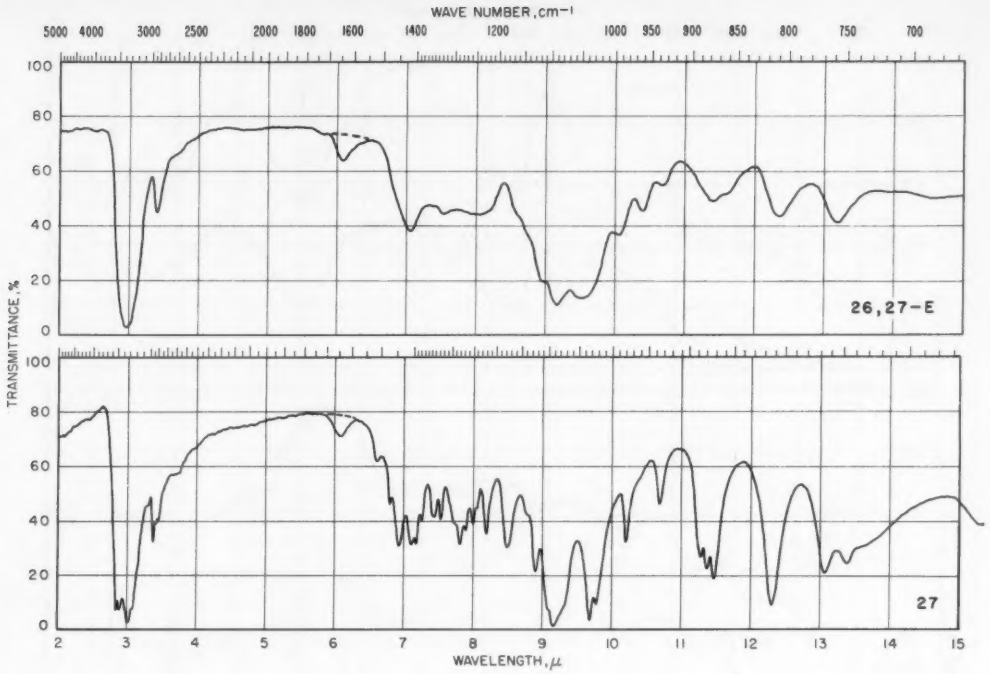

FIGURE 1. *Spectograms of materials in potassium chloride pellets.*—Continued

26,27-E, D-talose (equil.); **27,** β-D-talose.

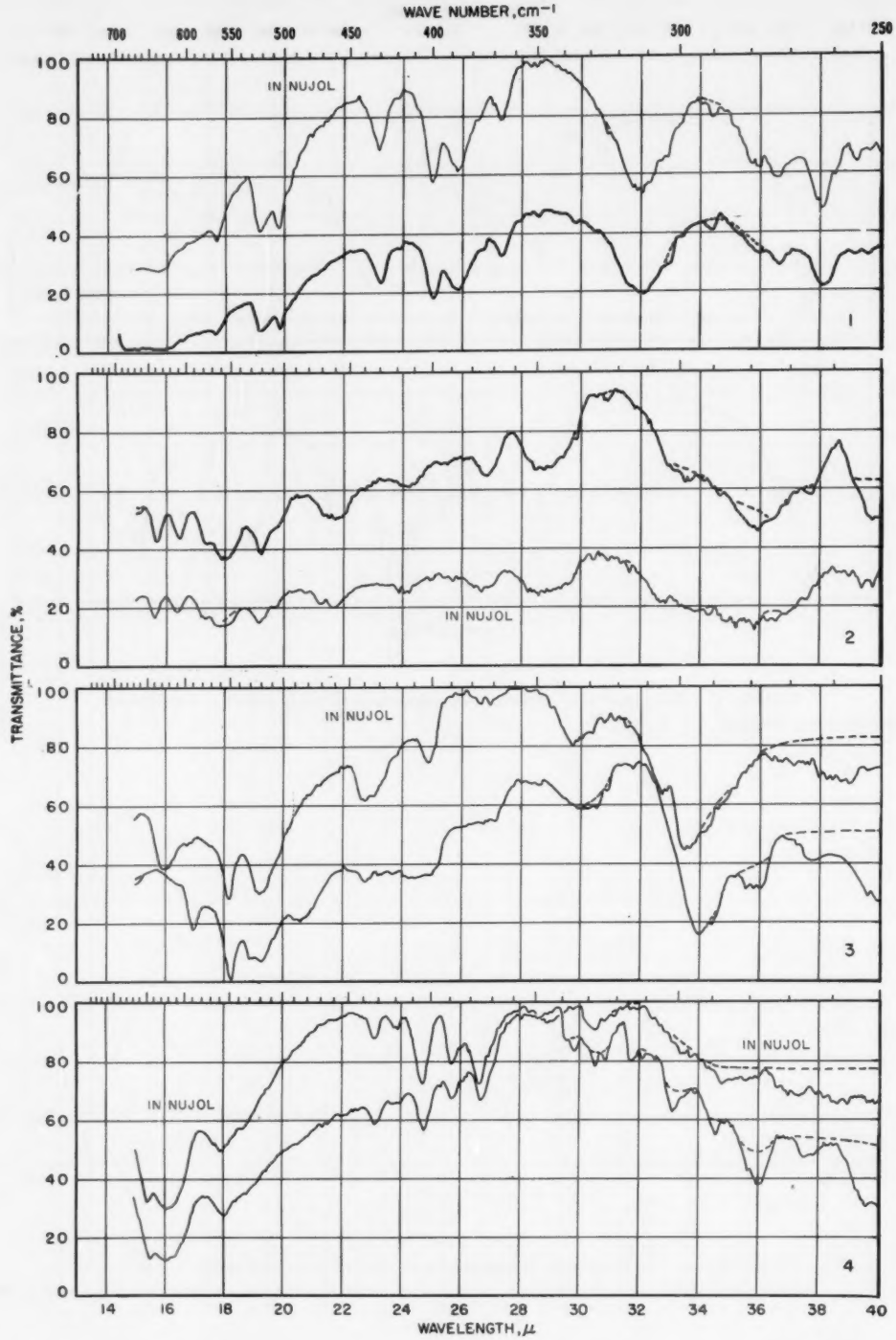

FIGURE 2. *Spectrograms of materials in Nujol mulls and in potassium iodide pellets.*

1, α-D-Xylose; 2, (?)-L-*xylo*-hexulose; 3, α-D-glucose·0.5 NaCl·0.5 H_2O; 4, α-D-glucose monohydrate.

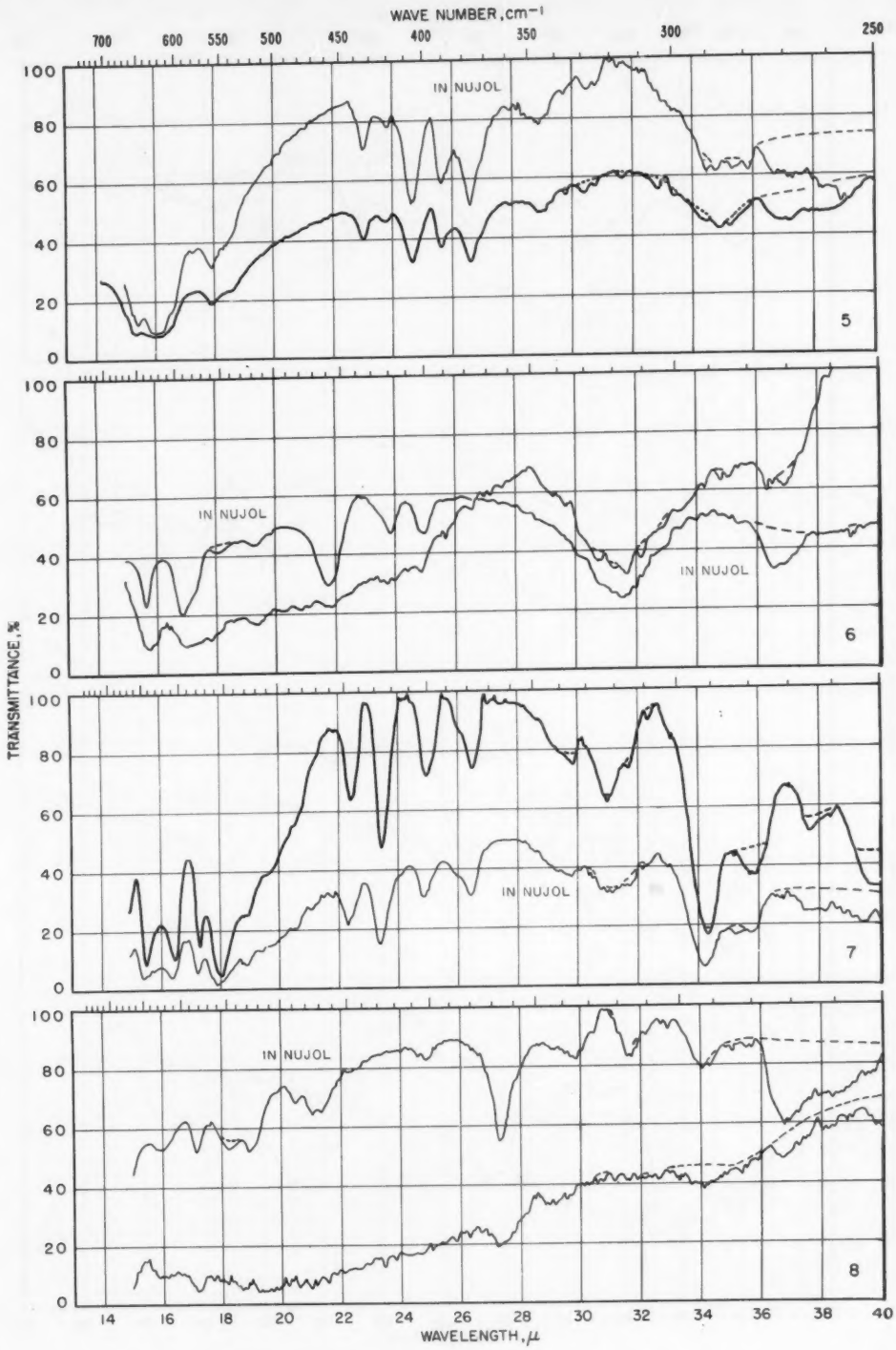

FIGURE 2. *Spectrograms of materials in Nujol mulls and in potassium iodide pellets.*—Continued

5, α-D-glucose; 6, β-D-glucose; 7, α(?)-D-*gluco*-heptulose; 8, α-D-lyxose.

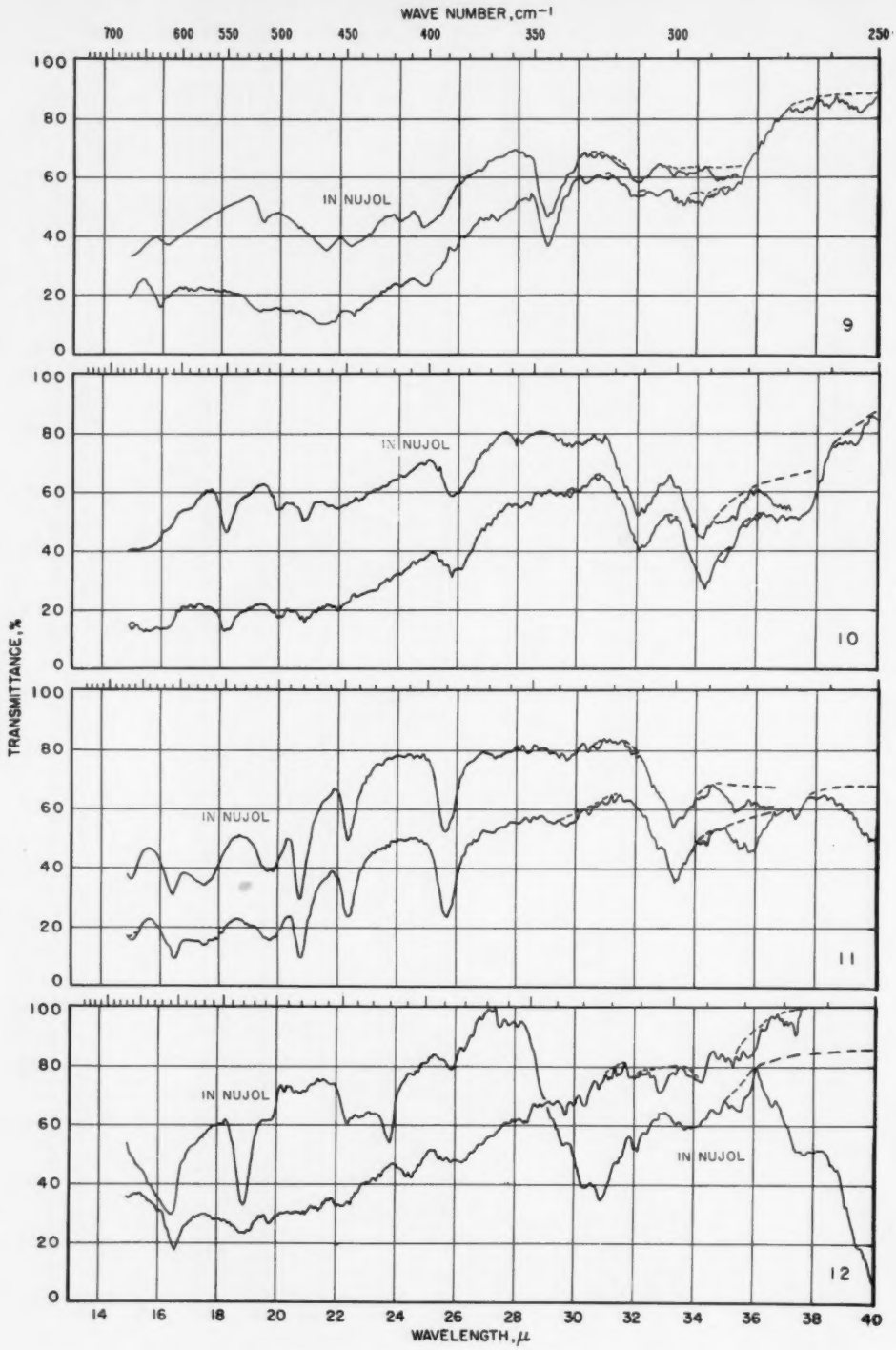

FIGURE 2. *Spectrograms of materials in Nujol mulls and in potassium iodide pellets.*—Continued

9, β-D-lyxose; 10, (?)-D-*lyxo*-hexulose; 11, 6-deoxy-α-L-mannose monohydrate; 12, 6-deoxy-β-L-mannose.

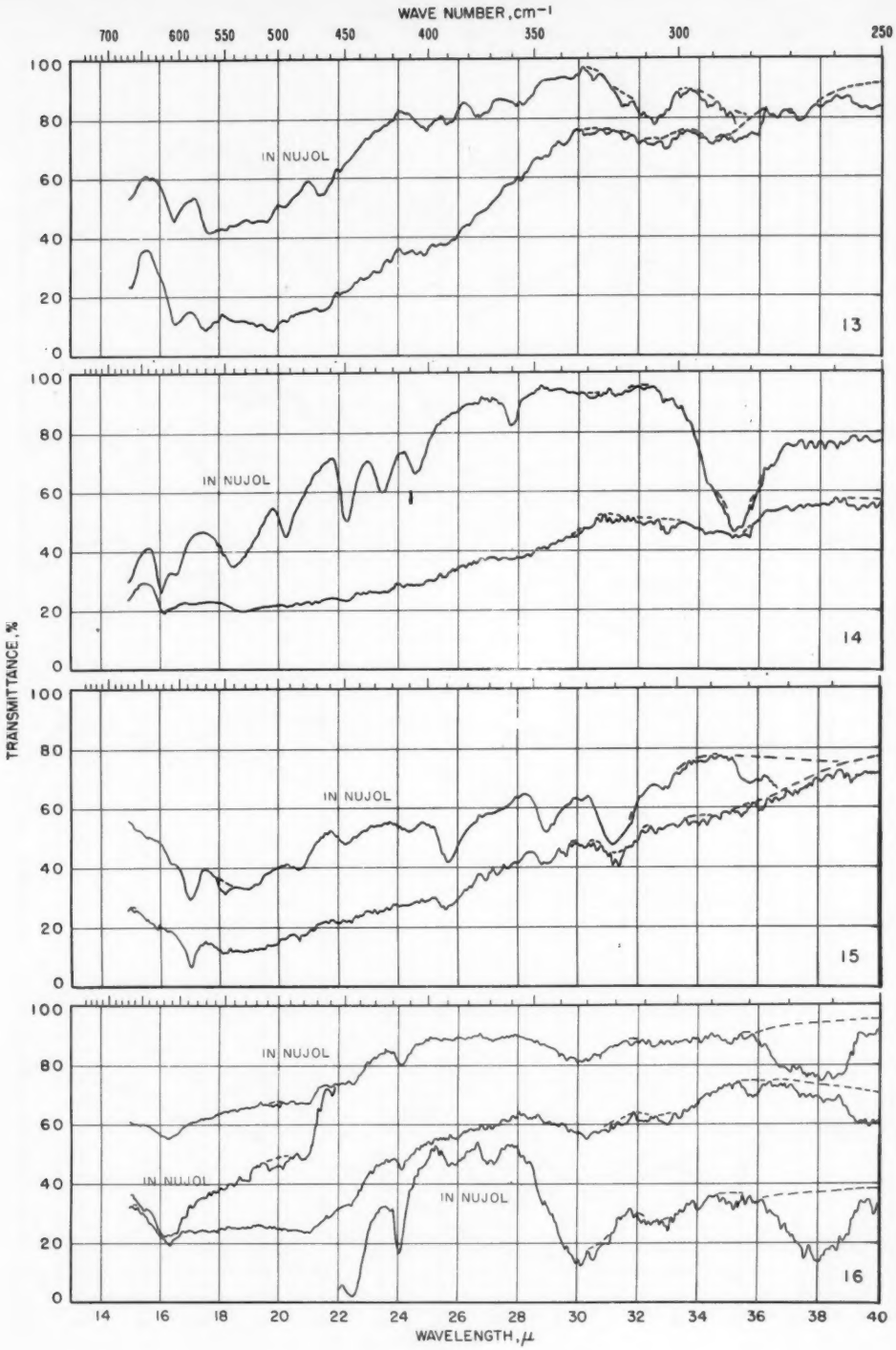

FIGURE 2. *Spectrograms of materials in Nujol mulls and in potassium iodide pellets.*—Continued

13, α-D-mannose; **14,** β-D-mannose; **15,** (?)-D-*manno*-heptulose; **16,** (?)-D-gulose·0.5 $CaCl_2$·0.5 H_2O.

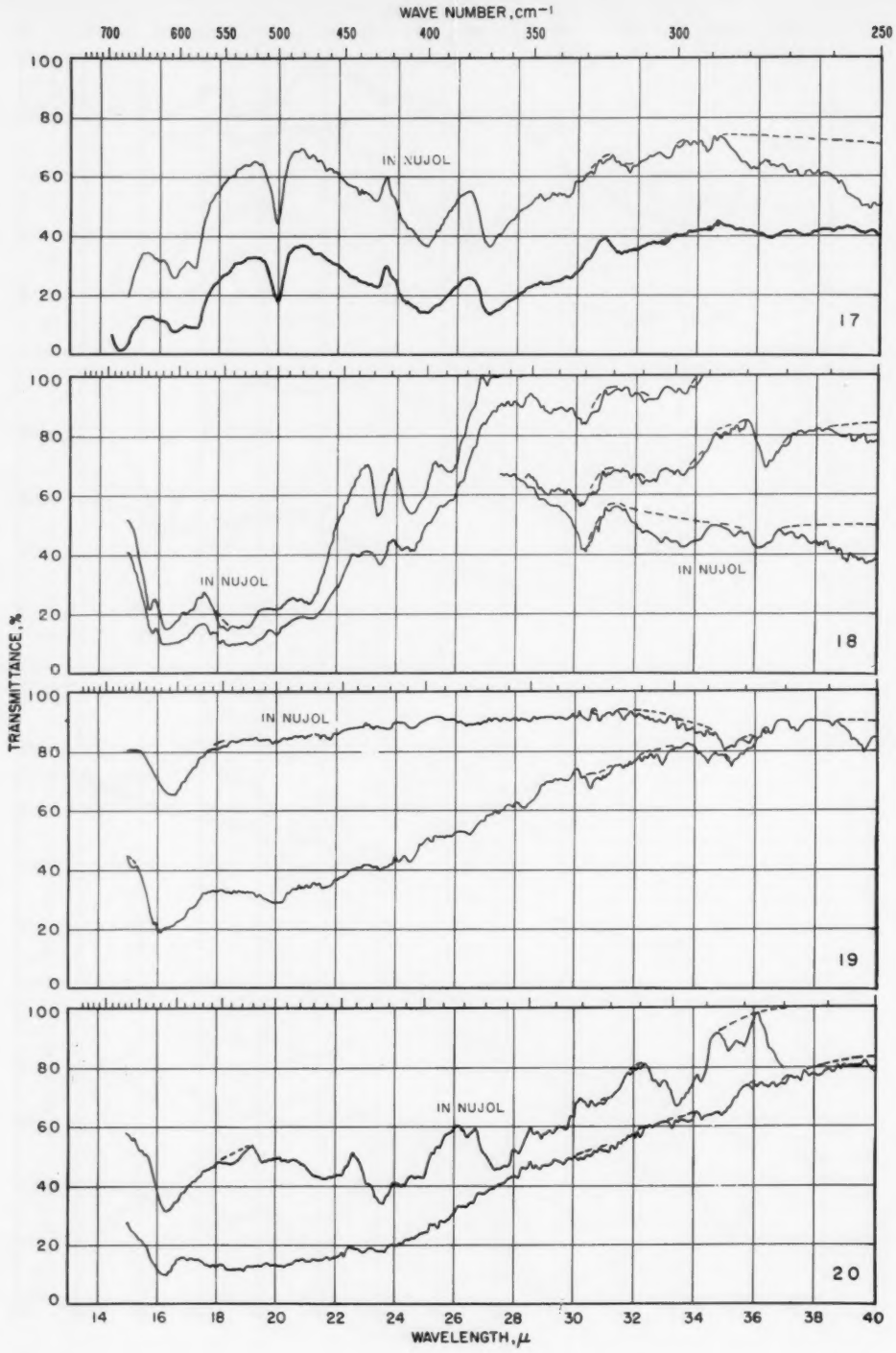

FIGURE 2. *Spectrograms of materials in Nujol mulls and in potassium iodide pellets.*—Continued

17, β-D-arabinose; **18**, (?)-D-*arabino*-hexulose-0.5 $CaCl_2$·1.5 H_2O; **19**, 3-*O*-methyl-(?)-D-*arabino*-hexulose; **20**, β-D-*manno*-3-heptulose monohydrate.

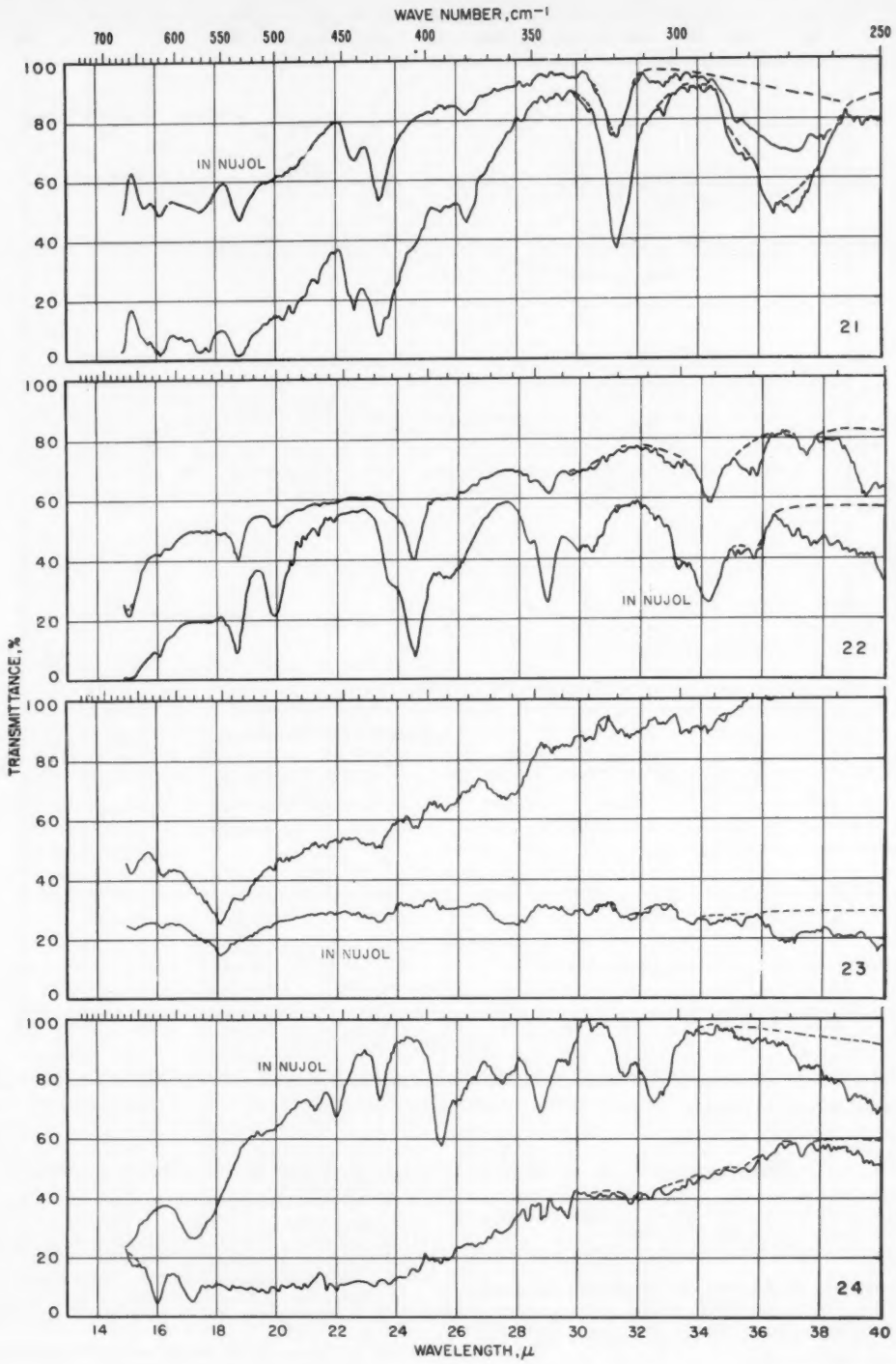

FIGURE 2. *Spectrograms of materials in Nujol mulls and in potassium iodide pellets.*—Continued

21, 6-deoxy-α-L-galactose; **22,** α-D-galactose; **23,** β-D-galactose; **24,** 2,7-anhydro-β-D-*altro*-heptulose monohydrate.

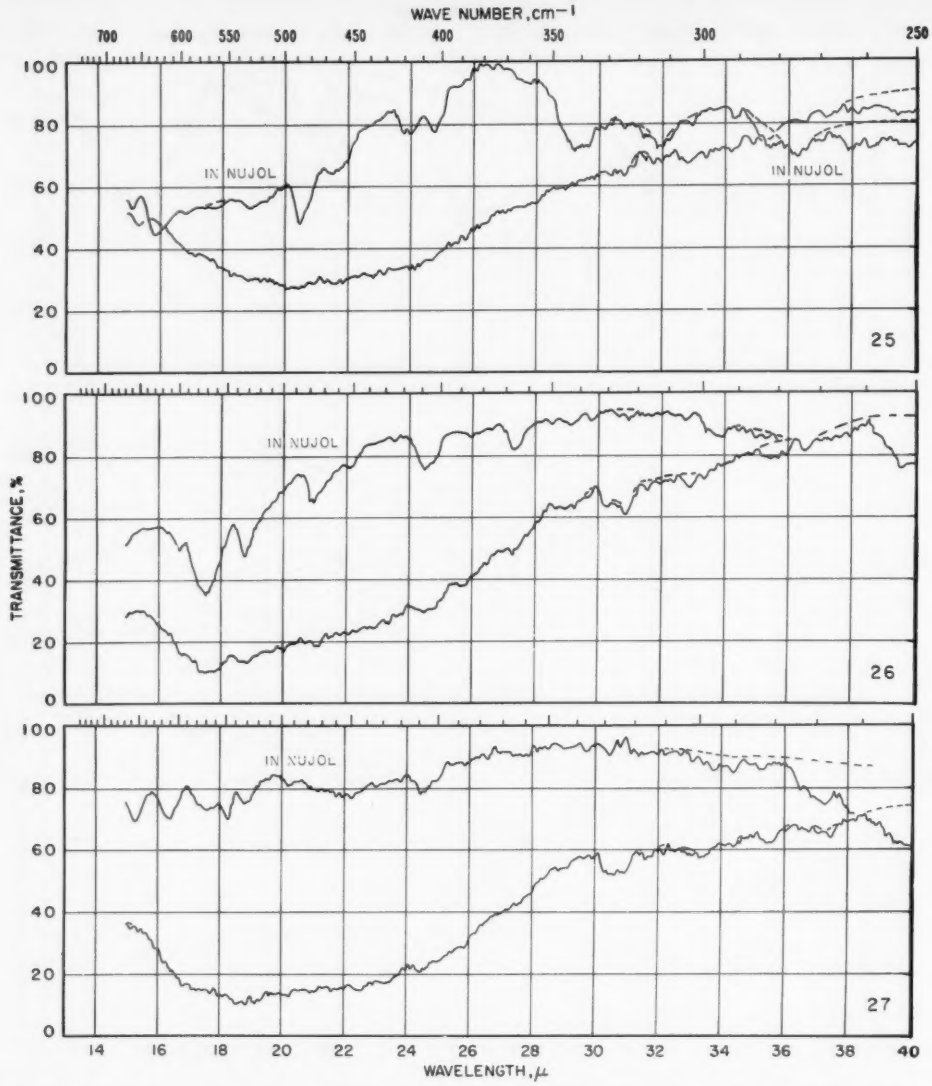

FIGURE 2. *Spectrograms of materials in Nujol mulls and in potassium iodide pellets.*—Continued

25, β(?)-D-ribose; 26, α-D-talose; 27, β-D-talose.

7. References

[1] H. S. Isbell, J. Research NBS **57,** 171 (1956) RP2707.
[2] L. P. Kuhn, Anal. Chem. **22,** 276 (1950).
[3] H. J. Marrinan and J. Mann, J. Appl. Chem. (London) **4,** 204 (1954).
[4] S. A. Barker, E. J. Bourne, R. Stephens, and D. H. Whiffen, J. Chem. Soc. **1954,** 3468.
[5] A. A. Konkin, D. N. Schigorin, and L. I. Nowikowa, Faserforsch. u. Textiltech. **8,** 85 (1957); Zhur. Fiz. Khim. **32,** 894 (1958).
[6] V. C. Farmer, Spectrochim. Acta **8,** 374 (1957).
[7] T. Urbański, W. Hofman, and M. Witanowski, Bull. acad. polon. sci., Sér. sci., Chim., géol. et géograph. **7,** 619 (1959).
[8] W. W. Coblentz, Carnegie Inst. Wash. Publ. **65,** 33 (1906).
[9] L. H. Rogers and D. Williams, J. Am. Chem. Soc. **60,** 2619 (1938).
[10] E. S. Barr and C. H. Chrisman, Jr., J. Chem. Phys. **8,** 51 (1940).
[11] F. S. Parker, Biochim. et Biophys. Acta **42,** 513 (1960).
[12] F. Lippich, Biochem. Z. **248,** 280 (1932).
[13] C. M. A. Kuyper, Koninkl. Ned. Akad. Wetenschap., Proc. Ser. B **62,** 137 (1959).
[14] N. K. Richtmyer and J. W. Pratt, J. Am. Chem. Soc. **78,** 4717 (1956).
[15] R. S. Tipson, H. S. Isbell, and J. E. Stewart, J. Research NBS **62,** 257 (1959) RP2960.
[16] R. S. Tipson and H. S. Isbell, J. Research NBS **64A,** 239 (1960).

(Paper 66A1-139)

JOURNAL OF RESEARCH of the National Bureau of Standards—A. Physics and Chemistry
Vol. 66A, No. 1, January–February 1962

Preparation of High Purity Trimethylborane [1]

Gaylon S. Ross, Delmo Enagonio, Clifford A. Hewitt, and Augustus R. Glasgow

(October 2, 1961)

The preparation of high-purity trimethylborane is described. Impurities were removed by fractionation of the ammonia adduct, NH_3:$B(CH_3)_3$. Mass spectrometric analyses were used during the fractionation to determine these impurities. After purification of the $B(CH_3)_3$ in the form of its ammonia adduct, high-purity hydrogen chloride was used to regenerate the $B(CH_3)_3$. This reaction and the subsequent distillation were carried out in a stainless steel system. Storage as a gas in stainless steel cylinders, rather than as a solid addition complex in glass vessels, eliminated the possibility of recontamination on regeneration. The purity of $B(CH_3)_3$ was determined cryoscopically to be 99.9 mole percent.

1. Introduction

Trimethylborane, $B(CH_3)_3$, is one of a series of boron compounds which have been prepared in high purity for use in the calorimetric [1][2] and spectrometric [2] research programs at the National Bureau of Standards. This highly purified material was successfully used as a neutron counting gas in proportional counters [3, 4] after trimethylborane prepared by other methods was found to be unsatisfactory because of impurities.

Trimethylborane is a toxic, reactive gas (bp −20 °C) which burns spontaneously on contact with air. These properties make purification and storage difficult. The compound is usually prepared in the form of the ammonia adduct, NH_3:$B(CH_3)_3$, which is subsequently treated with hydrogen chloride to liberate the trimethylborane gas. Inadequate purification of the adduct and further contamination during the reaction with the hydrogen chloride produces an impure product. In the preparation which is described in detail in this paper, the adduct was rigorously purified and then reacted with highly purified hydrogen chloride. This reaction and the subsequent fractional distillation of the trimethylborane were carried out in a stainless steel system. The product was stored as a liquid in stainless steel cylinders. Several hundred grams of trimethylborane were prepared, purified, and stored. The material was found to have a purity greater than 99.9 mole percent. This sample was used to establish reliable values for a large number of physical properties.

[1] Presented at the 128th meeting of the American Chemical Society at Minneapolis, Minn., September 11–16, 1955, before the Division of Industrial and Engineering Chemistry.

[2] Figures in brackets indicate the literature references at the end of this paper.

2. Purification of the Reactants

2.1. Ammonia Addition Compound

The ammonia addition compound of trimethylborane is a white crystalline solid that decomposes slowly in the presence of air and water vapor. All operations were therefore performed in sealed glass systems with the material under its own dissociation pressure. Two lots of the ammonia adduct, received from different sources,[3, 4] were used as starting material. The trimethylborane in these lots had been prepared from a methyl Grignard reagent and boron trifluoride in a *n*-butyl ether solution, under a nitrogen atmosphere, by a procedure similar to that described by Brown [6].

The system used in purifying and transferring the ammonia adduct is shown in figure 1. All parts of the glass system, except the glass ampoule containing the addition compound, were "flamed" to facilitate drying; the entire system was then evacuated to a pressure of 10^{-5} mm Hg. In the first lots processed, ampoules containing the original sample (D in fig. 1) were not equipped with break-off tips. In this case a scratch was filed on the narrowed neck of the ampoule at A so that it could be broken by the hammer B. The ampoule was attached to the transfer train at C by means of Apiezon wax W. Regular break-off tip ampoules were used in the second lots processed.

Fractionation of the ammonia adduct yielded six fractions as follows:

Fraction I—The addition compound in the ampoule D was cooled to approximately −78 °C and

[3] Robert C. Petry and Frank Verhoek, Ohio State Research Foundation Columbus, Ohio, supplied 280 g for use in the calorimetric and spectrometric studies of trimethylborane at the National Bureau of Standards.

[4] G. A. Ferguson, Jr., Naval Research Laboratories, Washington 25, D.C. supplied 282 g. The trimethylborane derived from this quantity of adduct was used as a neutron counting gas in proportional counters at the Naval Research Laboratories.

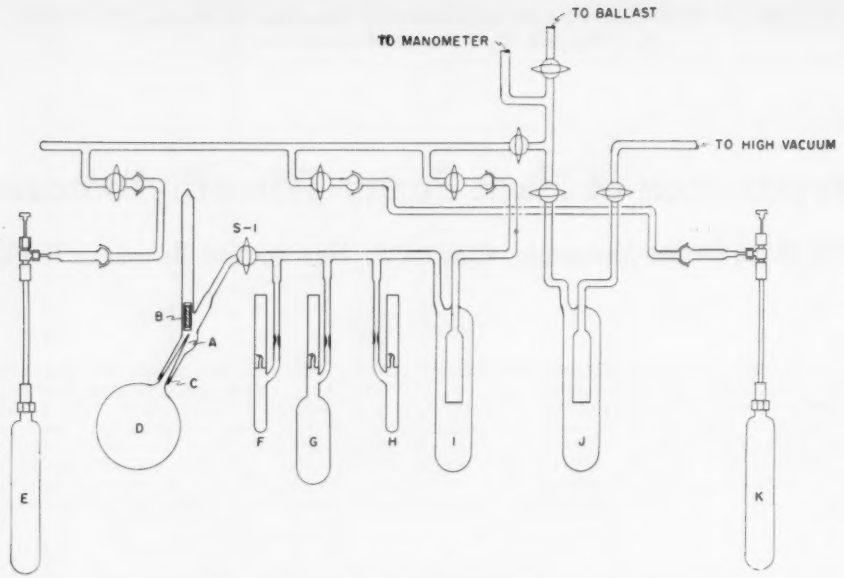

FIGURE 1. *Apparatus for purifying ammonia trimethylborane.*

then the tip of the ampoule was broken. The vapor phase existing above the sample at this temperature was collected in cylinder E, which was cooled with a liquid nitrogen bath. Mass spectrometric analysis showed this fraction to contain 30 percent air, 15 percent CCl_4, and 55 percent $B(CH_3)_3$.[5] These impurities could have been introduced during the original preparation or transfer because carbon tetrachloride was used to clean the system.

Fraction II—The material remaining in ampoule D was heated with a water bath at about 40 °C. The gaseous dissociation products were condensed in traps I and J, which were cooled with solid carbon dioxide and liquid nitrogen, respectively. The contents of this second trap (J) were transferred to metal cylinder K. Analysis of this material showed that it contained 60 percent CH_4, 20 percent CH_3OH, 5 percent air, 15 percent $Al(CH_3)_3$. Methane and methanol are logical oxidation and thermal degradation products of trimethylborane. The presence of aluminum trimethyl, while surprising, leads one to suspect that aluminum must have been present in the magnesium used in the preparation of the methyl Grignard reagent. At −78 °C, the temperature of the first trap I, there is little dissociation of the ammonia adduct, and the ammonia and trimethylborane generated by dissociation of the adduct at 40 °C [7] were successfully retained by reassociation. Aluminum trimethyl, however, has an appreciable vapor pressure at this temperature and consequently passed on into the liquid nitrogen trap.

Fraction III—The material retained at −78 °C in trap I was then transferred to trap J and subsequently to ampoule G. A sample for analysis was collected in ampoule F. In the analysis of the ammonia adduct, the sample was introduced as a gas into the spectrometer. Since ammonia is adsorbed on the walls of the inlet system, only the trimethylborane was detected. For this reason, the results indicated only the presence of trimethylborane rather than ammonia trimethylborane. The material in ampoule G was sealed and reserved for subsequent reaction with hydrogen chloride in the preparation of trimethylborane.

Fraction IV—After removal of fractions I, II, and III, a yellowish solid remained in the original ampoule. This ampoule was heated to 100 °C, and the gaseous products were collected in trap I, which was cooled with liquid nitrogen. After transfer to ampoule H, this material was found to contain $NH_2B(CH_3)_2$ (dimethylaminoboron), $B(CH_3)_3$, and NH_3.

Fraction V—The glass stopcock, S–1, was then closed and the glass tubing broken to the right of the stopcock. The residue remaining was heated to 150 °C and the gaseous products were introduced directly into the mass spectrometer. The primary components of this fraction were trimethylborane, ethyl-methyl boron compounds, and an unknown amino boron compound.

Fraction VI—Approximately two percent of the original material remained as a nonvolatile residue. This yellow solid is water-soluble and is presumed to be an organo-boron mixture of unknown composition.

2.2. Hydrogen Chloride

Commercial hydrogen chloride gas contains organic impurities and possibly carbon dioxide. The difficulty involved in removing these impurities suggested

[5] These analyses were performed by F. L. Mohler and V. H. Dibeler of this Bureau and are given in mole percent.

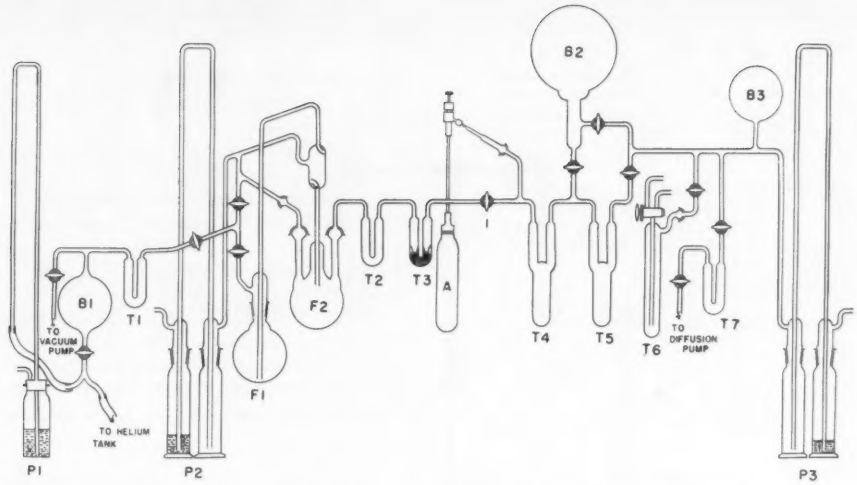

FIGURE 2. *Apparatus for preparing hydrogen chloride gas of high purity.*

the preparation of the hydrogen chloride gas by synthesis from purified sulfuric acid and recrystallized sodium chloride. The apparatus for preparing the hydrogen chloride is shown in figure 2. This apparatus was all glass except for the stainless steel cylinder A. This cylinder was one of a group of 3, all of which had been tested for leaks with a helium leak detector after filling with helium to a pressure of 800 lb/in^2. Sulfuric acid was placed in flask F–1 and sodium chloride in F–2. After several flushings with dry helium and subsequent evacuations, a portion of the sulfuric acid was introduced by means of helium pressure into flask F–2. The hydrogen chloride produced was carried along in a continuous stream of dry helium. Pressure regulators P–1, P–2, and P–3, partially filled with mercury as shown, were used to regulate pressures and flow of the helium and hydrogen chloride, and to act as safety valves.

Traps T–2 and T–3 were cooled to −78 °C and trap T–4 to −196 °C; T–3 was packed with glass wool to retain any solid particles. After being dried in traps T–2 and T–3, the hydrogen chloride gas was condensed in trap T–4. When the reaction was completed, stopcock 1 was closed and the portion of the apparatus to the right of this stopcock was evacuated. This process removed the bulk of the helium present. The residual helium was removed by alternately melting and freezing the hydrogen chloride. The released helium expanded into the ballast bulb B–2 and was removed by pumping through trap T–7, which was cooled to −196 °C to prevent fouling of the pumping system with hydrogen chloride. Finally, trap T–4 was warmed to approximately −120 °C and the hydrogen chloride transferred to T–5 by cooling this trap to −196 °C. The hydrogen chloride was transferred back to T–4 and finally collected in the weighed metal cylinder A. In this manner approximately 450 g of helium-free hydrogen chloride was prepared.

3. Preparation of Trimethylborane

The addition compound, NH_3:$B(CH_3)_3$ (fraction III), was reacted with hydrogen chloride in a stainless steel reactor. The reactor and the purification train are shown in figure 3. The metal cylinders of this train, including the reactor, were filled with helium to a pressure of 380 lb/in.^{2} and tested for leaks with a helium leak detector. Before use, all metal and glass components except joints and valves were heated to about 300 °C while the system was evacuated. Teflon-packed stainless steel valves of a modified Stimson type [8] and stainless steel connectors were located as shown. Trap T–1 and the section containing the ampoules of ammonia trimethylborane (A–1, 2, 3) were constructed of glass. Steel-to-glass connections were made by the use of a stainless steel male ball-joint and a glass female joint sealed with Apiezon N grease. The reaction vessel, a 500 ml stainless steel cylinder C–3, and the stainless steel trap T–2 were equipped with reentrant wells W–1 and W–2 for the insertion of thermocouples. Well W–2 contained three thermocouples: one at the bottom of the reactor, one in the middle of the distillation column R, and one near the top of this column.

The addition compound was treated with hydrogen chloride in the following manner. Batches of from 50 to 150 g of adduct were transferred from the glass ampoules A–1, etc., and deposited as uniformly as possible over the inside surface of the reactor. Total transfer of adduct was considered complete when no solid remained in the glass ampoules, at which time valve 5 was closed. Cylinder C–1 contained a weighed amount of hydrogen

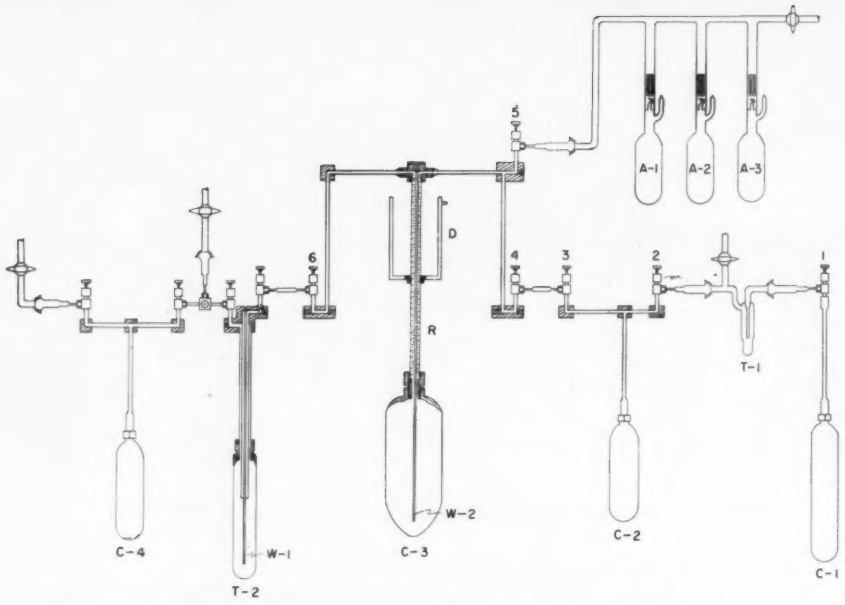

FIGURE 3. *Apparatus for preparing and purifying trimethylborane.*

chloride sufficient to react with 95 percent of the addition compound used, assuming that all of the hydrogen chloride reacted. Valves 1, 2, 3, and 4 allowed for transfer to or from vessels C–1, T–1, C–2, and C–3 and for isolation of parts. Five-gram amounts of hydrogen chloride from cylinder C–1 were condensed in trap T–1, cooled to −78 °C, and then distilled at this temperature into cylinder C–2 which was cooled by a liquid nitrogen bath. The contents of cylinder C–2, warmed to room temperature, were allowed to react with the adduct in the reactor C–3. The glass trap T–1 allowed one to see the amount of hydrogen chloride condensed in it from cylinder C–1 or recondensed from cylinder C–2. It was found that the reaction with 5-g increment-of hydrogen chloride was rapid and orderly. Substantially all the hydrogen chloride was transferred in this way; the residual gas in the weighed cylinder was then condensed directly in the reactor by cooling it with a liquid nitrogen bath. To react the last traces of hydrogen chloride, the reactor was allowed to warm to room temperature and, with all valves closed, was allowed to stand for at least 24 hr. Vigorous shaking of the reactor after removing it and its connections from the train also helped to complete the reaction.

Trimethylborane was separated from the reaction mixture by distillation. For this process the top of the reactor was equipped with a small distillation column R, which had a spiral of stainless steel wire as packing. During distillation, a liquid bath in container D was kept near −40 °C to provide reflux, and the reactor C–3 was kept near 0 °C. Trap T–2 was cooled to about −196 °C and the entire left side of the train (i.e., to the left of valve 6) was continuously evacuated. After a period of reflux, valve 6 was partially opened to allow distillation of a small portion of the trimethylborane into trap T–2. Then valve 6 was closed to return the column to total reflux. This process was repeated until all the trimethylborane was transferred.

During this process appreciable amounts of hydrogen, methane, and other gases, indentified by mass spectrometric analysis, were removed from the system while the trimethylborane was retained in trap T–2. After distillation was complete, T–2 was warmed to −78.5 °C and the vapor pressure of the liquid at that temperature was measured directly with a mercury manometer. If it was not greater than 31 mm Hg, the sample was transferred directly to cylinder C–4. From preliminary work, it was found that hydrogen chloride was the material chiefly responsible for any pressure greater than 31 mm Hg at −78.5 °C. If the pressure was greater than 31 mm Hg, the trimethylborane was transferred back to the reactor and allowed to come to room temperature and remain at this temperature for an additional 24 hr. After this, the distillation process was repeated. This procedure was found to give material free of hydrogen chloride as determined by the mass spectrometric analyses.

In the first series of runs, a total of 180 g of trimethylborane in a purified form was prepared. The first preparation (33 g) had a purity of 99.7 mole percent, the second and third (147 g) were 99.9 mole percent pure, as determined by cryoscopic-calorimetric procedures [1]. An additional 176 g of trimethylborane was prepared later and was also found to be 99.9 mole percent pure. Infrared analysis [2] of the material showed that several bands pre-

viously reported and ascribed to trimethylborane [5] were absent; these bands are presumed to have been caused by impurities.

Samples of the purified trimethylborane were stored at −78 °C pending measurements of certain physical constants. Later, the samples in stainless steel cylinders were kept at room temperature for several weeks and their vapor pressures at −78.5 °C redetermined. No significant change in pressure was observed, indicating that the compound is stable at room temperature.

The purified trimethylborane has been used in other laboratories of this Bureau for measurement of infrared spectrum [2], heat capacity, heats of fusion, transition, and vaporization and vapor pressure [1]. At the Naval Research Laboratory it has been used in a study of electron mobility in $B(CH_3)_3$ [3] and as a neutron counting gas for proportional counters [4].

(Paper 66A1–140)

4. References

[1] G. T. Furukawa and R. P. Park, Heat capacity, heats of fusion, transition, vaporization, and vapor pressure of trimethylborane, $B(CH_3)_3$, presented before the Symposium, From Borax to Boranes, of the Division of Inorganic Chemistry, 133d Meeting of the American Chemical Society, San Francisco, California, April 15–18, 1958.

[2] J. E. Stewart, J. Research NBS **56,** 337 (1956) RP2684.

[3] G. A. Ferguson, Jr., and F. E. Jablonski, Rev. Sci. Instru. **28,** 893 (1957).

[4] G. A. Ferguson, C. W. Peters, and F. E. Jablonski, An investigation of boron trimethyl counters, Progress Report of Naval Research Laboratories, March 1956 issue.

[5] G. Goubeau and H. J. Becher, Z. anorg. u. allgem. Chem. **268,** 1 (1952).

[6] H. C. Brown, J. Am. Chem. Soc. **67,** 374 (1945).

[7] H. C. Brown, H. Bartholomay, Jr., and M. D. Taylor, J. Am. Chem. Soc. **66,** 435 (1944).

[8] A. R. Glasgow and G. S. Ross, Anal. Chem. **26,** 2003 (1954).

JOURNAL OF RESEARCH of the National Bureau of Standards—A. Physics and Chemistry
Vol. 66A, No. 1, January–February 1962

Reaction of Several Aminopyrimidines With Formaldehyde

Gerald L. McLeod [1]

(August 29, 1961)

Formaldehyde has been shown to react with 2-aminopyrimidine (II) and 2-(methylamino)pyrimidine (V) at room temperature to give the corresponding methylol derivatives or the corresponding methylenebis(aminopyrimidines). The reaction of formaldehyde with 2-amino-4,6-dichloro-5-methylpyrimidine (VII) and also its failure to react with 2-(dimethylamino)pyrimidine (IX) are cited as evidence that the pyrimidine ring is not involved in the reaction.

1. Introduction

A number of investigations have been made on the melamine-formaldehyde reaction, and several mechanisms [1–5][2] have been suggested. The complex structures of the triamino-1,3,5-triazines made it desirable to study simpler model compounds. A logical model compound, 2-amino-1,3,5-triazine (Ia), has been reported [6–8] not to give the usual amine reactions because it tautomerizes to the iminoid structure (Ib). Addition of more amino groups to

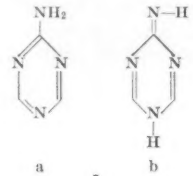

a b

I

the triazine ring shifts the equilibrium to the benzenoid structure [8], thereby increasing the tendency to give amine reactions.

In the present study, it was found that 2-amino-1,3,5-triazine does not react with formaldehyde under the conditions used. The 2-aminopyrimidines, which show a structural similarity to the aminotriazines, give many typical amine reactions and were selected as model compounds.

2. Results and Discussion

The reaction between equimolar amounts of 2-aminopyrimidine (II) and formaldehyde in neutral or slightly alkaline media at room temperature gave *N*-(2-pyrimidinyl)aminomethanol (III). The *N*-methylol structure is supported by infrared analysis. The spectrum of 2-aminopyrimidine has two absorption bands near 3,320 and 3,170 cm^{-1} which are attributed to N—H asymmetric and symmetric stretching modes [9]; the methylol compound, III, shows one fairly broad band at 3,225 cm^{-1}. The occurrence of both inter- and intra-molecular hydrogen bonding in III could cause a lowering of the OH stretching frequency, allowing it to overlap the N—H stretching band. Treatment of the methylol III with boiling, dilute hydrochloric acid gave 2,2′-(methylenediimino)dipyrimidine (IV). This compound was also prepared from 2-aminopyrimidine (II) and half a molar equivalent of formaldehyde, using a procedure similar to one previously reported [10]. Compound IV was also prepared by the reaction of 2-aminopyrimidine (II) with the methylol III.

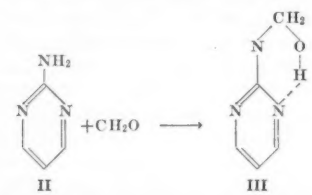

II III

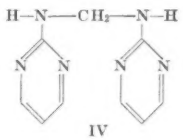

IV

The compound 2-(methylamino)pyrimidine (V) was also found to give a methylol derivative on reaction with formaldehyde. This methylol derivative of V was less stable than the methylol derivative III and was not obtained in a pure form. It did, however, react with 2-(methylamino)pyrimidine (V) to give 2,2′-methylenebis(methylimino)dipyrimidine (VI), which was also formed when V was reacted with half a molar equivalent of formaldehyde. In contrast with the methylol III, treatment of the methylol compound of V with dilute hydrochloric acid did not give the corresponding methylenebis derivative VI.

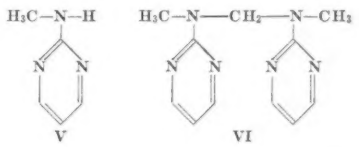

V VI

[1] Present address: Itek Laboratories, Inc., Lexington 73, Mass.
[2] Figures in brackets indicate the literature references at the end of this paper.

The following evidence indicates that formaldehyde reacts exclusively with the amino group and not with the pyrimidine ring. If formaldehyde reacted with the carbon atoms of II or V, the amino groups would be unchanged. This postulate is not in accord with the observed change in the infrared spectra. As mentioned previously, the two bands representing N – H stretching in II are transformed into a single broad band between the two when reacted with formaldehyde. Similarly, 2-(methylamino)pyrimidine (V), which shows a single N—H stretching vibration near 3,250 cm^{-1}, gives, on reaction with formaldehyde, a product showing no N – H stretching bands. Furthermore, an aminopyrimidine with the ring-carbon atoms blocked was found to react with formaldehyde. 2-Amino-4,6-dichloro-5-methylpyrimidine (VII) gave 2-2′-(methylenediimino) bis (4,6-dichloro-5-methylpyrimidine) (VIII). The infrared spectrum of VII shows, as expected, two, N—H stretching bands near 3,460 and 3,340 cm^{-1}, whereas

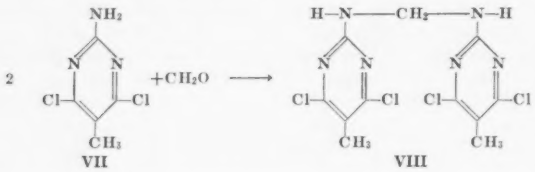

VII VIII

that of the methylenebispyrimidine VIII shows only one N—H absorption band near 3,300 cm^{-1}.

A compound with the amino group blocked, 2-(dimethylamino)pyrimidine (IX), was recovered

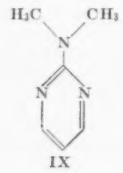

IX

unchanged after attempts to react it with aqueous formaldehyde. The failure to react demonstrates the reluctance of the pyrimidine-ring carbon atoms to react with formaldehyde under the conditions used.

The potential ability of 2-aminopyrimidine (II) to exist to a slight extent in the imine form [9,11] suggests the possibility that the reaction product with formaldehyde might have structure X and that the product from the reaction with 2-(methylamino)-pyrimidine (V)

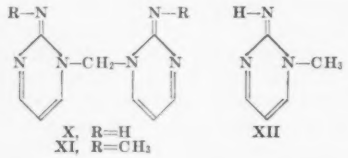

X, R=H
XI, R=CH_3 XII

might be XI. The infrared spectra of all the pyrimidines studied in the present investigation show an absorption band of medium intensity in the region near 800 cm^{-1}. This band is consistent with data observed elsewhere [12] and has been assigned to pyrimidine-ring vibration. Examination of the infrared spectrum of 1,2-dihydro-2-imino-1-methylpyrimidine (XII), which can be prepared from 2-aminopyrimidine (II) and methyl iodide, reveals that there is no band near 800 cm^{-1}. This observation might be explained by the fact that the benzenoid type of resonance present in the other pyrimidine rings cannot exist in the imine XII. The structural similarity of the imine XII to structures X and XI can readily be seen. Consequently, it might be expected that compounds with imine structures X and XI would not show a pyrimidine-ring vibration band near 800 cm^{-1}. In fact, the infrared spectra of the products actually obtained from the reaction of 2-aminopyrimidine (II) and 2-(methylamino)pyrimidine (V) with formaldehyde reveal the presence of the ring absorption-bands at 800 and 795 cm^{-1}, respectively. These bands further support the assignment of structures IV and VI to these compounds.

1,2-Dihydro-2-imino-1-methypyrimidine (XII) has been described [9] as a yellow compound. This fact was confirmed in the present investigation, and it suggested that compounds having the iminoid structures X and XI would also be colored. By contrast, 2,2′-(methylenediimino)dipyrimidine (IV) and 2,2′-[methylenebis(methylimino)]dipyrimidine (VI) are found to be, not colored, but white, crystalline compounds similar to the parent compounds 2-aminopyrimidine (II) and 2-(methylamino)pyrimidine (V).

This correlation of the absence of color, the presence of an absorption band in the 800 cm^{-1} region, and the benzenoid type of resonance is supported by the following facts. The hydriodide salt (XIII) of

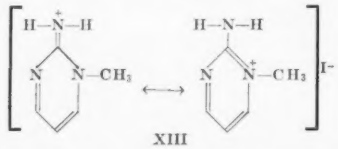

XIII

the yellow compound 1,2-dihydro-2-imino-1-methylpyrimidine (XII) is a white compound. The pyrimidine ring of the salt can have the benzenoid type of resonance and its infrared spectrum does show an absorption band at 795 cm^{-1}.

3. Conclusions

On the basis of the observed data, 2-aminopyrimidine (II) and 2-(methylamino)pyrimidine (V) react with neutral aqueous formaldehyde in *equimolar* proportions to give the corresponding methylol compounds; reaction with *half-molar* proportions of formaldehyde gives the corresponding methyleneiminodipyrimidines. The reaction of the aminopyrimidines with the methylol derivatives to give the substituted iminodipyrimidines suggests the possibility that the methylol derivatives are intermediates in the direct preparation of the methyleneimino-

dipyrimidines from the corresponding aminopyrimdines. There is no evidence of involvement of the pyrimidine ring in any of the reactions investigated.

The two *N*-methylolpyrimidines, as well as 2,2′-[methylenebis(methylimino)]dipyrimidine (VI) and 2,2′-(methylenediimino)bis(4,6-dichloro-5-methylpyrimidine) (VIII), are previously unreported compounds.

4. Experimental Procedures

Infrared analyses were made, on samples prepared as mineral-oil mulls or potassium bromide pellets, with a double-beam recording spectrophotometer (sodium chloride optics). All melting points were corrected.

2-Aminopyrimidine (*II*). Commercial material was recrystallized once from benzene, giving white crystals, mp 126 to 127.5° (Lit. [13] 127 to 128°). Infrared analysis showed two absorption bands near 3,320 and 3,170 cm^{-1} due to N—H stretching vibrations, bands at 1,650 and 1,570 cm^{-1} due to N—H deformation and aromatic ring–double bond interaction [9,12], and a band near 800 cm^{-1} probably due to pyrimidine-ring vibration [12].

Reaction of 2-aminopyrimidine (*II*) *with formaldehyde.—The preparation of N-(2-pyrimidinyl)aminomethanol* (*III*). A 37 percent aqueous solution of formaldehyde (9.7 g, 0.12 mole) was adjusted to a *p*H of 7–8 with several drops of 5 percent sodium hydroxide. To this solution, 11.4 g (0.12 mole) of 2-aminopyrimidine was added, with stirring, in small portions over a period of 10 min. The 2-aminopyrimidine dissolved during the addition. After approximately 20 min of continuous stirring at room temperature, a white, solid mass formed. After several hours of cooling in an icebox, the solid was collected by suction filtration, air dried, and recrystallized from 50 ml of dioxane in the following manner. A flask containing the product and dioxane was immersed in a water bath at 50 to 60°, the mixture was stirred until all solid had dissolved, and the warm solution was filtered. The clear filtrate was cooled slowly to room temperature and then cooled in an icebox for 24 hr. The white crystalline solid was collected by suction filtration, washed with a small amount of cold ethanol, and stored in a desiccator over calcium chloride for three days. The yield was 10.0 g (67 percent), mp 110 to 112°. The melting point, which was quite sensitive to the heating rate, was taken in a bath preheated to 100°.

Infrared analysis showed a band near 3,225 cm^{-1} which is probably a combination of N—H and O—H stretching vibrations. Four bands between 1,250 and 1,000 cm^{-1} (which are absent from the spectrum of 2-aminopyrimidine), including a relatively intense band at 1,018 cm^{-1}, are probably due to C—O stretching or OH deformation [14]. A band at 800 cm^{-1} is probably due to pyrimidine-ring vibration.

The product was identified as *N*-(2-pyrimidinyl)-aminomethanol (III) on the basis of the following analysis.

Anal. Calcd. for $C_5H_7N_3O$: C, 47.99; H, 5.65; N, 33.58; O, 12.78. Found: C, 47.94; H, 5.66; N, 33.91; O, 13.09.

Reaction of N-(2-pyrimidinyl)aminomethanol (*III*) *with hydrochloric acid.* A solution containing 6.25 g (0.050 mole) of methylol III and 150 ml of 0.05 *N* hydrochloric acid in a 250-ml flask was refluxed for 5 hrs and cooled to room temperature. The *p*H was adjusted to 8–9 with 5 percent sodium hydroxide. A white precipitate formed and the reaction mixture was cooled for three days in an icebox. The white solid was collected by suction filtration and air dried. This material slowly decomposed without melting above 350° and was not investigated further.

The filtrate was neutralized with dilute hydrochloric acid and evaporated to dryness. The white residue was extracted with four 25-ml portions of boiling ethanol. The combined extracts were evaporated to dryness and the residue, which contained sodium chloride, was extracted with a few milliliters of cold water. The remainder of the residue was recrystallized twice from ethanol, once from chloroform, and again from ethanol, giving large white needles, mp 187 to 188°. The product, 2,2′-(methylenediimino)dipyrimidine (IV) showed no melting point lowering (187 to 188°) when mixed with the dipyrimidine prepared directly from 2-aminopyrimidine and formaldehyde. The infrared spectra of the two samples were identical. The spectra show a band at 3,220 cm^{-1} due to N—H stretching and a band at 800 cm^{-1} due to pyrimidine-ring vibration. The purified product had the following analysis:

Anal. Calcd. for $C_9H_{10}N_6$: C, 53.45; H, 4.99; N, 41.56. Found: C, 53.63; H, 5.15; N, 41.70.

Attempts to prepare the picrate of 2,2′-(methylenediimino)dipyrimidine (IV) gave a product whose analysis and melting point agreed with those for the picrate of 2-aminopyrimidine. Apparently, hydrolysis occurred during the preparation. The picrate, prepared by the method of Shriner et al. [15], and recrystallized from 95 percent ethyl alcohol, melted at 237 to 238° (Lit. [13] 237 to 238°). A mixed melting point with authentic 2-aminopyrimidine picrate showed no depression (237 to 238°).

Anal. Calcd. for $C_{10}H_8N_6O_7$: C, 37.04; H, 2.49. Found: C, 36.8; H, 2.7.

Reaction of 2-aminopyrimidine (*II*) *with formaldehyde.—Preparation of 2,2′-(methylenediimino)dipyrimidine* (*IV*). This procedure is similar to one previously reported [10], but, because of several differences, details are given. Over a 5-min period, 2.0 g (0.025 mole) of 37 percent aqueous formaldehyde was added dropwise with stirring to a solution of 4.8 g (0.050 mole) of 2-aminopyrimidine in 20 ml of water. The stirring was continued for 1 hr, after which a white precipitate began forming. The reaction mixture was cooled for 4 hr in an icebox and the solid was collected by suction filtration. Successive concentrations gave more solid. The combined crude product, mp 176 to 181°, was recrystallized twice from ethanol and three times from chloroform to give 2.1 g (42 percent) of white crystals, mp 186 to 188° (Lit. [10] 180 to 182°). A mixed melting point with 2,2′-(methylenediimino)dipyrimidine, prepared form *N*-(2-pyrimidinyl)aminomethanol (III), showed no

lowering (186 to 188°), and the infrared spectra of the two samples were identical.

Reaction of 2-aminopyrimidine (II) with N-(2-pyrimidinyl)aminomethanol (III). A solution of 3.13 g (0.025 mole) of *N*-(2-pyrimidinyl)aminomethanol in 15 ml of water was added dropwise with stirring over a 10-min period to a solution of 2.38 g (0.025 mole) of 2-aminopyrimidine in 15 ml of water. The stirring was continued for an additional 90 min. After evaporation of the solution to one-third the origina vollume and cooling for several days in an icebox, a white solid was obtained. The product was collected by suction filtration and recrystallized twice from chloroform and once from ethanol, giving 2.5 g of shiny, white crystals, mp 187 to 189°. A mixed melting point with 2,2′-(methylenediimino)dipyrimidine (IV) showed no lowering (187 to 189°) and the infrared spectra of the two compounds were identical.

2-(Methylamino)pyrimidine (V). This procedure is similar to that of Overberger and Kogon [16] for the preparation of the hydriodide salt and to that of Brown et al. [9], for the preparation of the free amine. The hydriodide salt was prepared from 2-aminopyrimidine and methyl iodide in 91 percent yield.[3] The white crystals, after recrystallization from ethanol, melted at 242 to 244° (Lit. 241 to 242° [16]; 242 to 244° [9]).

The hydriodide salt was converted to 2-(methylamino)pyrimidine (V) by heating in an alcoholic sodium hydroxide solution for several minutes. After recrystallization from petroleum ether (bp 30 to 60°), the white crystalline solid (yield 77 percent based on amine salt) melted at 61.5 to 62.5°. (Lit. 58 to 59.5° [16]; 59 to 60° [9]).

The infrared spectra showed an N—H stretching vibration near 3,250 cm^{-1}, a band near 1,610 cm^{-1} probably due to ring double-bond stretching [9], and the pyrimidine-ring stretching-vibration at 800 cm^{-1}.

The picrate, prepared by the procedure of Shriner et al. [15], gave, on recrystallization from 95 percent ethyl alcohol, yellow needles, mp 194 to 195° (Lit. 195 to 196° [16]; 191° [9]).

Reaction of 2-(methylamino)pyrimidine (V) with formaldehyde.—Preparation of the methylol derivative. A mixture of 3.3 g (0.030 mole) of 2-(methylamino)-pyrimidine and 2.4 g (0.030 mole) of 37 percent aqueous formaldehyde solution was stirred in a small flask at room temperature for 1 hr. All of the solid dissolved in approximately 5 min. The reaction mixture was cooled for three days in an icebox and the white solid collected by suction filtration. The yield of product was 2.6 g (62 percent), mp 61 to 62°. An additional amount of white crystalline product (0.63 g), mp 60 to 62.5°, was isolated from the mother liquor. This methylol compound was unstable and was not further purified. It also gave poor and inconsistent analyses. On admixture with 2-(methylamino)pyrimidine, a noticeable softening or partial melting occurred at room temperature.

[3] Brown and coworkers [9] suggested that the alkylation of 2-aminopyrimidine with methyl iodide actually gives the hydriodide of 1,2-dihydro-2-imino-1-methylpyrimidine (XIII), which rearranges to 2-(methylamino)pyrimidine (V) on treatment with warm, alkaline solution.

Reaction of 2-(methylamino)pyrimidine (V) with formaldehyde.—The preparation of 2,2′-methylenebis-(methylimino)dipyrimidine (VI). A 37 percent aqueous solution of formaldehyde (1.0 g, 0.012 mole) was added dropwise with stirring over a period of several minutes to 2.75 g (0.025 mole) of 2-(methylamino)pyrimidine in 5 ml of water, and stirring was continued for 30 min. After being heated for 10 min on a steam bath, the solution became cloudy, and an oil separated. After ten more minutes of heating, the reaction mixture was stored in an icebox for four days, and the white solid was collected by suction filtration and air dried. Yield 2.35 g (85 percent), mp 86.5 to 88°. Recrystallization from 15 ml of petroleum ether (bp 30 to 60°) gave 2.23 g (81 percent) of long, white needles, mp 87 to 88°.

Infrared analysis of this product showed no N—H stretching vibration. Absorption bands near 1,590 and 1,555 cm^{-1} are probably due to interaction effects of ring double-bonds [12] and a band at 795 cm^{-1} is probably due to pyrimidine-ring vibrations.

Anal. Calcd. for $C_{11}H_{14}N_6$: C, 57.37; H, 6.13; N, 36.50. Found: C, 57.33; H, 6.24; N, 36.81.

Reaction of 2-(methylamino)pyrimidine (V) with N-methyl-N-(2-pyrimidinyl)aminomethanol. A mixture of 0.41 g (0.0037 mole) of 2-(methylamino)-pyrimidine, 0.52 g (0.0037 mole) of the methylol derivative, and 5 ml of water in a small flask was stirred and warmed on a steam bath for 10 min. All of the solid dissolved during the warming period. The clear solution was cooled to room temperature and, after standing for two days, deposited white crystals. After removal of the crystals, the filtrate, on standing two more days, deposited more solid. The total product, which, after air drying, weighed 0.7 g (82 percent), was recrystallized from petroleum ether (bp 30 to 60°), giving 0.65 g (76 percent) of white needles, mp 87 to 88°.

A mixed mp with 2,2′-methylenebis(methyleneimino)dipyrimidine (VI) prepared from 2-(methylamino)pyrimidine and formaldehyde showed no lowering (87 to 88°). The infrared spectra of the two samples were identical.

2-(Dimethylamino)pyrimidine (IX). The procedure used was similar to that of Overberger et al. [16, 17]. 2-Chloropyrimidine was prepared by diazotization of 2-aminopyrimidine with sodium nitrite and hydrochloric acid. The product, after three recrystallizations from petroleum ether (bp 38 to 55°), gave white crystals (23 percent), mp 65 to 66.5° (Lit [16] 64.5 to 65.5°).

2-(Dimethylamino)pyrimidine was prepared from 2-chloropyrimidine by bubbling anhydrous dimethylamine into a refluxing solution of the chloropyrimidine in absolute ethyl alcohol. The crude 2-(dimethylamino)pyrimidine was distilled through a 12-cm Vigreux column, giving a colorless liquid (85 percent), bp 79–81° (20 mm), n_D^{24} 1.5438 (Lit. [16] 88 percent, bp 86° (28 mm), n_D^{25} 1.5420; Lit. [11] 46 percent, bp 78 to 81° (17 mm), n_D^{22} 1.5438).

Infrared analyses of a liquid sample show several C—H stretching bands in the region of 3,150 to 2,800 cm^{-1}, several bands characteristic of ring double-bond interaction effects between 1,600 and 1,400

cm^{-1}, and the 800 cm^{-1} band due to pyrimidine-ring vibration.

The picrate was prepared by adding an ethereal solution of picric acid to an ethereal solution of 2-(dimethylamino)pyrimidine. Recrystallization from ethyl alcohol gave yellow crystals, mp 173 to 175° (Lit. [16] 170.5 to 171.5°).

Reaction of 2-(dimethylamino)pyrimidine (IX) with formaldehyde. A mixture of 1.23 g (0.010 mole) of 2-(dimethylamino)pyrimidine and 0.4 g (0.005 mole) of aqueous 37 percent formaldehyde solution was stirred at room temperature for 90 min. After an additional hour, no solid had deposited, and the reaction mixture was extracted with five 6-ml portions of ether. A small amount of sodium chloride was added to the reaction mixture to lower the solubility of any organic material present. The combined ether extracts were dried over anhydrous magnesium sulfate for 3 hr. Removal of the ether by distillation and of the remaining residue by vacuum distillation gave 1.18 g of 2-(dimethylamino)-pyrimidine, bp 84 to 86° (22 mm) n_D^{23} 1.5430.

In another experiment, the 2-(dimethylamino)-pyrimidine and formaldehyde were stirred together for 1 hr, heated on a steam bath for half an hour, and cooled for one day in an icebox. The reaction mixture, treated as previously described, gave 1.17 g of unchanged 2-(dimethylamino)pyrimidine. In both instances, nearly quantitative recovery of unchanged 2-(dimethylamino)pyrimidine was obtained.

Picrates prepared from the compound recovered from these attempted reactions with formaldehyde gave no melting-point lowering (173 to 175°) when mixed with a sample of the picrate of 2-(dimethylamino)pyrimidine.

Reaction of 2-amino-4,6-dichloro-5-methylpyrimidine (VII) with formaldehyde. Portions of commercial 2-amino-4,6-dichloro-5-methylpyrimidine were purified by vacuum sublimation (200°; 1 mm) or by recrystallization from ethyl alcohol, giving a white solid, mp 252 to 254° (Lit. [18] 249°). Sublimation was the preferable method, because of the low solubility of the chloropyrimidine.

A mixture of 0.9 g (0.05 mole) of 2-amino-4,6-dichloro-5-methylpyrimidine and excess (25 ml) of 37 percent aqueous formaldehyde solution was boiled for 10 min and filtered while still hot, to remove undissolved starting material. Concentration of the filtrate to one-third volume, followed by cooling to room temperature, gave a white solid. Two recrystallizations from ethanol gave about 50 mg of a white, crystalline solid, mp 240 to 242°, which is probably 2,2′-(methylenediimino)bis(4,6-dichloro-5-methylpyrimidine) (VIII), based on the following analysis.

Anal. Calcd. for $C_{11}H_{10}Cl_4N_6$: N, 22.83; Cl, 38.54. Found: N, 22.72; Cl, 38.39.

Infrared analysis of the starting material, VII, showed two N—H stretching bands near 3,460 and 3,440 cm^{-1}. The reaction product, VIII, showed a single N—H stretching band near 3,300 cm^{-1}. Both compounds showed the absorption band near 800 cm^{-1} characteristic of pyrimidine-ring stretching.

1,2-Dihydro-2-imino-1-methylpyrimidine (XII). This compound was prepared from 2-aminopyrimidine and methyl iodide according to the procedure of Brown et al. [9]. The product, a yellow solid, melted at 101 to 103° (Lit. [9] 102 to 104°).

Infrared analysis showed an N—H stretching band near 3,246 cm^{-1}, and a band near 1,646 cm^{-1} due to double-bond stretching [9]. There was no band near 800 cm^{-1} typical of pyrimidine-ring vibration.

The infrared spectrum of the hydriodide salt, XIII, showed two absorption bands near 3,400 and 3,200 cm^{-1} and a band near 1,650 cm^{-1}. An absorption band at 795 cm^{-1} was probably due to pyrimidine-ring vibration.

2-Amino-1,3,5-triazine (I). The procedure consisted of heating a mixture of formylguanidine [19] and formamide with powdered sodium hydroxide, and was essentially that of Grundmann et al. [7]. The product, a white crystalline solid, mp 224 to 226° (Lit [7] 225 to 226°) gave the following analysis.

Anal. Calcd. for $C_3H_4N_4$: C, 37.50; H, 4.19; N, 58.31. Found: C, 37.21; H, 4.21; N, 58.71.

Attempts to react 2-amino-1,3,5-triazine with formaldehyde in neutral solution were unsuccessful.

The author thanks Miss M. Kathryn Wharton and Max Tryon for assistance with the infrared analyses, and Mrs. Elli Hand for the preparation of several compounds.

5. References

[1] A. Gams, G. Widmer, and W. Fisch, Brit. Plastics **14,** 508 (1943).
[2] H. P. Wohnsiedler, Ind. Eng. Chem. **44,** 2679 (1952).
[3] H. P. Wohnsiedler, Ind. Eng. Chem. **45,** 2307 (1953).
[4] H. P. Wohnsiedler, Ind. Eng. Chem. **48,** 82 (1956).
[5] R. F. Goldstein, Plastics Inst. (London) Trans. **21,** 18 (1953).
[6] A. Burger and E. D. Hornbaker, J. Am. Chem. Soc. **75,** 4579 (1953).
[7] C. Grundmann, L. Schwennicke, and E. Beyer, Chem. Ber. **87,** 19 (1954).
[8] L. Paolini, Gazz. chim. ital. **84,** 735 (1954) [C.A. **50,** 1039*i* (1956)].
[9] D. J. Brown, E. Hoerger, and S. F. Mason, J. Chem. Soc. **1955,** 4035.
[10] B. Skowrońska-Serafinowa, Roczniki Chem. **29,** 932 (1955) [C.A. **50,** 6464*b* (1956)].
[11] D. J. Brown and L. N. Short, J. Chem. Soc. **1953,** 331.
[12] L. J. Bellamy, The infrared spectra of complex molecules (John Wiley & Sons, Inc., New York, N.Y., 2d ed., 1958, 277, 283).
[13] E. Büttner, Ber. deut. chem. Ges. **36,** 2229 (1903).
[14] L. J. Bellamy, The infrared spectra of complex molecules (John Wiley & Sons, Inc., New York, N.Y., 2d ed., 1958, 108, 188).
[15] R. L. Shriner, R. C. Fuson, and D. Y. Curtin, The systematic identification of organic compounds, (John Wiley & Sons, Inc., New York, N.Y., 4th ed., 1956, 229).
[16] C. G. Overberger and I. C. Kogon, J. Am. Chem. Soc. **76,** 1065 (1954).
[17] C. G. Overberger, I. C. Kogon, and R. Minin, Org. Syntheses **35,** 34 (1955).
[18] O. Gerngross, Ber. deut. chem. Ges. **38,** 3394 (1905).
[19] W. Traube, Ber. deut. chem. Ges. **43,** 3587 (1910).

(Paper 66A1–141)

JOURNAL OF RESEARCH of the National Bureau of Standards—A. Physics and Chemistry
Vol. 66A, No. 1, January–February 1962

Acidic Dissociation Constant and Related Thermodynamic Quantities for Diethanolammonium Ion in Water From 0 to 50 °C[1]

Vincent E. Bower, Robert A. Robinson, and Roger G. Bates

(August 29, 1961)

The dissociation constants of diethanolamine (2:2′-dihydroxydiethylamine) and its conjugate acid were determined by electromotive force measurements of the cell

$$Pt;\ H_2(g,\ 1\ atm),(HOC_2H_4)_2NH_2Cl(m_1),(HOC_2H_4)_2NH\ (m_2),\ AgCl\ (s);\ Ag$$

in the temperature range 0 to 50 °C. The acidic dissociation constant (K_{bk}) of the diethanolammonium ion is given by

$$-\log K_{bk}=\frac{1830.15}{T}+4.0302-0.0043261\ T,$$

where T, the temperature on the Kelvin scale, lies between 273.15 and 323.15°. From this equation were calculated $\Delta G°$, the change in free energy; $\Delta H°$, the change in heat content; $\Delta S°$, the change in entropy; and $\Delta C_p°$, the change in heat capacity that accompany the dissociation of 1 mole of diethanolammonium ion in the standard state. At 25 °C, $-\log K_{bk}=8.883$; $\Delta G°=50{,}682$ joule mole^{-1}; $\Delta H°=42{,}400$ joule mole^{-1}; $\Delta S°=-27.8$ joule deg^{-1}mole^{-1}; and $\Delta C_p°=49$ joule deg^{-1}mole^{-1}.

1. Introduction

The effect of changes of temperature upon the dissociation constants of neutral and negatively charged acids has been the object of considerable study over the past quarter century. This effort has resulted in much useful information concerning the thermodynamic quantities associated with the dissociation process in acids of these types. Until recently, however, the systematic study of positively charged acids has received little attention.

From the electrostatic point of view, the dissociation of a positively charged monobasic acid is of unusual interest. The dissociation process is isoelectric, and consequently it might be expected that the electrostatic contribution to the change of heat capacity would be zero [1, 2][2]. This prediction was confirmed for ammonium ion [3, 4], but rather large positive values of the heat-capacity change have been found for other acids of the same charge type.[3]

From the molecular point of view, the dissociation process appears to be a reaction of considerable complexity. Although considerable progress has been made, notably by Everett and Wynne-Jones and their coworkers [6, 7, 8], Evans and Hamann [9], Laidler [10], and others,[4] in identifying the several factors involved, it is not yet possible to account theoretically for the measured thermodynamic quantities. The empirical correlation of structure with the observed changes of entropy and heat capacity, on the other hand, has revealed a considerable amount of regularity, permitting useful predictions to be made.

Earlier papers have reported the dissociation constants of monoethanolammonium ion [12] and triethanolammonium ion [13] from 0 to 50 °C, as well as the changes of free energy, enthalpy, entropy, and heat capacity that accompany the dissociation process in the standard state. Similar data for diethanolammonium ion are now presented.

2. Method

The method was the same as that used in the determination of the dissociation constant of monoethanolammonium ion [12], and that of triethanolammonium ion [13, 14]. It has been described in detail in earlier publications and will only be summarized here.

Electromotive-force measurements of the cell

$$Pt;\ H_2(g,1\ atm),\ (HOC_2H_4)_2NH_2Cl(m_1),\ (HOC_2H_4)_2NH(m_2),\ AgCl\ (s);\ Ag$$

were made at intervals of 5 deg from 0 to 50 °C. The molalities m_1 and m_2 were approximately equal, and the partial pressure of diethanolamine over the buffer solutions was so low that no correction was

[1] Presented in part before the Division of Physical Chemistry at the 137th meeting of the American Chemical Society, Cleveland, Ohio, April 1960.
[2] Figures in brackets indicate the literature references at the end of this paper.
[3] For example, the value of $\Delta C°_p$, the change of heat capacity, for trimethylammonium ion is +183 j deg^{-1}mole^{-1} at 25 °C [5].
[4] See, for example, reference [11].

applied for volatility of the solute (diethanolamine boils at about 140 °C under a pressure of 2 mm Hg). It was also found that the correction for the complexing of silver chloride by the amine was negligible, and it was therefore omitted.[5]

The thermodynamic acidity function $p(a_{H}\gamma_{Cl})$ was computed for each buffer solution at each temperature by the equation

$$p(a_{H}\gamma_{Cl}) \equiv -\log(\gamma_{H}\gamma_{Cl}m_{H}) = (E-E^{\circ})F/(2.3026RT)+\log m_{Cl} \quad (1)$$

where E is the emf of the cell and E° the standard potential of the cell [15]. In addition, F is the Faraday, R the gas constant, T the temperature on the Kelvin scale, m is molality, and γ is the molal activity coefficient. Values of $2.3026RT/F$ have been tabulated elsewhere [16].

The acidity function $p(a_{H}\gamma_{Cl})$ is the same quantity for which the symbol pwH was earlier suggested [17] and has been widely used. In order to clarify the nature of this quantity, it has now been proposed that $p(a_{H}\gamma_{Cl})$ be used instead of pwH [18].

The hydrolysis (dissociation) of diethanolamine as a base is sufficiently extensive that the true equilibrium concentrations of diethanolammonium ion (BH^{+}) and of diethanolamine (B) in the solution differ somewhat from the stoichiometric molalities m_1 and m_2. This hydrolysis reaction is written as follows:

$$B+H_2O=BH^{+}+OH^{-}. \quad (2)$$

It is evident from this equation that the molality of BH^{+} will be equal to (m_1+m_{OH}) whereas that of B will be (m_2-m_{OH}). Accordingly the ionic strength (I) will be given by

$$I=m_1+m_{OH}. \quad (3)$$

It has been shown earlier [19] that the concentration of hydroxyl ion can be computed very conveniently and with sufficient accuracy by the approximation

$$\log m_{OH} \approx \log K_w + p(a_{H}\gamma_{Cl}), \quad (4)$$

where K_w is the ion product constant for water [20].

Experience has shown that the determination of the dissociation constant is facilitated by estimating the magnitude of the activity coefficient of the ionized diethanolammonium chloride in each of the solutions. The complete expression for the acidic dissociation constant of the diethanolammonium ion is therefore obtained by combining the mass-law expression for the dissociation process with the acidity function $p(a_{H}\gamma_{Cl})$ and with the Hückel expression for the activity coefficients. The resulting equation is

$$-\log K'_{bh} \equiv -\log K_{bh}-\beta I = p(a_{H}\gamma_{Cl}) + \log\frac{m_1+m_{OH}}{m_2-m_{OH}}-\frac{2A\sqrt{I}}{1+Ba^{*}\sqrt{I}}. \quad (5)$$

The apparent value of K_{bh} in any solution is designated K'_{bh}; A and B are constants of the Debye-Hückel theory [21], and a^{*} and β are adjustable parameters.

The thermodynamic constant was obtained by plotting the values of $-\log K'_{bh}$ as a function of ionic strength and extending the line so obtained to an ionic strength of zero. When too large a value of a^{*} was selected, the plot of the right side of eq (5) as a function of ionic strength was concave downward; when a^{*} was too small, the function was concave upward. For the measurements of diethanolamine, straight lines easily extrapolated to zero ionic strength were obtained by using a value of zero for a^{*}. The last term of eq (5) thus takes the form of the Debye-Hückel limiting law.

3. Experimental Procedures and Results

Diethanolamine was distilled at 143° C±3° at a pressure of 2 mm Hg. The middle third of the distillate was collected and subjected to another distillation at the same pressure and temperature, and the middle third of this new distillate was collected. This final sample was found by electrometric titration with a standard solution of hydrochloric acid to assay 100.1 percent, if assumed to contain only diethanolamine.[6]

The buffer solutions were prepared and studied in groups of five. The last four of each series were prepared by weight dilution of the first. This stock solution was prepared, for each series, by pipeting into a 0.1-m hydrochloric acid solution (standardized by weighing the chloride as silver chloride) an amount of diethanolamine sufficient to produce a solution about 0.1 m in diethanolamine hydrochloride and 0.1 m in uncombined diethanolamine. The exact molality of the hydrochloride was, of course, the same as that of the hydrochloric acid used in making the solution. The exact molality of the free amine was determined by weight titration.

The observed values of the electromotive force (the averages for two pairs of electrodes in each cell) were corrected in the usual way to the standard reference state for 1 atm partial pressure of hydrogen. The corrected average values are given in table 1. Values of $p(a_{H}\gamma_{Cl})$ were calculated by eq (1) from each corrected value of the emf and the chloride molality (m_1).

The quantity $-\log K'_{bh}$ was evaluated by eq (5) for each solution and was plotted at each temperature as a function of ionic strength. The calculated points at each temperature fell on a straight line when $a^{*}=0$ was chosen. By the method of least squares, the equations for these lines were determined and the intercepts ($-\log K_{bh}$) at $I=0$ were obtained. The values of $-\log K_{bh}$ from 0 to 50° C are listed in table 2 together with the standard deviation of the intercept.

The basic dissociation constant (K_b) of diethanolamine is also given in table 2. This is the equilibrium constant for eq (2) and was obtained by the

[5] The solubility of silver chloride in a 0.1 m solution of diethanolamine was found to be 0.0002 mole/liter. The corresponding correction to the emf can be calculated in the manner outlined by Bates and Pinching [4].

[6] An estimate of the effect of monoethanolamine as an impurity is given in the appendix, section 5 of this paper.

TABLE 1. *Electromotive force of the cell:* $Pt;H_2(g,1\ atm)$, *diethanolammonium chloride* (m_1), *diethanolamine* (m_2), $AgCl;Ag$ *from 0 to 50° C*

Series	m_1	m_2	0	5	10	15	20	25	30	35	40	45	50
A	0.10066	0.10833	0.82349	0.82387	0.82410	0.82411	0.82396	0.82364	0.82320	0.82254	0.82165	0.82068	0.81962
	.06207	.06680	.83254	.83285	.83327	.83333	.83394	.83363	.83320	.83260	.83194	.83114	.83018
	.03922	.04220	.84134	.84203	.84263	.84294	.84313	.84325	.84304	.84263	.84191	.84124	.84051
	.02924	.03147	.84704	.84762	.84854	.84908	.84911	.84961	.84918	.84893	.84847	.84795	.84724
	.02097	.02257	.85385	.85481	.85573	.85628	.85669	.85694	.85699				
B	.10239	.09148	.81879	.81904	.81917	.81902	.81883	.81877	.81781	.81675	.81583	.81490	.81364
	.09114	.08143	.82095	.82124	.82139	.82132	.82108	.82096	.82019	.81939	.81842	.81729	.81621
	.07174	.06410	.82543	.82584	.82608	.82613	.82600	.82588	.82533	.82466	.82387	.82294	.82161
	.05182	.04630	.83165	.83213	.83254	.83274	.83278	.83270	.83224	.83165	.83099	.83007	.82909
	.03138	.02804	.84125	.84192	.84250	.84287	.84305	.84320	.84285	.84254	.84196	.84130	.84048
C	.10239	.10575	.82202	.82236	.82256	.82253	.82246	.82230					
	.08678	.08963	.82526	.82570	.82597	.82603	.82594	.82573					
	.013163	.013595	.86239	.86352	.86444	.86508	.86573	.86612					
	.009087	.009385	.87017	.87143	.87250	.87334	.87407	.87475					
D	.10239	.10460							.82129	.82056	.81980	.81892	.81763
	.012161	.012423							.86739	.86743	.86734	.86718	.86671
	.008791	.008981							.87496	.87517	.87510	.87499	.87469
	.007109	.007262							.87979	.87998	.88013	.88008	.87980
	.005248	.005361							.88720	.88755	.88775	.88781	.88762
E	.08643	.07830	.82236	.82268	.82288	.82286	.82269	.82243	.82190	.82112	.82001	.81907	.81792
	.06103	.05529	.82881	.82917	.82946	.82954	.82950	.82958	.82902	.82838	.82757	.82658	.82560
	.04569	.04139	.83436	.83492	.83531	.83552	.83556	.83562	.83525	.83469	.83403	.83308	.83214
	.03521	.03190	.83950	.84018	.84062	.84093	.84111	.84117	.84092	.83959	.83993	.83916	.83829
	.02521	.02284	.84605	.84657	.84709	.84746	.84782	.84830	.84814	.84760	.84709	.84649	.84577

TABLE 2. *Summary of the dissociation constants of diethanolammonium ion* (K_{bh}) *and diethanolamine* (K_b) *from 0 to 50 °C*

t	$-\log K_{bh}$	σ_i	$-\log K_b$
°C			
0	9.550	0.001	5.394
5	9.404	.002	5.330
10	9.268	.001	5.267
15	9.133	.001	5.213
20	9.005	.001	5.162
25	8.883	.001	5.113
30	8.759	.001	5.074
35	8.632	.002	5.048
40	8.518	.001	5.017
45	8.406	.001	4.990
50	8.297	.001	4.965

formula

$$K_b = K_w / K_{bh}. \tag{6}$$

The constants given in the second column of table 2 may be expressed by the following equation, valid from 0 to 50 °C:

$$-\log K_{bh} = \frac{1830.15}{T} + 4.0302 - 0.0043261\,T, \tag{7}$$

where T is temperature in °K: T=°C+273.15. The constants of eq (7) were computed by the method of least squares. The standard deviation of a single value of $-\log K_{bh}$ from eq (7) was 0.003. Equation (7) is of the form proposed by Harned and Robinson [22].

Hall and Sprinkle [23], using a cell with a hydrogen electrode and a liquid junction, found a value of 8.88 for $-\log K_{bh}$ for diethanolammonium ion at 25 °C. In recent work [24], Chremos and Zimmerman have reported a value of 8.96 at the same temperature. This value was calculated from pH measurements made with a pH meter of the glass-electrode type. Our result agrees well with the earlier work of Hall and Sprinkle.

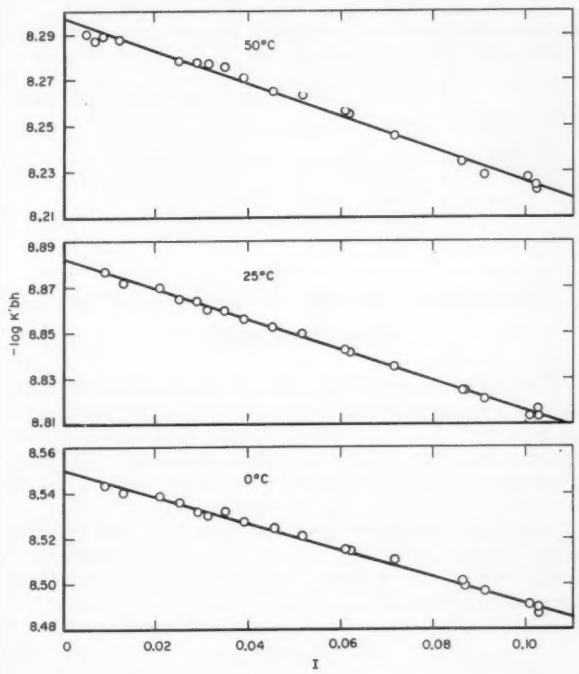

FIGURE 1. *Plots of* $-\log K'_{bh}$ *as a function of ionic strength at 0, 25, and 50 °C.*

4. Derived Thermodynamic Quantities

The changes of free energy ($\Delta G°$), enthalpy ($\Delta H°$), entropy ($\Delta S°$), and heat capacity ($\Delta C°_p$) for the dissociation for one mole of diethanolammonium ion in the standard state were calculated in the usual way from the change of the dissociation constant with temperature as given in eq (7). The results

are summarized in table 3. The thermodynamic quantities for the dissociation of monoethanolammonium ion [12], diethanolammonium ion, and triethanolammonium ion [13] at 25 °C are compared in table 4.

TABLE 3. *Thermodynamic quantities for the dissociation of diethanolammonium ion:* $BH^+ \rightleftarrows B + H^+$

t	$\Delta G°$	$\Delta H°$	$\Delta S°$	$\Delta C_p°$
°C	*j mole*$^{-1}$	*j mole*$^{-1}$	*j deg*$^{-1}$*mole*$^{-1}$	*j deg*$^{-1}$*mole*$^{-1}$
0	49,936	41,220	−31.9	45
5	50,094	41,440	−31.1	46
10	50,247	41,680	−30.3	47
15	50,396	41,910	−29.4	48
20	50,541	42,160	−28.6	49
25	50,682	42,400	−27.8	49
30	50,819	42,650	−27.0	50
35	50,952	42,910	−26.1	51
40	51,079	43,160	−25.3	52
45	51,204	43,420	−24.5	53
50	51,325	43,690	−23.6	53

TABLE 4. *Comparison of the thermodynamic quantities for the dissociation of monoethanolammonium, diethanolammonium, and triethanolammonium ions at 25 °C*

Acid (BH^+)	$-\log K_{bh}$	$\Delta G°$	$\Delta H°$	$\Delta S°$	$\Delta C_p°$
		j mole^{-1}	*j mole*$^{-1}$	*j deg*$^{-1}$*mole*$^{-1}$	*j deg*$^{-1}$*mole*$^{-1}$
Monoethanolammonium [12]	9.498	54,205	50,540	−12.3	−5
Diethanolammonium (present work)	8.883	50,682	42,400	−27.8	49
Triethanolammonium [13]	7.762	44,305	33,450	−36.4	52

5. Appendix. Effects of Impurities in the Diethanolamine

The effect of small amounts of monoethanolamine or other bases present as an impurity may be gaged as follows. In the measurements described above, a solution was made of diethanolamine (D) and hydrogen chloride in water. Let a be the weight of diethanolamine in 1 kg of water. The molality of D, on the assumption that this base was 100 percent pure, would be a/M_D, where M_D is the molecular weight of D, and hydrochloric acid would be added to a molality $a/(2M_D)$; thus

$$m'_D = m'_{DH} = \frac{a}{2M_D}. \tag{8}$$

Hence, the apparent concentration dissociation constant, k'_{DH}, can be written

$$k'_{DH} = \frac{m_H m'_D}{m'_{DH}} = m_H. \tag{9}$$

A relation between k'_{DH} and the true concentration dissociation constant is sought.

If a fraction x (by weight) of the base added is present as another base (e.g., monoethanolamine, M) whose conjugate acid has the dissociation constant k_{MH}, the total concentration of diethanolamine (as free base and hydrochloride) is

$$m_D + m_{DH} = \frac{(1-x)a}{M_D} \tag{10}$$

and the total concentration of monoethanolamine is

$$m_M + m_{MH} = \frac{xa}{M_M} \tag{11}$$

From the definition of the dissociation constants,

$$m_D = \frac{k_{DH}}{m_H} m_{DH} \tag{12}$$

and

$$m_M = \frac{k_{MH}}{m_H} m_{MH} \tag{13}$$

Hence, from eq (8), (10), and (12) one can write

$$m_{DH}\left(1 + \frac{k_{DH}}{m_H}\right) = \frac{(1-x)a}{M_D} = 2(1-x)m'_D \tag{14}$$

and from eq (8), (11), and (13) one finds

$$m_{MH}\left(1 + \frac{k_{MH}}{m_H}\right) = \frac{xa}{M_M} = 2x\frac{M_D}{M_M} m'_D. \tag{15}$$

Electroneutrality imposes the following condition:

$$m_H + m_{MH} + m_{DH} = m_{Cl} + m_{OH} \tag{16}$$

or

$$m_{MH} + m_{DH} \approx m_{Cl}, \tag{16a}$$

inasmuch as the hydroxyl ion concentration is very much smaller than the molality of the added hydrochloric acid. Hence, with the aid of eq (14) and (15) one obtains

$$\frac{2(1-x)m'_D}{1 + k_{DH}/m_H} + \frac{2xM_D m'_D}{M_M(1 + k_{MH}/m_H)} = m_{Cl}. \tag{17}$$

Remembering that $m_H = k'_{DH}$ and that $m_{Cl} = m'_D = m'_{DH}$, one can then write

$$\frac{1-x}{1 + k_{DH}/k'_{DH}} + \frac{xM_D}{M_M(1+\epsilon)} = 0.5, \tag{18}$$

where $\epsilon \equiv k_{MH}/k'_{DH}$. Finally, eq (18) can be rearranged to

$$\frac{k_{DH}}{k'_{DH}} = \frac{(1+\epsilon)(2-2x)}{(1+\epsilon) - 2x(M_D/M_M)} - 1. \tag{18a}$$

It is now possible, with the aid of eq (18a), to compute the error in the dissociation constant resulting from the presence of small amounts of a second base in the diethanolamine used. Inasmuch as the assay (100.1 percent) exceeded the theoretical value, it is evident that the impurity was a base of

equivalent weight less than that of diethanolamine. It is likely, therefore, that it was monoethanolamine (molecular weight=61.08) rather than triethanolamine (mol wt=149.19). The value of x is readily shown to be

$$x=\frac{\Delta A}{100}\frac{M_M}{M_D-M_M} \tag{19}$$

where ΔA is the observed assay value (in percent) minus 100, due consideration being given to sign.

For the measurements reported here, ΔA was +0.1, and x is therefore 0.0015. The value of k'_{DH} at 25 °C is 1.31×10^{-9} and k_{MH} is 3.18×10^{-10} [12]; hence ϵ is 0.243. The ratio of molecular weights, M_D/M_M, is 1.721. Substitution of these values in eq (18a) gives 1.0051 for k_{DH}/k'_{DH}. It may be concluded, therefore, that the presence of monoethanolamine (x=0.0015) could result in values of $-\log K_{bh}$ for diethanolamine that are too high by about 0.002 unit. This correction was not made in reporting the values of $-\log K_{bh}$ given in table 2.

6. References

[1] R. W. Gurney, J. Chem. Phys. **6,** 499 (1938), Ionic processes in solution, chap 7 (McGraw-Hill Book Co., Inc., New York, N.Y., 1953).
[2] E. C. Baughan, J. Chem. Phys. **7,** 951 (1939).
[3] D. H. Everett and W. F. K. Wynne-Jones, Proc. Roy. Soc. (London) **169A,** 190 (1938); D. H. Everett and D. A. Landsman, Trans. Faraday Soc. **50,** 1221 (1954).
[4] R. G. Bates and G. D. Pinching, J. Research NBS **42,** 419 (1949) RP1982.
[5] D. H. Everett and W. F. K. Wynne-Jones, Proc. Roy. Soc. (London) **177A,** 499 (1941).
[6] D. H. Everett and W. F. K. Wynne-Jones, Trans. Faraday Soc. **35,** 1380 (1939).
[7] D. H. Everett, D. A. Landsman, and B. R. W. Pinsent, Proc. Roy. Soc. (London) **215A,** 403 (1952).
[8] D. H. Everett and B. R. W. Pinsent, Proc. Roy. Soc. (London) **215A,** 416 (1952).
[9] A. G. Evans and S. D. Hamann, Trans. Faraday Soc. **47,** 34 (1951).
[10] K. J. Laidler et al., Trans. Faraday Soc. **55,** 1725, 1731, 1734, 1738, 1743 (1959).
[11] R. P. Bell, The proton in chemistry, chap 5 (Cornell University Press, Ithaca, N.Y., 1959).
[12] R. G. Bates and G. D. Pinching, J. Research NBS **46,** 349 (1951) RP2205.
[13] R. G. Bates and G. F. Allen, J. Research NBS **64A** (Phys. and Chem.) 343 (1960).
[14] R. G. Bates and G. Schwarzenbach, Helv. Chim. Acta **37,** 1437 (1954).
[15] R. G. Bates and V. E. Bower, J. Research NBS **53,** 283 (1954) RP2546.
[16] R. G. Bates, Electrometric *p*H determinations, p. 313. (John Wiley & Sons, Inc., New York, N.Y. 1954).
[17] R. G. Bates, Chem. Revs. **42,** 1 (1948).
[18] R. G. Bates and E. A. Guggenheim, Pure and Applied Chem. **1,** 163 (1960).
[19] R. G. Bates, G. L. Siegel, and S. F. Acree, J. Research NBS **31,** 205 (1943) RP1559.
[20] H. S. Harned and B. B. Owen, The physical chemistry of electrolytic solutions, 3d ed. (Reinhold Publishing Corp., New York, N.Y. 1958).
[21] R. A. Robinson and R. H. Stokes, Electrolyte solutions, 2d ed., app 7.1 (Academic Press, New York, N.Y., 1959).
[22] H. S. Harned and R. A. Robinson, Trans. Faraday Soc. **36,** 973 (1940).
[23] N. F. Hall and M. R. Sprinkle, J. Am. Chem. Soc. **54,** 3469 (1932).
[24] G. Chremos and H. K. Zimmerman, Jr., Texas J. Sci. **11,** 467 (1959).

(Paper 66A1–142)

JOURNAL OF RESEARCH of the National Bureau of Standards—A. Physics and Chemistry
Vol. 66A, No. 1, January–February 1962

Fiber Structure—Property Relationships II: Macroscopic Deformations of Alkylene Sulfide Crosslinked Polycaprolactam Fibers

Stephen D. Bruck

(October 9, 1961)

The introduction of alkylene sulfide crosslinks into oriented nylon-6 (polycaprolactam) homofiber is described. The resulting structural modifications are found to produce crimping and coiling in the dry and wet states of the fiber resembling the situation in wool. In a previous paper a similar phenomenon was reported for a disulfide crosslinked nylon-6 homofiber. The macroscopic deformations exhibited by the alkylene sulfide crosslinked fibers differ in at least three respects from the disulfide crosslinked samples: (1) the crimp frequency is much higher and the crimp amplitude smaller, (2) in addition to crimping, some helical coiling takes place even when the fiber is in the unswollen state, and (3) the extent of crimping and coiling is not decreased by gradual air-oxidation of some of the reactive groups. An explanation for this crimping and coiling previously advanced is corroborated by additional evidence provided by chemical analyses, and X-ray diffraction, birefringence, and swelling data.

1. Introduction

In previous communications [1, 2] [1] it was shown that under suitable conditions, self-crimping and helical coiling can be achieved with round cross-section nylon-6 (polycaprolactam) homofiber by the introduction of disulfide crosslinkages. The resulting chemically modified fiber resembled wool in its bulking characteristics. The present paper deals with the introduction of alkylene sulfide crosslinks into oriented nylon-6 homofibers and describes some of the properties of the resulting structures.

2. Discussion

2.1. Introduction of Alkylene Sulfide Crosslinks

Although wool exhibits excellent bulking and other desirable properties, the possibility of improving some of its negative characteristics has challenged many workers. For example, the disulfide (cystine) crosslinks in wool are subject to degradation, reduction to the sulfhydryl groups (cysteine), and attack by microorganisms and enzymes. These problems prompted several early investigators [3, 4] to study the chemical modifications of the cystine crosslinks in wool.

In view of this work on wool, it seemed of interest to introduce longer, more flexible crosslinks of the alkylene sulfide types into nylon-6 fiber and to compare the properties of these structures with the previously reported disulfide crosslinked fibers. Discussion of the methods used to introduce the alkylene sulfide crosslinks is facilitated by reference to the reactions schemes at the top of page 78 (for details refer to Experimental Section).

The introduction of methoxymethyl groups (B) into nylon-6 polymer has already been described [1,5,6]. In order to convert (B) into the intermediate (C), the methylmethoxylated fiber was reacted with thioacetamide in the presence of methyl alcohol as swelling agent, and concentrated hydrochloric acid. (In previous work, thiourea was used, but it has been found that thioacetamide gives a similar product.) To facilitate the synthesis of a large number of alkylene sulfide crosslinks, it was necessary to inhibit the tendency of disulfide crosslinks to form (E) by the oxidation of sulfhydryl groups (D). This was accomplished by reacting the intermediate (C) with an excess amount of potassium hydroxide to yield the potassium mercaptides (F) which are less sensitive to oxidation than sulfhydryls. The final steps involved the reaction of the potassium mercaptide groups with either methylene dihalide to yield the alkylene sulfide crosslinked product (G), henceforth referred to as type A, or alternatively, reacting the potassium mercaptide groups with ethylene dihalide to give the type B alkylene sulfide crosslinks (H). These last reactions are similar to the well-known Williamson synthesis of ethers from metallic alkoxides and alkyl halides [7].

Although the potassium mercaptide groups are less vulnerable to oxidation than the sulfhydryl groups, the final product undoubtedly contains some disulfide crosslinks and also some "blocked" (alkylated) groups of the type:

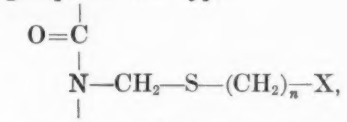

where, $n=1$ or 2, and X=I or Br. The presence of these latter groups could be expected since, because of steric factors, not all potassium mercaptide groups

[1] Figures in brackets indicate the literature references at the end of this paper.

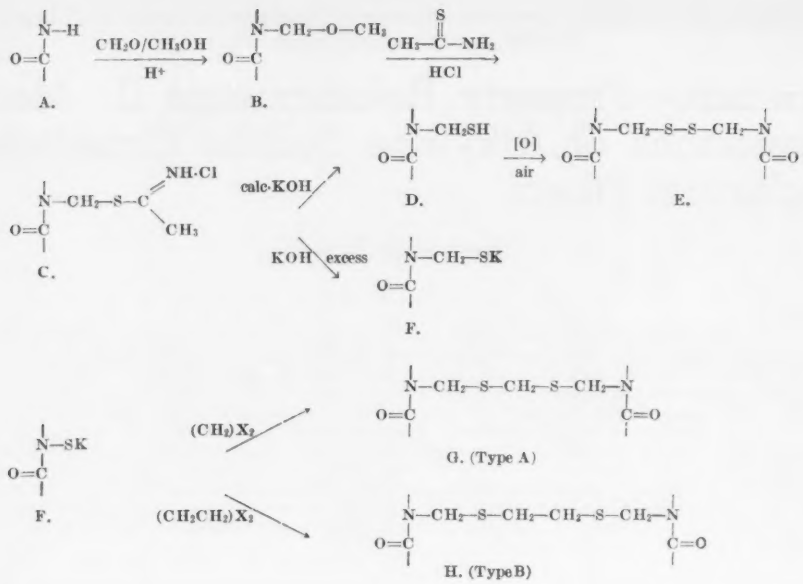

Where, X=I or Br.

can form crosslinks and therefore are subject only to the blocking reaction. No significant amounts of free potassium mercaptide or sulfhydryl groups were detected in the alkylene sulfide crosslinked fibers by a sensitive technique [8], specially devised for this purpose.

The pertinent analytical data are summarized in table 1. The percent sulfur represents the combined quantities of alkylene sulfide and disulfide crosslinks, as well as the "blocked" (alkylated) sulfhydryl groups. The total sulfur content of the samples varied between 2.7 to 3.7 percent depending on the type of crosslinks and on the experimental conditions. The relative extent of crosslinking was also estimated by a photomicrographic swelling technique [9,10]. The symbol q_m represents the ratio V/V_0 of the volumes of the swollen to the unswollen structures at equilibrium [11]. The minimum observed q_m values were between 5.1 and 5.8, indicating that a high density of alkylene sulfide crosslinks had been introduced into the fiber. Assuming that there were no side reactions, the total sulfur analyses indicates approximately 400 to 500 equivalents of crosslinks per 10^6 g of polymer. Although these crosslinks were probably not uniformly distributed in the fiber, dyed cross sections indicated that, as in the case of the disulfide crosslinks, the alkylene sulfide crosslinks extended throughout the entire structure and were not confined to the surface [12].

TABLE 1. *Analytical data on crosslinked nylon-6 fibers*

Experiment [1]	Total S	Predominant crosslink type [2]	Swelling ratio q_m [3]	Macroscopic deformation	
				Dry or wet	*m*-cresol
	wt %				
1	3.7	A	8.0	Very highly crimped; some helices.	Helices.
2	3.6	A	5.1	——do——	Do.
3	2.9	B	6.2	——do——	Do.
4	2.9	B	6.8	——do——	Do.
5	2.7	O	5.8	Crimped	Do.

[1] Refer to Experimental Section.

[2] Type A=N–CH_2–S–CH_2–S–CH_2–N

Type B=N–CH_2–S–$(CH_2)_2$–S–CH_2–N

Type O=N–CH_2–S–S–CH_2–N

[3] $q_m = V/V_0$ where V=volume of network at equilibrium swelling V_0=volume of network before swelling. Swelling agent; *m*-cresol.

Figure 1 is a photograph of the unmodified (scoured) nylon-6 fiber, the type A crosslinked fiber and the type B crosslinked fiber. Figure 2 shows a photomicrograph of a single helical coil in the unswollen fiber (type A) and a phase-photomicro-

2.2. Macroscopic Deformations of Alkylene Sulfide Crosslinked Nylon-6 Fibers and Their Structural Significance

The alkylene sulfide crosslinked nylon-6 homofibers exhibited self-crimping and helical coiling of uneven distribution and dimensions in both dry and wet states similar to those already reported for disulfide crosslinked fibers. However, these macroscopic deformations differed in at least three respects from those of the disulfide crosslinked samples: (1) the crimp frequency was much higher and the crimp-amplitude smaller, (2) in addition to crimping, some helical coiling occurred even when the fiber was in the unswollen state, and (3) the extent of crimping and coiling was not gradually decreased by air oxidation of unreacted sulfhydryl groups.

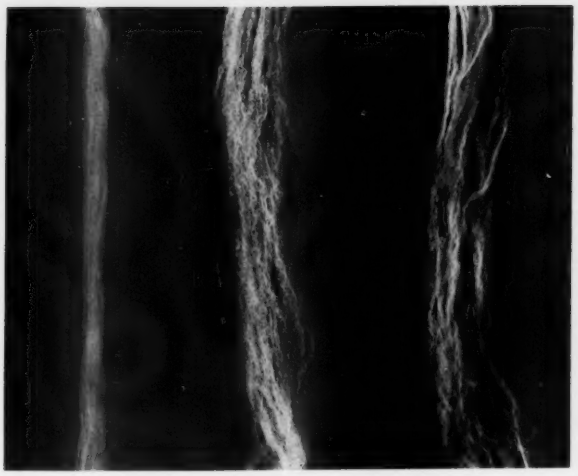

FIGURE 1. *Crimping of alkylene sulfide crosslinked nylon-6 fibers.*

Left: unmodified, Middle: type A crosslinks; Right: type B crosslinks.

graph of a portion of the same coil while swollen in *m*-cresol. The diameter of the fiber before swelling was between 16 and 18 μ and the magnification in both photographs is the same. The small spots appearing in the swollen fiber are due to particles of TiO_2 delustrant present in the fiber in small amounts. Figure 3 shows similar photographs of a fiber with type B crosslinks before and while swollen in *m*-cresol. The fiber diameter before swelling was between 20 and 23 μ, and the magnification in both photographs is the same. When either type A or B crosslinked fibers were swollen with *m*-cresol, additional helical coils were produced.

In the previous paper [1] a tentative hypothesis was advanced to explain the crimping and coiling tendency in terms of differential swelling and structural asymmetry resulting from the crosslinking process. Since then, additional data on the crystalline structure and internal orientation of crosslinked nylon-6 homofibers have been obtained, and the effect of alkylene sulfide crosslinks on fiber properties has been studied. These new data provide an increased understanding of the effects of crosslinking on fiber properties and will be presented as part of the following discussion.

From the chemical reaction series discussed above, it is noted that prior to the introduction of alkylene sulfide crosslinks, some disulfide crosslinks will have been formed due to partial oxidation of the mercaptide groups. These crosslinks exercise a local restraining effect upon the amorphous structure and some crimping results during the mild swelling that occurs at this stage. The next step actually involves two simultaneous reactions: (1) Further swelling of the fiber in a mixture of benzyl alcohol and ethyl alcohol, and (2) additional crosslinking by flexible alkylene sulfide groups. During this swelling process further internal plasticization of the fiber and partial disruption of the crystallites take place, thus

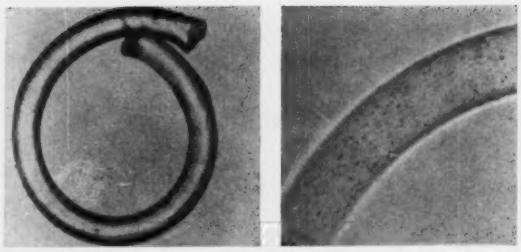

FIGURE 2. *Helical coiling of type A alkylene sulfide crosslinked nylon-6 fiber.*

Left: A single helical coil of the unswollen (dry) fiber; Right: A portion of the helical coil swollen in *m*-cresol.

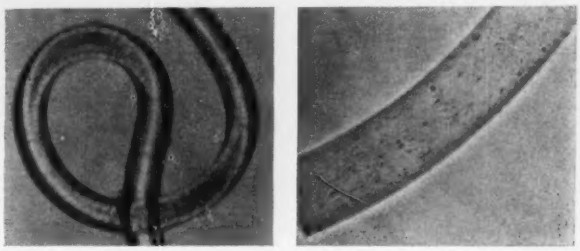

FIGUGE 3. *Helical coiling of type B alkylene sulfide crosslinked nylon-6 fiber.*

Left: A single helical coil of the unswollen (dry) fiber; Right: A portion of the helical coil swollen in *m*-cresol.

permitting the penetration of the alkylene dihalide reagent. The crystallites present resist the deformation of the fiber, but as the smaller crystallites are disrupted, some of this resistance is removed so that the crimping becomes more pronounced and some coiling occurs. It is likely that the introduction of alkylene sulfide crosslinks when the fiber is in this deformed state tends to reinforce this deformation, and to accentuate the extent of crimping and coiling even in the unswollen state. If complete destruction of the crystallites is permitted, such as during swelling in *m*-cresol, the fiber will undergo helical coiling because all counterforce to deformation has now been removed. This latter effect is similar to that previously observed in the disulfide crosslinked system [1, 2].

The above macroscopic deformations are associated with changes in the fine structure of the fiber as evidenced by birefringence and X-ray analyses. Birefringence measurements were carried out on the uncrosslinked and crosslinked nylon-6 fibers using a slot compensator (sodium D light) with samples approximately 2 in. in length. Birefrengence $=(n_1-n_2)=R/t$, where n_1 and n_2 are refractive indices along and across the fiber axis, respectively, R is retardation in millimicrons (measured with the compensator), and t is thickness of the fiber in millimicrons (measured with a micrometer eyepiece). The birefringence values of the uncrosslinked (scoured) samples varied between $+0.055$ and $+0.060$. On the other hand, the alkylene sulfide crosslinked fibers showed nonuniform birefringence values that ranged from $+0.019$ to $+0.0048$ for five measurements along approximately 2 in. length samples. The irregular decrease in birefringence

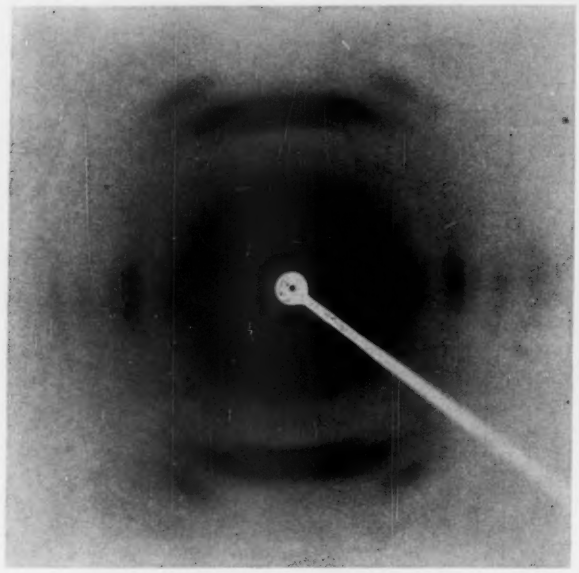

FIGURE 4. *X-ray diffraction photograph of unmodified (scoured) nylon-6 fiber.*

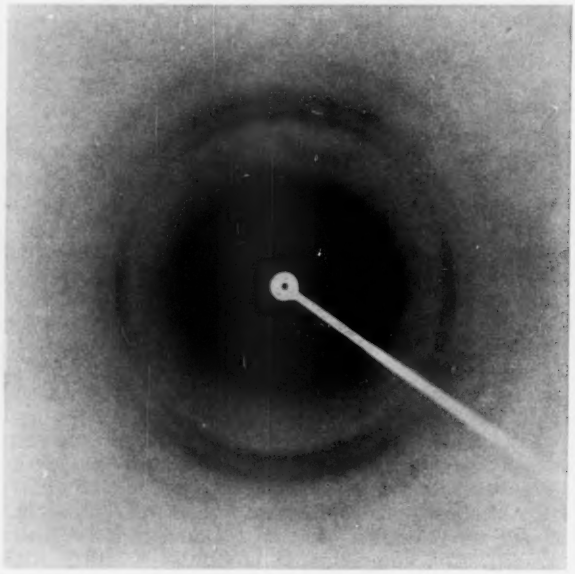

FIGURE 5. *X-ray diffraction photograph of disulfide crosslinked nylon-6 fiber.*

indicates decreased and nonuniform orientations of the polymer chains in the crosslinked fiber. This observation is similar to that reported earlier in the disulfide crosslinked samples [1]. The decrease in birefringence is probably the result of the partial disruption of the crystallites and the plasticizing effect of the swelling agent, and is limited by the structural strain caused by the crosslinks.

Additional evidence for important changes in the internal structure of crosslinked nylon-6 fibers is

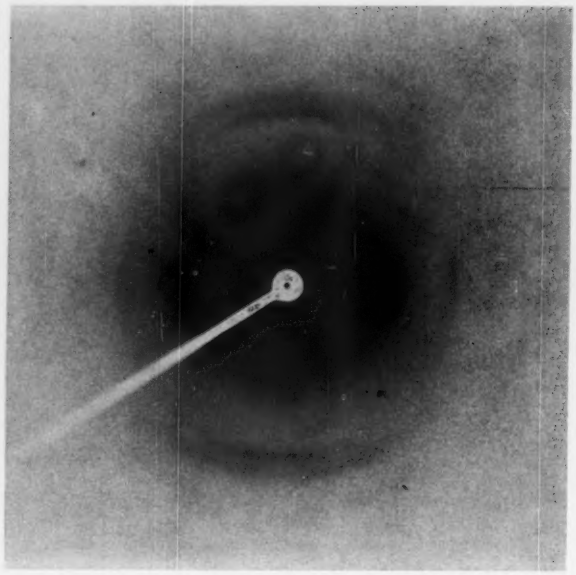

FIGURE 6. *X-ray diffraction photograph of alkylene sulfide crosslinked (type A) nylon-6 fiber.*

shown by X-ray analyses [13, 14, 15]. Figures 4 to 6 depict X-ray diffraction photographs of the uncrosslinked (scoured), disulfide crosslinked, and alkylene sulfide crosslinked fibers, respectively.

The unmodified nylon-6 (fig. 4) exhibits good orientation, whereas the alkylene sulfide crosslinked sample (fig. 6) shows appreciable orientation spread of up to around 20° from the ideal unit-cell alinement. The disulfide crosslinked sample (fig. 5) shows even less preferred orientation. The innermost of the two intense equatorial spots has been spread into a continuous Debye-Scherrer ring that shows only slightly greater intensity along the equatorial compared to that along the meridional radius.

It is not yet possible to differentiate between the relative effects of decreased orientation and decreased crystallite size on the observed macroscopic deformations exhibited by the disulfide and alkylene sulfide crosslinked samples. The partial disruption of the crystallites may be due to the combined effects of plasticization by the swelling agent and to internal strain caused by the crosslinks. The observed higher crimp frequency and partial helical coiling even in the unswollen (dry) state of the alkylene sulfide crosslinked fibers in comparison to the disulfide crosslinked samples may thus indeed be the result of the removal of some of the counterforce maintained by the crystallites, as already discussed above. (See note on p. 81.)

In contrast to the disulfide crosslinked nylon-6 fibers [1], the alkylene sulfide crosslinked samples showed no decrease in the extent of crimping and coiling after prolonged standing in air or when the fibers were treated with dilute solutions of an oxidizing agent, such as H_2O_2. This is probably due to the fact that in the case of the alkylene sulfide crosslinked fibers there were no significant amounts

of free labile sulfhydryl groups, these having been "blocked" (alkylated) by either methylene or ethylene halides from further oxidation. Thus, the "built-in" differential swelling effect [1] was maintained. The "blocking" of the free sulfhydryl groups can also be achieved by treatment with $AgNO_3$, thus forming the stable silver mercaptides, but this procedure causes blackening of the fibers due to reduction of some of the silver ions to free silver that cannot be readily removed.

The alkylene sulfide bonds are much less subject to chemical reductions, than are the disulfide groups [16]. This property should make the former crosslinkages more desirable from the point of view of stability. It is possible that other properties, such as heat and hydrolytic stability, as well as stress-strain characteristics, will also show decisive advantages for the alkylene sulfide type bonds over the disulfide crosslinkages.

3. Experimental Details

All work was carried out with 7.8 Tex (60 denier)/32 filament round cross-section nylon-6 homofiber.

3.1. *N*-methoxymethylation (B)

This reaction was carried out according to a procedure reported earlier [1, 5, 6].

3.2. Preparation of the Mercaptides (F), Experiment No. 1, Table 1

A small skein (0.1–0.2 grams) of the *N*-methoxymethylated nylon-6 fiber was soaked for 12 hr at room temperature in a solution containing 37.5 g (0.5 moles) of thioacetamide and 700 ml of methyl alcohol. Next, 35 ml of conc. HCl (0.42 moles) was added and the fiber soaked for 1 hr at room temperature. After this period 60.0 g (1.06 moles) of KOH was added in 200 ml of methyl alcohol and the fiber was permitted to soak at room temperature for 1 hr. The fiber was then washed thoroughly twice with methyl alcohol, twice with distilled water, and again twice with methyl alcohol.

3.3. Introduction of Type A Alkylene Sulfide Crosslinkages (G), Experiment No. 1, Table 1

(a) The fiber from (2) was soaked for 5 hr at room temperature in a solution of 150 ml of ethyl alcohol, 150 ml of benzyl alcohol, and 29 ml (0.36 moles) of methylene diiodide. After this period the sample was thoroughly washed twice with ethyl alcohol, twice with distilled water, and twice with methyl alcohol and allowed to dry at room temperature. S=3.7 percent.

(b) The procedure was the same as in (a), except that soaking time was 24 hr instead of 5 hr (Exp. No. 2, table 1). S=3.6 percent.

3.4. Introduction of Type B Alkylene Sulfide Crosslinkages (H), Experiment Nos. 3 and 4, Table 1

The fiber from (2) was soaked for 24 hr at room temperature in a solution of 90 ml of ethyl alcohol, 90 ml of benzyl alcohol, and 90 ml (1.04 moles) of 1,2,-dibromoethane. After this period the sample was thoroughly washed twice with ethyl alcohol, twice with distilled water, and twice with methyl alcohol, and allowed to dry at room temperature. S=2.9 percent.

3.5. Introduction of Disulfide Crosslinks (E), Experiment No. 5, Table 1

This reaction was carried out according to a procedure reported earlier [1]. S=2.7 percent.

The author thanks R. A. Paulson, Applied Analytical Research Section, National Bureau of Jtandards for the sulfur analyses, and Sylvia M. Bailey for technical assistance in some phases of this work.

4. References

[1] S. D. Bruck, J. Research, NBS **65A** (Phys. and Chem.), No. 5, 489 (Nov.–Dec. 1961).
[2] Technical News Bulletin, NBS **45,** 152 (1961). Structural modification of synthetic fibers.
[3] J. B. Speakman and C. S. Whewell, J. Soc. Dyers Colourists, **52,** 380 (1936).
[4] W. I. Patterson, W. B. Geiger, L. R. Mizell, and M. J Harris, J. Research NBS **27,** 89 (1941).
[5] W. R. Sorensen and T. W. Campbell, Preparative Methods of Polymer Chemistry, p. 64, Interscience Publishers, Inc., New York, 1961.
[6] T. L. Cairns, H. W. Gray, A. K. Schneider, and R. S. Schreiber, J. Am. Chem. Soc. **71,** 651 (1949).
[7] C. R. Noller, Chemistry of Organic Compounds, p. 136, W. B. Saunders Co., Philadelphia, 1951.
[8] S. D. Bruck and S. M. Bailey, J. Research NBS, in press.
[9] S. D. Bruck, J. Polymer Sci., In press.
[10] S. D. Bruck, J. Research NBS **65A** (Phys. and Chem.), No. 5, 485 (Nov.–Dec. 1961).
[11] P. J. Flory, Principles of Polymer Chemistry, Cornell University Press, Ithaca, N.Y., 1953.
[12] S. D. Bruck, Unpublished data.
[13] H. Steffen Peiser (private communication) and Boris Paretzkin (X-ray exposures), Analytical and Inorganic Chemistry Division, National Bureau of Standards.
[14] C. W. Bunn and E. V. Garner, Proc. Roy. Soc. **A189,** 39 (1947).
[15] D. R. Holmes, C. W. Bunn, and D. J. Smith, J. Polymer Sci. **17,** 159 (1955).
[16] A. Cantarow and B. Schepartz, Biochemistry, 2d Ed., p. 272, W. B. Saunders Co., Philadelphia, 1957.

NOTE ADDED IN PROOF. The importance of the fine crystalline structure of nylon-6 in the crimping process is further indicated from preliminary results on samples having predominantly *alpha* crystalline structure. These fiber samples exhibited a much greater crimping tendency than those samples in which both *alpha* and *beta* cryallinest structures were present in approximately equal amounts.

(Paper 66A1–143)

JOURNAL OF RESEARCH of the National Bureau of Standards—A. Physics and Chemistry
Vol. 66A, No. 1, January–February 1962

Ion Transport Across Membranes: I. Definitions of Membrane Electromotive Forces and of Flows of Electrolytic Solutes

Blanton C. Duncan

(October 10, 1961)

An analysis is given for the treatment of membrane transport phenomena in accord with the theory of steady state thermodynamics. A linear macroscopic theory for discontinuous systems is applied as a postulate. It is shown that as a consequence of the transformation properties of the Onsager reciprocal relations the definition of a membrane electromotive force gives corollary definitions of the flows of electrolytic solutes as a whole in the form of linear combinations of the flows of ionic constituents. It is shown that established conventions which set the activity coefficients of ionic constituents equal to unity at the reference state of infinite dilution lead to a particular definition of the membrane electromotive force which may be applied at any concentration.

1. Introduction

This paper reports the results of a part of a study directed toward the detailed application of the thermodynamics of steady state processes to the investigation of transport phenomena at junctions between electrolytic solutions. The work was undertaken as a part of a research project under the sponsorship of the Office of Saline Water of the U.S. Department of the Interior. This project had the aim of improving the methods of measuring and reporting the electrochemical characteristics of membranes.

In this paper we are concerned with the problem of treating permeability characteristics during steady states involving the transfer of electric charge without introducing the classical uncertainty involving the electrostatic potential difference between two chemical phases of different composition [1, 2, 3, 4].[1] The existence of such an electrostatic potential difference is postulated in discussions of the application of steady state thermodynamics to electrolytic transport problems. The usual practice [5] is to introduce the definition of the differential of the chemical potential of an ionic constituent in the form

$$d\mu_i^e = (d\mu_i^e)_{d\xi=0} + z_i^e \mathcal{F} d\xi \tag{1}$$

where $d\mu_i^e$ is the total differential of the chemical potential; z_i^e is the electrovalence; $\mathcal{F}$ is the faraday; and $d\xi$ is the differential of the electrostatic potential. The first term on the right, the "nonelectrical part," may be put formally

$$(d\mu_i^e)_{d\xi=0} = -\bar{S}_i^e dT + \bar{V}_i^e dP + RT d\ln m_i^e + RT d\ln \gamma_i^e \tag{2}$$

where $\bar{S}_i^e$, $\bar{V}_i^e$, m_i^e, and γ_i^e are, respectively, the partial molar entropy, the partial molar volume, the molality and the activity coefficient at constant temperature and pressure of the ionic constiuent. We note here that if ion constituents are defined as MacInnis [6] defines them, m_i^e and hence $d\ln m_i^e$ are operational quantities without extra-thermodynamic assumptions adopted as arbitrary conventions. The work of Guggenheim [7] as confirmed by de Groot and Tolhoek [8] shows that in ordinary electrochemical systems only the term $d\mu_i^e$ on the left in eq (1) may be included with $d\ln m_i^e$ as an operational quantity in a thermodynamic treatment.

de Groot and Tolhoek give demonstrations that, in principle, one may treat transport across junctions between electrolytic solutions without seeking to make the division of chemical potential differentials called for in eq (1). The first object of this paper is to set down a fundamental steady state treatment which makes explicit use of familiar electrochemical quantities but avoids the use of eq (1). The fundamental treatment given here is new only in the sense that it is a unified analysis applicable to the peculiar requirements of membrane studies. It may properly be viewed as first a restriction of Guggenheim's [9] treatment of galvanic cells to discontinuous systems. The treatment is then extended to nonisopiestic systems by including the flow of solvent in a membrane fixed frame of reference. It is further extended to the treatment of stationary states involving flows of electric charge. Finally, by following Temkin and Koroshin [10, 11] and Agar [12] in the treatment of electronic transport entropies we extend the analysis to nonisothermal systems.

In much theoretical and experimental work there appears to be a need to adopt conventions regarding single ion activities, membrane potentials, salt bridges, or ideal "inert" electrodes. In terms of the steady state theory these conventions are viewed as giving definitions to a "force"—the EMF—conjugate to a "flow"—the electric current—in the same sense that a pressure difference is a force conjugate to the flow of fluid volume. In the discussion given in section 10 we show an important case in which the ex-

[1] Figures in brackets indicate the literature references at the end of this paper.

plicit need for such a convention arises. The second object of this paper is to study the requirements to be met by an EMF convention if it is to lead to an internally consistent treatment of transport phenomena. We will show that the application of the steady state theory leads quite naturally to a particular conventional definition of the membrane EMF. This definition is developed in sections 8 and 9.

2. Analytical Model

In our analysis we will formally treat a one dimensional, discontinuous, open steady state system without chemistry [13]. Flows through a junction are treated as if they took place between two points. The points, α and β, are taken as representative of two parallel planes in a real system at each of which one may assign by experiments a truly representative average value of any intensive property. A "junction" is everything between α and β and its composition need not be defined. We only require flow continuity between α and β. The flow of a conserved quantity, i.e., energy, mass as a chemical constituent, and electric charge, across α in the direction of β must be equal to the flow of that quantity across β toward the surroundings of β. Flows are positive in the direction α to β and are to be measured with reference to α and β.

The postulate of local equilibrium is applied at α and β. A complete set of intensive equilibrium thermodynamic properties can be defined by the local temperature, pressures, and component concentrations when α and β are at the same gravitational potential with no other external fields operating. During a steady state these intensive properties are to be maintained constant by exchanges with the surroundings.

We give *a priori* emphasis to certain consequences of this model. The uncertainty which arises in discussions of transference numbers and diffusion coefficients continues to receive attention in the literature [14, 15, 16]. An analysis of the model chosen gives permeability characteristics as integral characteristics of a junction in a cell fix frame of reference. Thus if the real system were a simple Hittorf transference cell [17], an integral transference number of an ion constituent would be by definition a property of the middle cell region, a solution filled glass tube. A transformation to an ordinary Hittorf or Washburn [12] number given with reference to the center of mass of the solvent would yield another integral property of the solution filled glass tube. The identification of these latter properties as properties of the solution would, in the usual way, require a demonstration that wall effects in large tubes contribute only to the extent that the tube defines the geometry of the solution.

3. Fundamental Steady State Formulation

de Groot gives a detailed discussion of the fundamental principles of the steady state theory. We accept the theory here in the manner of a formal postulate. The material of this section sets forth the way in which quantities of established operational significance are to be employed to define flows and forces in the steady state description of junction processes without resort to eq (1).

The choice of a concentration scale is immaterial to the essential results of this paper. In nonisothermal systems it is generally preferable to avoid volume concentrations [37]. We find it convenient to employ molalities, mole kg^{-1} of solvent. The compositions of the solutions at α and β are defined by the concentrations of r *constituents*. The first m, including the solvent, are nonelectrolytes. The next r-m are ionic constituents. We define a *constituent* composition vector, $\{m^f\}$, the elements of which are the molalities of these constituents. We define the constituent electrovalence vector, $\{z^f\}$, where the elements are the electrovalences of the respective constituents represented in $\{m^f\}$. The restriction of the electroneutrality condition is expressed by

$$\{z^f\}^\dagger \{m^f\} = 0 \tag{3}$$

where the superscript dagger, †, denotes transposition.

Under the restriction imposed by eq (3) it will always be possible to express the composition of solutions α and β in terms of $r-1$ independent components [38]. We define a *component* composition vector, $\{m^*\}$, where the respective elements are the molalities of electrically neutral isolable chemical compounds. These composition vectors must be connected by a relation,

$$[\![\nu]\!]\{m^*\} = \{m^f\} \tag{4}$$

or, in more detail,

$$\begin{bmatrix} 1 & \cdots & 0 & 0 & \cdots & 0 \\ \cdots & \cdots & \cdots & \cdots & \cdots & \cdots \\ 0 & \cdots & 1 & 0 & \cdots & 0 \\ 0 & \cdots & 0 & \nu_{m+1,\,m+1} & \cdots & \nu_{m+1,r-1} \\ \cdots & \cdots & \cdots & \cdots & \cdots & \cdots \\ 0 & \cdots & 0 & \nu_{r-1,m+1} & \cdots & \nu_{r-1,r-1} \\ 0 & \cdots & 0 & \nu_{r,m+1} & \cdots & \nu_{r,r-1} \end{bmatrix} \begin{Bmatrix} m_1^* \\ \cdots \\ m_m^* \\ m_{m+1}^* \\ \cdots \\ m_{r-1}^* \end{Bmatrix} = \begin{Bmatrix} m_1^f \\ \cdots \\ m_m^f \\ m_{m+1}^* \\ \cdots \\ m_{r-1}^f \\ m_r^f \end{Bmatrix} \tag{5}$$

An element, ν_{ij}, of the matrix $[\![\nu]\!]$ is zero or a positive integer. It is the number of moles of the ith constituent contained in one mole of the isolated jth neutral component. The particular combinations of ionic constituents chosen as neutral components are a matter of convenience except that the *independence* of the components requires that $[\![\nu]\!]$ be of rank $r-1$. A unique solution must exist for the molalities of components in terms of molalities of $r-1$ constituents. We note that the requirement of electroneutrality for every component is expressed by

$$\{z^f\}^\dagger[\![\nu]\!]=[\![0]\!]. \tag{6}$$

We also note that convenience is best served if $[\![\nu]\!]$ is chosen such that the elements of the solution vector $\{m^*\}$ of eq (4) satisfy the condition

$$m_j^*\geq 0; \qquad (j=1, 2, \ldots, r-1). \tag{7}$$

It is important to note that in equilibrium thermodynamics one can treat the properties of a three component system such as H_2O-NaCl-KBr. In a steady state treatment of transport processes—"without chemistry"—such as the interdiffusion of the components between solutions with differing concentrations of NaCl and KBr we must regard such solutions as special cases in which the concentration of a fourth component, either KCl or NaBr, is zero. In practice such special cases would be treated as the result of special restraints upon the possible transport processes in a system under study.

Writing

$$\Delta\mu_i=\mu_i^\beta-\mu_i^\alpha. \tag{8}$$

as the difference in chemical potential of a chemical component or constituent between α and β and using the equilibrium property

$$\mu_j^*=\sum_{i=1}^{r}\nu_{ij}\mu_i; \qquad (j=1, \ldots, r-1) \tag{9}$$

we secure the equation,

$$[\![\nu]\!]^\dagger\begin{Bmatrix}\Delta\mu_1^*\\ \cdots\\ \Delta\mu_m^*\\ \Delta\mu_{m+1}^e\\ \cdots\\ \Delta\mu_{r-1}^e\\ \Delta\mu_r^e\end{Bmatrix}=\begin{Bmatrix}\Delta\mu_1^*\\ \cdots\\ \Delta\mu_m^*\\ \Delta\mu_{m+1}^*\\ \cdots\\ \Delta\mu_{r-1}^*\end{Bmatrix} \tag{10}$$

The superscript, *, indicates quantities which are functions of only temperatures, compositions, and pressures in accord with classical thermodynamics. The superscript, e, indicates quantities requiring an auxiliary electrochemical operation involving measured transfers of electric charge coupled with measured transfers of material constituents [19, 20]. The algebraic theorem that eq (10) possesses no unique solution for the elements of the vector on the left is equivalent to Guggenheim's conclusion that where α and β are formally treated as electrically isolated phases, the elements $\Delta\mu_i^e$ have no general thermodynamic significance. However, when α and β are not electrically isolated but communicate through a junction permeable to at least one ion constituent, the elements $\Delta\mu_i^e$ are operationally meaningful. Guggenheim considers the case when α and β are at the same temperature and pressure. He shows that when a reversible current can be passed between the terminals of a pair of identical electrodes reversible to the ith constituent, one at α and one at β, the relation

$$\Delta_{T,P}\mu_i^e=z_i^f\mathcal{F}(E_i^\beta-E_i^\alpha) \tag{11}$$

defines the chemical potential differences when $E_i^\beta-E_i^\alpha$ is the electric potential difference measured between the electrode terminals. Equation (11) is easily modified to include cases where the temperatures and pressures at the electrodes are not equal. Here we follow Temkin and Koroshin [10, 11], Agar [12], and deBethune [21] by choosing to have the leads from the electrodes at α and β be wires of identical composition which come out to terminals which are at the same temperature, but we specifically require the use of platinum wire for these leads.[2] We write the electrode reaction

$$\sum_k\lambda_{ik}\mathscr{A}_{ik}+\frac{1}{z_i^f}\mathscr{B}_i^f+e^-=0 \tag{12}$$

for an electrode reversible to the ith constituent. $\mathscr{B}_i^f$ denotes the chemical symbol of the constituent corresponding to the ith element of $\{m^f\}\cdot\mathscr{A}_{ik}$ denotes neutral components of the electrode which are virtually insoluble in the solutions at the electrodes and, hence, are not represented in the vector $\{m^*\}$. For example, for a silver–silver chloride electrode we write

$$-\mathrm{Ag}+\mathrm{AgCl}-\mathrm{Cl}^-+e^-=0 \tag{12a}$$

with k taking the values 1 and 2. $\mathscr{A}_{i1}$ is silver; $\mathscr{A}_{i2}$ is silver chloride; and λ_{i1} and λ_{i2} are -1 and 1, respectively.

We then write for each ion constituent

$$\Delta\mu_i^e=z_i^f\mathcal{F}\Delta\phi_i; \qquad (i=m+1, \ldots, r) \tag{13}$$

[2] In nonisothermal systems it is necessary to indicate the reference medium implied for electrons when one writes an electrode reaction. The established use of platinum in constructing hydrogen electrodes and in resistance thermometers makes it convenient to regard platinum at 25 °C as the reference medium for electrons.

where $\Delta\phi_i$ is the EMF obtained by correcting the measured EMF, $E_i^\beta - E_i^\alpha$, for the homogeneous thermoelectric effect in the platinum leads and for the chemical potential differences of the insoluble components involved in the electrode reaction, i.e.,

$$\Delta\phi_i = (E_i^\beta - E_i^\alpha) + \frac{\overline{\overline{S}}_{pt}}{\mathcal{F}}\Delta T - \frac{1}{\mathcal{F}}\sum_k \lambda_{ik}\Delta\mu_k \qquad (14)$$

where $\overline{\overline{S}}_{pt}$ is the transported entropy for electrons in platinum.[3]

For silver–silver chloride electrodes under ordinary conditions eq (14) becomes

$$\Delta\phi_{Cl^-} = (E^\beta_{Cl^-} - E^\alpha_{Cl^-}) + \frac{\overline{\overline{S}}_{pt}}{\mathcal{F}}\Delta T$$

$$-\frac{1}{\mathcal{F}}[(\overline{S}_{Ag} - \overline{S}_{AgCl})\Delta T - (\overline{V}_{Ag} - \overline{V}_{AgCl})\Delta P] \qquad (14a)$$

where the term in square brackets is derived from eq (16) below with the condition that

$$\left(\frac{\partial\mu_k}{\partial m_j^*}\right)_{TP,m} = 0 \qquad (15$$

for compounds in their standard states.

Equation (13) defines the last r-m elements of the vector on the left in eq (10). The first m elements are defined using the classical equilibrium thermodynamic relation resulting from the choice of temperature, pressure, and molality as independent intensive variables, i.e.,

$$d\mu_i^* = -\overline{S}_i^* dT + \overline{V}_i^* dP + \sum_{j=2}^{r-1}\left(\frac{\partial\mu_i^*}{\partial m_j^*}\right)_{T,P,m} dm_j^* \qquad (16)$$

$\overline{S}_i^*$ denotes the partial molal entropy; $\overline{V}_i^*$ denotes the partial molal volume; and the summation is over the independent solute components represented in the vector $\{m^*\}$. Since we wish to express the thermodynamic "forces", $\Delta\mu_i^*$, as *linear* functions of the experimental "forces" it is convenient to write

$$\Delta\mu_i^* = -\overline{S}_i^*\Delta T + \overline{V}_i^*\Delta P + \sum_{j=2}^{r-1}\cdot\Theta_{ij}^*\,\Delta\log\, m_j^* \qquad (17)$$

where

$$\Theta_{ij}^* \equiv \left(\frac{\partial\mu_i^*}{\partial\log m_j^*}\right)_{T,P,m} \qquad (18)$$

with log denoting logarithms to the base 10. This gives a condensed symbol for our constant coefficient; we expect $\Delta\mu_j^*$ to be more nearly proportional to $\Delta\log m_j^*$ than to Δm_i^*. We restrict our attention here to steady states representing displacements from a definite reference state of complete equilibrium between α and β when the solutions α and β have the same temperature, pressure, and concentrations of components with no net flows of energy, chemical constituents, or electric charge taking place between them.[4] The vectors $\{m^f\}$ and $\{m^*\}$ are defined at this state.

It is useful to show how Θ_{ij}^* is to be expressed in terms of the solution compositions and activity coefficients.

We have the defining relation

$$(\mu_i^*)_{T,P} = \mu_i^0 + RT\sum_{k=1}^{r}\nu_{ki}\ln m_k^f\gamma_k^f; \quad (i=1,2,\ldots,r-1) \qquad (19)$$

where the summations are over the elements of $\{m^f\}$. Here, for ion, constituents, γ^f is a single ion activity coefficient[5] which in this paper has no more than the ordinary significance of a formal device. It disappears when eq (19) is written in the meaningful form

$$(\mu_i^*)_{T,P} = \mu_i^0 + RT\sum_{k=1}^{r}\nu_{ki}\ln m_k^f + \nu_i^* RT\ln\gamma_i^* \qquad (20)$$

where

$$\nu_i^* \equiv \sum_{k=1}^{r}\nu_{ki} \qquad (21)$$

and γ_i^* is the molal activity coefficient for nonelectrolytes and the mean molal activity coefficient for electrolytes. From eq (20) and the definition given by eq (18) we find

$$\Theta_{ij}^* = \frac{RT}{0.4343}\left[m_j^*\sum_{k=1}^{r}\frac{\nu_{ki}\nu_{kj}}{m_k^f} + \nu_i^*\left(\frac{\partial\log\gamma_i^*}{\partial\log m_j^*}\right)_{T,p,m}\right]. \qquad (22)$$

There is a real advantage of simplicity and convenience in the form of eq (22) where ionic molalities are retained. The introduction of mean ionic molalities as suggested by textbooks leads to an almost hopelessly unwieldly expression in the general case.

We recognize the experimental fact that the solutions may be of such a composition that no reversible electrode will function as required by eq (14). However, as demonstrated in section 6, if a single pair of reversible electrodes is available to measure $\Delta\phi_i$; for any one of the ion constituents represented in $\{m^f\}$, the added equation supplements eq (10) to give a solution for the remaining terms, $\Delta\mu_i^*$. Thus, given a satisfactory pair of reversible electrodes, we may define every term in eq (10) in terms of operational quantities without resort to eq (1).

---

[3] At temperatures near 25 °C the work of Koroshin and Temkin gives

$$\overline{\overline{S}}_{pt} = -8.66\times10^{-4} + 0.044\times10^{-4}T; \quad (T>220\ °k)$$

with temperature in degrees Kelvin and $\overline{\overline{S}}_{pt}$ in volt faraday deg^{-1}.

[4] The steady state postulate can be applied with reference to other equilibrium states, e.g., osmotic equilibrium. However, in writing eq (17) we imply the one indicated because we regard $\overline{S}_i^*$; $\overline{V}_i^*$ and Θ_{ij}^* as constants.

[5] It should be noticed that we distingush γ^* in eq (2) and γ^f here. We regard γ^* as being defined on the basis of a postulate that the electrostatic potential, $\Delta\xi$, can be operationally defined between solutions of different compositions at finite concentrations. This postulate has been rejected.

A fundamental set of phenomenological relations

$$\{J^I\}=[\![L^I]\!]\{X^I\} \tag{23}$$

with

$$[\![L^I]\!]=[\![L^I]\!]^\dagger \tag{24}$$

may now be set down by choosing

$$\{J^I\}=\begin{Bmatrix} J_1^I \\ \cdots \\ J_m^I \\ J_{m+1}^I \\ \cdots \\ J_r \\ J_q \end{Bmatrix}, \text{ and } \{X^I\}=\begin{Bmatrix} -\Delta\mu_1^* \\ \cdots \\ -\Delta\mu_m^* \\ -\Delta\mu_{m+1}^e \\ \cdots \\ -\Delta\mu_r^e \\ -\Delta \ln T \end{Bmatrix} \tag{25}$$

This choice of flows and forces is similar to that employed by Kirkwood [22] in differential form. We have already defined the first r elements of $\{X^I\}$ and grant that $\Delta \ln T$ is a meaningful quantity. The first r elements of $\{J^I\}$ are flows of chemical constituents corresponding to the respective elements of $\{m^I\}$. Since the chemical constituents are defined as having fixed identities in cell processes including exchanges with the surroundings of α and β it may be granted that the first r elements of $\{J^I\}$ are meaningful quantities. It is this conservation of chemical identity in the complete specification of concentrations and of flows of matter which permits the analysis "without chemistry" [13].[6]

The flow of "entropic heat," J_q^I, must be given special notice. We select the name, entropic heat, on the basis of the discussion set down by de Groot [24] who notes that various flows are termed "flows of heat" by different authors. The flow of entropic heat is defined by

$$J_q^I=J_u-\sum_{i=1}^{m}\mu_i^*J_i^I-\sum_{i=m+1}^{r}\mu_i^eJ_i^I \tag{26}$$

where J_u is the flow of energy. Energy is of course conserved in all cell processes. Entropic heat is not. However, we cannot rely upon eq (26) alone to define J_q^I since the chemical potential of a single ion constituent, μ_i^e, has been given no meaningful definition. Only its significance in the particular linear combinations of eq (9) has been established. It is necessary to state conditions which are at least sufficient to establish an operational definition of J_q^I.

We first note that by eq (23)

$$J_q^I=-L_{qq}^I\Delta \ln T-\sum_{j=1}^{r}L_{qj}^IX_j^I. \tag{27}$$

A measurement of the thermal conductivity of the junction when all flows of matter are zero gives

$$J_q^I=J_u; \quad (J_{j\neq q}^I=0) \tag{28}$$

from which L_{qq}^I may be determined using

$$L_{qq}^I=-\frac{J_u}{\Delta \ln T}+\sum_{j=1}^{r}L_{qj}^I\frac{X_j^I}{\Delta \ln T}; \qquad (J_{j\neq q}=0) \tag{29}$$

when the experiment is designed to simultaneously evaluate the elements of $\{X^I\}$ and the elements L_{qj}^I are already known. Since by eq (24)

$$L_{qj}^I=L_{iq}^I \tag{30}$$

the equations

$$L_{qj}^I=L_{iq}^I=-\frac{J_i^I}{\Delta \ln T}+\sum_{i=1}^{r}L_{ij}^I\frac{X_j^I}{\Delta \ln T} \tag{31}$$

applied to measurements of the flow of each material constituent in the presence of a temperature difference would evaluate each term L_{qj}^I when again the elements of $\{X^I\}$ are simultaneously evaluated and the elements L_{ij}^I are known. We finally require the measurement of a complete set of isothermal permeability characteristics to define the elements of the isothermal admittance matrix in the equation

$$[\![L_{ij}^I]\!]\begin{Bmatrix} X_1^I \\ \cdots \\ X_r^I \end{Bmatrix}=\begin{Bmatrix} J_1^I \\ \cdots \\ J_r^I \end{Bmatrix} \tag{32}$$

which is obtained from eq (23) by setting $\Delta \ln T$ equal zero. Isothermal measurements dealing with flows of conserved quantities require no special discussion.

This formulation of a *linear* macroscopic theory requires an additional postulate to put a restriction upon the magnitude of any admissible displacement of equilibrium from the reference state. We have chosen to give the treatment of a discontinuous system in order to avoid operational uncertainties which often arise in attempts to apply an analysis of a continuous system [25]. In general we are unable to measure intensive properties at an arbitrarily dense succession of planes lying between α and β. Our choice is in line with the suggestions of Kirkwood [22] and Scatchard [26]. Thus the specification of a junction such as one including a membrane or porous plug must include the specification of the composition of the contacting solutions at the reference state. At the reference state we formally assume that equilibrium is established with respect to all solution components throughout the region α to β. The integral admittance matrix, $[\![L^I]\!]$, can in principle include linear "polarization" effects in the boundary layers. However, with

[6] The treatment of water as a nonelectrolytic solvent limits the participation of hydrogen and hydroxyl ions in the net transfer of electric charge to those systems where either a strong acid or strong base is present as a solute. The treatment of weak electrolytes requires the introduction of "chemistry" [23].

reference to Kirkwood's treatment of thed tirec transformation of the analysis of a continuous system into the analysis of a discontinuous system, Schlögl [27] has demonstrated the possibility of "apparently" linear phenomenological relations where the elements of $[\![L']\!]$ are not proper constants. In such a case the respective elements of a series of differential admittance matrices defined as functions of position between α and β would not, upon integration, give the corresponding elements of $[\![L']\!]$. In a purely phenomenological approach no basis can exist for distinguishing "really" and "apparently" valid applications of eqs (23) and (24). Schlögl's analysis suggests that no difficulty exists in the limit of the reference state and that if the forces represented in $\{X'\}$ are "sufficiently small," the experimental demonstration of any such distinction would be difficult and would require measurements of the highest accuracy and precision. We require some quantitative criterion for judging what forces are "sufficiently small."

Miller [28] has recently reviewed the experimental evidence which bears upon the validity of the Onsager relations in macroscopic processes. Miller [29] and Dunlop and Gosting [30, 31] have given detailed attention to ternary diffusion in electrolytic solutions. It is clear from a study of these papers that any criterion will necessarily be somewhat arbitrary. Nevertheless, since a major part of the intuitive support for the postulation of a linear macroscopic theory involves the established validity of linear free energy relationships such as eq (17) it is reasonable to assume that the range of validity of eq (17) is of fundamental significance in applications of the theory. Therefore, we choose to apply the following minimum condition:

It is assumed that determinations of the elements of $[\![L']\!]$ will involve displacements of equilibrium with forces and flows of such a magnitude that the uncertainty in the value of an element L'_{ij} arising from uncertainties in measurements of temperatures, concentrations, pressures, and potentials will be equal to or greater than the errors introduced by neglecting variations of $\overline{V}_i^*, \overline{S}_i^*$, and Θ_{ij}^*.

This criterion has the practical advantage of setting "sufficiently small" at magnitudes consistent with the precision and accuracy of any particular experimental investigation.

4. Transformation Properties

In the fundamental formulation, a flow of electric charge is identified with the flow of each ionic constituent and a conjugate electromotive force is defined for each such flow. However, no net flow of charge or overall electromotive force occurs as an element of the vectors $\{J'\}$ and $\{X'\}$. The thermodynamic theory does not require us to define vectors containing such elements, but the definition of all elements of $\{J'\}$ during all processes including electric charge flows depends upon our extrathermodynamic definitions of ionic constituents and our use of the established conservation relation

$$\frac{I}{\mathcal{F}} = \sum_{i=m+1}^{r} z_i^f J_i^f. \tag{33}$$

The electric current in amperes is denoted by I. Equation (33) suggests a linear transformation of flows to give a new flow vector, say $\{J'\}$, where one element is the flow of electric charge. A corresponding transformation of forces to give a new force vector, $\{X'\}$, would contain an element conjugate to the flow of charge. In this paper we identify such an element of $\{X'\}$ as a junction EMF.

The steady state theory explicitly defines restrictive conditions which must be applied in carrying out linear transformations of flows and forces. The transformation properties are summarized by de Groot [32]. We set them down briefly in the notation of this paper.

We take as given

$$\{J'\} = [\![L']\!]\{X'\} \tag{23}$$

with

$$[\![L']\!] = [\![L']\!]^{\dagger} \tag{24}$$

and

$$T\sigma = \{J'\}^{\dagger}\{X'\} \tag{34}$$

where σ is the rate of entropy production during a steady state process described by the vectors $\{J'\}$ and $\{X'\}$.

We may choose an alternative description of the same steady state process in terms of vectors $\{J'\}$ and $\{X'\}$ where

$$\{J'\} = [\![L']\!]\{X'\} \tag{35}$$

with

$$[\![L']\!] = [\![L']\!]^{\dagger} \tag{36}$$

and

$$T\sigma = \{J'\}^{\dagger}\{X'\} \tag{37}$$

The entropy production, σ, must be invariant under a linear transformation of flows and forces. We must define a new force vector by

$$\{X'\} = [\![b''']\!]\{X'\} \tag{38}$$

where the order of the superscripts in the matrix of the linear transformation indicates the direction of the transformation, i.e.,

$$[\![b''']\!] = [\![b'']\!]^{-1} \tag{39}$$

The elements of the vector $\{X'\}$ must be linearly independent combinations of the elements of $\{X^f\}$, i.e.,

$$det\,[\![b'']\!] \neq 0 \tag{40}$$

where the prefix, *det*, denotes the determinant of the matrix. The corresponding transformation of flows is uniquely defined by

$$\{J'\}=[\![a'']\!]\{J''\} \tag{41}$$

where

$$[\![a'']\!]=[\![b'']\!]^{\dagger-1} \tag{42}$$

Alternatively, since the reciprocal of the transpose of a matrix is the same as the transpose of its reciprocal the transformations may be defined in reverse order with

$$[\![b'']\!]=[\![a'']\!]^{\dagger-1} \tag{43}$$

Tne matrix $[\![a'']\!]$ takes the role of de Groot's matrix β and we note that an application of the transformation

$$[\![L']\!]=[\![a'']\!][\![L'']\!][\![a'']\!]^{\dagger} \tag{44}$$

is required to complete the definition of an alternative set of phenomenological relations to replace eq (23).

Finally, we note that in the general case we are dealing with a force vector whose elements are formally linearly independent in terms of their definitions from measurements of intensive properties. We may state that if not all the elements X_i^f are zero,

$$\sum_{j=1}^{q}\epsilon_i X_i^f \not\equiv 0 \tag{45}$$

for any choice of constants, ϵ_i. The transformation properties given remain valid regardless of the permeability characteristics of any junction permeable to at least one ion constituent. In a real system if any one flow or a linear combination of flows is identically zero in all steady state flow processes, the elements of $\{J'\}$ will not be linearly independent. We will study such a special case in section 7 below and set a linear combination of forces to zero. de Groot demonstrates that the *a priori* definition of independent forces secures the validity of the transformation properties despite any linear dependence of flows in a special case.

5. Restrictive Condition Upon a Defined EMF

We consider first a matrix $[\![a'']\!]$. Certain general restrictions upon the form of this matrix may be adopted on the basis of elementary considerations. The nonelectrolytes are *independent* components of conserved chemical identity. The law of conservation of mass is applied to the flow of each such nonelectrolyte. The flows of $r-m-1$ electrolytes and of electric charge are an interdependent group subject to the laws of conservation of mass and of electric charge, but the electroneutrality condition only operates as a restriction upon the flow of ionic constituents with respect to other ionic constituents. It does not restrict the independence between flows of nonelectrolytes and electrolytes. We take these points into consideration when we write

$$[\![a'']\!]=\left[\!\left[\begin{array}{ccc|ccc|c}
1 & \cdots & 0 & 0 & \cdots & 0 & 0 & 0 \\
\cdots & \cdots & \cdots & \cdots & \cdots & \cdots & \cdots & \cdots \\
0 & \cdots & 1 & 0 & \cdots & 0 & 0 & 0 \\
\hline
0 & \cdots & 0 & a_{m+1,m+1} & \cdots & a_{m+1,r-1} & a_{m+1,r} & 0 \\
\cdots & \cdots & \cdots & \cdots & \cdots & \cdots & \cdots & \cdots \\
0 & \cdots & 0 & a_{r-1,m+1} & \cdots & a_{r-1,r-1} & a_{r-1,r} & 0 \\
0 & \cdots & 0 & z_{m+1}^f & \cdots & z_{r-1}^f & z_r^f & 0 \\
\hline
0 & \cdots & 0 & 0 & \cdots & 0 & 0 & 1
\end{array}\right]\!\right] \tag{46}$$

where the last column and the last row indicate that we retain the flow of entropic heat as a fundamental flow. It is convenient to have the rth element of our new vector $\{J'\}$ equal to the flow of electric current. This is indicated in the matrix where

$$a_{rj}''=0; \quad (j=1,\ldots,m,q); \tag{47}$$

and

$$a_{rj}''=z_j^f; \quad (j=m+1,\ldots,r). \tag{48}$$

The rth flow defines the flow of electric charge. The flows J_1' through J_m' are the flows of neutral components not involving a transfer of electric charge. It is natural to inquire into the possibility of defining as set of $r-m-1$ independent flows of the neutral electrolytic components represented by the last $r-m-1$ elements of the vector $\{m^*\}$ in such a way that these flows do not imply a flow of electric charge. On the most elementary rational grounds a net transfer of a quantity of an electrolytic component from α to β must represent some combination of the transfers of ionic constituents. It is not obvious that any established rules or conventions dictate these combinations, but we identify the respective conjugate forces defined by a matrix $[\![b'']\!]$ with the chemical potential differences of neutral electrolytic components defined as linear combinations in eq (10). The fact that the eq (42) describes a unique operation permits us to carry out an inverted development.

Before setting down a matrix $[\![b'']\!]$ we note that in the matrix $[\![a'']\!]$ given above the dashed lines show how the matrix may be partitioned to give a pseudo-diagonal matrix;

$$[\![a'']\!]=\left[\!\left[\begin{array}{ccc} M & 0 & 0 \\ 0 & N & 0 \\ 0 & 0 & Q \end{array}\right]\!\right] \tag{49}$$

The submatrices $[\![M]\!]$ and $[\![Q]\!]$ are identity matrices, and the submatrices $[\![0]\!]$ are zero matrices. It re-

sults as a property of such forms [33] that when the matrix $[\![N]\!]$ is not singular,

$$[\![b'']\!]=[\![a'']\!]^{\dagger-1}=\begin{bmatrix} M & 0 & 0 \\ 0 & N^{\dagger-1} & 0 \\ 0 & 0 & Q \end{bmatrix} \tag{50}$$

with

$$det\,[\![b'']\!]=det\,[\![N]\!]^{\dagger-1} \tag{51}$$

Thus we write the pseudodiagonal form

$$[\![b'']\!]= \tag{52}$$

$$\left[\begin{array}{ccc|ccc|c} 1 & \cdots & 0 & 0 & \cdots & 0 & 0 & 0 \\ 0 & \cdots & \cdots & \cdots & \cdots & \cdots & \cdots & \cdots \\ 0 & \cdots & 1 & 0 & \cdots & 0 & 0 & 0 \\ \hline 0 & \cdots & 0 & \nu_{m+1,m+1} & \cdots & \nu_{r-1,m+1} & \nu_{r,m+1} & 0 \\ \cdots & \cdots & \cdots & \cdots & \cdots & \cdots & \cdots & \cdots \\ 0 & \cdots & 0 & \nu_{m+1,r-1} & \cdots & \nu_{r-1,r-1} & \nu_{r,r-1} & 0 \\ 0 & \cdots & 0 & b''_{r,m+1} & \cdots & b''_{r,r-1} & b''_{r,r} & 0 \\ \hline 0 & \cdots & 0 & 0 & \cdots & 0 & 0 & 1 \end{array}\right]$$

with the matrix $[\![\nu]\!]^{\dagger}$ from eq (10) comprising the first $r-1$ rows and first r columns. Only the elements, b''_{rj}, in the rth row and columns $m+1$ through r are left to be determined.

The restriction upon $[\![b'']\!]$ can be demonstrated. For the moment we assume that $det\,[\![b'']\!]$ does not vanish. The definition of an element of the ith row of the reciprocal of a transposed matrix is [33],

$$a''_{ij}=\frac{cof\,b''_{ij}}{det\,[\![b'']\!]}, \tag{53}$$

where the numerator on the right is the cofactor of the element indicated. Following eq (53) we write the definitions of the elements of $[\![a'']\!]$ within the submatrix $[\![N]\!]$ as

$$a''_{ij}=\frac{cof\,N^{\dagger-1}_{i-m,j-m}}{det\,[\![N]\!]^{\dagger-1}} \tag{54}$$

The electrical neutrality of each component represented in the vector $\{m^*\}$ as stated in eq (6) gives the condition,

$$\sum_{j=m+1}^{r} z^j\,N^{\dagger-1}_{i-m,j-m}=0; \qquad (i=m+1,\ldots,r-1) \tag{55}$$

Equation (55) applied in the first $r-m-1$ rows of $det\,[\![N]\!]^{\dagger-1}$ gives zeros as the first $r-m-1$ elements of any column when the other $r-m-1$ columns are added to it. The last element of that column then becomes

$$\sum_{j=m+1}^{r} z^j\,N^{\dagger-1}_{r-m,j-m}=\sum_{j=m+1}^{r} z^j\,b''_{rj} \tag{56}$$

for any jth column. It then follows that

$$det\,[\![b'']\!]=\frac{cof\,b''_{rj}}{z^j}\left(\sum_{j=m+1}^{r} z^j\,b''_{rj}\right) \tag{57}$$

for any jth column $m+1$ through r. Substituting from eq (57) for $det\,[\![b'']\!]$ in eq (53) gives

$$a''_{rj}=z^j\left(\sum_{j=m+1}^{r} z^j\,b''_{rj}\right)^{-1} \tag{58}$$

Clearly, if

$$\sum_{j=m+1}^{r} z^j\,b''_{rj}=1, \tag{59}$$

eqs (47) and (48) will be satisfied provided $[\![b'']\!]$ is not singular. The nonsingularity of $[\![b'']\!]$ is assured by the requirement that $[\![\nu]\!]$ be of rank $r-1$. At least one $cof\,b''_{rj}$ will not vanish. When the condition of eq (59) is applied the determinant will be given by

$$det\,[\![b'']\!]=\frac{cof\,b''_{rj}}{z^j}\neq 0. \tag{60}$$

6. Reference Ion Electromotive Force

An extremely important class of experimental systems including concentration cells and various cells with transference have identical reversible terminal electrodes [1] and can be designed to fall into the class of systems discussed in section 2. It is proper to inquire as to whether or not the EMF between a single pair of identical reversible probe electrodes, one at ϕ and one at β, may be formally regarded as the junction electromotive force. We may choose to order the elements of $\{m^j\}$, $\{X^j\}$ and $\{J^j\}$ to have the rth constituent be that one to which the electrode pair is reversible. We define a "reference ion" force vector with

$$X^r_i=X^j_i; \qquad (i=1,\ldots,m); \tag{61}$$

$$X^r_i=\sum_{j=m+1}^{r} \nu_{ji}X^j_i; \qquad (i=m+1,\ldots,r-1); \tag{62}$$

$$X^r_r=\frac{X^j_r}{z^j_r} \tag{63}$$

and

$$X^r_q=X^j_q. \tag{64}$$

The matrix $[b^{jr}]$ is thus of the class of $[b^{j\prime}]$ in eq (52). The elements

$$b^{jr}_{rj}=0; \qquad (j=1,\ldots,r-1,q) \tag{65}$$

and

$$b^{jr}_{rr}=\frac{1}{z^j_r}. \tag{66}$$

clearly satisfy the restriction imposed by eq (59). Therefore, any one of the $r-m$ EMF's $\Delta\phi_i$ defined by eq (14) may be chosen as *the* junction EMF.

This reference ion formulation is important for practical applications. In most systems one can at

best discover a single pair of adequate reversible electrodes. Experimental flows will normally be expressed most directly in terms of the vector $\{J^r\}$ with the forces being in terms of the vector $\{X^r\}$, A transformation,

$$\{X^r\}=[\![b^{rr'}]\!]\{X^r\}, \tag{67}$$

must be applied with

$$[\![b^{rr'}]\!]=[\![b^{rr'}]\!]^{-1}. \tag{68}$$

7. Junctions With Zero Electric Current Flow

Treatments of electromotive forces acting across junctions are most often encountered in discussions of the thermodynamics of galvanic cells. In such treatments one is concerned with the apparently reversible EMF measured at the limit of zero electric current flow. Guggenheim [9] has given a treatment of isothermal, isopiestic cells with liquid-liquid junctions without employing eq (1). The treatment is one of a continuous steady state system without chemistry in a solvent fixed frame of reference. His work is an exception to the apparent universal practice of using eq (1) or its equivalent. Therefore, some indication must be given of the relationship between the treatment here and the more common treatments. In addition the treatment of junctions at states of zero current gives an important relationship for use in connection with eq (10).

It can be shown [34] that when no electric current is flowing through the junction,

$$\sum_{j=1}^{r}\tau_j^f\Delta\mu_j=0\,; \qquad \left(\frac{I}{\mathscr{F}}=0\right). \tag{69}$$

The coefficients, τ_j^f, are the integral stoichiometric transference numbers in a cell fixed frame of reference when no difference of temperature, pressure, or composition exists between α and β, i.e.,

$$\tau_j^f=J_j^f\left(\sum_{j=1}^{r}z_j^f\,J_j^f\right)^{-1}; \qquad (\Delta T=\Delta P=\{\Delta m^*\}=0). \tag{70}$$

The numbers τ_j^f are properties of the junction defined as functions of the elements of the admittance matrix $[\![L^{rr'}]\!]$.
These functions are

$$\tau_j^f=\frac{1}{L_E}\sum_{i=1}^{r}z_i^fL_{ji}^f \tag{71}$$

where

$$L_E=\sum_{j=1}^{r}\sum_{i=1}^{r}z_i^fz_j^fL_{ji}^f \tag{72}$$

with

$$\sum_{j=m+1}^{r}z_j^f\tau_j^f=1. \tag{73}$$

The detailed manipulations leading to the above relations need not be repeated. However, in existing analyses the use of eq (1) as an elementary postulate gives a familiar result in differential form as

$$-\mathscr{F}d\xi=\sum_{j=1}^{r}\tau_j^f(d\mu_j)_{d\xi=0}=RT\sum_{j=1}^{r}\tau_j^f(d\ln a_j)_{d\xi=0} \tag{74}$$

which because of uncertainties in notation may appear to be inconsistent with eq (69). The relationship may be seen clearly if we write

$$\Delta\mu_j=(\Delta\mu_j)_{\Delta\xi=0}+z_j^f\mathscr{F}\Delta\xi \tag{75}$$

and substitute for $\Delta\mu_j$ in eq (69). The use of eq (73) to reduce the coefficient of $\mathscr{F}\Delta\xi$ then gives

$$-\mathscr{F}\Delta\xi=\sum_{j=1}^{r}\tau_j^f(\Delta\mu_j)_{\Delta\xi=0}. \tag{76}$$

Of course this only demonstrates a formal abstract relationship since the operational significance of eq (1) has not been established for ordinary electrochemical systems.

Nevertheless, we note that eq (69) is a linear combination of chemical potential differences defined as a function of the permeability characteristics of the junction. Thus when this relation is added to the set of equations in eq (10) we have a set of r equations in r unknowns,

$$\begin{bmatrix}
1 & \cdots & 0 & 0 & \cdots & 0 & 0 \\
\cdots & \cdots & \cdots & \cdots & \cdots & \cdots & \cdots \\
0 & \cdots & 1 & 0 & \cdots & 0 & 0 \\
0 & \cdots & 0 & \nu_{m+1,m+1} & \cdots & \nu_{r-1,m-1} & \nu_{r,m-1} \\
\cdots & \cdots & \cdots & \cdots & \cdots & \cdots & \\
0 & \cdots & 0 & \nu_{m+1,r-1} & \cdots & \nu_{r-1,r-1} & \nu_{r,r-1} \\
\tau_1^f & \cdots & \tau_m^f & \tau_{m+1}^f & \cdots & \tau_{r-1}^f & \tau_r^f
\end{bmatrix}$$

$$\begin{Bmatrix}
\Delta\mu_1^* \\ \cdots \\ \Delta\mu_m^* \\ \Delta\mu_{m+1}^e \\ \cdots \\ \Delta\mu_{r-1}^e \\ \Delta\mu_r^e
\end{Bmatrix}=\begin{Bmatrix}
\Delta\mu_1^* \\ \cdots \\ \Delta\mu_m^* \\ \Delta\mu_{m+1}^* \\ \cdots \\ \Delta\mu_{r-1}^* \\ 0
\end{Bmatrix} \tag{77}$$

The elements τ_{m+1}^f through τ_r^f obey eq (73); therefore the condition of eq (59) required for $b_{r,m+1}^{rr'}$ through $b_{rr}^{rr'}$ in treating the matrix $[\![b^{rr'}]\!]$ applies. It may be shown by a treatment similar to that applied to $[\![b^{rr'}]\!]$ that the matrix here does not vanish unless

$$\tau_{m+1}^f=\ldots=\tau_r^f=0 \tag{78}$$

Thus if the junction is permeable to at least one ionic constituent of the solutions at α and β, eq (77) possesses a unique solution. This result confirms the statement given after eq (10).

It should be noted that eq (77) has the distinct practical advantage of unifying the treatment of galvanic cells having identical terminal electrodes in compartments separated by a defined junction through which flow continuity is established. It is clear that a solution for any $\Delta\mu_i^f$ will after applying eq (13) give the EMF, $\Delta\phi_l$, at the limit of zero electric current flow in terms of the transference numbers and the thermodynamic properties of independent isolable components.

8. Electromotive Force at Infinite Dilution

The reference state of unit activity coefficient established for treating the thermodynamic properties of solutes is infinite dilution in pure solvent. In the limit of infinite dilution aqueous solutions of strong electrolytes are "nearly" insulators and the Debye-Hückel limiting law is valid for electrolytic solutes as a whole. In accord with the discussion of Tolhoek and de Groot [8] and Guggenheim [7] we may regard it as meaningful to speak of a difference of electrostatic potential acting as a part of the "force" conjugate to the transfer of an ionic constituent between solutions of infinitesimally different compositions in the neighborhood of infinite dilution. To define this "force" we make use of several commonly used extrathermodynamic conventions, and we need only consider isothermal, isopiestic systems.

We assume that the activity coefficients of solute nonelectrolytes approach unity much more rapidly than their concentrations approach zero in the limit as a solution is diluted with pure solvent. We write

$$(d\mu_i^*)_{T,P}=RTd\ln m_i^*;\quad (i=2,\ldots,m). \tag{79}$$

For ionic solute constituents we apply the same assumption and write

$$(d\mu_i^e)_{T,P}=RTd\ln m_i^f+z_i^f\mathcal{F}d\xi;\quad (i=m+1,\ldots,r) \tag{80}$$

It will be noted that the Debye-Hückel theory supports the assumption underlying eq (80) since the limiting law

$$(\ln\gamma_i^e)_{T,P,d\xi=0}=-A(z_i^f)^2\sqrt{\mathrm{u}} \tag{81}$$

where u is the ionic strength, i.e.,

$$\mathrm{u}=\frac{1}{2}\sum_{j=m+1}^{r}(z_j^f)^2 m_j^f, \tag{82}$$

suggests that $(\ln\gamma_i^e)_{T,P,d\xi=0}$ approaches zero in the limit of infinite dilution as $\ln m_i^f$ approaches minus infinity.

Using the relation.

$$d\ln m_i^f=\frac{dm_i^f}{m_i^f} \tag{83}$$

in eqs (79) and (80) and then applying the electroneutrality condition

$$\sum_{j=m+1}^{r} z_i^f dm_i^f=0 \tag{84}$$

gives a set of r equations in r unknowns.

$$\begin{bmatrix}
\frac{RT}{m_2^f} & \ldots & 0 & 0 & \ldots & 0 & 0 \\
\ldots & \ldots & \ldots & \ldots & \ldots & \ldots & \ldots \\
0 & \ldots & \frac{RT}{m_m^f} & 0 & \ldots & 0 & 0 \\
0 & \ldots & 0 & \frac{RT}{m_{m+1}^f} & \ldots & 0 & z_{m+1}^f \\
\ldots & \ldots & \ldots & \ldots & \ldots & \ldots & \ldots \\
0 & \ldots & 0 & 0 & \ldots & \frac{RT}{m_r^f} & z_r^f \\
0 & \ldots & 0 & z_{m+1}^f & \ldots & z_r^f & 0
\end{bmatrix}$$

$$\begin{Bmatrix} dm_2^f \\ \ldots \\ dm_m^f \\ dm_{m+1}^f \\ \ldots \\ dm_r \\ \mathcal{F}d\xi \end{Bmatrix} = \begin{Bmatrix} (d\mu_2^*)_{T,P} \\ \ldots \\ (d\mu_m^*)_{T,P} \\ (d\mu_{m+1}^e)_{T,P} \\ \ldots \\ (d\mu_r^e)_{T,P} \\ 0 \end{Bmatrix} \tag{85}$$

The coefficient matrix is nonsingular; its determinant is given by

$$2(RT)^{r-2}\mathrm{u}\left(\prod_{i=2}^{r} m_i^f\right)^{-1}>0. \tag{86}$$

The solution,

$$\mathcal{F}d\xi=\sum_{j=m+1}^{r}\frac{z_j^f m_j^f}{2\mathrm{u}}(d\mu_j^e)_{T,P}, \tag{87}$$

gives the differential of the electrostatic potential at infinite dilution as a linear combination of the differentials of chemical potential. The coefficients in eq (87) satisfy eq (59).

It is clear from the form of eq (80) that $d\xi$ is introduced as the "force" conjugate to any infini-

tesimal transfer of electric charge, hence, eq (87) defines the electromotive force at infinite dilution. We use eq (87) to define the elements of the rth row of the linear transformation matrix in

$$[\![b^{fd}]\!]\{X^f\}=\{X^d\} \tag{88}$$

where $[\![b^{fd}]\!]$ is of the class required by eq (52). By eqs (41) and (43) we have the transformation

$$[\![a^{fd}]\!]\{J^f\}=\{J^d\} \tag{89}$$

where each element J^d_{m+1} through J^d_{r-1} is a linear combination of the flows of ionic constituents defining the "flow" conjugate to the "force" acting on an isolable electrolytic component as a whole. The combinations are necessary consequences of established extra-thermodynamic conventions and assumptions. They are implicit in our established methods of treating the properties of completely dissociated electrolytes.

9. The Membrane EMF at Higher Concentrations

The definition of the membrane EMF at higher concentrations follows directly from the definition at infinite dilution. In order to remove any implication of a definition of an electrostatic potential difference at finite concentrations and concentration differences we write

$$\mathcal{F}\psi=\sum_{i=m+1}^{r}\frac{z_i^f m_i^f}{2\mathrm{u}}\Delta\mu_i^* \tag{90}$$

where ψ is the electromotive force between α and β. We regard ψ as representing the action of an electric field in the sense that it denotes a force acting to produce a flow of electric charge, but it is not a gradient of an external electrostatic potential field [35]. The EMF, ψ, is fully meaningful since every term on the right hand side is meaningful. It is arbitrary in the sense that our choice of the reference state of infinite dilution and the applications of eqs (79) and (80) are arbitrary. It depends upon our definitions of the elements of the vector $\{m^f\}$ and our use of these ion constituent concentrations in writing the ionic strength, u, given in eq (82) and the electroneutrality condition given as eq (3). It is, however, quite independent of any arbitrary choice of the matrix $[\![\nu]\!]$ to give the elements of $\{m^*\}$. The matrix $[\![a^{fd}]\!]$ of eq (89) defined at infinite dilution fixes the stoichiometry governing exchanges of radical chemical constituents. The most elementary considerations of internal consistency dictate the use of this same stoichiometry regardless of the absolute concentrations of the solutions.

10. Discussion

The need for defining a membrane electromotive force and the corollary flows of electrolytes as a whole arises quite naturally if we consider the treatment of electrokinetic phenomena. However, we must first establish certain points in terms of a specific example.

Consider a membrane cell with compartments filled with HCl solutions. Let it be arranged in the manner of a four lead resistor with a pair of probe electrodes close to the membrane—one on each side. These probe electrodes establish the positions of the planes, α and β, indicated in section 2. They are potential indicating devices and carry no steady electric currents. Let each compartment also be provided with a working or current electrode more remote from the membrane than α and β. The electrode reactions at the current electrodes are to involve virtually insoluble components and either the chloride or the hydrogen ion constituent of the solution. Let us also provide for continuous, adjustable flows through each compartment utilizing feed solutions of adjustable composition.

A little reflection will show that we can establish a particular steady state—defined by giving the elements of $\{X^f\}$—regardless of whether it is the hydrogen ions or the chloride ions which are exchanged with the solutions at the current electrodes. The adjustments of feed solution compositions and rates of flow serve as our compensating variables. If the phenomenological relations, eq (23), describe a steady state process taking place between α and β, they describe it independently of the specific nature of the processes at current electrodes which may in practice be at virtually infinite distances from the region between α and β. This statement of independence, the independence of dissipative processes occuring in different regions of space, expresses an elementary requirement of the steady state theory [39]. Processes which are described as coupled—having phenomenological relations with cross coefficients—in the production of entropy must take place in the same system. By system we mean an open system, the region of space between α and β as defined in section 2. If we wish to describe a particular process in terms of some set of phenomenological relations resulting from a linear transformation of eq (23), the second form of the phenomenological relations will describe the *same* and *only the same* process if and only if it is defined so as not to include *external* dissipative processes. This elementary requirement is expressed in the steady state theory when we state that the rate of entropy production given by eq (34) must be independent of a linear transformation of the forces and flows.

Ordinary isothermal electrokinetic phenomena at membranes are investigated by making experimental measurements—in a membrane fixed frame of reference—of flows of fluid volume and electric current under the influence of their conjugate forces—pressure difference and electric potential difference. We can site, for example, de Groot's [40] and Guggenheim's [36] demonstrations of the application of the steady state theory in the special case where no differences of temperature or of composition are present to act as forces. They show that the well

known experimental relation, the Saxén relation, between the streaming potential and the electroosmotic transport, i.e.,

$$\left(\frac{\Delta\xi}{\Delta P}\right)_{I=\Delta T=\{\Delta m^*\}=0}=\left(\frac{J_V}{I}\right)_{\Delta P=\Delta T=\{\Delta m^*\}=0} \tag{91}$$

may be regarded as a consequence of the Onsager reciprocal relations. J_V is the rate of flow of fluid volume and $\Delta\xi$ is, as before, the difference in electrostatic potential. The electrostatic potential, $\Delta\xi$, is of course a meaningful quantity when measured between phases of identical composition and temperature; it is the EMF measured between the terminals of any pair of identical electrodes. Hence, neither of the treatments cited makes any reference to the nature of the electrodes employed to measure $\Delta\xi$. The fact that these analyses impose the restriction

$$\Delta T=\{\Delta m^*\}=0 \tag{92}$$

and the fact that in practice the experimental measurements do not include measurements of the flows of heat and of the relative flows of constituents obscures certain features of the phenomena involved. J_V is computed from the measured rate of change of the volume of solution in a cell compartment with due allowance for the change of the volume of a compartment arising from the reactions of insoluble components at the working electrodes. In such treatments there is normally an implicit understanding that the reactions at the probe and working electrodes are identical. The problem of separating electrode and membrane processes simply does not arise in such a restricted case. However, we may, for example, study Guggenheim's [9] treatment of concentration cells with transference. This is a case where $\{\Delta m^*\}$ is not restricted to zero. Although our formulation is first to be distinguished from his treatment of concentration cells by the fact that his is in a Hittorf, i.e., solvent fixed, frame of reference, the essential point is that Guggenheim explicitly requires the use of electrodes reversible to one of the ionic constituents. Such a treatment avoids the classical uncertainty involving $\Delta\xi$. Since he restricted his treatment to steady states not involving flows of electric charge, the requirement of specific electrodes does not introduce any difficulty with respect to the separation of electrode and junction processes.

Since the phenomenological relations of eq (23) describe processes which involve electrokinetic effects as well as diffusion effects, we are led immediately to attempt to set down a treatment in which heat flows and temperature differences and diffusion flows and concentration differences are added to the flows and forces of the electrokinetic treatment. However, we find that not only the meaning of $\Delta\xi$ but also the meaning of J_V, is uncertain. We must require our formulation to describe the processes in the "membrane", i.e., α to β, region. It is to result from a linear transformation of the fundamental phenomenological relations, eq (23).

At first glance it appears that we would write

$$J_V^e=\sum_{i=1}^{m}\overline{V}_i^e J_i+\sum_{i=m+1}^{r}\overline{V}_i^e J_i \tag{93}$$

where the terms $\overline{V}_i^e$ are the partial molal volumes of the nonelectrolytes and the terms $\overline{V}_i^e$ are the partial molal volumes of ionic constituents represented in the vector $\{m^I\}$. However, we have already indicated in the discussion of eq (2) that $\overline{V}_i^e$ has no operational meaning when we reject the postulate that $\Delta\xi$ is operationally defined. We could consider a convention which defines $\overline{V}_i^e$ for any constituent. Such a convention would permit us to retain the distinction between electrode and membrane processes. However, there is an alternative approach which has to be considered.

We recognize that in the study of combined hydrodynamic and diffusion flow processes during steady states not involving net flows of electric current, we have by definition

$$(J'_V)_{I=0}\equiv\sum_{j=1}^{r-1}\overline{V}_j^*(J_j^*)_{I=0} \tag{94}$$

where $(J_j^*)_{I=0}$ are the flows of the neutral components represented in the vector $\{m^*\}$ and $\overline{V}_j^*$ are their partial molal volumes. We recognize that in practice the flows $(J_j^*)_{I=0}$ will be computed from experimental measurements of changes of ion constituent concentrations with explicit dependence upon the requirement of electroneutrality, i.e., as linear combinations of the flows $(J_i^I)_{I=0}$. We are thus led to write

$$J'_V=\sum_{j=1}^{r-1}\overline{V}_j^* J'_j\,;I\neq 0 \tag{95}$$

where the flows J'_j are linear combinations of the flows of ion constituents which represent flows of electrolytes as a whole. It was necessary to discover what conditions are to be met in defining J'_j.

In section 5 of this paper we showed that we are first led to the conclusion that when we define the membrane EMF in terms of the potentials measured between pairs of identical probe electrodes with specific electrode reactions, we at the same time define, by implication, a particular method of combining the flows of ionic constituents into the flows of neutral electrolytes as a whole. Thus, by implication, we establish the definitions of J'_j and, hence, J'_V in eq (95). Therefore, we conclude that it is not proper to introduce any auxiliary convention which defines $\overline{V}_i^e$ in eq (93) when we set down a transformation of eq (23) into an electrokinetic formulation.

In section 6 we showed that we can choose a "reference ion" EMF, $\Delta\phi_r$, by choosing to employ probe electrodes reversible to some particular ion constituent. Formally, there will be $r-m$ distinct choices possible. In general there will be a family of $r-m$ pairs of matrices $[\![b^{Ir}]\!]$ and $[\![a^{Ir}]\!]$. The definition of the flow of any jth neutral electrolyte

$$J_j^r = \sum_{i=m+1}^{r} a_{ji}^{rr} J_i^r \,; (j=m+1, \ldots, r-1) \qquad (96)$$

will in general be different for each choice of a "reference ion." Although the arbitrariness of a "reference ion" electromotive force is objectionable, one can always employ such a device in order to define electrokinetic effects in terms of a general treatment. We can employ the essentially "direct experimental variables" such as appear in Saxén's relation, eq (91), in conjunction with diffusion flows and concentration difference forces without including *external* dissipative processes in our description of membrane processes.

The arbitrariness of a "reference ion" treatment can only be removed by adopting an additional convention—an "averaging" convention. In Sections 8 and 9 we showed that such a convention is implicit in the conventions already established for the treatment of the thermodynamic properties of electrolytic solutions. A general treatment which is consistent with the elementary defining stoichiometric relationships employed at the reference state of infinite dilution results when we write

$$J_v^h \equiv \sum_{j=1}^{r-1} \overline{V}_j^* J_j^d \qquad (97)$$

where J_j^d is defined by the transformation given in eq (89).

It is important to emphasize that the treatment which defines ψ is complete only with respect to the requirement of consistency with established convention. We have implied that ψ is a physically significant quantity. The developments of this paper are not adequate to demonstrate any real physical significance. Our development in sections 8 and 9 follows the formal procedure of defining the Lagrangian multiplier corresponding to the electroneutrality condition.[7] Although as a formal device in section 8 ψ is uniquely defined when we write eq (85), the approach to ideal behavior implied by eq (80) is not subject to an adequate experimental test [42]. The use of the concept of "almost" insulators is not satisfying as a basis for attaching physical significance to $\Delta\xi$ in extremely dilute solution and, hence, to ψ in more concentrated solutions.

An important problem for further investigation is the comparison of experimentally determined values of ψ with the EMF's measured between pairs of saturated calomel electrodes. A study of representative attempts to set down meaningful conventions for junctions potentials [4, 43, 44] based upon established common practice shows that saturated solutions of potassium chloride are regarded as special experimental devices. It is abundantly clear that they are assumed to represent a practical approach to some ideal of "inert" behavior in experimental systems. We can, for example, accept ψ as a physically significant quantity if a general study of a large class of experimental systems shows that saturated calomel electrodes can be regarded as experimental devices which measure ψ directly with a degree of accuracy which is adequate for most practical purposes—"to within a few millivolts." We suggest this hypothesis here because our first tests support it, but we regard it, for the present, as only an example.

[7] Lagrangian multipliers as physically significant quantities are common in statistical mechanics. Onsager [41] suggests the use of such a multiplier to represent the electric potential in electrochemical systems. However, he gives no explicit definition and, further, he chooses to have his dissipation function include electrode processes.

11. Summary of Symbols and Notation

a_i	Activity of a constituent, eq (74).
$[\![a'']\!]$	Matrix of transformation of $q=r+1$ flows, r of chemical constituents and one of entropic heat, into the flows of $r-1$ chemical components, electric current, and entropic heat, eq (46).
$[\![a']\!]$	$[\![a'']\!]^{-1}$, the reciprocal of $[\![a'']\!]$.
$[\![a^{fd}]\!]$	Matrix of the class $[\![a'']\!]$ consistent with the conventional EMF, ψ, section 9.
$[\![a^{fr}]\!]$	Matrix of the class $[\![a'']\!]$ consistent with a particular reference ion EMF, $\Delta\phi_r$, section 6.
$\mathscr{A}_k$	Chemical symbol of electrode component, eq (12).
$[\![b'']\!]$	Matrix of transformation of forces, eqs (50) and (52); $[\![b'']\!]=[\![a'']\!]^{\dagger-1}$.
$[\![b^{fd}]\!]$	Matrix of the class $[\![b'']\!]$; $[\![b^{fd}]\!]=[\![a^{fd}]\!]^{\dagger-1}$.
$[\![b^{fr}]\!]$	Matrix of the class $[\![b'']\!]$; $[\![b^{fr}]\!]=[\![a^{fr}]\!]^{\dagger-1}$.
$\mathscr{B}_i^f$	Chemical symbol of ion constituent, eq (12).
$cof\, a_{ij}''$	Cofactor of ijth element of $[\![a'']\!]$.
$det[\![a'']\!]$	Determinant of matrix $[\![a'']\!]$.
$E_i^\beta - E_i^\alpha$	EMF measured between electrode terminals.
$\mathscr{F}$	Faraday.
I	Electric current.
J_i^r	$i=1, \ldots, r$; rate of flow of a chemical constituent.
J_i', J_i^d, J_i^r	$i=1, \ldots, r-1$; rate of flow of a neutral component.
J_r', J_r^d, J_r^r	$I/\mathscr{F}$, eq (33).
$(J_i^*)_{I=0}$	$i=1, \ldots, r-1$; rate of flow of a neutral component when $I=0$, eq (94).
$J_q^r, J_q', J_q^d, J_q^r$	$q=r+1$; rate of flow of entropic heat.
J_V	Rate of flow of fluid volume, section 10.
$[\![L^r]\!], [\![L']\!]$	Admittance matrices.
$\{m^r\}$	Constituent composition vector having r elements which are the molalities of m nonelectrolytes and $r-m$ ion constituents.
$\{m^*\}$	Component composition vector having $r-1$ elements which are the molalities of m nonelectrolytes and $r-m-1$ neutral electrolytes.
P	Pressure.

R	Gas constant.
$\overline{S_i^*}$	Partial molal entropy of ith component in $\{m^*\}$.
$\overline{S_i^e}$	(Undefined) partial molal entropy of an ion constituent.
T	Temperature.
$\overline{V_i^*}$	Partial molal volume of ith component in $\{m^*\}$.
$\overline{V_i^e}$	(Undefined) partial molal volume of an ion constituent.
$X_i^f, X_i^r, X_i^d, X_i^r$	$i=1, \ldots, m$; forces, $-\Delta\mu_i^*$, acting conjugate to the flows of nonelectrolytes.
X_i^f	$i=m+1, \ldots, r$; forces, $-\Delta\mu_i^e$, acting conjugate to the flows of ion constituents.
X_i^r, X_i^d, X_i^r	$i=m+1, \ldots, r-1$; forces, $-\Delta\mu_i^*$, acting conjugate to the flows of neutral electrolytes.
X_r^d	Conventionally averaged force, $-\mathcal{F}\psi$, acting conjugate to the flow of electric charge, section 9.
X_r^r	Force, $-\mathcal{F}\Delta\phi_r$, acting conjugate to the flow of electric charge in accord with a reference ion convention, section 6.
$X_q^f, X_q^r, X_q^d, X_q^r$	$q=r+1$; force, $-\Delta \ln T$, acting conjugate to the flow of entropic heat.
z_i^f	Electrovalence of a constituent.
α,β	Denote boundaries of membrane region; α to β positive.
γ_i^*	$i=1, \ldots, m$; molal activity coefficient of a nonelectrolyte; and $i=m+1 \ldots, r-1$; mean molal activity coefficient of an electrolyte.
γ_i^e	(Undefined) electrostatic molal activity coefficient of an ion constituent.
γ_i^f	Formal device denoting the molal activity coefficient of an ion constituent; eq (19).
Θ_{ij}^*	Thermodynamic composition coefficient, eq (18).
λ_{ik}	Stoichiometric coefficient of a neutral component in an electrode reaction, eq (12).
μ_i^e	Formal device denoting the chemical potential of an ion constituent.
$\Delta\mu_i^e$	Difference in the chemical potential of an ion constituent between α and β, eq (13).
μ_i^*	The chemical potential of a component represented in $\{m^*\}$.
$[\![\nu]\!]$	The stoichiometry matrix, eq (4).
τ^f	The integral stoichiometric transference number of a constituent in a cell fixed frame of reference; eq (69).
ξ	(Undefined) the absolute electrostatic potential.
$\Delta\phi_i$	Equation (13).
ψ	Conventionally defined EMF, section 9.

12. References

[1] D. A. MacInnes, Principles of electrochemistry (Rheinhold Publishing Company, 1939).
[2] H. S. Harned and B. B. Owen, Electrolytic solutions, 3d Ed. (Rheinhold Publishing Company, New York, 1954).
[3] E. A. Guggenheim, Thermodynamics (Interscience Publishers, Inc., New York, N.Y., 1957).
[4] R. G. Bates, Electrometric pH determinations (John Wiley & Sons, Inc., New York, N.Y., 1954).
[5] S. R. de Groot, Thermodynamics of irreversible processes (North-Holland Publishing Company, Amsterdam, 1952), p. 127.
[6] Ref. [1], p. 60.
[7] Ref. [3], p. 372.
[8] S. R. de Groot and H. A. Tolhoek, Proc. Konink. Ned. Akad. Wetens. **54B,** 42 (1951).
[9] Ref. [3], p. 456.
[10] M. I. Temkin and A. V. Koroshin, Zhur. Fiz. Khim. **26,** 500 (1952).
[11] A. V. Koroshin and M. I. Temkin, Zhur. Fiz. Khim. **26,** 773 (1952).
[12] J. N. Agar, The Structure of electrolytic solutions, W. J. Hamer, Editor (John Wiley & Sons, Inc., New York, N.Y., 1959), p. 200.
[13] Ref. [5], p. 54.
[14] M. Spiro, Trans. Faraday Soc. **55,** 1207 (1959).
[15] R. P. Wendt and L. J. Gosting, J. Phys. Chem. **63,** 1287 (1959).
[16] D. G. Miller, Am. J. Phys. **24,** 433 (1956).
[17] Ref. [1], p. 62.
[18] Ref. [3], p. 340.
[19] Ref. [1], p. 109.
[20] Ref. [3], p. 386.
[21] A. J. de Bethune, J. Electrochem. Soc. **107,** 829 (1960).
[22] J. G. Kirkwood, Ion transport across membranes, J. T. Clarke, Editor (Academic Press, Inc., New York, 1954), p. 119.
[23] Ref. [5], p. 73.
[24] Ref. [5], p. 66.
[25] Ref. [5], p. 94.
[26] G. Scatchard, Enlarged Abstracts of Symposium of Electrokinetic and membrane phenomena, Electrochemical Society Meeting, April 1958, New York.
[27] R. Schlögl, Discussions Faraday Soc. **21,** 46 (1956).
[28] D. G. Miller, Chem. Rev. **60,** 15 (1960).
[29] D. G. Miller, J. Phys. Chem. **63,** 570 (1959).
[30] P. J. Dunlop and L. J. Gosting, J. Phys. Chem. **63,** 86 (1959).
[31] P. J. Dunlop, J. Phys. Chem. **63,** 612 (1959).
[32] Ref. [5], p. 208.
[33] H. Margenau and G. M. Murphy, Mathematics of and chemistry (D. Van Nostrand Company, Inc., New York, 1943), p. 293.
[34] E. H. Wiebenga, Rec. trav. chim. **65,** 273 (1946); A. J. Staverman, Trans. Faraday Soc. **48,** 176 (1952).
[35] W. V. Houston, Principles of mathematical physics (McGraw-Hill Book Company, Inc., New York, N.Y., 1948), p. 287.
[36] Ref. [3], p. 453.
[37] Ref. [3], p. 299.
[38] Ref. [3], p. 338.
[39] I. Prigogine, Thermodynamics of irreversible processes (Charles C. Thomas, Springfield, Ill., 1955), p. 17.
[40] Ref. [5], p. 185.
[41] L. Onsager, Ann. N.Y. Acad. Sci. **46,** 256 (1945).
[42] Ref. [3], p. 341.
[43] G. Scatchard, Science **95,** 27 (1942); G. Scatchard and P. C. Breckenridge, J. Phys. Chem. **58,** 602 (1954).
[44] Proceedings, International Committee of Electrochemical Thermodynamics and Kinetics, Eighth Meeting, (Butterworth, London, 1958) p. 34.

(Paper 66A1–144)

JOURNAL OF RESEARCH of the National Bureau of Standards—A. Physics and Chemistry
Vol. 66A, No. 1, January–February 1962

Publications of the National Bureau of Standards*

(Including papers in outside journals)

Selected Abstracts

International practical temperature scale of 1948, text revision of 1960, H. F. Stimson, *NBS Mono. 37 (1960) 10 cents.*
The International Practical Temperature Scale of 1948 is a text revision of the International Temperature Scale of 1948, the numerical values of temperatures remaining the same. The adjective "Practical" was added to the name by the International Committee on Weights and Measures. The scale continues to be based upon six fixed and reproducible equilibrium temperatures to which values have been assigned, and upon the same interpolation formulas relating temperatures to the indications of specified measuring instruments. Some changes have been made in the text to make the scale more reproducible than its predecessor. The triple point of water, with the value 0.01 °C replaces the former ice point as a defining fixed point of the scale. It is also recommended that the zinc point, with the value 419.505 °C, be used instead of the sulfur point. The recommendations include new information that has become available since 1948.

An evaluation of Kacser's second order Born approximation to the bremsstrahlung differential cross section, G. S. Ofelt, *NBS Tech. Note 81 (PB161582) (1961) 75 cents.*
The second order term, as derived by C. Kacser [Proc. Roy. Soc. A253 (1959)], of the Born approximation series for the bremsstrahlung cross section differential with respect to photon energy, photon direction, and final electron direction averaged over initial and summed over final polarization states has been put in a form that admits to numerical evaluation for the coplanar case. The results are valid for relativistic as well as non-relativistic incident electrons.
Completely general (non-coplanar) expressions are included for the first order (Bethe-Heitler) and second order terms. However, the latter has not been given in a form admissible to numerical evaluation.
Tabulated values are given for the case of the incident electron kinetic energy=500 kev, photon energy=450 kev, and photon direction 20° from the incident electron direction. For this case the second order term increases the differential cross section by about 50 percent for Al and about 200 percent for Au for the various angles of electron emission. A rough approximation to the integrated (over final electron direction) cross section is included and a comparison is made with experimental values. The inclusion of the second order term brings the theoretical cross section closer to the experimental values.

A compilation of the physical equilibria and related properties of the hydrogen-carbon monoxide system, D. E. Drayer and T. M. Flynn, *NBS Tech. Note 108 (PB161609) (1961) $2.25.*
Literature data have been used to calculate K factors (K= the ratio of vapor phase to condensed phase compositions) for the hydrogen-carbon monoxide system over the range of 68.2 to 122.2°K and 10 to 225 atmospheres. K factors are presented graphically for eight isotherms over this range.
Published data on the solid-vapor region are presented separately as composition versus pressure at constant temperature.
A bibliography of approximately 450 references is also presented on related properties for this system and for the pure components.

A compilation of the physical equilibria and related properties of the hydrogen-helium system, D. E. Drayer and T. M. Flynn, *NBS Tech. Note 109 (PB161610) (1961) $1.25.*
Published data have been used to calculate K factors (K= the ratio of vapor phase to condensed phase compositions) for the helium-hydrogen system over the range of 17.4° to 21.8°K and 2 to 32 atmospheres pressure. K factors are presented graphically for three isotherms over this range. A bibliography of approximately 290 references is also presented on related properties for this system and for the pure components.

A compilation of the physical equilibria and related properties of the hydrogen-nitrogen system, D. E. Drayer and T. M. Flynn, *NBS Tech. Note 110 (PB161611) (1961) $1.75.*
Published data have been used to calculate K factors (K= the ratio of vapor phase to condensed phase compositions) for the hydrogen-nitrogen system over the liquid-vapor range of 68.2 to 122.2°K, and 10 to 225 atmospheres. K factors are presented graphically for eleven isotherms within this range.
Published data on the solid-gas and solid-liquid regions are presented separately as composition versus pressure at constant temperature.
A bibliography of 250 references pertaining to the hydrogen-nitrogen system is included.

The structure of B-type vibrational-rotational bands of an asymmetric rotor, H. C. Allen, Jr., *Phil. Trans. Roy. Soc. of London, Series A. Mathematical and Physical Sciences, No. 1030, 253, 335 (1961).*
The structure of B-type vibrational-rotational bands of an asymmetric rotor is related to the band types of the two limiting symmetric rotors. The effect of the degree of asymmetry on the band structure is shown. The type of information which can be obtained from the analysis of a B-type band is pointed out.

Complex conductivity of some plasmas and semiconductors, P. H. Fang, *J. Appl. Research Soc. B (The Hague)* **9,** *51(1960).*
The complex conductivities of plasmas and semiconductors have been calculated for several cases where collision frequency can be expressed as a power function of the energy. From the result, some characteristic parameters of the plasma originally investigated by Spitzer are estimated. The problem of determining the relaxation time from a nonsymmetrical dispersion is discussed.

Electric field distribution in a dense plasma, J. L. Jackson, *Phys. Fluids* **3,** *927–931 (1960).*
A calculation is presented of the probability distribution function of the electric field at the center of an ion or atom in a plasma in the high ion density limit. In this limit, it is possible to take into account rigorously the effect of the Coulomb interactions on the distribution function. The distribution function in the high density limit is Gaussian. The Coulomb interaction decreases the mean square electric field by the multiplicative factor $(1+ka_0+(ka_0)^2/3)^{-1}$, where k is the reciprocal Debye length and a_0 the radius of the ion or atom at whose center the field is evaluated.

Absorption spectrum and magnetic properties of osmium hexafluoride, J. C. Eisenstein, *J. Chem. Phys.* **34,** *310–318 (1961).*
This paper is devoted to a discussion of the optical absorption spectrum and the susceptibility of OsF_6. It is assumed that two 5d electrons, which move in a ligand field of octahedral symmetry, are responsible for the magnetic and optical properties of the molecule. The calculated positions of the energy levels depend on the strength of the ligand field, the Coulomb integrals and the spin-orbit coupling constant. These quantities are treated as parameters. If they are given appropriate values excellent agreement

with observed energy level positions is obtained. The calculated susceptibility is also in good agreement with experimental values. In order to fit the magnetic data it is necessary to assume that the orbital reduction factor is approximately 0.7.

Effect of departures from local thermodynamic equilibrium on inferences on stellar atmospheric temperatures, R. N. Thomas, *Book,* **Optical Spectrometric Measurements of High Temperatures,** P. J. Dickerman, *ed., 14–26 (University of Chicago Press, Chicago, Ill., 1961).*

A summary, representing the astrophysical approach to the spectrometric diagnosis of a gaseous atmosphere, for the Chicago conference on Optical Spectrometric Diagnostics of a High-temperature Gas. Problems of departure from Local Thermodynamic Equilibrium, in their bearing on the assignment of a local value of temperature in a gaseous atmosphere, are discussed.

Thermal degradation of organic polymers, S. L. Madorsky, *Polymer Sci.* **17,** *No. 7, (July 1961).*

When pyrolyzed in a vacuum or in a neutral atmosphere at about 200° to 1200°C, simple vinyl polymer chains break into molecular fragments of various sizes. The mechanism of the chemical reactions involved and the nature and relative amounts of the resulting products depend on the molecular structure of the polymer undergoing pyrolysis. Some polymers decompose into a molecular spectrum of fragments containing from 1 to 50 or more carbon chain atoms; some yield monomers exclusively; some yield a mixture of monomers and various other chain fragments; yet another group of polymers yield fragments which are unrelated to the structural unit of the chain. Generally, the higher the temperature and pressure of pyrolysis the greater the fragmentation of the decomposition products.

Infrared spectra of solid hydrocarbons at very low temperatures, J. J. Comeford and J. H. Gould, *J. Mole. Spectroscopy* **5,** *474 (1960).*

Mixtures of various hydrocarbons with argon were condensed on a CsI window cooled with liquid helium or hydrogen and the absorption spectra recorded in the region 700–3500 cm^{-1}.

Microwave Zeeman effect of free hydroxyl radicals: $^2\Pi_{1/2}$ levels, H. E. Radford, *Phys. Rev.* **122,** *114 (1961).*

Two new paramagnetic resonance spectra of the free $O^{16}H$ radical have been observed at 3 cm wavelength in the products of an electric discharge in water vapor. The spectra arise from Λ-type doubling transitions in the $^2\Pi_{\frac{1}{2}}$, J=3/2 and $^2\Pi_{\frac{1}{2}}$, J=5/2 levels. Molecular magnetic moments and hyperfine structure constants measured from the spectra lead to refinements in the theory developed earlier to account for similar measurements on $^2\Pi_{3/2}$ levels. A consistent analysis of the combined $^2\Pi_{\frac{1}{2}}$ and $^2\Pi_{3/2}$ data is then possible, and yields a much better understanding of the molecular Zeeman effect and hyperfine structure.

Kinetic isotope effects in the reaction of methyl radicals with ethane, -d_6 and ethane-1, 1, 1-d_3, J. R. McNesby, *J. Phys. Chem.* **64,** *No. 11, 1671 (Nov. 1960).*

Photolyses of acetone-d_6 in the presence of a mixture of C_2H_6 and C_2D_6 and in the presence of CH_3CD_3 were carried out to measure kinetic isotope effects for the reactions

$$(1)\quad CD_3+C_2H_6 \rightarrow CD_3H+C_2H_5 \rightarrow$$
$$(2)\quad CD_3+CH_3CD_3 \rightarrow CD_3H+CH_2CD_3 \rightarrow$$
$$(3)\quad CD_3+CH_3CD_3 \rightarrow CD_4+CH_3CD_2$$
$$(4)\quad CD_3+C_2D_6 \rightarrow CD_4+C_2D_5$$

The conclusion drawn from the results is that the relative rate constants are within experimental error:

$$k_1/k_4=\exp(1500/RT)$$
$$k_2/k_3=\exp(1500/RT)$$
$$k_1/k_2=2.0$$

Theory of vibrational relaxation in liquids, R. Zwanzig, *J. Chem. Phys.* **34,** *1931–1935 (1961).*
A new formulation of the theory of vibrational relaxation, based on Zener's semi-classical approximation, is presented here. The relaxation rate is shown to be proportional to the spectral density of the force exerted on the oscillator by its environment. The isolated binary collision theory is derived, but only with the condition that the collision frequency is much smaller than the oscillator frequency. This requirement is not satisfied in a liquid: we conclude that Litovitz's application of the isolated binary collision theory to liquid CS_2 is not justified. A possible relation between vibrational relaxation and the self-diffusion coefficient in a liquid is discussed.

Nomenclature of carbohydrates, R. S. Tipson, *J. Chem. Documentation* **2,** *No. 3, 3–7 (1961).*
In naming a carbohydrate, the name chosen should not conflict with the general principles of established organic nomenclature; it should concisely show the number of carbon atoms, the number and configuration of all asymmetric carbon atoms, the functional groups, the size of any sugar-ring, and the anomeric form, if any.
The present paper describes methods which have evolved for naming sugars having either one or two aldehydic or ketonic functions, or an aldehydic plus a ketonic function. The system is then extended to derivatives having either one or two carboxyl groups, an aldehydic plus a carboxyl function, or a ketonic plus a carboxyl function. Naming of derivatives of such compounds are also discussed.

The oxide films formed on copper single crystal surfaces in water II. Rate of growth at room temperature, J. Kruger, *J. Electrochem. Soc.* **108,** *No. 6, 503 (June 1961).*
Measurements utilizing polarized light were made of the increase in film thickness with time on {100}, {110}, {111}, and {311} surfaces of a copper single crystal immersed in water in equilibrium with atmospheres containing either pure oxygen or oxygen-helium mixtures containing 1%, 10%, or 20% oxygen. With the pure oxygen atmosphere a Cu_2O film rapidly reached a limiting thickness that remained constant for 1.5 to 2 hours after which time the formation of CuO was observed. Stirring increased the time required to observe the formation of CuO. Similar behavior was observed for 10% and 20% oxygen atmospheres, the limiting film thickness of Cu_2O and the time required to observe the formation of CuO increased with decreasing oxygen content in the atmosphere. When a 1% oxygen atmosphere was used, parabolic film growth was observed. In all cases the {111} plane exhibited the lowest growth rate.

Line shape of ultraviolet absorption in solid noble gases, P. H. E. Meijer, *J. Chem. Phys.* **34,** *2078–2082 (1961).*
The absorption of ultraviolet in solid noble gases shows lines that are a few inverse centimeters broad. An attempt is made to explain and calculate the width and shape of these lines on the basis of a tentative energy versus configuration. curve. It is shown that the width has the proper order of magnitude. The line shape can be easily calculated at the long wave length end. It should show an exponential tail. If we inspect the expression for small values of the energy, we find a rapidly rising exponential, which would give rise to a smeared out edge appearance, provided the normalization constant (which cannot be determined in the approximation used) is relatively insensitive to variations in the energy. The line will have a nonsymmetrical shape.

Exponential temperature dependence of Young's modulus for several oxides, J. B. Watchman, Jr., W. E. Tefft, D. G. Lam, Jr., and C. S. Apstein, *Phys. Rev.* **122,** *1754 (June 1961).*
Young's modulus was measured over the temperature range 77 °K to 850 °K by an accurate resonance technique. Data are presented for single crystals of aluminum oxide with various orientations of the crystallographic axes and for polycrystalline aluminum oxide, thorium oxide, and magnesium oxide. The results show that the range of validity of a T^4 temperature dependence predicted by theory must be quite small. The temperature dependence is very well described over the whole temperature range by $T\exp(-T_0/T)$ where T_0 is an empirical parameter.

The X- or gamma-ray energy absorption of transfer coefficient: Tabulations and discussion, R. T. Berger, *Radiation Research* **15,** *No. 1, 1–29 (July 1961).*
The energy absorption coefficient is defined and its significance for the calculation of absorbed dose is discussed.

Values of the energy absorption coefficient are tabulated for X-ray photon energies between 3 kev and 10 Mev, for various materials. This tabulation is an extension of previous work of G. R. White Grodstein and takes into account the latest values of the relevant cross sections. Auxiliary data are given to facilitate adaptation of the energy absorption coefficient to practical applications. The uncertainties of the tabulated values are discussed.

Adsorption of nitrogen and argon on mineralogical graphite and diamond at 77 and 90° K, J. de Dios Lopez-Gonzalez, F. G. Carpenter and V. R. Deitz, *J. Phys. Chem.* **65,** *No. 7, 1112–19 (July 1961).*
Adsorption isotherms of argon and nitrogen on mineralogical graphite and diamond powder were determined in the relative pressure range from 10^{-9} to about 1. The sample was outgassed at 450° C for 18 hours before each of a series of measurements. Upon the first exposure to the adsorbate, there was in many cases a very slow adsorption. This was followed by a much higher rate of adsorption and finally by attainment of a steady state. An induction period in physical adsorption is postulated to explain this phenomenon. The isotherms on diamond followed the Freundlich equation over a very wide pressure range and the B.E.T. relationship from 0.01 to 0.4 relative pressure. The isotherms on graphite showed a definite step at a relative pressure range between 10^{-3} and 10^{-4}, and indicated another step at about 10^{-7}. The isotherms on graphite followed the B.E.T. relationship in the relative pressure range 0.001 to 0.1.

Absorption of carbon dioxide by solutions of 2-amino-2-(hydroxymethyl)-1, 3-propanediol, R. G. Bates and H. B. Hetzer, *Anal. Chem.* **33,** *No. 9, 1285 (Aug. 1961).*
Tris(hydroxymethyl)aminomethane, or 2-amino-2-1,3-propanediol, is finding wide use in acidimetry and in *p*H control. This useful base and its aqueous solutions have been reported to be stable in air. Nevertheless, an appreciable change of *p*H can occur if these solutions are exposed to atmospheres containing normal amounts of carbon dioxide.

Quantum theory of interference effects in the mixing of light from phase-independent sources, U. Fano, *Am. J. Phys.* **29,** *No. 8, 539–545 (August 1961).*
Correlations in space and time of the light intensity from extended sources, observed by Brown and Twiss and by Forrester, were analyzed by these authors primarily in terms of field oscillations. This paper discusses an atomic process which brings out the intensity correlations, namely, the photoionization of a pair of atoms following photon emission by another pair of independently excited atoms. The calculated probability of this process depends sinusoidally on the relative positions of the four atoms and also, when the source atoms emit different frequencies, on the time interval between the photoionizations, in agreement with the macroscopic treatment. The oscillations arise from an interference of probability amplitudes which is not affected by the random phases of the source atoms. The calculation follows a standard approach but involves some novel detail.

Heats and volumes of mixing in several C_{12} hydrocarbon systems, R. S. Jessup and C. L. Stanley, *J. Chem. Eng. Data* **6,** *No. 3, 368–371 (July 1961).*
Measurements have been made of the heats and volumes of mixing of two binary systems, one of which was composed of two kerosines, and the other of the C_{12} hydrocarbons bicyclohexyl and *n*-dodecane. In addition, measurements of volume of mixing were made on four other binary systems, in each of which one component was *n*-dodecane while the other was, in turn, *n*-heptylcyclopentane, *n*-hexylcyclohexane, *n*-hexylbenzene, and phenylcyclohexane.

Low-angle X-ray diffraction of crystalline nonoriented polyethylene and its relation to crystallization mechanisms, L. Mandelkern, A. S. Posner, A. F. Diorio, and D. E. Roberts, *J. Appl. Phys.* **32,** *No. 8, 1509–1517 (Aug. 1961).*

X-ray diffraction maxima at low angles have been observed in crystalline but nonoriented linear polyethylene, the crystallization process being conducted from the melt of the pure undiluted polymer. Several orders of diffraction are observed in favorable cases, and the spacings corresponding to the first-order reflections range from 150–850 A. The values of the maxima depend on the mode of crystallization. Previous assertions that in such systems the maxima are limited to 100–200 A are shown to be very restrictive and typical only of crystallization processes conducted at very large undercooling. Major attention is focused on the properties of specimens crystallized isothermally at relatively low values of the undercooling. The spacings are very sensitive to the crystallization temperature in this range. The highest values are observed at low undercooling, and substantial decreases occur as the temperature is lowered. Concomitantly, the density observed after isothermal crystallization significantly decreases with a lowering of the crystallization temperature.

The fact that a periodicity can be developed in such systems, the magnitude of the maxima, and their dependence on the crystallization temperature, is explicable by the application of nucleation theory. It is assumed that subsequent to the formation of critical-size nuclei from a bundle of polymer chains, crystal growth along the chain direction is severely retarded, while in the transverse direction essentially unimpeded crystallization occurs. From the observed temperature coefficient of the low-angle spacings, the ratio of the excess free energy (resulting from the junction of crystalline and amorphous regions at the crystallite ends) to the bulk enthalpy of fusion is found to be 2.6. The magnitude of this ratio receives confirmation from another type of experiment.

Density fluctuations and heat conduction in a pure liquid, R. E. Nettleton, *Phys. Fluids* **4,** *No. 1, 74 (Jan. 1961).*
Two components of the heat flux in a pure liquid are identified—one carried by sound waves and the other by diffusing molecules. Coupled relaxation equations are obtained for these components, both depending on the density gradient $\nabla\rho$, and this dependence is interpreted thermodynamically as a further coupling of these equations with the equation determining $(\partial/\partial t)\ (\nabla\rho)$. The latter can be immediately written down with the aid of Onsager's theorem and an inertial principle developed in a previous paper. The thermodynamic interpretation of these rate equations also leads to an explicit expression for the coefficient of $(\nabla\rho)^2$ in a Taylor expansion, about equilibrium, of the Helmholtz free energy. This result is compared with similar free energy terms assumed to exist by other authors.

Low temperature properties of cerous magnesium nitrate, R. P. Hudson, R. S. Kaeser, and H. E. Radford, *Proc. VIIth Intern. Conf. Low Temperature Physics, University of Toronto, Canada, p. 45–48 (1960).*
A variety of measurements have been made on cerous magnesium nitrate between room temperature and the region of millidegrees Kelvin. In the range 10^{-3} to 1° K the entropy temperature relation varies from specimen to specimen and at the high temperature end the curve for any one sample does not entropolate to coincidence with that derived from spin-lattice relaxation measurements in the 1°–4° K region. The spectroscopic splitting factor is probably exactly zero along the c-axis. Evidence for the presence of low-lying doublets is supplied by departures of the X-T relation from the Curie Law in the 4°–300° K range.

Other NBS Publications

Journal of Research 65B (Math. and Math. Phys.) No. 4 (Oct.–Dec. 1961) 75 cents.

Physical entities and mathematical representation. C. H. Page.

On the range of a fleet of aircraft. A. J. Goldman.

Measurement of wave fronts without a reference standard: Part I. The wave-front-shearing interferometer. J. B Saunders.

On the evaluation of the function $\Phi(\lambda)=\frac{1}{2\pi i}\int_{\sigma-i\infty}^{\sigma+i\infty} e^{u\ln u+\lambda u}du$ for real values of λ. W. Börsch-Supan.

Analyticity and probability properties of one-dimensional Brownian motion. A. Ghaffari.

Some higher order integral identities with application to bounding techniques. J. H. Bramble and B. E. Hubbard.

A priori bounds in the first boundary value problem in elasticity. J. H. Bramble. and L. E. Payne.

Journal of Research 66D (Radio Prop.) No. 1 (Jan.–Feb. 1962) 70 cents.

A survey of very wide band antennas—1945 to the present J. D. Dyson.

Numerical investigation of the equivalent impedance of a wire grid parallel to the interface between two media. T. Larsen.

Current on and input impedance of a cylindrical antenna. Y. M. Chen and J. B. Keller.

Radar corner reflectors for linear or circular polarization. G. Latmiral and A. Sposito.

On the theory of wave propagation through a concentrically stratified troposphere with a smooth profile. H. Bremmer.

On the propagation of VLF and ELF radio waves when the ionosphere is not sharply bounded. J. R. Wait.

Fields of electric dipoles in sea water—the earth-atmosphere-ionosphere problem. W. L. Anderson.

Reflection of electromagnetic waves from thin ionized gaseous layers. F. H. Northover.

Reflection and transmission of radio waves at a continuously stratified plasma with arbitrary magnetic induction. J. R. Johler and J. D. Harper, Jr.

On the diffraction of spherical radio waves by a finitely conducting spherical earth. L. C. Walters and J. R. Johler.

An approximate full wave solution for low frequency electromagnetic waves in an unbounded magneto-ionic medium. W. C. Hoffman.

VHF radio propagation data for the Cedar Rapids-Sterling, Anchorage-Barrow, and Fargo-Churchill test paths, April 1951 through June 1958. G. R. Sugar and K. W. Sullivan.

Stopping powers for use with cavity chambers, NBS Handb. 79 (1961), 35 cents.

Hydraulic research in the United States, H. K. Middleton, NBS Misc. Publ. 238 (1961), $1.25.

Fractional factorial designs for experiments with factors at two and three levels, W. S. Connor and S. Young, NBS Applied Math. Series 58 (1961), 40 cents.

Quarterly radio noise data, March, April, May 1961, W. Q. Crichlow, R. T. Disney, and M. A. Jenkins, NBS Tech. Note 18–10 (PB151377–10) (1961) $1.50.

Mean electron density variations of the quiet ionosphere, No. 5—July 1959, J. W. Wright, L. R. Wescott, and D. J. Brown, NBS Tech. Note 40–5 (PB151399–5) (1961) $1.50.

Flux switching mechanisms in ferrite cores and their dependence on core geometry, G. W. Reimherr, NBS Tech. Note 90 (PB161591) (1961) $1.25.

An experimental study of beta decay using the radiations from oriented nuclei, D. D. Hoppes, NBS Tech. Note 93 (PB161594) (1961) $1.50.

Bibliography on meteoric radio wave propagation, W. Nupen, NBS Tech. Note 94 (PB161595) (1961) $2.75.

The integrated starlight over the sky, L. R. Megill and F. E. Roach, NBS Tech. Note 106 (PB161607) (1961) $2.00.

Load carrying capacity of gas-lubricated bearings with inherent orifice compensation using nitrogen and helium gas, H. Sixsmith, W. A. Wilson, and B. W. Birmingham, NBS Tech. Note 115 (PB161616) (1961) $1.00.

Matrix elements in the forbidden beta decay of Ce^{141}, D. D. Hoppes, E. Ambler, R. W. Hayward, and R. S. Kaeser, Phys. Rev. Letters **6,** 115–118 (1961).

The electromagnetic fields of horizontal dipole in the presence of a conducting half space, J. R. Wait, Can. J. Phys. **39,** No. 7, 1017–1028 (July 1961).

Simple adiabatic demagnetization apparatus, V. D. Arp and R. H. Kropschot, Rev. Sci. Instr., Note **32,** 217–218 (Feb. 1961).

4-Nitrophenyl esters, carbonates, and bi-carbonates as leather fungicides, S. Dahl and A. M. Kaplan, J. Am. Leather Chemists Assoc. **55,** 480 (Sept. 1960).

The organization of international intercomparisons of radioactivity standards, with special reference to such measurements of NBS standards, L. M. Cavallo and W. B. Mann, Proc. 1959 Symp. Metrology Radioactive, IAEA, Vienna, 117 (1960).

The physical environment as affected by radiation, D. M. Gates, Proceedings of the 50th Anniversary Celebration of the University of Michigan Biological Station (1960).

Second revision American Dental Association specifications No. 4 for dental inlay casting wax, J. W. Stanford, K. V. Weigel, and J. W. Paffenbarger, J. Am. Dental Assoc. **62,** 45 (Jan. 1961).

Measurement of contrast in the aerial image, F. W. Rosberry, Photogrammetric Eng. 155–159 (March 1961).

An interferometric instrument for the rapid measurement of small diameters, D. H. Blackburn, Rev. Sci. Instr. **32,** No. 2, 137 (Feb. 1961).

Vapor-phase photolysis of formic acid, R. Gordon, Jr., and P. Ausloos, J. Chem. Phys. **65,** 1033 (1961).

Binary silicate glasses in the study of alkali-aggregate reaction, R. G. Pike, D. Hubbard, and E. S. Newman, Highway Research Board Bull. No. 275, 39–44 (1960).

Physical measurement—challenge to science and engineering, A. V. Astin, SPE J. **17,** No. 5. 455–458 (May 1961).

Low-temperature thermocouples I. Gold-cobalt or constantan versus copper or "normal" silver, R. L. Powell, M. D. Bunch, and R. J. Corruccini, Cryogenics **1,** 139–150 (Mar. 1961).

Dielectric properties of polyamides, A. J. Curtis, J. Chem. Phys. **34,** No. 5, 1849–1850 (May 1961).

Natural and synthetic rubbers: Review of test methods, F. J. Linnig, M. Tryon, and E. J. Parks, Anal. Chem. **33,** 1272 (Apr. 1961).

Simple calculus for all-dielectric interference filters, K. D. Mielenz, J. Opt. Soc. Am. **50,** No. 10, 1014 (Oct. 1960).

Magnetic susceptibility of tetratonal titanium dioxide, F. E. Senftle, T. Pankey, and F. A. Grant, Phys. Rev. **120,** 820 (Nov. 1960).

Equipment and procedures for the evaluation of total hemispherical emittance, J. C. Richmond and W. N. Harrison, Bull. Am. Ceram. Soc. **39,** No. 11, 668 (Nov. 1960).

Limitations of radiosonde punch-card records for radio-meteorological studies, B. R. Bean and B. A. Cahoon, J. Geophys. Research **66,** No. 1, 328–331 (Jan. 1961).

Evaluations of some oxide glasses for use as infrared materials, G. W. Cleek and T. G. Scuderi, Proc. Infrared Information Symp. **5,** No. 4 (Aug. 1960).

Improvement of some of the properties of sole leathers by impregnation with polymers, J. R. Kanagy, J. Am. Leather Chemists Assoc. **LVI,** No. 7, 322–342 (July 1961).

A transistor frequency meter, F. R. Bretemps and S. Saito, Electronic Inds. **19,** No. 10, 196–198 (Oct. 1960).

Studies on the flame-spraying of aluminum oxide, D. G. Moore, Metal Finishing J. **6,** No. 70, 397 (Oct. 1960).

Self-qualification of laboratories, A. T. McPherson, Instr. and Control Systems **34,** No. 7. 1265 (July 1961).

Four-color achromats and superchromats, R. E. Stephens, J. Opt. Soc. Am. **50,** No. 10, 1016–1019 (Oct. 1960).

Bounds for determinants with positive diagonals, E. V. Haynsworth, Trans. Am. Math. Soc. **96,** 395–399 (1960).

Refining measurements by capacitance techniques, F. K. Harris and R. D. Cutkosky, ISA—J. Instr. Soc. Am. **8,** No. 2, 63–66 (Feb. 1961).

Standards for plastic pipe fittings, F. W. Reinhart, SPE J. **17,** 160 (Feb. 1961).

Post office mechanization, B. M. Levin, M. C. Stark, and P. C. Tosini, Elec. Engr. **80,** 105–110 (Feb. 1961).

Comparison of observed tropospheric refraction with values computed from the surface refractivity, B. R. Bean, IRE Trans, Ant. Prop. **AP–9,** 415–416 (July 1961).

The precision measurement of transformer ratios, R. D. Cutkosky and J. Q. Shields, IRE Trans, Instrumentation **I–9,** No. 2, 243–250 (Sept. 1960).

Studies of environmental factors in a family-size underground shelter, P. R. Achenbach, F. J. J. Drapeau, and C. W. Phillips, Report OCDM–NBS–60–1 issued Office of Civil Defense Mobilization (Mar. 1961).

Electrodes for pH measurements, R. G. Bates, J. Electroanalytical Chem. **3,** 93 (1961).

Phase-shift method for one-dimensional scattering, A. H. Kahn, Am. J. Phys. **29,** 77 (1961).

The classical field theories, C. Truesdell and R. Toupin, Handb. der Physik, Springer, Berlin, **III,** No. 1, 226–793 (1960).

A precision RF attenuation calibration system, C. M. Allred and C. C. Cook, IRE Trans. Instrumentation **I–9,** No. 2, 268–274 (Sept. 1960).

A vibrating sample magnetometer, N. V. Frederick, IRE Trans. Instrumentation **I–9,** No. 2, 194–196 (Sept. 1960).

Standards development by ASTM committee D–20 on plastics, F. Reinhart, SPE J. **16,** 800 (Aug. 1960).

A nuclear magnetic resonance study of *syn-anti* isomerism in ketoximes, E. Lustig, J. Phys. Chem. **65,** 491 (1961).

A standard current transformer and comparison method—A basis for establishing ratios of currents at audio frequencies, B. L. Dunfee, IRE Trans. Instrumentation **I–9,** No. 2, 231–236 (Sept. 1960).

Evaluating the freezing-and-thawing durability of concrete by laboratory tests in the U.S.A., H. T. Arni and R. L. Blaine, Preliminary Report on Symposium on Durability of Concrete of RILEM, Prague, Czechoslovakia, 218–231 (July 1961).

Spectroscopic standard samples of titanium and high-temperature alloys, R. E. Michaelis, J. Appl. Spectroscopy **15,** 7 (1961).

Analytical laboratory problems, J. Mandel, Trans. Metropolitan Conf. Am. Soc. Quality Control, 99–107 (Feb. 1960).

Some experimental aspects of nuclear orientation, E. Ambler, Proc. 10th Inter. Congress of Refrigeration, Copenhagen, Denmark, 1959, Progress in Refregeration in Science and Technology **I,** 195–198 (Pergamon Press, London, England, 1960).

Rapid method for interpolating refractive index measurements, O. N. Stavroudis and L. E. Sutton, J. Opt. Soc. Am. **51,** No. 3, 368–370 (Mar. 1961).

Comparison of four different methods of determining drying shrinkage of concrete masonry units, J. O. Bryson and D. Watstein, J. Am. Concrete Inst. **58,** No. 2, 163–184 (Aug. 1961).

The retannage of chrome-tanned leather with vegetable tannins, J. R. Kanagy, J. Am. Leather Chemists Assoc. **LVI,** No. 6, 252–272 (June 1961).

Improved electron filter lens, J. A. Simpson and L. Marton, Rev. Sci. Instr. **32,** No. 7, 802–803 (July 1961).

Static and dynamic calibrations of pressure measuring instruments at the National Bureau of Standards, E. C. Lloyd and D. P. Johnson, Automatic and Remote Control Proc. 1st Intern. Congress of IFAC, 274–280 (1960).

X-ray diffraction study of acellular teleost bone, M. L. Moss and A. S. Posner, Nature **188,** 1037 (Dec. 1960).

The NBS absolute gravity experiment, D. R. Tate, Proc. 2d Air Force Cambridge Research Center Military Geodesy Seminar, GRD Research Notes, 40 (Jan. 12–14, 1960).

Adsorption of polyesters and other polymers on glass and other substrates, R. R. Stromberg and G. M. Kline, Modern Plastics **38,** 123 (Apr. 1961); **38,** 241 (May 1961); Poliplastic **9,** 15 (Jan.–Feb. 1961).

Tunnel diode large-signal simulation study, S. B. Geller and P. A. Mantek, Proc. IRE **49,** No. 4, 803 (Apr. 1961).

Determination of carboxyl in cellulose—comparison of various methods, W. K. Wilson and J. Mandel, Tappi **44,** No. 2, 131 (1961).

A recalibration of NBS carbon-14 standards by Geiger-Müller and proportional gas counting, W. B. Mann, H. H. Seliger, W. F. Marlow, and R. W. Medlock, Rev. Sci. Instr. **31,** No. 7, 690 (1960).

Computer for weather data acquisition, P. Meissner, J. Cunningham, and C. Kettering, Proc. Eastern Joint Computer Conf. **18,** No. 2.1, 57–66 (Dec. 1960).

The solar spectrum from 2635 to 2085 A, H. H. Malitson, J. D. Purcell, R. Tousey, and C. E. Moore, Astrophys. J. **132,** 746 (1960).

Winter thermal radiation studies in Yellowstone Park, D. M. Gates, Science **134,** 32–35 (July 7, 1961).

Vapor phase γ-radiolysis of acetone, L. J. Stief and P. Ausloos, J. Phys. Chem. **65,** 877 (1961).

Amine buffers for *p*H control, R. G. Bates, Ann. N. Y. Acad. Sci. **92,** 341 (1961).

Cryogenic adhesive properties of bisphenol-A epoxy resins, M. J. Hiza and P. L. Barrick, SPE Trans. **1,** 73–79 (Apr. 1961).

Resonance characteristics of a corrugated cylinder excited by a magnetic dipole, J. R. Wait and A. M. Conda, IRE Trans. Ant. Prop. **AP–9,** 330–333 (July 1961).

Recent work with compensated internal gas counters for the standardization of gaseous radionuclides, W. B. Mann, Proc. Symp. Metrology of Radioactive IAEA, Vienna, 307 (1960).

Vanadium oxytrichloride [Vanadyl(V) chloride], R. B. Johannesen, Book, Inorganic Syntheses, E. G. Rochow, Editor-in-Chief (McGraw-Hill Book Co., New York, N.Y.), IV. Chapt. 5B, No. 38, 119–120 (1960).

Concerning the potential refractive index and the molecular refractivity, B. R. Bean and J. D. Horn, J. Meteorol. **18,** No. 3, 427–428 (June 1961).

Standard samples and related materials for spectrochemical analysis, R. E. Michaelis, Am. Soc. Testing Materials Spec. Tech. Publ. No. 58–D, 116 (1960).

Aromatic fluorocarbons: Thermal stability and synthesis, L. A. Wall, Proc. 6th Joint Army-Navy-Air Force Elastomer Conf., Oct. 18–20, 1960, I. 150 (U.S. Army Quartermaster Research & Engineering Command, Natick, Mass.).

The ionization constant of hydroxylamine, R. A. Robinson and V. E. Bower, J. Phys. Chem. **65,** 1279–1280 (1961).

The calculation of the energy levels of nearly symmetric rotors, S. C. Wait, Jr., J. Mol. Spectroscopy **6,** 276 (1960).

Multiple layer insulation for cryogenic applications, R. H. Kropschot, Cryogenics **1,** 171–177 (Mar. 1961).

Extinguishment effectiveness of some powdered materials on hydrocarbon fires, T. G. Lee and A. F. Robertson, Fire Research Abstracts and Reviews, Natl. Acad. Sci.-Natl. Research Council Publ. 786 (June 1961).

Forty years of dental research at the National Bureau of Standards, W. T. Sweeney, Capital Chemist **10,** 228 (Oct. 1960).

A stainless steel for standard weights, S. J. Rosenberg and T. P. Royston, Materials Research & Standards (ASTM Bull.) **1,** No. 1, 21 (Jan. 1961).

Long-term working stress of thermoplastic pipe, F. W. Reinhart, SPE J., 751–754 (Aug. 1961).

NBS atomic frequency standards, R. C. Mockler and R. E. Beehler, Proc. 14th Annual Symp. Frequency Control, Atlantic City, N.J., May 31–June 3, 1960, p. 298–309 (Signal Corps Eng. Laboratories, Fort Monmouth, N.J., 1961).

A precision RF power transfer standards, P. A. Hudson, IRE Trans. Instrumentation **I–9,** 280-283 (Sept. 1960).

The fluorescence and phosphorescence of trifluoroacetone vapor, P. Ausloos and E. Murad, J. Am. Chem. Soc. **83,** 1327 (1961).

The morphology of sporadic E, E. K. Smith, Jr., Proc. XIIIth Gen. Assembly URSI (London, England, 1960), Natl. Acad. Sci.-Natl. Research Council Publ., Report No. 880, 218 (1961).

How to determine stack load limits, R. S. Wyly, Contractor, p. 19–20 (Aug. 15, 1961). γ-Irradiation of liquid and solid oxygen, D. W. Brown and L. A. Wall, Phys. Chem. **65,** 915 (1961).

Testing of ball bearings with five different separator materials at 9200 RPM in liquid nitrogen, J. A. Brennan, W. A. Wilson, R. Radebaugh, and B. W. Birmingham, Am. Soc. Mech. Engrs., No. 61–LUBS–18, 1–8 (Apr. 1961).

The CRPL electron density profile program: Some features and early results, J. W. Wright, Proc. URSI–AGI Symp. (Brussels, Belgium, 1959), Book, Some Ionospheric Results Obtained During IGY, Ed. W. J. G. Beyon (Elsevier Publ. Co., Princeton, N.J.), 215 (1960).

Digest of a general description of D–C digital voltmeters, C. Stansbury, AIEE Trans. Paper 61–721 (Apr. 1961).

Determination of wax in paper, W. L. Marrow, Tappi **44,** No. 2, 120 (1961).

Mortar for cavity walls, C. C. Fishburn, Building Research Institute, 1960 Spring Conf. Program on Insulated Cavity Walls, Natl. Acad. Sci.-Natl. Research Council Publ. **793,** 37 (1960).

Variations of [OI] 5577 Å emission in the upper atmosphere, F. E. Roach, Ann. Geophys. **17,** 172–180 (Apr.–June 1961).

Continuously operating He^3 refrigerator for producing

temperature down to ¼° K, E. Ambler and R. B. Dove, Rev. Sci. Instr. **32,** No. 6, 737–739 (June 1961).

Location of the plane of best average definition for airplane camera lenses, F. E. Washer and W. P. Tayman, Photogrammetric Eng. **26,** No. 3, 475–488 (1960).

A review of the hydraulics of circular sewers in accordance with the Manning formula, R. S. Wyly, Yearbook of Am. Soc. of Sanitary Engineering **38,** 154 (1960).

Non-reciprocity and time-reversal in microwave circuits, H. A. Fowler, Academie royale de Belgique (Classe Des Sciences) **V–46**, No. 11, 963–977 (Dec. 1960).

A screening method for large information retrieval systems, R. T. Moore, Proc. Western Joint IRE–AIEE–ACM Computer Conf., Los Angeles, Calif. 6.3, 259–274 (1961).

Humidity standards, A. Wexler, Tappi **44**, No. 6, 180a (June 1961).

Tchebycheff approximations by ab^x+c, J. R. Rice, J. Soc. Ind. Appl. Math. **8**, No. 4, 691–702 (1960).

Ionospheric "forward" scattering, D. K. Bailey, Proc. XIIIth Gen. Assembly of URSI (London, England, 1960), Natl. Acad. Sci.-Natl. Research Council Publ. Report No. 880, 281 (1961).

Apparatus for controlled slack quenching, N. L. Carwile, M. R. Meyerson, and S. J. Rosenberg, Materials Research and Standards (ASTM Bull.) **1**, No. 7, 532–536 (July 1961).

A high-resolution ammonia-maser-spectrum analyzer, J. A. Barnes and L. E. Heim, IRE Trans. Instrumentation **I–10**, 4–8 (June 1961).

Electron spin resonance spectra of free-radical intermediates formed by reaction of polystyrene with atoms of hydrogen and deuterium, R. B. Ingalls and L. A. Wall, J. Chem. Phys. **35**, No. 1, 370–371 (July 1961).

Reinhart, F. M., Twenty-year atmospheric corrosion investigation of zinc-coated and uncoated wire and wire products, Am. Soc. Testing Materials Spec. Tech. Publ. **290**, 1–141 (June 1961).

Time standards, A. G. McNish, Instr. and Control Systems **33**, 1340–1341 (Aug. 1960).

Stress-strain relationships in yarns subjected to rapid impact loading; Part 7. Stress-strain curves and breaking-energy data for textile yarns, J. C. Smith, P. J. Shouse, J. M. Blandford, and K. M. Towne, Textile Research J. **31**, No. 8, 721–734 (Aug. 1961).

V. Mutual interference between surfaces and satellite communication systems, B. Hartman, M. T. Decker, ch. 5, p. 111–157, Book, Frequency Allocations for Space Communications (Report of the Joint Tech. Adv. Comm. of IRE–EIA to the Federal Communications Commission, Mar. 1961).

Some observations of copper deposits on single crystals of copper, I. Giron and F. Ogburn, J. Electrochem. Soc. **108**, No. 9, 842–846 (Sept. 1961).

Binary oxide systems, H. R. Hoekstra and H. S. Parker, ch. 6, sec. 6, p. 271–304, Book, UO_2, Properties and Nuclear Applications (U. S. Superintendent of Documents, Government Printing Office, Washington 25, D. C., Aug. 1961).

Wind resistance of asphalt shingle roofing, W. C. Cullen, Natl. Acad. Sci.-Natl. Research Council, 33–42 (1961).

Pulse voltage comparator measures height of positive or negative pulses, O. B. Laug, Electronics **34**, No. 36, 70–71 (Sept. 1961).

Spectroscopic observations of the stratosphere and mesosphere D. M. Gates, Instr. Soc. Am. J. Conf. Preprint No. 2-NY60 (Sept. 1960).

Supercooling in the barnyard, C. P. Saylor, The Capital Chemist **10**, No. 9, 292–293 (Dec. 1960).

References to contemporary papers on acoustics, W. Koidan, Acoust. Soc. Am. **33**, No. 5, 705–716 (May 1961).

**Publications for which a price is indicated (except for Technical Notes) are available only from the Superintendent of Documents, U. S. Government Printing Office, Washington 25, D. C. (foreign postage, one-fourth additional). Technical Notes are available only from the Office of Technical Services, U. S. Department of Commerce, Washington 25, D. C. (Order by PB number). Reprints from outside journals and the NBS Journal of Research may often be obtained directly from the authors.*

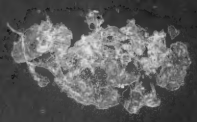

UNIVERSITY MICROFILMS INC
EDITORIAL DEPARTMENT
313 NORTH FIRST ST
ANN ARBOR MICH
SJR-A OCT

UNITED STATES
GOVERNMENT PRINTING OFFICE
DIVISION OF PUBLIC DOCUMENTS
WASHINGTON 25, D.C.

OFFICIAL BUSINESS

PENALTY FOR PRIVATE USE TO AVOID PAYMENT OF POSTAGE, $300 (GPO)

JOURNAL OF RESEARCH of the National Bureau of Standards Vol. 66A, No. 1 January–February 1962
A. Physics and Chemistry

Contents

Page

Absolute isotopic abundance of terrestrial silver. William R. Shields, Ernest L. Garner, and Vernon H. Dibeler. 1

Temperature of a copper arc. Charles H. Corliss. 5

Melting process and the equilibrium melting temperature of polychlorotrifluoroethylene. John D. Hoffman and James J. Weeks. 13

Tritium-labeled compounds VIII. Confirmation of the position of the tritium in D-glucose-*6-t* and D-glucitol-*5-t*. Lorna T. Sniegoski and Horace S. Isbell. 29

Infrared absorption spectra in the study of mutarotational equilibria of monosaccharides. R. Stuart Tipson and Horace S. Isbell. 31

Preparation of high purity trimethylborane. Gaylon S. Ross, Delmo Enagonio, Clifford A. Hewitt, and Augustus R. Glasgow. 59

Reaction of several aminopyrimidines with formaldehyde. Gerald L. McLeod. 65

Acidic dissociation constant and related thermodynamic quantities for diethanolammonium ion in water from 0 to 50 °C. Vincent E. Bower, Robert A. Robinson, and Roger G. Bates. 71

Fiber structure—property relationships II: Macroscopic deformations of alkylene sulfide crosslinked polycaprolactam fibers. Stephen D. Bruck. 77

Ion transport across membranes: I. Definitions of membrane electromotive forces and of flows of electrolytic solutes. Blanton C. Duncan. 83

Publications of the National Bureau of Standards. 97

For sale by the Superintendent of Documents, U.S. Government Printing Office, Washington 25, D.C. Price 70 cents (single copy)
Subscription price: $4.00 a year; 75 cents additional for foreign mailing.

UNITED STATES GOVERNMENT PRINTING OFFICE, WASHINGTON : 1962